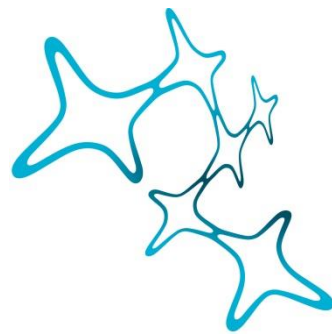


LOCAL AND REMOTE EFFECTS OF
PATHOLOGICAL CONDITIONS ON PYRAMIDAL
NEURITES

A LONGITUDINAL STUDY USING
IN VIVO TWO-PHOTON MICROSCOPY

Susana Valero Freitag



Graduate School of
Systemic Neurosciences

LMU Munich



Dissertation at the
Graduate School of Systemic Neurosciences
Ludwig-Maximilians-Universität München

May, 2020

Supervisors

Prof. Dr. med. Nikolaus Plesnila

Dr. Farida Hellal

Institute for Stroke and Dementia Research

Klinikum der Universität München

First Reviewer: Prof. Dr. med. Nikolaus Plesnila

Second Reviewer: Prof. Dr. rer. nat. Juergen Bernhagen

External Reviewer: Prof. Dr. Frank Kirchhoff

Date of Submission: May 7th, 2020

Date of Defense: September 7th, 2020

Table of content

List of abbreviations	4
Abstract	6
1. Introduction	8
1.1. Insight into the cortical network	8
1.2. Neurites of pyramidal neurons, interaction via synapses and synaptic rearrangement under normal physiological conditions	10
1.2.1. Synapses	10
1.2.2. Synaptic plasticity	12
1.3. Neuritic alterations in pathological conditions	13
1.4. Axonal pathology in Alzheimer's Disease	14
1.4.1. AD and main pathological hallmarks	14
1.4.2. Axonal dystrophies in close proximity to amyloid plaques	16
1.5. Ischemic stroke as a pathological condition, evolution over time and neuritic alterations	17
1.5.1. Stroke, epidemiology, causes, and symptoms	17
1.5.2. Pathophysiology, temporal course of ischemic stroke and infarct growth	18
1.5.3. Expansion of the focal ischemic damage to remote areas	20
1.5.4. Neuronal plasticity after ischemic stroke: dendritic remodeling	22
1.5.5. Impact of structural changes on the neuronal circuits: interhemispheric imbalance and role of the corpus callosum	22
1.5.6. Current clinical management of ischemic stroke and disabilities	24
1.6. Experimental approach used in our study to investigate structural and functional alteration	26
1.6.1. Chronic two-photon imaging and optical access to cortical structures	26
1.6.2. AD models and models of unilateral ischemic stroke	27
1.6.3. Laser speckle imaging as a tool to measure functional outcome	28
2. Aim	30
3. Research articles	31
3.1. High plasticity of axonal pathology in Alzheimer's Disease mouse models	31
3.2. Transcallosal deafferentation induces contralesional cortex reorganization after stroke	59
4. Discussion	110
4.1. Critical reasoning of the results	110
4.2. Technical considerations	112
4.3. Considerations about the findings and future directions	114
5. References	116
6. List of publications	129
7. Acknowledgments	130
8. Declaration of author's contribution	131
9. Affidavit	132
10. Curriculum Vitae	133
11. Copyrights	136

List of abbreviations

Aβ	Amyloid beta
AAV	Adeno associated virus
AD	Alzheimer's disease
AMPA	Alpha-amino-3-hydroxy-5-methyl-4-isoxazole-propionic acid
APP	Amyloid precursor protein
ATP	Adenosine triphosphate
BACE1	β -Secretase enzyme 1
BOLD	Blood oxygen level dependent imaging
CIMT	Constraint-induced movement therapy
CC	Corpus callosum
CNS	Central nervous system
DN	Dystrophic neurite
DTI	Diffusion tensor imaging
EC	Extracellular
EM	Electronic microscope
5XFAD	Five familial AD mutations
FIB-SEM	Focused ion beam-scanning electron microscope
fMRI	Functional magnetic resonance imaging
GABA	Gamma-aminobutyric acid
GFP	Green fluorescent protein
IACD	Intracellular domain of APP
IC	Intracellular
IL-1β	Interleukin-1 β
INs	Interneurons
IT	Intratelencephalic
LC3-II	Microtubule-associated protein 1A/1B-light chain 3
MCA	Middle cerebral artery
MCAo	Middle cerebral artery occlusion
MRI	Magnetic resonance imaging
NMDA	N-methyl-D-aspartate

NFT	Neurofibrillary tangles
NIBS	Non-invasive brain stimulation
NVC	Neurovascular coupling
P3	Small peptide
PCR	Polymerase chain reaction
PHF-tau	Hyperphosphorylated tau
PN	Projection neurons
PNs	Pyramidal neurons
PSD-95	Post-synaptic density protein 95
PSEN1	Presenilin 1
PSEN2	Presenilin 2
rTMS	Repetitive transcranial magnetic stimulation
SNAP25	Synaptosomal nerve-associated protein 25
SST	Somatostatin
TEM	Transmission electron microscope
Th	Thalamus
TM	Transmembrane
TNFα	Tumor necrosis factor alpha
tPA	Tissue plasminogen activator
TPLSM	Two-photon laser scanning microscopy
Vglut-1	Vesicular glutamate transporter 1
3D	3-Dimensional
2P	Two-photon

Abstract

When neurons change their activity pattern, they remodel their synapses. Synaptic remodeling is characterized by changes in synaptic stability, number, and morphology. Remodeling occurs during normal CNS function, but also under pathological conditions, such as Alzheimer's Disease (AD) and stroke. Under these circumstances, when the brain undergoes substantial functional and morphological alterations, loss of synaptic connections have been reported to be the anatomical correlate of decreasing cognitive function.

In addition to loss of synapses, AD is also characterized by axonal pathology. Axons form axonal dystrophies (DNs), bundles of pathologically altered axons in the vicinity of A β plaques. The role of DNs in AD are, however, not well defined. For example, it is not even known whether A β plaques induce DNs or whether DNs form first and trigger the formation of A β plaques later on. Since this question can only be answered by longitudinal observation of DN and A β formation *in vivo* with cellular resolution, one aim of the current thesis was to use a mouse AD model and co-register DNs and A β plaques by repetitive 2-photon microscopy, a technique able to observe these processes in the living brain. For this purpose, we used two transgenic AD mouse lines each crossed to a mouse line with green fluorescent neurons (dE9xGFP-M and APP-PS1xGFP-M). Plaques were stained with the specific dye methoxy-X04. Over a follow up of 210 days, we found that DNs were formed in only 25% of GFP-expressing axons near plaques, indicating selective vulnerability. We observed that DNs were highly dynamic and plastic structures with large variations in size and shape (axonal regrowth). These changes were more prominent in larger DNs. Large A β plaques appeared around imaging day 130 and smaller, satellite plaques appeared later (day 232).

Moreover, the analysis of the neurochemical and ultrastructural characteristics of DNs revealed that most GFP-expressing DNs widely express presynaptic, autophagy, and lysosomal markers while APP/A β is selectively present in 50-60% of the GFP-expressing DNs. Our data suggests a relationship between different plaques and DNs, where dystrophies are involved in the plaque formation and development. Larger DNs might be the main source of A β peptide and thus, an active participant in the amyloid pathology, whereas smaller DNs seem to be a consequence.

Taking these results together, the existence of neuronal plasticity increases the likelihood that the synaptic abnormalities associated with pathological conditions can be influenced within a certain time window. Indeed, our data demonstrated that the axonal pathology linked to the presence of dystrophies could be reversed within a longer time window than previously thought.

Moreover, ischemic stroke is associated to the presence of disabilities in patients. Previous studies have demonstrated that the chronic impairment may be related to a maladaptive plasticity after ischemia. However, it is not clear which structural and functional alterations underlie this process. It is known that stroke leads to alterations in remote areas (diaschisis) through the loss of neuronal input from the damaged region (deafferentation). Focusing on the contralesional cortex, we aimed to characterize the long-term effect of cerebral ischemia on its reorganization and dendritic dynamics in correlation with sensorimotor behavior and neuronal activity.

Here, we benefit from two-photon imaging through a cranial window and retrograde virus tracing in C57BL/6N mice (1-2 months old). Ischemic stroke was induced by electrocoagulation

of the distal part of the MCA (dMCAo) or by 1h occlusion with a filament (fMCAo). A post-operative care protocol was applied to mice subjected to fMCAo to facilitate a better surgery recovery and higher survival chances. Global and focal neurological deficits were assessed by a modified neurological severity score. The contralesional NVC response was measured after whisker stimulation by using laser speckle imaging. Nissl staining, immunofluorescence and PCR were performed as well as MRI scanning.

Our post-operative care protocol enabled optimal survival (90-100%) of mice after fMCAo. The evaluation of global and focal neurological deficits in this model, demonstrated a general recovery of the sickness behavior but the presence of sustained neurological deficits over time (40% residual deficit). We found a decrease in the cortical thickness (11%) without any cell death and a significant decrease in the neuropil fraction (14%). By using retrograde viral tracing, we could unequivocally follow the dendritic arbor of transcallosal neurons connected to the infarct. We observed dendritic remodeling and dynamic changes in the apical dendrites of transcallosal neurons after stroke reflected by more transient spines together with a decrease in spine density (35%). Thus the dendritic reorganization of these neurons might explain this remote effect. In parallel we demonstrated changes in relative excitatory/inhibitory balance between both hemispheres but also at the level of transcallosal neurons which became hyperexcitable. Using laser speckle imaging, we showed that the observed structural reorganization was accompanied by functional hyperemia (increase in blood flow during stimulation) up to one month, followed by a decrease at three months post-stroke. These data indicates that at one month, neurons in the contralesional cortex would show an increase in activity reflected by more demand of blood flow (higher laser speckle signal) when the whiskers are stimulated (NVC principle). In contrast, the scenario would be inverted at three months and the decrease in neuronal activity would be also supported by our previous observation, the reduction of spine density in that area.

Our findings suggest that the ongoing atrophy, at the level of the infarcted hemisphere, would lead to an extension of the damage through the transcallosal pathway to the contralesional side. The triggered alterations would lead to spine remodeling resulting in both structural and functional reorganization of the contralesional cortex. These findings might therefore give insight into the neurophysiological underpinnings through which neurorehabilitation therapies benefit to stroke recovery.

In sum, we demonstrate the relevance of neuritic integrity and plasticity in AD and ischemic stroke and highlighted the importance that axons and dendrites own as a therapeutic target to reduce structural damages and preserve cognitive and functional abilities.

1. Introduction

The brain represents the most complex organ in the human body, providing us with the ability to think, act, generate memories, feel, and experience the world that surrounds us. It is formed by billions of neurons (Sotelo, 2003) that are connected through synapses. Brain activity is mediated by the reinforcement or loss of the connecting patterns. Functions such as memory storage, learning of habits, or personality will be shaped through dynamic changes these synapses undergo.

In the brain, the cerebral cortex is responsible for the execution of higher-order functions, including cognition, sensory perception, and sophisticated motor control. It represents a complex circuit where neurons are allocated together with blood vessels and a wide range of other cell types, e.g. glial cells. These cells interact as a unit to enable the well-functioning of the nervous system responding to external and internal signals (Attwell et al., 2010).

1.1. Insight into the cortical network

The cortical neuronal network is organized into six horizontal layers defined as molecular (Layer I containing very few neurons), supragranular (layers II/III), granular (layer IV) and infragranular (layer V and VI). Neurons within the cortex communicate horizontally across cortical areas and radially within functional columns that contain neurons from different layers connected in a highly stereotyped fashion (**Figure 1**). Neurons constitute a very heterogeneous cell population, and their classification into different subtypes may still not be complete. In general, they are divided into excitatory pyramidal (or projection) neurons (PNs) and inhibitory local cortical interneurons (INs) (Lodato and Arlotta, 2015).

PNs are excitatory, glutamatergic neurons that connect the cerebral cortex with its distal intracortical and subcortical targets. These cells represent the vast majority of the neurons of the cortex (70–80%) and are distributed within all cortical layers (Han and Sestan, 2013; Lodato and Arlotta, 2015). They can be broadly classified into intracortical and corticofugal neurons based on both, the layer where their soma is located and the area where their projections are sent. A set of projections, formed by a bundle of axons directed to a specific target, gives rise to the different fiber tracts in the nervous system (Friederici, 2009).

The intracortical PNs type is located in all layers (predominantly layer II/III) and further divided into “associative” and “commissural”. Associative PNs project their axons either to targets in the same hemisphere or to different layers of the same area or column (association fibers). In contrast, they are classified as “commissural” when their axons project to targets located in the opposite hemisphere (commissural fibers) (Molyneaux et al., 2007). Here three main commissural tracts, the anterior and posterior commissures together with the corpus callosum (CC), enable interhemispheric communication (Ribas et al., 2018).

Moreover, corticofugal neurons are mainly located in the deep cortical layers sending their axons to distal targets outside the cortex such as the thalamus or spinal cord (projection fibers) (Guo et al., 2017).

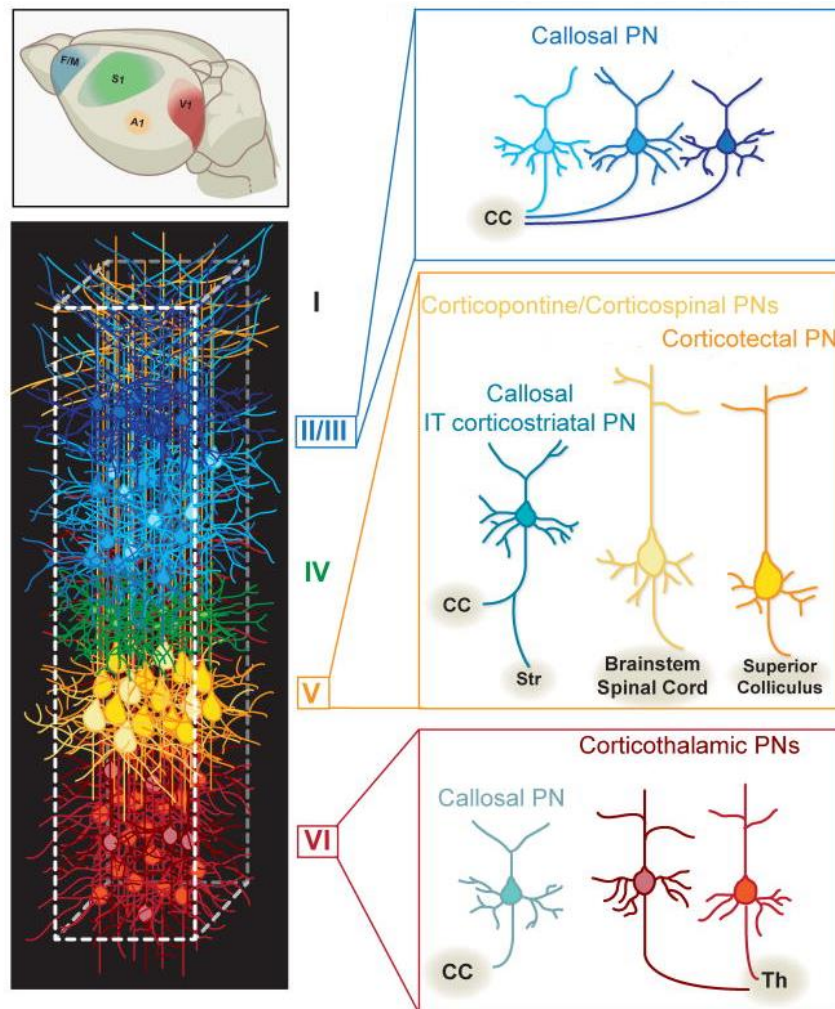


Figure 1. Organization of the cortex into layers and columns where the different types of excitatory projection neurons are distributed. Colors correspond to the frontal/motor cortex (blue), somatosensory cortex (green), auditory cortex (yellow) and visual cortex (red). PNs project to different areas depending on their location. Abbreviations: CC, corpus callosum; Th, thalamus; IT, intratelencephalic; PN, projection neuron. Roman numerals refer to the six cortical layers. Modified from (Lodato and Arlotta, 2015).

Interneurons, also known as short-axon neurons, represent 20-30% of cortical neurons. They expand through all layers, and their classification is most likely also not complete (Lodato et al., 2015). In general, interneurons are subdivided into spiny pyramidal cells and aspiny non-pyramidal cells. Spiny cells are excitatory glutamatergic neurons located in layer IV that receive sensory input from the thalamus, while the aspiny type consists of inhibitory GABAergic neurons located in all layers of the cortex. They represent the main inhibitory component of the cortical circuit, modulating projection neurons activity by regulating both synaptic function and the timing of action potential generation (Kepecs and Fishell, 2014). Cortical GABAergic interneurons are very diverse, containing subtypes that differ in morphology, molecular identity, firing properties, and patterns of connectivity.

Both populations of excitatory and inhibitory neurons interact through stereotypical connectivity patterns within and across cortical layers, forming functional units in the cortical circuit (Wolf et al., 2014). The connections between the large population of excitatory cells are

believed to underlie the generation of persistent activity in the cortex. In contrast, INs would provide a dense “blanket of inhibition” constantly modulating this resulting activity (Karnani et al., 2014). In this manner, the cortical network would operate according to a strong and dynamic interaction between recurrent excitation and feedback inhibition (Isaacson and Scanziani, 2011; Wolf et al., 2014). Under pathological conditions, this equilibrium can be disturbed, leading to important functional alterations (Scharfman, 2007; Malcolm et al., 2015; Ren et al., 2018).

Besides the key interaction of PNs and INs, the successful functioning of the cortex also involves other types of connecting patterns. Inhibitory neurons are known, for instance, to interact with each other, contributing to spike synchronization and coordination of inhibitory input (Galarreta and Hestrin, 2001; Gibson et al., 2005).

Moreover, the excitatory and inhibitory activity can be affected by glia-mediated processes that affect mainly the transmission of information and remodeling of the connecting patterns (Henstridge et al., 2019).

1.2. Neurites of pyramidal neurons, interaction via synapses and synaptic rearrangement under normal physiological conditions

During embryonic development of the cortex, neuronal progenitors differentiate into mature neurons. This process includes the formation of neurites as well as the acquisition of mature electrophysiological properties and functional excitatory synaptic network formation (Hobert, 2011; Shi et al., 2012). The term neurite refers to the emerging processes from the neuronal body and is either classified into an axon or dendrite (Flynn, 2013). Axons constitute long, slender projections that typically conduct electrical impulses (action potential) away from the cell body while dendrites refer to branched protoplasmic extensions that propagate the electrochemical stimulation received from other neurons to the soma, from which dendrites project (Chklovskii, 2004).

1.2.1. Synapses

In the cortex, neurites will enable the integration and communication of neurons in the cortical network through the establishment of synapses. Although axon-dendrite synaptic connections are the main norm, other variations (e.g., dendrite-dendrite, dendrite-axon, axon-axon) are also possible (**Figure 2**). In normal conditions, electrical impulses will travel through the pre-synaptic component (axon) until the synaptic terminal, where the release of neurotransmitters is activated. The dendritic spines, small membranous protrusion allocated on dendrites, constitute the post-synaptic component where receptors will be involved in the recognition and integration of the sent signal. In addition, the pre- and postsynaptic components are surrounded by a third element (tripartite synapse concept), the astrocytic processes, which control synaptic transmission (Perea et al., 2009; Chung et al., 2015).

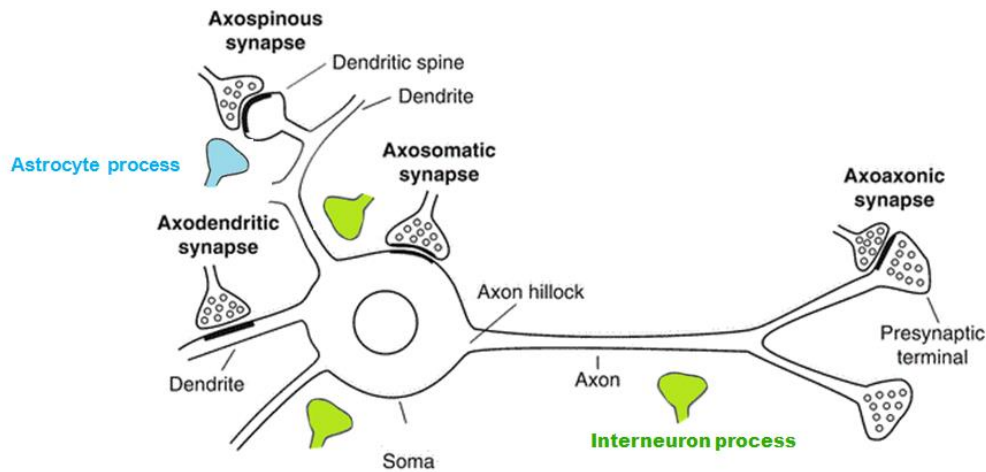


Figure 2. Types of synapses at different levels of the pyramidal neuron together with inputs from astrocytes (blue) and interneurons (green) to regulate neuronal activity. Modified from Rochelle S. Cohen 2013.

Glutamate is the major excitatory neurotransmitter in the mammalian central nervous system (Zhou and Danbolt, 2014). Glutamate receptors are classified into ionotropic (NMDA, Kainate, and AMPA receptors) and metabotropic (mGluR1-8). Ionotropic receptors tend to be quicker in relaying information while metabotropic are associated with a more prolonged stimulus. Gamma-aminobutyric acid (GABA) refers to the most common inhibitory neurotransmitter with two classes of receptors: GABA_A (ligand-gated ion channels) and GABA_B (G protein-coupled receptors). The main source of GABA are interneurons with GABA_A receptors being the most abundant type of receptor in the brain (Farrant and Nusser, 2005). They are localized at both synaptic and extrasynaptic membranes.

Synaptic-localized GABA_A receptors (low affinity for GABA) mediate phasic inhibition which shows a transient effect. On the other hand, extrasynaptic GABA_A receptors mediate tonic inhibition. Here, receptors own a higher affinity for GABA resulting in a more persistent GABAergic conductance and longer effect (Lee and Maguire, 2014). Both phasic and tonic inhibitions regulate neuronal activity, but whether they control each other is not very clear (Wu et al., 2013).

The sent signal is recognized by the post-synaptic element. Dendritic spines are thin protrusions, primarily localized in the excitatory synapses. They consist of a dense network of cytoskeletal, transmembrane, scaffolding molecules and numerous surface receptors (Chidambaram et al., 2019). Spines arise from filopodia like structures and are formed through their interaction with molecules such as ephrins and telencephalin that regulate their motility and transformation. Trans-synaptic signaling involving nitric oxide, proteases, adhesion molecules, and Rho GTPases further controls contact formation or the structural remodeling of spines and their stability (Yoshihara et al., 2009). Their morphology is variable and ranges from filopodia-like protrusions to more stubby, thin, or mushroom-shaped structures (Peters and Kaiserman-Abramof, 1970) (**Figure 3**).

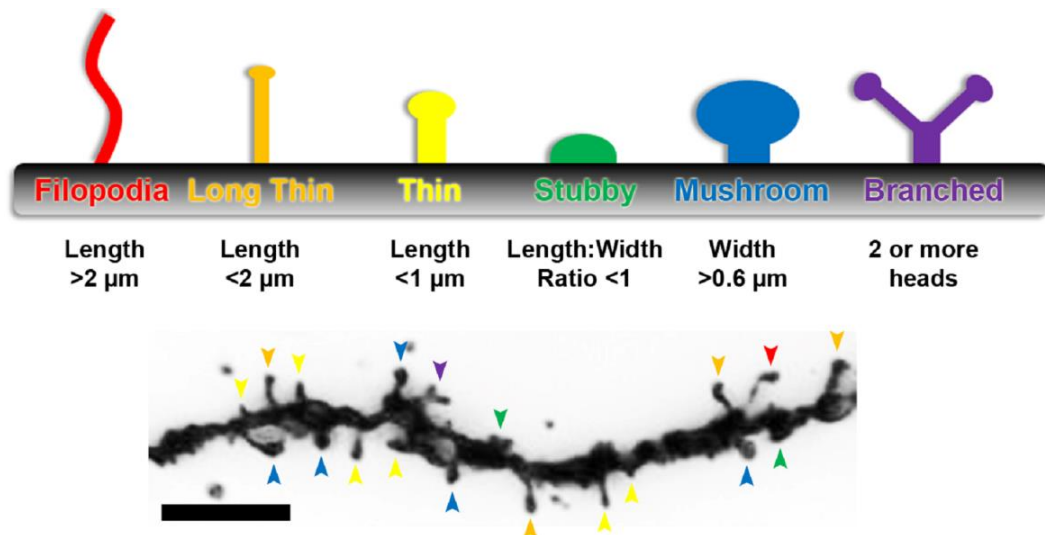


Figure 3. Illustration of different types of dendritic spines. Top: from left to right, the distinct maturity stages can be identified together with length and width change. Bottom: Golgi-cox stained dendritic branch of a Layer II/III pyramidal neuron in mouse primary visual cortex. The different spine types are indicated by arrowheads, color-coded to match previous illustration. Scale bar, 5 μm . (Risher et al., 2014).

The morphology of spines, has great impact on their function (Rocheffort and Konnerth, 2012; Berry and Nedivi, 2017). Using electron microscopy and labeling with post-synaptic markers (PSD-95) it was shown that filopodia-like spines are the precursors of mushroom spines (mature stage) while thin and stubby represent intermediate shapes. Indeed, many filopodia lack mature synaptic structures, show none or little synaptic function (smaller synaptic cleft and fewer synaptic vesicles) and lack PSD-95. On the other hand, mushroom shaped spines, contain the largest number of excitatory synapses and high synaptic function as well as PSD-95 (Berry and Nedivi, 2017).

Through the interaction with actin-binding proteins, postsynaptic signaling messengers, and the dynamics of actin filaments, spines are formed, maintained, and eliminated. This process plays an essential role in the refinement of the brain circuits, neuronal development, and cognitive functions including memory and learning (Borovac et al., 2018). Considering their dynamic properties, spines are classified into persistent or transient (Berry and Nedivi, 2017). The first type includes spines which are formed and remain for an extended time (months to years) or disappear and never return. Transient spines are added and then removed with a mean lifetime of approximately two days. These spines tend to be smaller, but spines of all sizes and morphological subtypes from mushroom spines to filopodia can fall into either dynamic class. From a functional point of view, persistent spines are associated with the maintenance of learned skills while more dynamic spines are related to skill acquisition (Xu et al., 2009; Yang et al., 2009; Berry and Nedivi, 2017).

1.2.2. Synaptic plasticity

During early postnatal development, the synapses undergo a pruning phase that eliminates unnecessary or improper connections. In the adult brain, synaptic formation and elimination are believed to be at equilibrium with a fraction of connections been consistently added and removed (Petanjek et al., 2011; Chen et al., 2014). The ability to change their number and

morphology, which is usually activity-dependent, gives rise to the concept of synaptic plasticity, which entails the weakening or strengthening of synapses over time as well as synapse formation and elimination (structural plasticity).

The idea that synapses could change depending on how active or inactive they are, was first proposed by the Canadian psychologist Donald Hebb in 1949 (Berlucchi and Buchtel, 2009). Hebbian plasticity is divided into short-term and long-term. Short-term plasticity takes place when changes in synaptic strength occur on a sub-second timescale, a fast up or down adjustment to determine the importance of the connection and to decide if ongoing communication is essential or not. This type of plasticity might be involved in decision making as well as working memory (Deng and Klyachko, 2011). In contrast, long-term synaptic plasticity lasts anywhere from minutes to hours, days, or years and constitutes the dominant model for how the brain stores information (Takeuchi et al., 2014).

According to the Hebbian theory, an increase in synaptic efficacy arises from repeated and persistent stimulation of a postsynaptic cell by a presynaptic cell. The formation and elimination of synapses are, therefore, dependent on activity. The input that neurons receive is converging on dendrites and would differ in synaptic activity. Inputs with less active synaptic regions would be ultimately eliminated giving rise to the “use it or lose it” concept (Shors et al., 2012).

Dendritic spine turnover plays a crucial role in synaptic plasticity (Frankfurt and Luine, 2015). The changes in the synaptic strength are related mainly to the rapid modification of the expression of membrane glutamate receptors in an activity-dependent manner. In contrast, structural plasticity would be an enlargement, growth, pruning, and stabilization of dendritic spines. These rearrangements have the potential to continuously modify the organization of the synaptic network and are thereby tightly linked to brain activity, cognitive, and functional function. Plasticity can be triggered by external signals such as learning, storage of new memories (Howland and Wang, 2008), sleep (Rao et al., 2007) or environmental enrichment (Baroncelli et al., 2010).

1.3. Neuritic alterations in pathological conditions

In response to pathology-induced alterations, neurons reorganize their projections (Kempermann et al., 2000) as a way to compensate for the damage. As main components of synapses, the induced changes will lead to disrupted synaptic stability, number, and connecting patterns that define normal brain functioning (Masliah et al., 1994; Scheff and Price, 2006). Neuritic pathology would thus contribute to disease’s progression and worsening of the associated symptoms. In pathologies, such as Alzheimer’s Disease (AD) and stroke, synaptic and neuritic alterations have been reported and related to deficits in the disease’s outcome (Masliah et al., 1994; Serrano-Pozo et al., 2011; Jang, 2013).

In the context of aging and Alzheimer’s Disease (AD), neurons are affected by beta-amyloid toxicity and deposition (plaques) that lead to the formation of dystrophic structures, neurite malfunction, and degeneration (Reitz et al., 2011). Although processes to counteract the damage such as axonal regrowth have been observed (Blazquez-Llorca et al., 2017), very often, these neurons fail to successfully integrate into the circuit and propagate information (Stern et al., 2004). In ischemic stroke, especially the infarct core, neurons undergo irreversible damage that will avoid any chances of self-repairing by these cells. Nevertheless, other more distant areas from the core could represent a potential source for repair and compensation mainly

through dynamic changes of dendritic spines (Brown et al., 2007). Although this structural rearrangement might play a key role in stroke recovery, a wide range of patients keeps lifelong disabilities, pointing out that the repair is not entirely successful and the function not fully restored.

1.4. Axonal pathology in Alzheimer's Disease

1.4.1. AD and main pathological hallmarks

AD is the leading cause of dementia worldwide, representing 60-80% of all cases (Garre-Olmo, 2018). It is characterized by a progressive decline in cognitive function, which usually begins with deterioration in memory and continues affecting intellectual functions leading to complete dependence for basic daily activities as well as premature death (Mayeux and Stern, 2012). The AD brain is characterized by neuropathological hallmarks, including extracellular amyloid plaques, intracellular neurofibrillary tangles and dystrophic neurites surrounding plaques (Reitz et al., 2011). The term “dystrophic neurites” (DNs) refers to abnormal, swollen and tortuous neuronal processes. These pathologies are often accompanied by the presence of reactive microglia as well as a loss of neurons, synapses, and white matter (Serrano-Pozo et al., 2011). The etiology of AD remains unclear, but environmental factors, advancing age, and genetic factors such as mutations in APP, PSEN1, and PSEN2 genes are believed to play an important role (Giri et al., 2016).

In the past decades, two hypothesis about the pathogenesis of AD are discussed (Kametani and Hasegawa, 2018). Some researchers support the notion that the accumulation and deposition of oligomeric or fibrillar amyloid β ($A\beta$) peptide (β -amyloidopathy) is the primary cause of AD (Masters et al., 1985). In contrast, others claim that the microtubule-associated protein tau is the main responsible factor. The production of $A\beta$ peptide synthesis requires the cleavage of the amyloid precursor protein (APP) by the β and γ secretases, respectively through the so-called amyloidogenic pathway (**Figure. 4**).

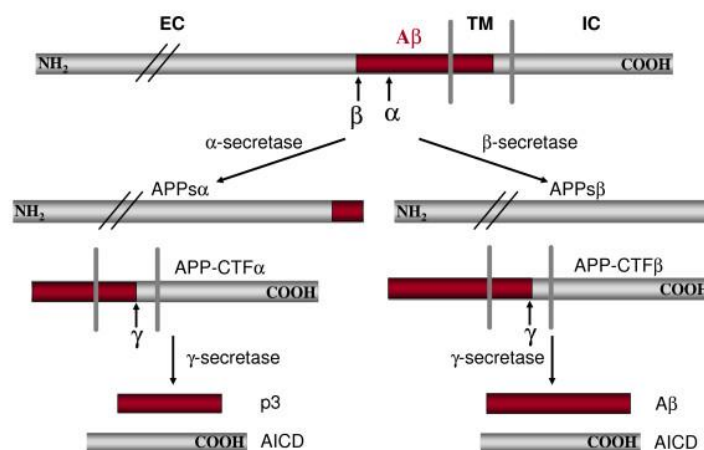


Figure 4. Diagram of APP processing. EC: extracellular; TM: transmembrane; IC: intracellular; AICD: intracellular domain of APP; p3: small peptide. Domain A β highlighted in red. From (Zheng and Koo, 2006).

$A\beta$ is not an abnormal protein and is produced during healthy cell metabolism (Seubert et al., 1992; Shoji et al., 1992). Under normal conditions, the soluble $A\beta$ peptide found in the extracellular space is degraded by peptidases (Carson and Turner, 2002). It can also be

internalized and degraded by activated microglia or removed by an out-input balance process from the brain through the blood-brain barrier (Tanzi et al., 2004). An imbalance between the production and/or degradation of A β would increase the levels of this peptide in the brain. While in familial AD, the overexpression of A β is related to mutations in the genes APP, PSEN1, and PSEN2, in sporadic AD, a failure in the degradation processes of this peptide is involved (Wang et al., 2006).

APP has been found in the plasma membrane as well as in the membrane layers of the trans-Golgi region, endoplasmic reticulum, endosomes, lysosomes and mitochondria. Thus these compartments might be the source of A β . Part of this process takes place in the distal axons and dendrites, both in the pre-synaptic and post-synaptic compartments. Also, synaptic activity appears to promote the transport of APPs to synaptic terminals, their endocytosis, and subsequent formation of A β (Cirrito et al., 2008; Tampellini et al., 2009). Moreover, the extracellular A β can be recaptured and internalized, increasing the intracellular reservoir (Mohamed and Posse de Chaves, 2011).

Amyloid plaques result from the extracellular accumulation of fibrillar A β and constitute an important hallmark of the AD pathology. There are classified into primitive, classic, and compact plaques (Wisniewski et al., 1973). Primitive plaques are formed by degenerated neurites with some amyloid deposits visible at the ultrastructural level. Classic plaques are generated from the previous ones, forming a central amyloid nucleus, while compact plaques are a result of complete degeneration of neurites leaving only the amyloid mass (Probst et al., 1987).

The amyloid plaques have other components besides dystrophic neurites and A β . A classic plaque, for example, is formed by a central nucleus of A β 42 surrounded by a halo formed by active microglia and astrocytes arranged in the periphery (Figure 5).

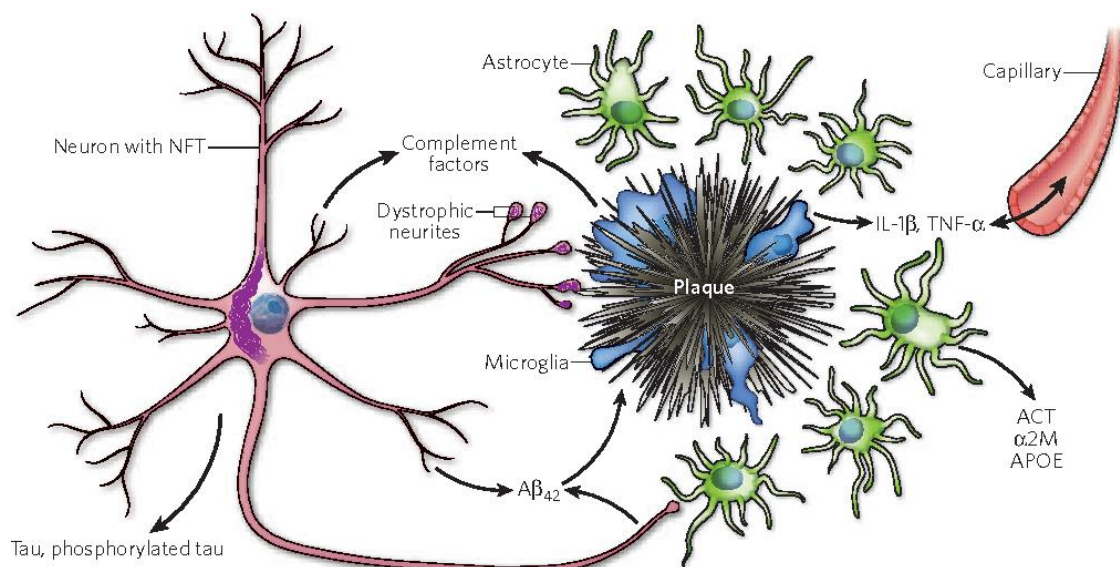


Figure 5. Main components of a senile plaque. The A β 42 produced by the neurons deposited in the plaques. Microglia is then activated and begins to release cytokines such as IL-1 β and TNF- α that can cross the blood-brain barrier and induce the activation of astrocytes. Hyperphosphorylated tau protein is added in neurofibrillary tangles (NFT) to neurons (in the soma and neuritic dystrophies) around the plaques. Modified from (Perrin et al., 2009).

1.4.2. Axonal dystrophies in close proximity to amyloid plaques

DNs are found around amyloid plaques and contain mainly autophagocytic vacuoles, lipofuscin, degenerating mitochondria, and hyperphosphorylated tau (PHF-tau) (Sanchez-Varo et al., 2012; Mitew et al., 2013) (**Figure 6**). Dystrophies can develop in both, axons and dendrites, but axons seem to show greater vulnerability for their formation (Yang et al., 2013; Blazquez-Llorca et al., 2017). The reason for this distinct degree of vulnerability remains unknown but differences in the arrangement of microtubules and different maturation of autophagosomes in both compartments may be related (Yang et al., 2013).

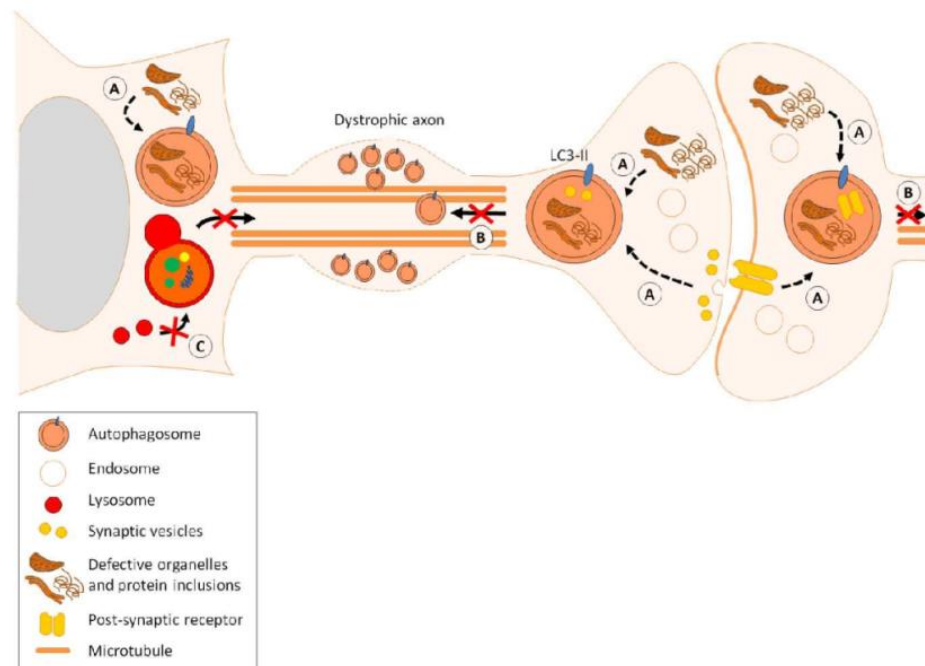


Figure 6. Impaired steps of neuronal autophagy in neurodegenerative disorders. (A) Defective autophagosome biogenesis and disruption of axonal transport leading to the accumulation of autophagosomes in dystrophic neurites (B). Failure of autophagosomes to fuse with lysosomes (C). LC3-II: Microtubule-associated protein 1A/1B-light chain 3, present in autophagosomal membranes and marker for autophagic activity. From Audrey Ragagnin 2013.

Moreover, several factors might contribute to the formation of dystrophies in axons. Some of them rely on the neurotoxic effect of A β as key player. For example, a study performed on cultured cortical neurons, demonstrated that treatment with fibrillar A β , resulted in the development of neuritic dystrophy in a concentration-dependent manner (Grace et al., 2002). In addition, it has been shown that soluble oligomeric assemblies of A β , which surround plaques, induce calcium-mediated secondary cascades that lead to dystrophic changes. Soluble A β oligomers would lead to the activation of the calcium-dependent phosphatase calcineurin altering neuritic structure (Wu et al., 2010).

Other important factors involved in the formation of dystrophies are autophagy and autophagic vacuoles (Sanchez-Varo et al., 2012). In AD, an increased number and accumulation of vesicles is observed in axons, event that might be associated to an altered lysosomal activity (Lee et al., 2011). Lysosomes contain enzymes that are important for the degradation and digestion of compounds either from the cell (autophagy) or from the extracellular space (heterophagy). Mutations in the presenilin gene make lysosomes unable to maintain an

optimal acidic pH for their enzyme activity. As a result, they cannot function normally, as binding to the autophagosomes, and degradation of their content would not take place properly. Therefore, vesicles would start accumulating and would lead to an alteration of the axonal structure as well as transport. At the same time, A β can damage cellular organelles such as mitochondria which would become targets of more autophagy promoting the accumulation of additional vesicles worsening the dystrophic pathology (Perez-Gracia et al., 2008). A β would lead to mitochondrial dysfunction by impairment of oxidative phosphorylation, elevation of reactive oxygen species production, and alteration of the mitochondrial proteins and membrane (Pagani and Eckert, 2011).

Once dystrophies are formed, they behave as dynamic structures with complex and variable morphologies over time (Blazquez-Llorca et al., 2017). The more numerous and severe they are, the more vulnerable the nerve cell will be to lysis and cell death. Even so, it seems that the cells try to resist the maximum time possible presenting severe dystrophies that at first sight could indicate that the neuron is no longer functional when it really is (Adalbert et al., 2009). Not surprisingly when considering the effect that dystrophies have on axons, they have been related to synaptic dysfunction and progression of AD (Knowles et al., 1999; Stern et al., 2004).

1.5. Ischemic stroke as a pathological condition, evolution over time and neuritic alterations

1.5.1. Stroke, epidemiology, causes, and symptoms

Affecting 13.7 million people worldwide and causing about 5.5 million deaths every year, stroke is the second most frequent cause of death and the leading cause of disability globally (Campbell et al., 2019). Patients can suffer two types of stroke: ischemic and hemorrhagic. Hemorrhagic stroke is caused by the rupture of a cerebral vessel which results in the formation of a hematoma (intracerebral or subarachnoid hemorrhage), while ischemic stroke is caused by vessel occlusion, most often (71%) of the middle cerebral artery (MCA) (Fluri et al., 2015). Ischemic strokes are mainly unilateral (Ilyayeva et al., 2018) and are thromboembolic of origin. The main risk factors for occurrence are, among others, atherosclerosis, small vessel disease, cerebral vasculitis, or atrial fibrillation (Previtali et al., 2011). Besides, non-modifiable risk factors, including age, sex, and genetic factors, are also believed to have an influence (Boehme et al., 2017). Symptoms will vary depending on the location and size of the tissue damaged by the reduced blood flow (infarct), but the most common symptoms include weakness of the limbs or face, trouble speaking or understanding speech, impaired vision, headache and dizziness (Musuka et al., 2015).

For the diagnose and patient's follow-up, different imaging techniques are used including computed tomography (CT), magnetic resonance imaging (MRI), and sometimes even positron emission tomography (PET) (Wey et al., 2013; Lin and Liebeskind, 2016).

Even though current strategies based on reperfusion have improved survival, patients are often confronted with lifelong disabilities such as motor/sensory disturbances, aphasia or personality and emotional changes together with cognitive impairment (Schaapsmeeders et al., 2013). A major explanation for this is that the pathophysiological events happening in the later stages of ischemic stroke are poorly understood (Dirnagl et al., 1999). A better knowledge about the progression of ischemic stroke together with a detailed understanding of the brains endogenous mechanisms for neuroprotection, repair and neuroanatomical rewiring are needed to develop new strategies and improve stroke care.

1.5.2. Pathophysiology, temporal course of ischemic stroke and infarct growth

The brain has high energy demands and almost exclusively relies on oxidative phosphorylation (Hossmann, 1994). When a cerebral vessel is occluded and the blood supply is interrupted, the previously irrigated tissue undergoes oxygen and glucose deprivation (Kalogeris et al., 2012). The brain area affected by irreversible tissue damage, forms the infarct core, while the surrounding area where cells are still viable but dysfunctional is known as penumbra (Paciaroni et al., 2009). Once stroke occurs, brain tissue inside and outside the infarct undergoes considerable changes over time.

The time course of ischemic stroke can be in general divided into three clinical phases: acute, sub-acute and chronic (Zhao and Willing, 2018) (**Figure 7**).

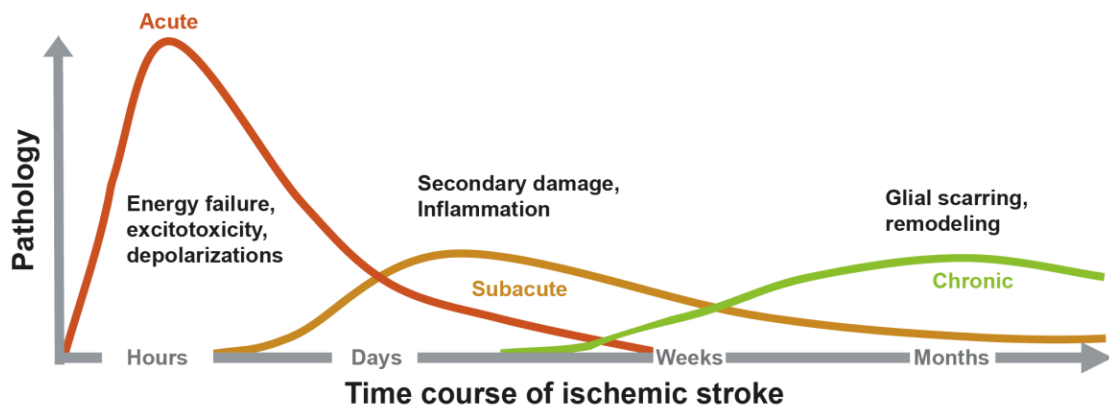


Figure 7. Time course of the progression of stroke from the acute over the subacute to the chronic phase. Modified from (Dirnagl et al., 1999).

The acute phase of stroke lasts 48 hours after symptom onset. As blood flow within the core drops, energy depletion and metabolic failure leads to anoxic depolarization and activation of the “ischemic cascade” that leads to neuronal death already minutes after onset of ischemia (Dirnagl et al., 1999; Doyle et al., 2008). In normal physiological conditions, neurons polarize by building up ion gradients in an ATP-dependent manner to be able to generate action potentials. During occlusion, the reduced blood flow leads to a reduction in ATP production and failure of energy dependent membrane receptors, ion channels and ionic pumps. This, at the same time, results in a collapse of transmembrane potential as ions such as sodium (Na^+), potassium (K^+) and calcium (Ca^{2+}) flow freely down their concentration gradients, leading to anoxic depolarization and the release of additional excitatory neurotransmitters (primarily glutamate) (Belov Kirdajova et al., 2020). The resulting excitotoxicity is potentiated even more by the disruption of energy dependent glutamate reuptake from the synaptic cleft (Lai et al., 2014), and the ensuing activation of the glutamatergic NMDA and AMPA receptors causing further depolarization and excitotoxicity. The over activation of the excitatory AMPA and NMDA receptors, leads to a higher influx of calcium ions triggering a cascade of harmful events including proteolytic cleavage of cytoskeletal and extracellular proteins such as actin and laminin, generation of reactive oxygen species, and oxidative stress (Dirnagl et al., 1999; Atochin and Huang, 2011). Beyond the direct effect on cell death, increased levels of reactive oxygen and nitrogen species also induce release of pro-inflammatory factors from immune cells, leading to inflammation (Dirnagl et al., 1999).

Moreover, the alterations in ion concentrations also result in water entering the cells producing cytotoxic oedema, an important pathophysiological marker of ischemia (Dostovic et al., 2016).

In general, the described processes of energy failure, depolarization, and excitotoxicity represent the main pathological events during acute ischemia at the level of the core (Dirnagl et al., 1999).

The penumbra surrounding the stroke core is a band of tissue in which blood flow is partially preserved due to collateral circulation (Rusanen et al., 2015). However, its viability is variable and time dependent. Peri-infarct depolarizations, apoptosis, and inflammation constitute the main factors leading to an ongoing cell death and expansion of the infarct core into the penumbra (Lakhan et al., 2009; Dreier, 2011).

The tissue at this level would still have the potential to repolarize, but it depolarizes again in response to the increased levels of glutamate coming from the core. These depolarizations spread in waves running from the ischemic core throughout the penumbra and would contribute to the progression and expansion of excitotoxic cell death (Dirnagl et al., 1999). Each new wave of these peri-infarct depolarizations would lead to infarct volume growth (Strong et al., 2007).

In addition, while neurons in the infarct core undergo necrotic cell death, neurons in the penumbra are affected by apoptosis which contributes to the expansion of the damage. Apoptosis is the systematic degradation of a cell in response to injury and is characterized by the condensation of chromatin, nuclear fragmentation, preserved membrane integrity and blebbing of the plasma membrane (Bredesen, 2000). At the level of the penumbra, apoptosis is induced by several factors. For instance, the excessive Ca^{2+} influx occurring due to excitotoxicity or persistent NMDA receptor activation leads to alterations in mitochondrial membrane permeability increasing the release of pro-apoptotic factors including cytochrome c (Garrido et al., 2006).

Another key factor is the activated inflammatory response which is characterized by the infiltration and proliferation of immune cells, and the secretion of chemokines and pro- and/or anti-inflammatory cytokines (Ahmad and Graham, 2010). Inflammation facilitates the elimination of cellular debris and pathogens but is also known to contribute to cell death and infarct growth even days after ischemic onset (Dirnagl et al., 1999). Leukocytes, monocytes, neurons, and glial cells, all participate in the inflammatory response to stroke. During and after ischemia, leukocytes aggregate and adhere to the vascular endothelium, in part due to increased release of adhesion molecules such as selectins in ischemic territories (Marquardt et al., 2009). Selectin promotes cellular interactions with leukocytes and aggregates of leukocytes that accumulate platelets and fibrin. Thus, vessels are occluded, perfusion reduced, and the infarct expands (Ritter et al., 2000).

Furthermore, glial cells are major contributors to post-stroke inflammation. After stroke, microglia becomes activated and migrates to the stroke penumbra. Therein, they adopt an activated morphology and participate in modulating inflammation through the secretion of pro- and anti-inflammatory cytokines able to trigger multiple signaling pathways relevant to cell death (Kim et al., 2016).

In the following days to weeks after stroke onset, the subacute phase starts. Excitotoxicity and the induction of oxidative and nitrative stress declines, but cell death together with the

expansion of the damage continues due to the previous described inflammation (Dirnagl et al., 1999).

Later in time, the subacute phase transitions into the chronic phase where the observed inflammation and ongoing apoptosis will also decrease and the infarct begins to be resolved (Doyle et al., 2008). The chronic phase characterized by the formation of a glial scar (Wang et al., 2018) together with tissue remodeling (Silver and Miller, 2004; Karki et al., 2010). The chronic phase starts the earliest at 3 months and the latest at 6 months post-stroke (Zhao and Willing, 2018). Glial scarring and tissue remodeling might be important to minimize damage, however, they are likely to be detrimental for recovery later on (Lo, 2008). For instance, the glial scar helps to seal off the lesioned area, preventing further microbial infections and the spread of cellular damage (Silver and Miller, 2004). In contrast, the scar hinders regeneration by creating a barrier for axonal regrowth (Yiu and He, 2006). In addition to the lack of recovery, also progressive neurodegeneration occurs in the chronic phase. This is reflected by the fact that a great amount of patients develop delayed cognitive impairment or even dementia after stroke (Brainin et al., 2015). The ongoing neurodegeneration is not fully understood yet but some mechanisms have been suggested.

In stroke survivors, increased homocysteine levels were found 3 months after infarction (Meiklejohn et al., 2001). Homocysteines are known to promote free-radical formation and oxidative damage, showing that oxidative stress could play a key role (Sibrian-Vazquez et al., 2010). Another contributor to the delayed neurodegeneration is Wallerian degeneration. According to this concept, when an axon is damaged, its remaining distal part undergoes delayed degeneration too. This process may occur over weeks after the initial damage (Hinman, 2014) and is linked to the infiltration of macrophages to clear the cell debris (Gaudet et al., 2011). These macrophages have a pro-inflammatory status and may cause sustained damage and cell death (Gaudet et al., 2011). Due to damage of axons projecting to areas outside the lesion side, Wallerian degeneration may also cause delayed damage in unaffected areas connected to the lesion.

1.5.3. Expansion of the focal ischemic damage to remote areas

The damage due to ischemic stroke extends beyond the ischemic territory to distant regions that are anatomical connected to the lesioned area, an effect known as diaschisis. This phenomenon can appear soon after ischemia and persist for weeks, and includes, changes in blood flow, metabolism, as well as atrophy in remote areas. The term was first described by Constantin von Monakow in 1914, a Russian-Swiss neurologist (Seitz et al., 1999). The main primary mechanism of diaschisis explanation is thought to be deafferentation also defined as loss of neuronal input from the damaged area (Butz et al., 2014). Additionally, other potential processes have been suggested to interfere.

For instance, brain edema and spreading depression (depolarization waves) as well as neuroanatomical disconnection might contribute to diaschisis. Cytotoxic and vasogenic edema are induced by stroke, and persistent water accumulation occurs in the brain over the days following ischemia (Witte et al., 2000). Edema in remote areas can occur and probably results from the migration of extravasated fluid and protein (Izumi et al., 2002). Brain swelling can directly compress the contralesional hemisphere and remote ipsilesional regions (Izumi et al., 2002) inducing secondary damage directly through physical compression or inducing secondary hypoperfusion and ischemia due to pressure on low resistance vasculature (Witte et al., 2000).

Moreover, it has been proved that spreading depolarization contributes to the expansion of the damage to non-ischemic regions. The resulting waves induce significant metabolic stress, with an initial increase in brain metabolism followed by profound hypometabolism and transient changes in the expression of a number of neurotrophic and inflammatory cytokines as well as molecular signaling cascades (Witte et al., 2000). *In vivo* calcium imaging studies demonstrated that spreading depression is associated with calcium waves propagating through both neurons and astrocytes, and that these waves elicit vasoconstriction enough to stop capillary blood flow in affected cortex (Chuquet et al., 2007).

By means of positron emission tomography (PET), computed tomography, and magnetic resonance imaging, changes in cerebral blood flow have been observed in remote areas. Approximately one half of stroke patients exhibit “mirror diaschisis” during the first two weeks after stroke, indicated by a decrease in oxygen metabolism and blood flow in the contralateral hemisphere, in the homotopic regions to the infarct (Lenzi et al., 1982). Together with these alterations in the blood flow, hypometabolism has been also reported in human patients as well as animal models after focal stroke. In patients, oxygen consumption measured by PET decreased throughout the ipsilesional hemisphere (including the thalamus and remote, non-ischemic tissue) acutely and three weeks after MCAo (Iglesias et al., 2000). Similarly, a study performed by Carmichael et al. (2004) demonstrated impaired glucose metabolism (a reflection of neuronal activity) one day after stroke throughout ipsilesional cortex, striatum, and thalamus, effect that was resolved eight days post-stroke (Carmichael et al., 2004).

Moreover, crossed cerebellar diaschisis is a well known effect after stroke characterized by a reduction in cerebral blood flow and metabolism in the cerebellar hemisphere contralateral to the lesion. This is attributed to a disruption of the cortico-ponto-cerebellar pathways with consecutive cerebellar functional inactivation which still persists in the chronic phase (Gold and Lauritzen, 2002).

Another important mechanism involved in stroke’s remote effect might be related to the alterations that damaged axons undergo. Their lesion would lead to inflammation triggering secondary damage and atrophy in structures with neuroanatomical links to the infarct. Indeed, studies have demonstrated that white matter fiber tracts may represent a crucial mechanism underlying the communication of the damage to other areas (Ho et al., 2005; Wang et al., 2016). Infarcts at the level of the white matter have also shown to induce remote effects translated, into cortical thinning (Duering et al., 2015). These findings highlight the idea that the ischemic damage and its consequences can spread through the white matter tracts resulting in alterations in distant areas too. Previous studies have demonstrated that local axonal damage leads to alterations in microtubule-associated protein (MAP-2) together with altered phosphorylation levels of neurofilaments in distant and connected regions (Wiley et al., 2016). Therefore axonal lesions would affect the intracellular neuronal transport and machinery, supporting that consequences would not just be evident locally where the damage took place but also transmitted along the neuron, altering its functioning as well as its connected targets.

Thus, the organization and distribution of fiber tracts in the nervous system would enable the effect to be communicated to several distant structures. As the most prominent fiber tract linking both hemispheres, the CC represents the main structure involved in the contralesional remote effect. Changes in excitation/inhibition levels, as well as blood flow, have been observed previously in this context (Andrews et al., 1993; Ruan et al., 2017).

Overall, the described remote effect of stroke highlights that the pathology is not just restricted to the damaged area. In the past, great effort has been made to understand the alterations during the acute phase but very little is known about the long term effect that stroke has on the brain as well as the mechanisms underlying stroke's effect on distant regions. In this context, mainly functional alterations have been described lacking information about the anatomical or structural changes underlying this effect.

The lifelong disabilities patients suffer, which up to now remain untreatable, could be explained by the ongoing alterations that the brain undergoes at this level. Additionally, distant areas might represent a highly interesting target for stroke treatment since they are formed by healthy tissue and constitute a possibility for structural and functional compensation.

1.5.4. Neuronal plasticity after ischemic stroke: dendritic remodeling

In the first days following ischemic stroke, to even 6 months after, neurons in damaged and intact brain regions undergo spontaneous alterations involved in brain self-repairing or nontreatment-induced recovery (Zhao and Willing, 2018). Early recovery has been associated to the resolution of oedema (Lo, 1986; Hallett, 2001) and reperfusion of the ischemic penumbra (Barber et al., 1998) while later recovery may be related to brain plasticity (Nudo, 2003). Especially in later phases of this repairing process, neuronal plasticity related to the sprouting and retraction of dendritic spines plays a critical role (Zhao and Willing, 2018).

This remodeling takes place in different cortical areas and results on the rewiring of neuronal circuits and changes in synaptic connectivity (Trachtenberg et al., 2002). Dendritic remodeling after ischemic stroke has been extensively investigated in perfused peri-infarct and distant regions within the ipsilateral cortex, notably by Tim Murphy's team (Brown et al., 2007; Brown et al., 2008; Brown et al., 2010). The dendritic tuft of layer II/III as well as of layer V pyramidal neurons were analyzed mainly through two-photon or Golgi-Cox staining after inducing stroke in the photothrombotic model. Altogether spine turnover and remodeling were observed and associated with cortical map displacement within the first three months. This would represent an adaptive mechanism where functional gaps due to the lesion are taken over by other areas to compensate for the missing function (Harrison et al., 2013).

Moreover, the dendritic remodeling at the level of the contralesional hemisphere is still under debate. Some studies claim that dendritic changes take place after stroke (Takatsuru et al., 2009; Takatsuru et al., 2013; Miquelajauregui et al., 2015) while other research lines support the fact that there are no evidence of dendritic plasticity or functional remapping in the contralateral hemisphere (Johnston et al., 2013).

Currently, it remains unclear whether the observed dendritic changes are beneficial or if they might lead to an imbalance hindering recovery. Probably both, an adaptive as well as a maladaptive plasticity take place over stroke recovery (Dalise et al., 2014). Understanding how this remote and still healthy tissue responds to the damage would be crucial to enhance the capacity of brain self-repairing and recovery after stroke (Cirillo et al., 2020).

1.5.5. Impact of structural changes on the neuronal circuits: interhemispheric imbalance and role of the corpus callosum

The multiple short and long-term alterations in the brain after stroke result in an imbalance of excitatory and inhibitory neuronal circuits (Naghavi et al., 2019). During the acute phase,

cortical hyperexcitability occurs in both the ipsi- and the contralateral hemisphere (Xerri et al., 2014). Later in the subacute and chronic phases, the excitability of the ipsilateral cortex decreases while it remains elevated in the contralateral side (Liepert et al., 2000). As a result, the inhibition towards the ipsilateral cortex is increased too, interfering in activity-dependent mechanism such as synaptic plasticity and functional recovery (Johansson, 2000; Carmichael, 2012).

The concept is based on a disruption of the interhemispheric communication through the corpus callosum important for the coordination of interhemispheric information and functions (Bertolucci et al., 2018).

The CC represents the largest commissure in the brain and is formed by fibers, which arise mainly from layer II/III (Mooshagian, 2008). Through the CC, the information from both cerebral hemispheres is integrated and transferred to process sensory, motor, and high-level cognitive signals (Schulte and Muller-Oehring, 2010). Experiments based on performing motor/visual tasks, simultaneous imaging (MRI, DTI), and paired-pulse transcranial magnetic stimulation (TMS) have significantly contributed to understand the CC topographic structure and functioning, especially related to right/left motor coordination (Wahl et al., 2007; Battal et al., 2010). Imagine a skilled pianist who needs to coordinate different movements in each hand (bimanual coordination) but also individuated finger control. Such skillful act will require that hand movement is coordinated in space and time, with minimal inter manual crosstalk or interference (Bloom and Hynd, 2005). The ability to successfully coordinate such movements by the two cortical hemispheres relies on callosal mediated communication (Carson, 2005).

This interhemispheric communication is based on a complex equilibrium between facilitatory and inhibitory interactions (interhemispheric inhibition). The action potentials transmitted via transcallosal neurons are primarily excitatory; however, the fiber tracts between the primary motor cortices project primarily to inhibitory interneurons, and thus the effect of transcallosal potentials between them results in an inhibitory effect (Meyer et al., 1995).

In other words, the activation of a motor function in one hemisphere, triggered in normal conditions by task performance or induced artificially by transcranial stimulation, leads to the inhibition of the contralateral motor cortex within several milliseconds. This effect would be controlled by excitatory transcallosal fibers that connect to interneurons in the opposite cortex leading to inhibition of the targeted area (Fling and Seidler, 2012).

While interhemispheric inhibition would be important to prevent interference of control processes between the two hemispheres (Fling et al., 2011), previous studies show that low levels of interhemispheric inhibition could be beneficial to conduct independently controlled bimanual tasks (Ridding et al., 2000; Shim et al., 2005).

In stroke conditions, the interhemispheric competition and coordination would be affected leading to interhemispheric activity imbalance (**Figure 8**). In this scenario, inhibition of the overexcited contralateral hemisphere, which in return would also lead to reduced inhibition of the damaged area, would promote plasticity and help to restore function (Xerri et al., 2014). Studies based on drug administration targeting inhibition in mice (Clarkson et al., 2010) or transcranial magnetic stimulation in patients (Mansur et al., 2005), have shown that rebalancing the disturbed interhemispheric inhibition is a promising therapeutic intervention.

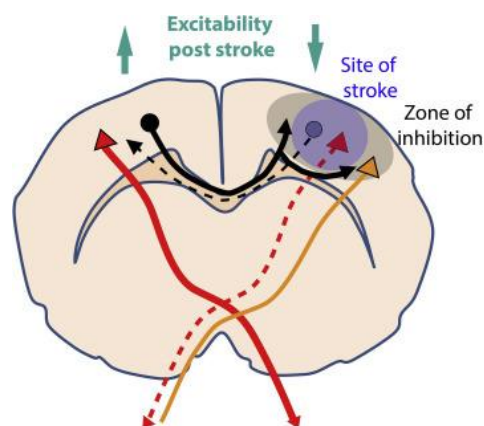


Figure 8. Interhemispheric imbalance model. According to this model, each side of the brain inhibits each other equally. After unilateral cortical stroke, this equilibrium is altered and the inhibition coming from the affected side is decreased (dashed line). The unaffected hemisphere, therefore, becomes more excitable and sends stronger inhibition onto the peri-lesional tissue. From (Boddington and Reynolds, 2017).

1.5.6. Current clinical management of ischemic stroke and disabilities

Nowadays the only pharmaceutical treatment of stroke is limited to the acute phase where drugs (alteplase and tenecteplase) are applied intravenously to break up the formed clot (Campbell et al., 2019). However, this treatment has a short therapeutic window of 3 - 4.5 hours after onset of symptoms (Hacke et al., 2008). Another available treatment is endovascular thrombectomy where the clot is removed using different techniques such as a vacuum to suck the thrombus out or a mechanical equipment (saline jets or ultrasound waves) to break it up (Tawil and Muir, 2017).

Up to date, research has mainly focused on reducing the primary damage (Dirnagl et al., 1999) explaining the absence of treatment for later phases of stroke to counteract secondary damage and facilitate brain repair. This leads to the situation where stroke-survivors are often confronted with lifelong disabilities (Campbell et al., 2019). A major reason explaining the sustained functional deficit could be related to the alterations that the brain undergoes during these later phases and mechanisms of maladaptive plasticity (Zhao and Willing, 2018). Understanding the ongoing pathophysiological events would be crucial for the development of new treatments with an increased therapeutic window in order to stop the progression of symptoms promoting deficits. In this context, the study of stroke-induced alterations in remote areas such as the contralesional hemisphere represent a high interesting target. Since this tissue is still healthy, therapies can be used to induce beneficial changes leading to a reduction in patient's functional impairment.

Considering this concept, rehabilitation therapies are currently used to improve motor disabilities. Here repetitive transcranial magnetic stimulation (rTMS) and constraint-induced movement therapy (CIMT) have proven to be potent therapeutic interventions to rebalance the disturbed interhemispheric inhibition. rTMS studies provided evidence that inhibiting the contralateral cortex (overexcited after stroke) would hypothetically lead to decreased

transcallosal inhibition of the ipsilateral side improving motor function in stroke patients (**Figure 9**) (Mansur et al., 2005; Fregni et al., 2006).

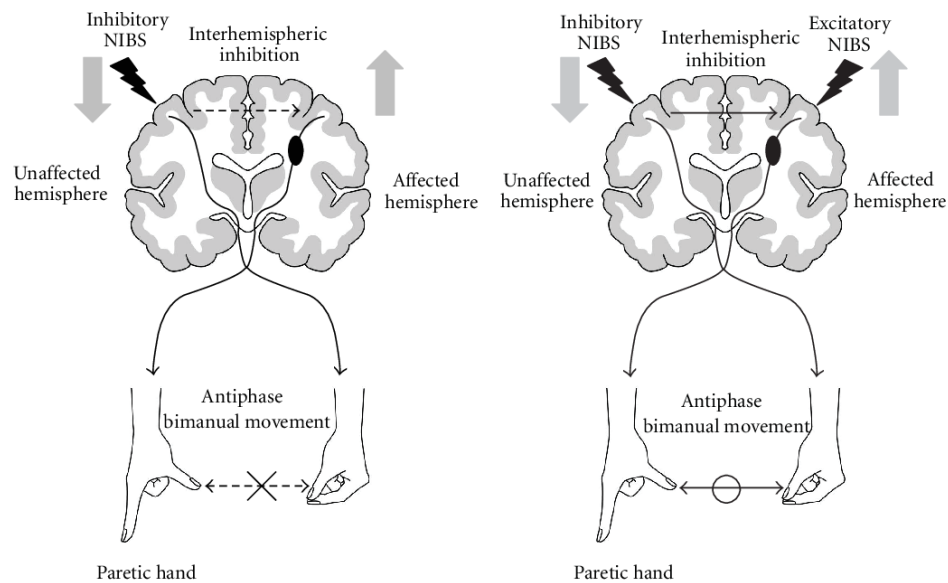


Figure 9. Principle of non-invasive brain stimulation (NIBS) such as rTMS to prevent bimanual movement deterioration in stroke patients. Inhibitory NIBS over the unaffected hemisphere (left picture) decreases the excitability of the contralesional motor cortex. It increases excitability of the ipsilesional motor cortex by reducing interhemispheric inhibition from the unaffected to the affected hemisphere. Moreover, excitatory NIBS, along with inhibitory NIBS (right picture), decreases excitability of the contralesional motor cortex and increases excitability of the ipsilesional motor cortex. However, bilateral NIBS limits the reduction in interhemispheric inhibition induced by inhibitory NIBS and prevents antiphase bimanual movement deterioration. From (Takeuchi and Izumi, 2012).

In the CIMT method, stroke patients with a paretic arm are subjected to physiotherapy (already 24 to 48 hours after stroke onset) of the affected arm while the unaffected arm is immobilized (Corbetta et al., 2010). The paretic arm is connected to the damaged cortical area, and forced use should increase the activity and excitability in this area promoting functional recovery. In contrast, the absence of activation of the contralateral cortex due to the constraint of the unaffected arm should reduce excitation in this area and therefore inhibition of the connected damaged ipsilateral cortex (Xerri et al., 2014). Clinical studies using this principle reported improvement of functional recovery of the affected limb (Sterr et al., 2002; Page et al., 2005).

Although both techniques seem to contribute to rebalance interhemispheric inhibition and promote functional recovery their use still needs to be further investigated (Xerri et al., 2014). Besides the described strategies, the level of cortical inhibition/excitation could be also influenced using a pharmacological approach. In animal models, the reduction of tonic GABA inhibition was shown to improve motor function (Clarkson et al., 2010; Jaenisch et al., 2016). Since tonic inhibition is controlling overall excitability, reducing it could help to increase the diminished activity of the damaged ipsilateral cortex. Moreover, studies performed in animal

models, also have targeted phasic inhibition by enhancing it with the positive allosteric modulator Zolpidem and observed an improved motor function (Hiu et al., 2016).

Last but not least, promising advances are made in the field of experimental stroke to develop putative therapies to enhance brain self-repairing and recovery. Accumulating evidence showed that enriched environment leads to adaptive plasticity. Indeed, it promoted dendritic branching, increasing spine density, glial numbers and vascular arborization together with better functional outcomes (Zhao and Willing, 2018). Other therapeutic approaches include stem cell transplantation (Misra et al., 2012), modulation of the inflammatory responses (Leonardo et al., 2010) or the use of optogenetic tools (Cheng et al., 2016). The latest consists of targeting specific cell types, GABAergic neurons, manipulating their activity by light. Although optogenetics itself cannot be applied directly to clinical patients, it is a powerful method to identify specific excitatory or inhibitory circuitry that may work in human patients. This would allow more precise and effective outcomes for noninvasive and mature stimulation toolboxes such as rTMS.

The key to successful stroke treatment may reside in the optimal combination of rehabilitative training and pharmacological intervention in accordance with defined plastic time windows (Wahl and Schwab, 2014). There is still a high controversy regarding the best time window for stroke treatment (Zhao and Willing, 2018), and future studies should focus on understanding what changes take place and when to plan the best treatment accordingly.

1.6. Experimental approach used in our study to investigate structural and functional alterations

1.6.1. Chronic two-photon imaging and optical access to cortical structures

GFP expression in neurites from cortical neurons was visualized and follow over time after cranial window implantation using two-photon excited fluorescence laser scanning microscopy (TPLSM). TPLSM was developed in the 1990s and remained a powerful technique used to understand many neurobiological phenomena, including the plasticity of individual synapses and neuronal network activity (Helmchen and Denk, 2005; Svoboda and Yasuda, 2006).

The application of fluorescence microscopy to living systems has always been limited by photobleaching and phototoxicity (photodamage effect). Each time the sample is excited, there is a risk of photodamage. Two-photon (2P) microscopy optimizes this problem by dramatically improving the detection of signal photons per excitation event (Svoboda and Yasuda, 2006). Usually, two low-energy photons from the same laser, contribute to induce a higher-energy electronic transition in a fluorescent molecule (e.g., GFP). 2P excitation is a nonlinear process where the absorption depends on the second power of the light intensity. When the laser is focused, the intensity is higher in the vicinity of the focus and reduces quadratically with distance below and above. As a consequence, fluorophores are excited in a small diffraction-limited focal volume. If the beam is focused by a high numerical aperture objective, the majority of fluorescence excitation occurs in a focal volume that can be as tiny as $\sim 0.1 \mu\text{m}^3$ (Zipfel et al., 2003). Through the scanning of the sample, fluorescence light is collected and an image obtained. Two-dimensional, as well as volume, can be acquired using different scanning methods (raster-like, line-by-line, plane-by-plane).

Compared to one-photon techniques, 2P excitation offers major advantages for microscopy in scattering specimens (Denk, 1994). First, excitation light is of longer wavelength compared to single-photon absorption, typically in the near-infrared wavelength range, enabling the penetration into deeper areas of the sample since longer-wavelength light is less scattered in

biological tissue. Second, the fluorescence signal depends nonlinearly on excitation light intensity. This nonlinear dependence is highly beneficial because it confines fluorescence generation to the focus spot. At each time point photons are generated only locally, and they can be correctly assigned to their point of origin in 3D space irrespective of whether they are scattered on their way out of the tissue to the detector (Helmchen and Denk, 2005; Kerr and Denk, 2008).

Despite its advantages and its high value as a tool there are still some problems that might be considered when observing, for example, fluorescently labeled neuronal structures or microvasculature. The strong scattering caused by the skull over the cortex is one of the main factors hindering the imaging process (Kneipp et al., 2016). In prevention various cranial window methods were developed, including the open-skull glass window (Levasseur et al., 1975; Holtmaat et al., 2009), the thinned-skull cranial window (Yang et al., 2010; Yu and Zuo, 2014) and their variants (Shih et al., 2012; Dombeck and Tank, 2014; Goldey et al., 2014; Roome and Kuhn, 2014).

In the open skull glass window, a glass coverslip is placed on top of the brain parenchyma after having removed a section of the skull while in the thinned-skull cranial window, the skull needs to be thinned down before imaging. Both techniques induce inflammatory responses and bone regrowth.

To solve this problem, researchers are working on the development of safe and easy-handling cranial window technique. Tissue optical clearing, already shows promising results for the observation of cortical structures acutely (Erturk et al., 2012; Pan et al., 2016; Zhao et al., 2018) as well as chronic (Zhang et al., 2018).

1.6.2. AD models and models of unilateral ischemic stroke

For the study of AD's pathophysiology as well as the testing of new drugs, experimental models rely on the utilization of genetic mutations associated with familial AD such as APP, PSEN1, APOE4 (Esquerda-Canals et al., 2017) or genetically modified mice that lack genes associated with this disorder, for example, knockout mice for APP secretases (BACE and ADAM10) (LaFerla and Green, 2012). Although none of the existing models fully reproduces the complete spectrum of the human disease, important characteristics can be recapitulated such as A β accumulation, tau pathology together with memory impairments and cognitive deficits (Elder et al., 2010; LaFerla and Green, 2012).

The mice used in our study correspond to two lines: APPswe/PS1dE9 (Jankowsky et al., 2004b) and the APP-PS1 line (Radde et al., 2006). These are double transgenic mice that express a chimeric mouse/human amyloid precursor protein (Mo/HuAPP695swe) and mutant human preseniline 1, both of which are targeted to neurons in the CNS. In addition, these mice were crossed with the GFP-M line, resulting on a subpopulation of pyramidal cells of layers III and V of the neocortex expressing GFP under the Thy-1 promoter (Feng et al., 2000). As relevant data, it is important to highlight that in the APP-PS1 mouse, amyloid pathology and related dystrophic neuritic changes around the A β plaques developed earlier (at 2 months) (Radde et al., 2006) than in the APPswe/PS1dE9 mouse (at 6 months) (Jankowsky et al., 2004a). Once extracellular A β deposits were formed, we could further analyze the axonal pathology in close proximity to senile plaques with the two-photon microscope.

In contrast to AD transgenic models, stroke conditions needed to be induced by surgery in mice. Nowadays, there is a wide range of experimental models available in the field of

ischemic stroke. Some of the most common methods used in rodents are the photothrombotic model, endothelin-I model, the intraluminal suture of the MCAo, and the embolic stroke model (Fluri et al., 2015). In the photothrombotic stroke model, infarcts are induced by photoactivation of a systemically given dye (e.g., Rose Bengal) through the intact skull. Illumination is followed by the activation of the dye causing singlet oxygen that damages components of endothelial cell membranes. As a result, subsequent platelet aggregation takes place as well as thrombi formation, which determines the interruption of local blood flow (Labat-gest and Tomasi, 2013).

Endothelin-I is a potent vasoconstrictor that allows the induction of transient focal ischemia in different areas of the brain. The two other models are mimicking human stroke most closely (Sommer, 2017). They are characterized by the occlusion of the MCA using sutures or an injection of homologous blood clots (Ren et al., 2012).

In our study, we made use of the transient MCA occlusion for 60 min (filament model). The MCA and its branches are the cerebral vessels that are most often affected in human ischemic stroke. The model is less invasive than others since it does not require craniectomy and thus avoids additional damage to cranial structures. Depending on the duration of the occlusion, the extension of the damage can be controlled. For example, when using the filament model, ischemia times larger than 60 min, induce large cortico-striatal infarcts together with significant focal neurological deficits (Lourbopoulos et al., 2017).

Furthermore, it resembles the damage of the vascular endothelium observed in clinical conditions (Peschillo et al., 2017) by the use of stent retrievers. The same effect is mimicked with a silicone-coated filament inserted in the MCA.

A relevant consideration of this model is the fact that animals show sustained neurological and behavioral deficits, which represents crucial factors for the assessment of treatment efficiency not always reached with other models (Freret et al., 2009).

Nevertheless, the model is associated with high mortality. The severe weight loss, together with body temperature changes (hypo- and hyperthermia), inflammation, difficulty to chew or swallow, scarring of wounds, motor deficits, and sometimes even blindness which compromises the food and water intake, represent the leading causes (Lourbopoulos et al., 2017).

1.6.3. Laser speckle imaging as a tool to measure functional outcome

In our stroke study, we used laser speckle imaging as main tool to translate structural alterations in the cortical network to functional outcome.

Laser speckle imaging is a powerful tool for full-field imaging of blood flow. This method can instantly visualize microcirculatory tissue blood perfusion combining high resolution with high speed (Boas and Dunn, 2010). When an object, such as red blood cells in a tissue, is illuminated by laser light, the backscattered light forms an interference pattern consisting of dark and bright areas. This pattern is defined as a speckle pattern. If the illuminated object is static, the speckle pattern is stationary. When there is movement in the object, the speckle pattern changes over time. The software records these changes in the speckle pattern, and hemodynamic signals can be monitored. In our experimental setup, the hemodynamic signal is generated by the activation through the whisker's stimulation of the neurons in the barrel cortex.

Based on the NVC coupling principle (del Zoppo, 2010), this activation, together with the communication between neurons, astrocytes, and cerebral blood vessels, leads to more blood flow in the activated area and a measurable hemodynamic signal (Wey et al., 2013)

Laser speckle imaging readout is comparable to blood oxygenation level-dependent (BOLD) imaging in human. Therefore, we used it as main technique providing results that would be comparable to those obtained in translational research.

In stroke patients, BOLD imaging is the standard technique used to generate images in functional MRI (fMRI) studies. It relies on regional differences in cerebral blood flow too. When a specific region of the cortex increases its activity in response to a task, the extraction fraction of oxygen from the local capillaries leads to an initial drop in oxygenated hemoglobin (oxyHb), an increase in local carbon dioxide (CO₂), and deoxygenated hemoglobin (deoxy-Hb). Following a lag of some seconds, cerebral blood flow also increases, delivering an excess of oxygenated hemoglobin, washing away deoxyhemoglobin (Gore, 2003). It is this substantial rebound in local tissue oxygenation, which is imaged. The reason fMRI can detect this change is due to a fundamental difference in the paramagnetic properties of oxyHb and deoxy-Hb.

2. Aim

Considering the critical role that neurites play for the maintenance and normal functioning of synapses in the cortical circuit, we aimed to understand the alterations they undergo under two pathological scenarios (AD and ischemic stroke).

On one hand, we focused on axonal pathology in close proximity to A β plaques. Our objective was to get a better insight into the formation and evolution over time (210 days of imaging) of axonal dystrophies revealing their potential contribution to the disease and plaque growth.

On the other hand, we aimed to investigate the long-term effect of cerebral ischemia on dendritic dynamics in an area distant to the damaged tissue. We therefore focused on the contralesional hemisphere, and targeted the dendritic arbor of transcallosal neurons connected to the infarct. Our main purpose is to understand if the observed alterations could be a source of maladaptive plasticity involved in the presence of functional impairment, since disabilities in stroke patients are extremely frequent and an important consequence associated to the disease.

3. Research articles

3.1. High plasticity of axonal pathology in Alzheimer's Disease mouse models

Alzheimer's disease (AD) is commonly associated with a set of neuronal cytoskeletal alterations – neurofibrillary tangles (NFTs), neuropil threads and dystrophic neurite (DN) formation, causing spine and synapse loss – as well as neuronal degeneration. DNs are swollen and tortuous neurites that are intimately associated with extracellular depositions of amyloid β (A β). They show a variable morphology and composition depending on the pathological stage of AD.

Using chronic two-photon *in vivo* imaging, correlative electron microscopy, and immunohistochemical techniques, we performed a detailed long-term study (up to 210 days of imaging) on the formation, development, and elimination of DNs in two transgenic mice (dE9xGFP-M and APP-PS1xGFP-M) to understand the temporal course of the dystrophic pathology and its relationship with the development of the amyloid pathology. The three-dimensional reconstruction and study of the GFP-expressing dystrophic axons and Methoxy-X04 stained A β plaques we followed *in vivo* has allowed us to observe different A β plaques and DNs near them. Regarding DNs, we observed they are highly plastic structures that present great variations in size and morphology (axonal sprouting) over time. These changes are more prominent in those DNs that reach larger volumes at some time point in comparison to smaller DNs. Regarding A β plaques, we distinguished those that reach large volumes and appear early in the animal lifetime (large A β plaques) and those others that are smaller and appear later in the animal lifetime near previous existing large A β plaques (satellite A β plaques). We found interesting relationships between different A β plaques and DNs since larger DNs are associated specifically with large A β plaques (but not to satellite A β plaques) and present an earlier development in the animal lifetime in comparison to smaller DNs. Moreover, most DNs are formed and develop during the cubic phase of the A β plaque volume growth, and numerous DNs are already disappeared at the end of this phase (the cubic phase is characterized, first by the formation of new A β plaques and second, by the increase in the growth rate of A β plaques). The analysis of the neurochemical and ultrastructural characteristics of DNs revealed that most GFP-expressing DNs widely express presynaptic, autophagy and lysosomal markers while APP/A β is selectively present in 50-60% of the GFP-expressing DNs, independently of their volume.

Based on these results, we propose that DNs are directly involved in the A β plaque formation and development, and due to the spatiotemporal segregation of distinct DNs, they could have different roles in the A β pathogenesis. Larger DNs might be the main source of A β peptide and thus, an active participant in the amyloid pathology, whereas smaller DNs seem to be a secondary consequence of it. However, both processes are not mutually exclusive and could occur concomitantly in the same DN. We consider that the development of DNs is a more dynamic and plastic event than previously thought, and this fact could also have important implications on the possible reversion of the pathology by treatments within a defined temporal window.

Contribution of V.F.S to this work: equal contribution to the performance of all experiments, data analysis, interpretation of the results, writing and correcting the manuscript than B.L.L. Moreover, I performed surgeries for cranial window implantation, chronic 2P imaging, immunostainings, and confocal imaging together with 3D reconstruction of the dystrophic axons (please see section 8 for further details).

RESEARCH

Open Access



High plasticity of axonal pathology in Alzheimer's disease mouse models

Lidia Blazquez-Llorca^{1,7*}, Susana Valero-Freitag^{1†}, Eva Ferreira Rodrigues¹, Ángel Merchán-Pérez^{2,3}, J. Rodrigo Rodríguez^{2,4}, Mario M. Dorostkar¹, Javier DeFelipe^{2,4,5} and Jochen Herms^{1,6*}

Abstract

Axonal dystrophies (AxDs) are swollen and tortuous neuronal processes that are associated with extracellular depositions of amyloid β (A β) and have been observed to contribute to synaptic alterations occurring in Alzheimer's disease. Understanding the temporal course of this axonal pathology is of high relevance to comprehend the progression of the disease over time. We performed a long-term in vivo study (up to 210 days of two-photon imaging) with two transgenic mouse models (dE9xGFP-M and APP-PS1xGFP-M). Interestingly, AxDs were formed only in a quarter of GFP-expressing axons near A β -plaques, which indicates a selective vulnerability. AxDs, especially those reaching larger sizes, had long lifetimes and appeared as highly plastic structures with large variations in size and shape and axonal sprouting over time. In the case of the APP-PS1 mouse only, the formation of new long axonal segments in dystrophic axons (re-growth phenomenon) was observed. Moreover, new AxDs could appear at the same point of the axon where a previous AxD had been located before disappearance (re-formation phenomenon). In addition, we observed that most AxDs were formed and developed during the imaging period, and numerous AxDs had already disappeared by the end of this time. This work is the first in vivo study analyzing quantitatively the high plasticity of the axonal pathology around A β plaques. We hypothesized that a therapeutically early prevention of A β plaque formation or their growth might halt disease progression and promote functional axon regeneration and the recovery of neural circuits.

Keywords: Alzheimer's disease, Dystrophic neurites, FIB/SEM microscopy, Three-dimensional, Two-photon microscopy

Introduction

Alzheimer's disease (AD) is typically associated with a set of neuronal cytoskeletal alterations – the formation of neurofibrillary tangles (NFTs), neuropil threads and dystrophic neurites, which are associated with dendritic spine and synapse loss, as well as neuronal degeneration (e.g., [2, 42, 53, 61]). These pathological changes develop in a characteristic spatiotemporal progression across the cerebral cortex and other brain regions in AD patients [12] and AD mouse models [10]. Dystrophic neurites are swollen and tortuous neurites, which were originally detected by Alois Alzheimer because of their argyrophilia [1]. They have a variable morphology and composition depending on the pathological stage of AD [44, 51, 58, 60, 62].

They are closely associated with extracellular deposits of amyloid β (A β), known as “A β plaques”, which represent another hallmark of AD pathology. Dystrophic neurites are normally formed in axons [18, 24, 25, 36, 38, 57, 58, 62]. From now on we will refer to axonal dystrophies as AxDs.

Synaptic loss is the major neurobiological basis of cognitive dysfunction in AD. Synaptic failure is an early event in the pathogenesis that is already clearly detectable in patients with mild cognitive impairment (MCI), a prodromal state of AD. Compelling evidence suggests that different forms of A β peptide and abnormal phosphorylated tau induce synaptic loss in AD and transgenic mice models [6]. Synaptic breakdown in AD mouse models with no relation to amyloid plaques but as a consequence of high level of soluble amyloid beta has been reported [3, 4]. A β plaques are associated to alterations of dendrites and axons that are in contact or in the proximity to them, and with a clear decrease of synapses. The majority of studies has been focused on alterations of dendrites in contact with A β plaques [8, 9, 28, 32–35, 43, 52, 53, 59].

* Correspondence: lblazquez@psi.uned.es; Jochen.Herms@med.uni-muenchen.de

†Equal contributors

¹German Center for Neurodegenerative Diseases-Munich site (DZNE-M) and Center for Neuropathology and Prion Research (ZNP), Ludwig-Maximilians University, Munich, Feodor-Lynen-St 23, 81377 Munich, Germany
Full list of author information is available at the end of the article

However, less attention has been paid to the alterations of axons [2]. This is unfortunate since the loss of synapses found in or around A β plaques could be related to alterations of postsynaptic targets (dendrites), presynaptic elements (axons) or both.

For this reason, we consider that understanding the temporal course of the axonal pathology is of high relevance to comprehend the progression of the disease over time and define possible therapeutic targets and the window time where a treatment might be effective. The dystrophic pathology is one of the alterations of the disease that has been better resembled in the animal models [2, 13, 53, 59]. Previous *in vivo* studies have been undertaken to analyze the dystrophic pathology over time [13, 15, 23, 53, 59]. One of the main findings from these studies was that the elimination rates were significantly higher than the formation rates, suggesting that there is a gradual net loss of neuronal structures over time near A β plaques, causing a permanent disruption of neuronal connections [59]. Furthermore, it has been reported that the dystrophic pathology is reversible with an anti-A β antibody treatment [13] and curcumin [23]. However, these studies did not perform either a detailed quantitative analysis of the observed changes or a long-term study of the dystrophic pathology (the longest was only 35 days). Moreover, the relationship of specific axonal dystrophic changes to A β accumulation has not been addressed. In the present work, we performed a detailed long-term study (of up to 210 days and weekly imaging) focusing on the formation, development and elimination of AxDs with the aim of examining the plasticity of AxDs and their potential to be reversed. To achieve these objectives, we have used two-photon *in vivo* imaging and electron microscopy including transmission electron microscopy (TEM) and focused ion beam/scanning electron microscopy (FIB/SEM).

Materials and methods

Animals and housing

Mouse lines Amyloid Precursor Protein – Preseniline 1 (APP-PS1) (dE9) [30], APP-PS1 [48] and the Green Fluorescent Protein-M (GFP-M) [19] were used in this study. The dE9 and GFP-M lines were purchased from The Jackson Laboratory (Bar Harbor, USA). The APP-PS1 mice were provided by Matthias Jucker (University of Tübingen and German Center for Neurodegenerative Diseases, Tübingen, Germany). Heterozygous dE9 and APP-PS1 mice were crossed with heterozygous GFP-M mice resulting in triple transgenic dE9xGFP-M and APP-PS1xGFP-M mice, which were inbred. Heterozygous triple transgenic mice of mixed gender were used for experiments at the ages indicated below. Mice were group-housed under pathogen-free conditions until surgery, after which they were singly housed in standard

cages with food and water *ad libitum*. The studies were carried out in accordance with an animal protocol approved by the Ludwig-Maximilians-University Munich and the government of Upper Bavaria (Az. 55.2-1-54-2531-188-09).

Two-photon *in vivo* imaging

For *in vivo* imaging, a chronic cranial window was prepared as described previously [22]. Surgery was performed in six 6-month-old dE9xGFP-M and seven 2-month-old APP-PS1xGFP-M mice. *In vivo* imaging began after a 4–5-week post-surgery recovery period, using an LSM 7 MP setup (Zeiss) equipped with a MaiTai laser (Spectra Physics). Around 24 h before imaging, Methoxy-X04 (0.4 to 2.4 mg/Kg body weight, Xcessbio, San Diego, CA, USA) was intraperitoneally injected to visualize A β plaques *in vivo* [31]. Imaging was performed once a week for 24 weeks in dE9xGFP-M mice and for 30 weeks in the APP-PS1xGFP-M mice. In the dE9 model, the imaging began when the mice were around 7 months-old (the age corresponding to the initial stage of the amyloid pathology) and was prolonged until they were approximately 13 months-old (corresponding to the advanced stage of the disease). In the APP-PS1 mouse, the imaging began when the mice were around 3 months-old (the age corresponding to the initial stage of the amyloid pathology) and was prolonged until they were approximately 10 months-old (which corresponds to the advanced stage of the disease).

Two-photon excitation of Methoxy-X04-labeled A β plaques was performed at 750 nm and the signal was detected using a short pass (SP) 485 nm filter. Two-photon excitation of GFP-expressing neuronal structures was performed at 880 nm and the signal was detected using a bandpass (BP) 500–550 nm filter. To exclude false positive fluorescent spots from the analysis, we also recorded emissions at 590–650 nm. These auto-fluorescent spots were found both in the neuropil and within neuronal and glial cells (Additional file 1). A $\times 20$ 1.0 NA water-immersion objective (Zeiss) was used. Stereological coordinates were used to locate the somatosensory cortex [29]. Overview images were taken at low resolution (logical size 512×512 pixels; physical size x, y, z : $424.3 \times 424.3 \times 300 \mu\text{m}$; z -step = $3 \mu\text{m}$) to a depth of $300 \mu\text{m}$ (supragranular layers) to find the same position over time. At least 2–3 overviews were taken per animal at each imaging session. Note that performing long-term *in vivo* two-photon imaging weekly during near 6 months is challenging. Although more imaging positions were acquired only those that were successfully imaged during the whole time period were used for the quantitative analysis. These numbers are shown in Additional file 2. Two types of images were taken to perform the analysis:

- i) The three-dimensional (3D) reconstruction of AxDs over time: High magnification images (logical size 512×512 pixels; physical size x, y, z : $84.9 \times 84.9 \times 40\text{--}60$ μm ; $z\text{-step} = 1$ μm) of single A β plaques stained with Methoxy-X04 and the GFP-expressing neurites around them (46 GFP-expressing axons around 6 A β plaques in the dE9xGFP-M mouse model ($n = 6$), 10 of which became dystrophic and were 3D reconstructed; 58 GFP-expressing axons around 6 A β plaques were followed in the APP-PS1xGFP-M mouse model ($n = 7$), 16 of which became dystrophic and were 3D reconstructed). Care was taken to ensure similar fluorescence levels in space and time.
- ii) The spatiotemporal relationship between A β plaques and AxDs: Panoramic high resolution images (logical size 1400×1400 pixels; physical size x, y, z : $202.3 \times 202.3 \times 39.9\text{--}50.1$ μm ; $z\text{-step} = 0.3$ μm) showing several A β plaques stained with Methoxy-X04 and GFP-expressing neurites near and far from them (33 A β plaques and 52 AxDs were followed over time in the APP-PS1xGFP-M mouse model ($n = 7$)). AxDs were not 3D reconstructed at all time points, but rather only on those days when the volume of the AxD was visually observed to be largest. Thus, we recorded “the maximum volume data” over time. Moreover, the day of appearance and disappearance and the type of axon in which the AxD appeared was also annotated for every single AxD. Care was taken to ensure similar fluorescence levels in space and time.

Electron microscopy preparation and TEM and FIB/SEM imaging

A correlative two-photon *in vivo* imaging and TEM or FIB/SEM microscopy method was used to analyze the ultrastructure of the same A β plaques (and AxDs around them) as those previously studied *in vivo* [11]. Briefly, after the final *in vivo* imaging session, three dE9xGFP-M mice were transcardially perfused with 2% paraformaldehyde and 2.5% glutaraldehyde in 0.12 M PB, pH 7.4. Later, regions of interest in a thick section cut from the window region were marked by laser, using the two-photon-laser system according to the Near Infrared Branding (NIRB) technique [7]. This thick section was resectioned in thinner sections of 50 μm with a Leica Vibratome (VT1200, Leica Microsystems, Wetzlar, Germany). After the cutting, sections were analyzed again under the two-photon microscope to find those slices where the marked regions of interest were present. Selected 50 μm sections containing the regions of interest were post-fixed in 2.5% glutaraldehyde/2% paraformaldehyde in 0.1 M cacodylate buffer for 1 h, treated with 1% osmium tetroxide in 0.1M cacodylate buffer for 1 h, dehydrated,

and flat embedded in Araldite resin [17, 41]. The postfixation, dehydration and embedding steps were done with a laboratory microwave oven with a vacuum chamber and cooling stage (Ted Pella, Redding, CA, USA).

In those samples that were analyzed by TEM, plastic-embedded sections were studied by correlative light and electron microscopy, as described in detail elsewhere [17]. Briefly, sections were photographed under the light microscope and then serially cut into semithin (2- μm thick) sections on a Leica ultramicrotome (EM UC6, Leica Microsystems). The semithin sections were stained with 1% toluidine blue in 1% borax, examined under the light microscope, and then photographed to locate the NIRB-marked region of interest. Serial ultrathin sections (50- to 70-nm thick) were obtained from selected semithin sections on a Leica ultramicrotome, and collected on formvar-coated single-slot nickel grids and stained with uranyl acetate and lead citrate. Digital images were captured at different magnifications on a Jeol JEM-1011 TEM (JEOL Inc., MA, USA) equipped with an 11 Mega-pixel Gatan Orius CCD digital camera.

In those samples that were analyzed by FIB/SEM, semithin sections (1- μm thick) were obtained by means of a Leica ultramicrotome from the surface of the block until the most superficial NIRB marks around the region of interest were reached (Additional file 3). The blocks containing the embedded tissue were then glued onto aluminum sample stubs using conductive carbon adhesive tabs (Electron Microscopy Sciences, Hatfield, PA). All surfaces of the Araldite blocks, except for the top surface containing the sample, were covered with colloidal silver paint (Electron Microscopy Sciences, Hatfield, PA) to prevent charging artifacts. The stubs with the mounted blocks were then placed into a sputter coater (Emitech K575X, Quorum Emitech, Ashford, Kent, UK) and were coated with platinum for 10 s to facilitate charge dissipation. The marks were still visible on the surface of the block with the FIB/SEM. The ultrastructural 3D study of these samples was carried out using a combined FIB/SEM microscope (Neon40 EsB, Carl Zeiss NTS GmbH, Oberkochen, Germany). The sequential automated use of alternating FIB milling and SEM imaging allowed us to obtain long series of images representing 3D sample volumes of selected regions. Images of 2048×1536 pixels at a resolution of 6.203 nm per pixel were taken; each individual photomicrograph therefore covered a field of view of 12.7×9.5 μm . The layer of material milled by the FIB in each cycle (equivalent to section thickness) was 30 nm. A total of 305 serial sections were obtained. Thus, the physical size of the stack was (x, y, z) $12.7 \times 9.5 \times 9.15$ μm .

Images, data processing and statistics

The deconvoluted two-photon images (AutoQuantX2, Media Cybernetics) were processed later by means of

Imaris software (Bitplane AG, Zurich, Switzerland) to obtain the 3D reconstructions of the dystrophic axons and the A β plaques, as well as the volumes of each of them at the different time points. For the alignment (registration) of the stack of FIB/SEM images, we used Fiji (<http://fiji.sc>). Reconstruct Software v1.1.0.0 [21] was used to carry out the 3D reconstruction of the AxDs and the microglial cell.

Regarding A β plaques: the images were analyzed as time series of 3D images in Imaris. First, images were contrast-normalized (i.e., based on the average and standard deviation of the 3D stack intensities). Plaque volumes were extracted by 3D-surface-rendering with background subtraction and a threshold of 500. Newly formed A β plaques were tracked back to the first time point when they appeared and were only assessed when present for at least 3 time points. Regarding AxDs: they were manually segmented in the images stacks. Only those AxDs and parent axons that were present in the whole imaging stack at all time points were reconstructed. An axonal segment was considered dystrophic when its volume was double that of the non-dystrophic axonal segment. When possible, non-dystrophic axonal volume was calculated as the average of three measurements at three different time points for the same axonal segment that would later go on to show the AxD. When the AxD was already present from the first day of observation, non-dystrophic segments of the same axon outside the A β plaque were averaged at three different time points. In all cases, reference non-dystrophic axonal segments had the same length as the maximal segment affected by the AxD (Additional file 4).

Photoshop CS6 (Adobe Systems Inc., San José, CA, USA) software was used to generate the figures.

All data sets were tested for normality with the Kolmogorov-Smirnov and D'Agostino and Pearson omnibus normality tests with a significance level set to $p = 0.05$, before the appropriate parametric or non-parametric statistical comparison test was carried out with GraphPad Prism 5.04 (GraphPad Inc., La Jolla, CA, USA).

Results

Kinetics of formation, development and elimination of AxDs: 3D reconstructions

In the dE9 mouse, we observed a total of 46 axonal segments located not further than 40 μm from the border of the adjacent Methoxy-X04-stained amyloid plaques. Out of all of these axonal segments, we detected the formation of AxDs in only 22% of them ($n = 10$ AxDs; all were reconstructed with Imaris software) (Figs. 1, 2 and 3). In the APP-PS1 mouse, we examined a total of 58 axonal segments located not further than 40 μm from the border of the adjacent Methoxy-X04-stained amyloid plaques. Out of all these axonal segments, we only

detected the formation of AxDs in 28% of them ($n = 16$ AxDs, all were reconstructed with Imaris software) (Figs. 1 and 3). We observed that a given AxD presented size variations over time (intra-size variations) and distinct AxDs could have very different sizes (inter-size variations) (Figs. 1 and 2). Due to this heterogeneity, we performed a detailed quantitative study of the morphological changes that take place and the kinetics of formation, development and elimination of single AxDs over time. Each AxD was independently named and they are referred to in the text and graphs as “dys 1–10” in the dE9 mouse and “dys 1–16” in the APP-PS1 mouse. Axons of control mice (GFP-M) displayed unchanged morphology after long-term in vivo two-photon imaging (observations are not shown).

Using Imaris software, 3D reconstructions of the AxDs were performed and it was possible to quantify their volume and study their morphological changes over time (Figs. 1 and 2).

Morphological changes of AxDs: size and shape

AxDs were highly variable in terms of their size both in the dE9 and the APP-PS1 models. AxDs sizes varied between 45 and 3081 μm^3 in the dE9 model and between 25 and 2814 μm^3 in the APP-PS1 model (Fig. 3). Moreover, AxDs did not grow continuously; indeed their volume grew and decreased over time. Changes in volume were more prominent in the larger AxDs than in the smaller ones. For example, dys 3 in the dE9 model ranged between 159 and 3081 μm^3 (Figs. 3a and 4e–g), while smaller AxDs showed less pronounced changes (e.g., dys 5 in the dE9 model only changed between 45 and 76 μm^3 ; Fig. 3a). Thus, it can be observed that larger AxDs at some point are similar in size to those AxDs that are smaller over their whole lifetime.

When we calculated the ratio between the volume of an AxD and the volume of the non-dystrophic axonal segment of the same AxD (size ratio) (Fig. 3c, d; Additional file 4), we observed that the volume increase of the AxDs ranged between 2 and 39 times in the dE9 model and between 2 and 35 times in the APP-PS1 model (Table 1).

In some cases, both in the dE9 and the APP-PS1 mice, we observed significant changes in the shape of the AxDs and the formation of more than one swollen varicosity of irregular shape with new short axonal segments leaving from the dystrophic structures (axonal sprouting) (Fig. 2). This phenomenon was observed in those AxDs reaching larger sizes (greater than 500 μm^3) — $n = 3$ in the dE9 and $n = 7$ in the APP-PS1 mice, see Table 1 and Fig. 3— but was not seen in the smaller ones that normally remained as single spherical swollen varicosities (Fig. 1a–c). To quantify this observation, we estimated the mean sphericity factor of each AxD over time. The

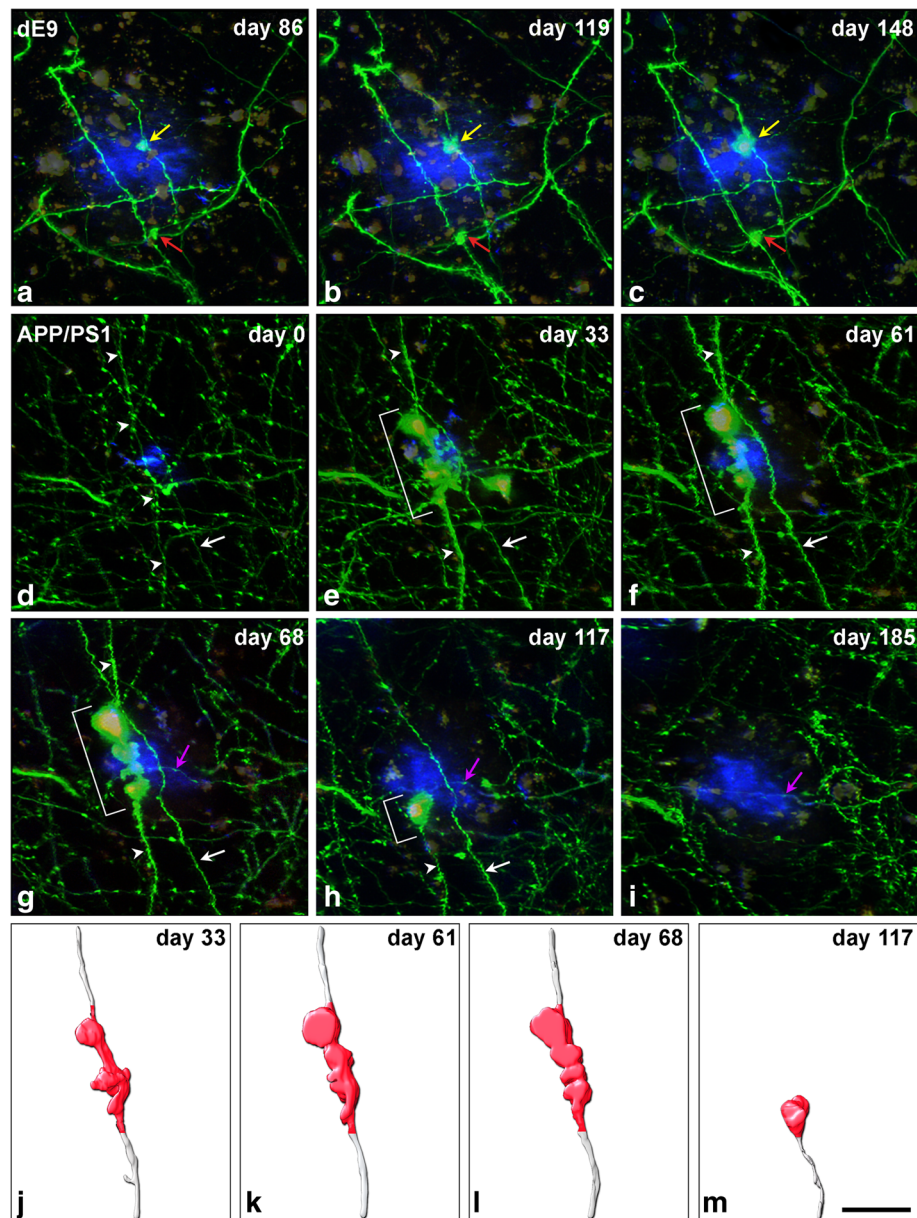


Fig. 1 Intra- and inter-size variations of AxDs over time. **(a-c)**, Maximum projection (40 optical sections, z-step = 1 μ m) of a stack of images taken with a two-photon microscope in the somatosensory cortex of a dE9 mouse at three different time points. Small AxDs (yellow and red arrows, dys 6 and 7, respectively) in GFP-expressing axons (green) are present around an A β plaque stained with Methoxy-X04 (blue). **(d-i)**, Maximum projection (32 optical sections, z-step = 1 μ m) of a stack of images taken with the two-photon microscope in the somatosensory cortex of the APP-PS1 mouse at six different time points. A large AxD (brackets in **e-h**; dys 4) in a GFP-expressing axon (green; arrowheads) is present around an A β plaque stained with Methoxy-X04 (blue). This plaque was observed growing in size from its birth (**d**) to maturation (**i**). There is a degeneration of the distal part of the axon and the AxD remains at the edge of the proximal part of the axon (**h**). On the final day of imaging, the whole axon had disappeared (**i**). AxDs in panels **a-c** do not show strong variations in size and shape over time as compared to the AxD in panels **d-i**, and numerous axons and dendritic processes do not become dystrophic. There is an axon segment that does not become dystrophic and disappears (white arrow). **(j-m)**, 3D reconstructions of the AxD showed in images **e-h**, respectively, using Imaris software. The dystrophic segment of the axon is shown in red and this is the portion of the axon that was used to calculate the AxD volume (Fig. 3b). The days shown refer to the number of days after day 0 (when imaging began). Purple arrows in **g-i** point out a re-growing axon that is also shown in greater detail in Fig. 5. Scale bar (in **m**): 19.5 μ m in **a-m**

sphericity factor, defined as the ratio of the surface area of a sphere to the surface area of the structure analyzed (both with the same volume) provides a quantitative

record of the morphological complexity of the 3D-reconstructed AxDs, since spherical objects would yield a sphericity value close to 1, while more complex shapes

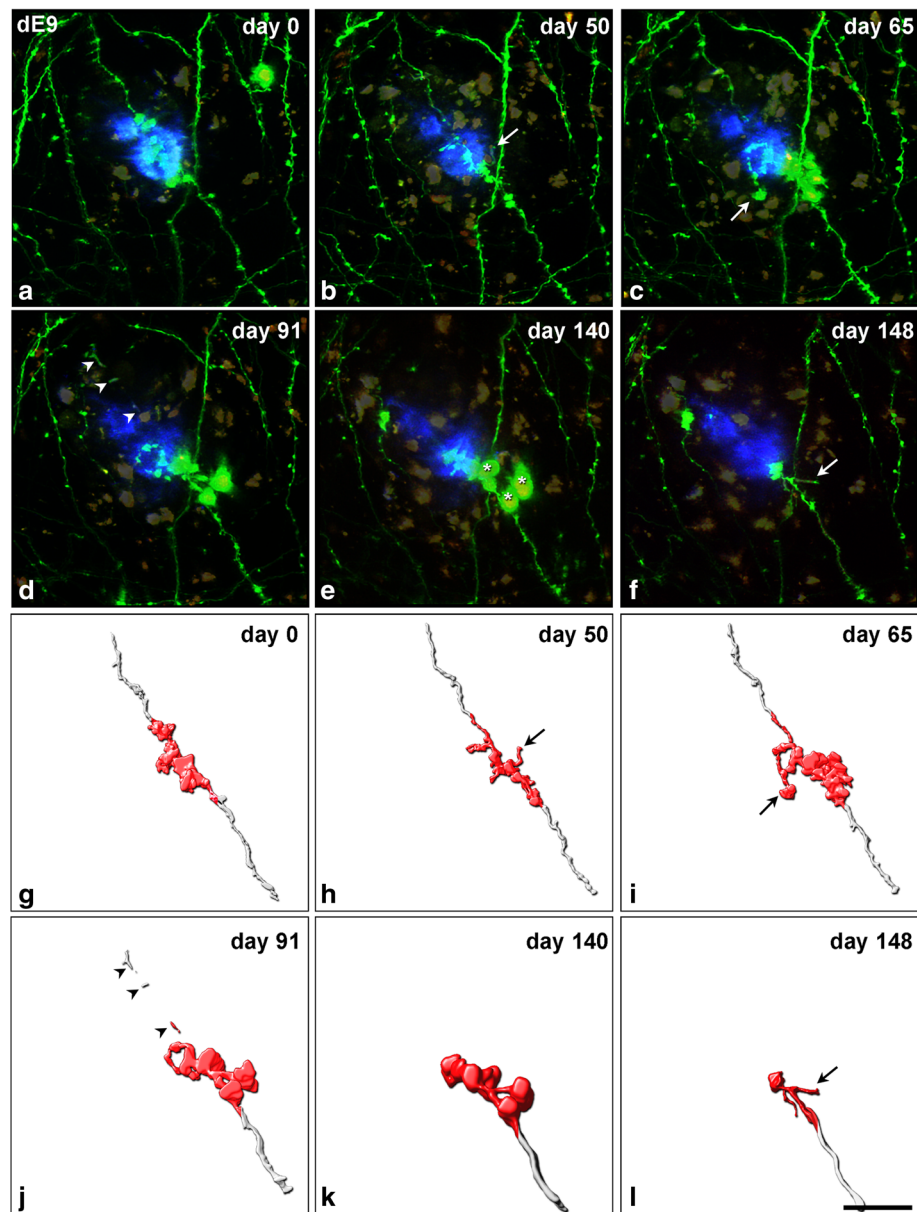
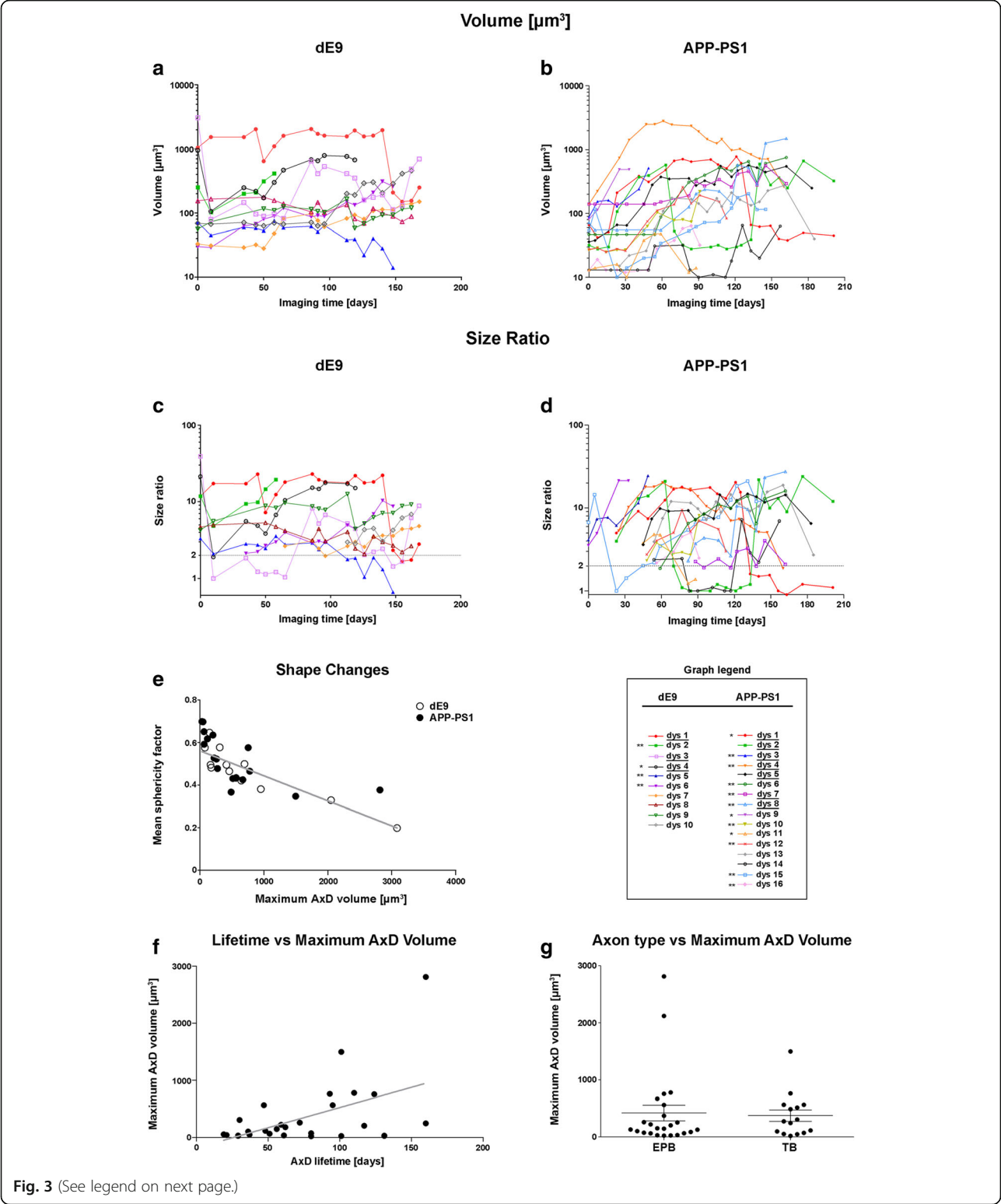


Fig. 2 Three-dimensional reconstructions of AxDs. **(a-f)**, Images obtained (over 148 days) of the same dystrophic axon expressing GFP (dys 1) in contact with an Aβ plaque stained with Methoxy-X04 (blue) in the supragranular layers of the somatosensory cortex of a dE9 mouse (two-photon microscopy). **(g-l)**, Three-dimensional reconstructions of the AxD showed in panels **a-f**, respectively, using Imaris software. On day 91 (**j**) the degeneration of the distal part of the axon (arrowheads) begins. This degenerative process is completed in the successive days but the AxD remains at the end of the cut axon (**k, l**). Note that the AxD presents numerous changes in volume and shape. The existence of more than one swollen varicosity (asterisks in **e** show an example) and short axonal sprouting can be identified (arrows in **b, c, f, h, i** and **l**). Note that the dystrophic segment of the axon is shown in red and from this part the numerical AxD volume was calculated and plotted in Fig. 3a. The days shown refer to the number of days after day 0 (when imaging began). Scale bar (in **l**): 19.5 μm in **a-l**

with larger surface-to-volume ratios would yield progressively lower values. We found an inverse correlation (Pearson's r : -0.7366 , $p < 0.0001$; Fig. 3e) between the sphericity and the maximum volume that the AxD reaches, so larger AxDs showed smaller sphericity factors and vice versa. Thus, larger AxDs tend to be complex, non-spherical shapes.

Axonal sprouting: re-growth phenomenon

In the case of the APP-PS1 mouse only, the formation of new long axonal segments in dystrophic axons (re-growth phenomenon, $n = 3$ (out of 17)) was observed (Fig. 5 and Additional file 5). These new axonal segments were observed either (i) leaving from a dystrophic structure ($n = 1$ (dys 13)) with a maximum



(See figure on previous page.)

Fig. 3 Volume and morphological changes of in vivo AxDs over time. **(a, b)**, Graphs showing the changes in volume of the different AxDs studied over time in the dE9 **(a)** and the APP-PS1 **(b)** mice. **(c, d)**, Size ratio indicates the ratio between the volume of an AxD and the volume of its equivalent non-dystrophic axonal segment. Graphs correspond to the same AxDs represented in **a, b**, respectively. With the aim of simplifying the graph visualization, the AxD size ratio was plotted only from the imaging day in which the AxD became dystrophic (size ratio ≥ 2 , *dashed line*). Note that in **a-d** the scale has been transformed to Log 10 to illustrate that volume values of larger and smaller AxDs can be very similar at some time points. The days shown refer to the number of days after day 0 (when imaging began). Graph legend: Asterisks refer to those AxDs that disappear at the end of the imaging period (*one asterisk* means the parental axon stays and *two asterisks* mean that the AxD disappears due to the loss of the parental axon); *underlined AxDs (dys)* are those that show morphology changes (more than one swollen varicosity of irregular shape and new short axonal segments). **(e)**, Correlation between the mean sphericity value over time and the maximum volume that the AxD reaches. Larger AxDs tend to be more complex, non-spherical shapes (Pearson's r : -0.7366 , $p < 0.0001$). **(f)**, Correlation between the AxD lifetime and the maximum AxD volume in the APP-PS1 mouse. Larger AxDs tend to have longer lifetimes (Pearson's r : 0.4974 , $p = 0.0071$). **(g)**, Comparison between the axon type (*EPB* en passant bouton axons, *TB* terminal bouton axons) and the maximum volume that the AxD reaches in the APP-PS1 mouse. The size of AxDs is not related to the type of axon in which they are formed (Mann-Whitney U: 163.0 ; $p = 0.6339$)

observed length of the new axonal segment of $53 \mu\text{m}$ or (ii) re-growing from axons that were previously sectioned at a dystrophic point ($n = 2$) with a maximum observed length of the new axonal segments of $104.5 \mu\text{m}$ (dys 9, Fig. 5) and $32 \mu\text{m}$ (this AxD was not 3D reconstructed, but is shown in Additional file 5). The re-grown segment followed a different trajectory from the previously existing axon segment (Fig. 5 and Additional file 5, Table 1).

Lifetime and elimination of AxDs

We found that on average AxDs had a very long lifetime. It was common to find AxDs that were present for more than 100 days both in the dE9 and the APP-PS1 mice — $n = 7$ (out of 10) and $n = 7$ (out of 16), respectively— (see Table 1). In the APP-PS1 mouse, it was feasible to analyze a larger number of AxDs (see next section and Additional file 6). In this case, the average lifetime of AxDs was 76.43 ± 7.8 days

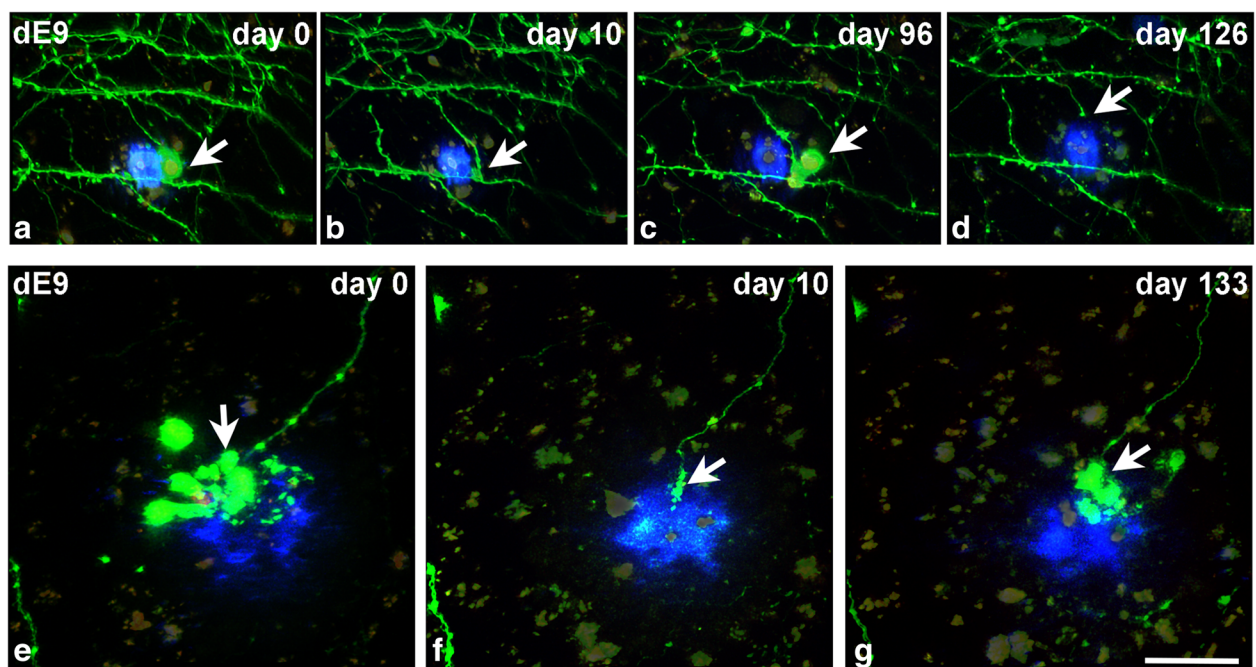


Fig. 4 Re-formation of AxDs. Dendrites and axons expressing GFP (*green*) in contact with A β plaques stained with Methoxy-XO4 (*blue*) in the supragranular layers of the somatosensory cortex of the dE9 mouse (two-photon microscopy). **(a-d)**, Maximum projection of images taken around an A β plaque (40 images, $z = 1 \mu\text{m}$) at different time points. The AxD (dys 4; *arrow*) is smaller on day 10 **(b)**, and has disappeared on day 126 **(d)**. Notice that the parental axon on day 126 is shortened. **(e-g)**, Maximum projection of images taken around another A β plaque (40 images, $z = 1 \mu\text{m}$) at different time points. The AxD (dys 3; *arrow*) disappeared on day 10 **(f)** but the parental axon remains. A new large AxD is generated at the same point on day 133. The days shown refer to the number of days after day 0 (when imaging began). Scale bar (in **g**): $25.9 \mu\text{m}$ in **a-d** and $19.5 \mu\text{m}$ in **e-g**

Table 1 Characteristics of the 3D reconstructed AxDs

dE9xGFP-M									
	Type of axon	Lifetime (days)	Disappearance of AxDs at the end of the imaging period	Disappearance of the parent axon	Reformation of AxDs	Maximum AxD volume (μm^3)	Maximum AxD size ratio	Axonal sprouting	
Dys 1	TB	>168	No	No	No	2049	22.98	Yes	
Dys 2	EPB	>75	Yes	Yes	No	414	19.40	No	
Dys 3	EPB	3a: >10 3b: 62 3c: >6	No	No	Yes	3a: 3081 3b: 646 3c: 697	3a: 39 3b: 8.18 3c: 8.82	Yes	
Dys 4	TB	4a: >10 4b: 116	Yes	No	Yes	4a: 952 4b: 789	4a: 21.3 4b: 17.64	Yes	
Dys 5	EPB	>155	Yes	Yes	No	76	3.57	No	
Dys 6	EPB	120	Yes	Yes	No	310	10.33	No	
Dys 7	EPB	>110	No	No	No	150	4.83	No	
Dys 8	EPB	>168	No	No	No	176	5.33	No	
Dys 9	EPB	>168	No	No	No	165	12.58	No	
Dys 10	EPB	>49	No	No	No	458	6.83	No	
APP-PS1xGFP-M									
	Type of axon	Lifetime (days)	Disappearance of AxDs at the end of the imaging period	Disappearance of the parent axon	Reformation of AxDs	Maximum AxD volume (μm^3)	Maximum AxD size ratio	Axonal sprouting	Regrowth
Dys 1	EPB	110	Yes	No	No	778	20.2	Yes	No
Dys 2	EPB	2a: 47 2b: >88	No	No	Yes	2a: 565 2b: 669	2a: 9.81 2b: 35.20	Yes	No
Dys 3	TB	>63	Yes	Yes	No	514	24.49	Yes	No
Dys 4	EPB	160	Yes	Yes	No	2814	20.14	Yes	No
Dys 5	TB	>138	No	No	No	565	14.77	Yes	No
Dys 6	EPB	124	Yes	Yes	No	755	16.01	No	No
Dys 7	TB	95	Yes	Yes	No	565	4.03	Yes	No
Dys 8	TB	101	Yes	Yes	No	1496	27.46	Yes	No
Dys 9	TB	>47	Yes	No	No	512	21.30	No	Yes
Dys 10	EPB	59	Yes	Yes	No	221	8.10	No	No
Dys 11	EPB	51	Yes	No	No	64	5.00	No	No
Dys 12	EPB	72	Yes	Yes	No	259	9.45	No	No
Dys 13	TB	>131	No	No	No	274	18.84	No	Yes
Dys 14	EPB	14a: 29 14b: >40	No	No	Yes	14a: 32 14b: 65	14a: 2.45 14b: 7.20	No	No
Dys 15	EPB	15a: >23 15b: 117	Yes	Yes	Yes	15a: 116 15b: 203	15a: 14.43 15b: 21.05	No	No
Dys 16	TB	37	Yes	Yes	No	48	4.80	No	No

($n = 28$) —not taking into account those AxDs that were present on the first and/or last day of imaging. Moreover, we found a correlation (Pearson's r : 0.4974, $p = 0.0071$) between the AxD lifetime and the maximum volume that the AxD reaches, that is, larger AxDs had longer lifetimes and vice versa (Fig. 3f).

When AxD loss occurred, it happened in two ways:

1- Loss of the whole axon where the AxD was present (Figs. 1d–i and 3, Table 1). In addition, around A β plaques, both normal-looking axons and dystrophic axons could disappear (see Fig. 1d–i). However, we cannot rule out the possibility of the normal axon being dystrophic at a segment close to an A β plaque in another microscopic field.

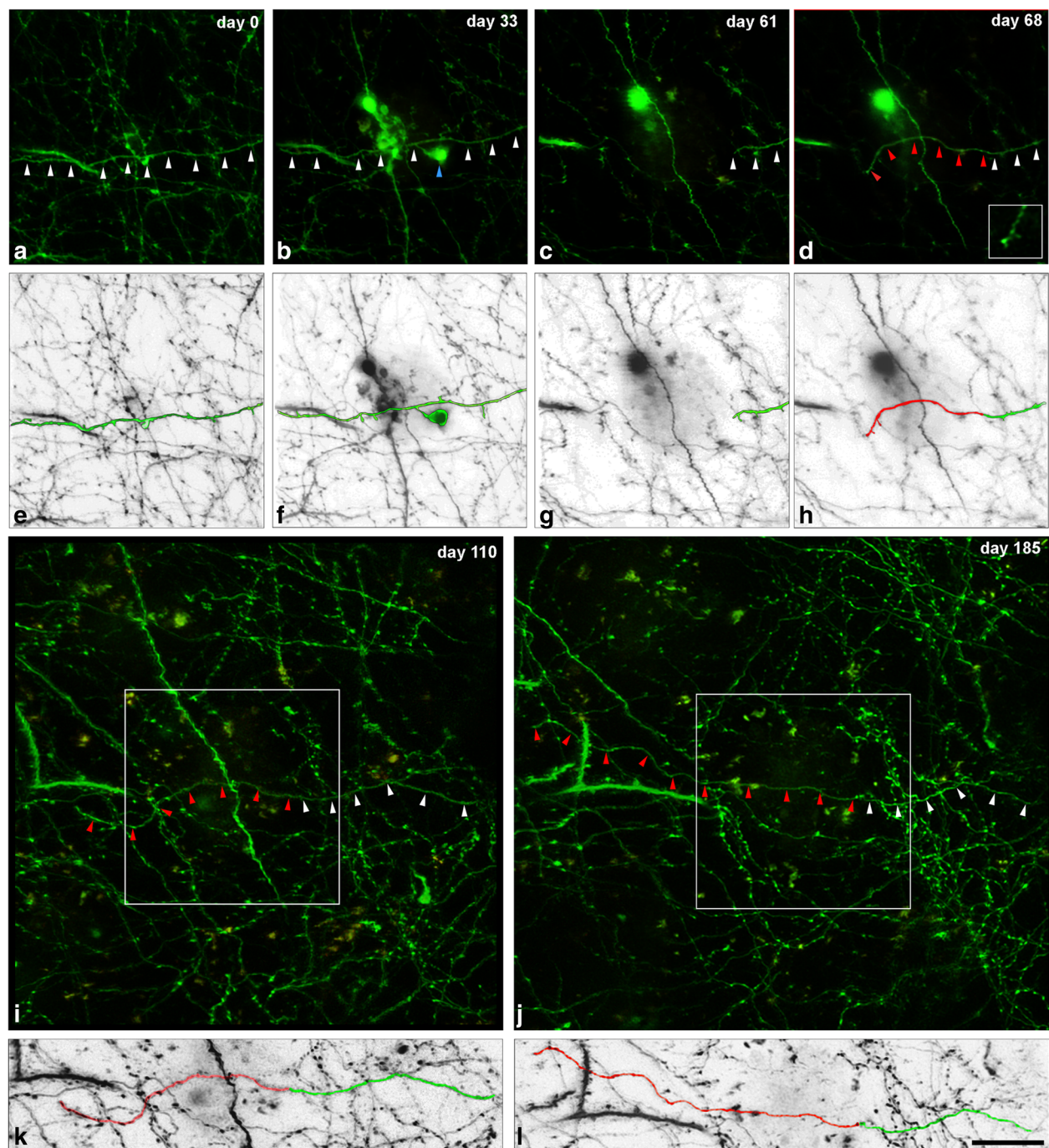


Fig. 5 Re-growing phenomenon in a dystrophic axon. (**a-d**), Maximum projection of a stack of images taken in the supragranular layers of the somatosensory cortex of the APP-PS1 mouse at four different time points (two-photon microscopy). To facilitate the visualization of the axon of interest, only those optical sections where this axon was present were used for the maximum projections (32 sections in **a**, 30 in **b**, 10 in **c** and 15 in **d**; z-step: 1 μ m). Panels **a-d** correspond to the same regions and days as those also illustrated in Fig. 1d-g. In day 61 (**c**), the distal part of the axon (white arrowheads) was lost just before the dystrophic part (dys 9, blue arrowhead in **b**). In day 68 (**d**), the axon starts to re-grow (red arrowheads). The inset in **d** shows the growth cone. (**e-h**), Schematic representation from images **a-d**, respectively, showing the axon of interest (green) and the re-growth segment (red). (**i, j**), Maximum projection of a stack of lower magnification images (89 sections in **i** and 98 in **j**; z-step: 0.7 μ m), showing that the new axon segment (in **d**) can re-grow (red arrowheads) longer distances over time (re-growth segment: 73.9 μ m in **i** and 104.5 μ m in **j**). The square delimits the size of the regions shown in **a-d**. (**k, l**), Schematic representation from images **i-j**, respectively, showing the axon of interest (green) and the re-growth segment (red). Note that the re-growth axonal segment has changed its trajectory whereas the original axon segment maintains the original trajectory. The days shown refer to the number of days after day 0 (when imaging began). Scale bar (in **l**): 24 μ m in **a-h**, 11.6 μ m in **d** (inset) and 20.6 μ m in **i-l**

- 2- Loss of the dystrophic structures only, but not the parental axon. Interestingly, in some of these cases, after a variable period of time, new AxDs appeared at the same point of the axon where the previous AxD had been located. This re-formation phenomenon of AxDs always occurred at the edge of the axon (Figs. 3 and 4; Additional file 5; Table 1).

Electron microscopy Using correlative FIB/SEM, we were able to analyze a region of approximately $1200 \mu\text{m}^3$ where an AxD had been observed in vivo to have disappeared (Fig. 6). In this region, at the ultrastructural level, we found an activated microglial cell containing a large amount of electron-dense material, full of phagocytosed fragments of membranes and organelles. This accumulation of electron-dense material corresponded to the auto-fluorescence observed with the two-photon microscope (Additional file 1) and maintained days later at a point where an AxD was lost (Additional file 7). Furthermore, we used correlative two-photon in vivo imaging and TEM of GFP-expressing AxD near to A β plaque. We found that in some cases, microglial cells with numerous phagocytic inclusions were in close apposition to AxDs, suggesting that these cells are participating in phagocytosis of AxDs (e.g., see [56]) (Fig. 7d).

Type of axon and dystrophic pathology

We were also interested in knowing if different types of axons seem to be selectively vulnerable to the amyloid pathology. We distinguished two main types of axons: En Passant Bouton (EPB) axons and Terminal Bouton (TB) axons. EPB axons had a high density of en passant boutons and relatively few spine-like terminal boutons. TB axons were similar to the EPB axons but had a high density of spine-like terminal boutons. Moreover, we could distinguish thin and thick EPB axons. In the dE9 mouse, 80% (8 out of 10) of the AxDs were present in EPB axons (see Fig. 4e–g) and the remaining 20% (2 out of 10) were in TB axons (see Fig. 2). In the APP-PS1 mouse, it was possible to analyze a larger number of AxDs ($n = 39$) (see next section and Additional file 6). In this case, 60% (24 out of 39) of the AxDs were present in EPB axons —Fig. 1d–i; 1 out of these 24 AxDs was present in a thick-EPB axon, see Fig. 8a, b— and the remaining 40% (15 out of 39) were in TB axons (Additional file 4 a–i). In addition, we calculated the number of EPB and TB axons in our images (on day 0 of imaging) in the APP-PS1 mouse model and it was estimated to be 71 and 29%, respectively. Thus, the presence of higher numbers of AxDs in EPB axons could be explained by the higher numbers of EPB axons. When we compared the maximum AxD volume depending on the type of axon, we did not observe significant differences between AxDs in EPB axons ($419.6 \pm 138.5 \mu\text{m}^3$) and TB axons (374.3

$\pm 100.4 \mu\text{m}^3$) (Mann–Whitney U: 163.0; $p = 0.6339$). Thus, the size of AxDs was not related to the type of axon in which they were formed (Fig. 3g).

In summary, our data suggest that AxDs were formed in a quarter of GFP-expressing axons, which indicates a selective vulnerability. AxDs, especially those reaching larger sizes, had long lifetimes and appeared as highly plastic structures with large variations in size and shape and axonal sprouting over time. Moreover, they seemed to be formed on different types of axons. Finally, it appeared that microglial cells which are associated with phagocytic activity, may contribute to the disappearance and morphological changes of AxDs. These and other results are summarized in Table 1.

Relationship between A β plaques and AxD formation and development

In order to study early events regarding the formation of AxDs and A β plaques, the APP-PS1 mouse was used due to the early A β plaque development and high density of A β plaques in the neocortex in this mouse compared to the dE9 mouse. Using panoramic and high resolution images (Additional file 6 a–f), it was possible to study 52 AxDs (5 of which were not associated with A β plaques) and 33 A β plaques (Additional file 6), 15 of which were pre-existing A β plaques (A β plaques that were already present on the first day of imaging) and 18 were new A β plaques (A β plaques that appeared during the imaging period).

- The vast majority of AxDs were associated with A β plaques and in all these cases the formation of AxDs was observed after the appearance of the A β plaques ($n = 18$). However, in a small number of cases we observed an axon with two AxDs ($n = 5$ out of 52); one small AxD that was not associated with A β plaques, and another which was close to an A β plaque (Fig. 8e).
- There was a correlation (Spearman r : 0.6173, $p < 0.0001$) between the maximum size of a given AxD and the maximum size of the A β plaque with which it is associated, in such a way that large AxDs were present only around large A β plaques, whereas small A β plaques were associated only with small AxDs. Nevertheless, both large and small AxDs were present around large A β plaques (Fig. 8a–d, h).
- There was a correlation (Spearman r : -0.4711 , $p = 0.0022$) between the maximum AxD volume and the time of AxD appearance, such that larger AxDs developed earlier than smaller AxDs in the animal lifetime (Fig. 8a–d, g).
- When we studied the distribution of the 47 AxDs associated with A β plaques over time, we observed that most of them developed during the imaging

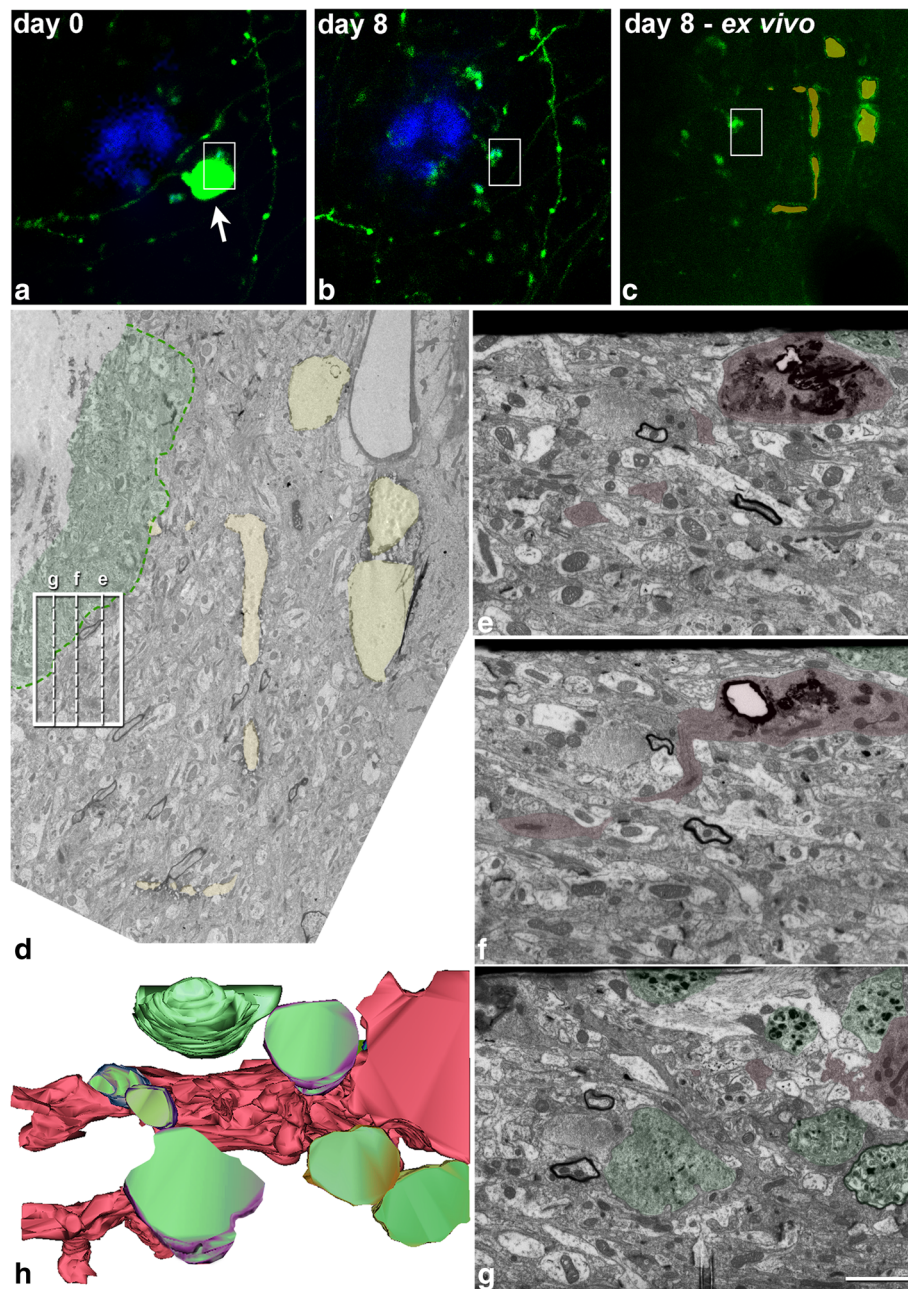


Fig. 6 Correlative two-photon in vivo imaging and FIB/SEM microscopy. (**a**, **b**), Optical single plane images taken at two different time points at the same region in layer I of the somatosensory cortex of the dE9 mouse, showing a Methoxy-X04-stained plaque (*blue*) and GFP-expressing processes. There is a loss of an AxD (*arrow*) in the space of 1 week. (**c**), Same region as in **a**, **b** taken ex vivo after the perfusion of the animal on day 8. This image was obtained by the combination of two optical single planes: one taken at the same z-level as in **a**, **b** and the other taken 4 μ m above it, showing the NIRB marks (pseudocolored in *yellow* and *orange*) performed to locate the region of interest at the ultrastructural level. (**d**), Electron-micrograph picture from the last ultrathin section taken from the surface of the block that was further analyzed by FIB/SEM microscopy. The same NIRB marks (pseudocolored in *yellow* and *orange*) as in **c** can be seen. The plaque halo is pseudocolored in *green*. The *rectangle* shows the position and the x, z dimensions of the FIB/SEM stack that was obtained. The same *rectangle* is shown in **a-c**. The three *dashed lines* inside the rectangle show the perpendicular plane in the approximate region where images **e-g** were obtained by FIB/SEM. (**e-g**), Examples of FIB/SEM images that were taken in the z = 9.15 μ m image stack (305 images of 30 nm thickness). Using Reconstruct software, the AxDs (*green*) and the microglial cell (*red*) that were present in the stack of images were segmented every 2 sections. (**h**), 3D visualization of the segmented elements (microglial cell: *red*, AxDs: *green*). There is an activated microglia cell in the region where the loss of a GFP-expressing AxD was observed. Scale bar (in **g**): 18.2 μ m in **a-c**; 5.1 μ m in **d**; 1.8 μ m in **e-h**

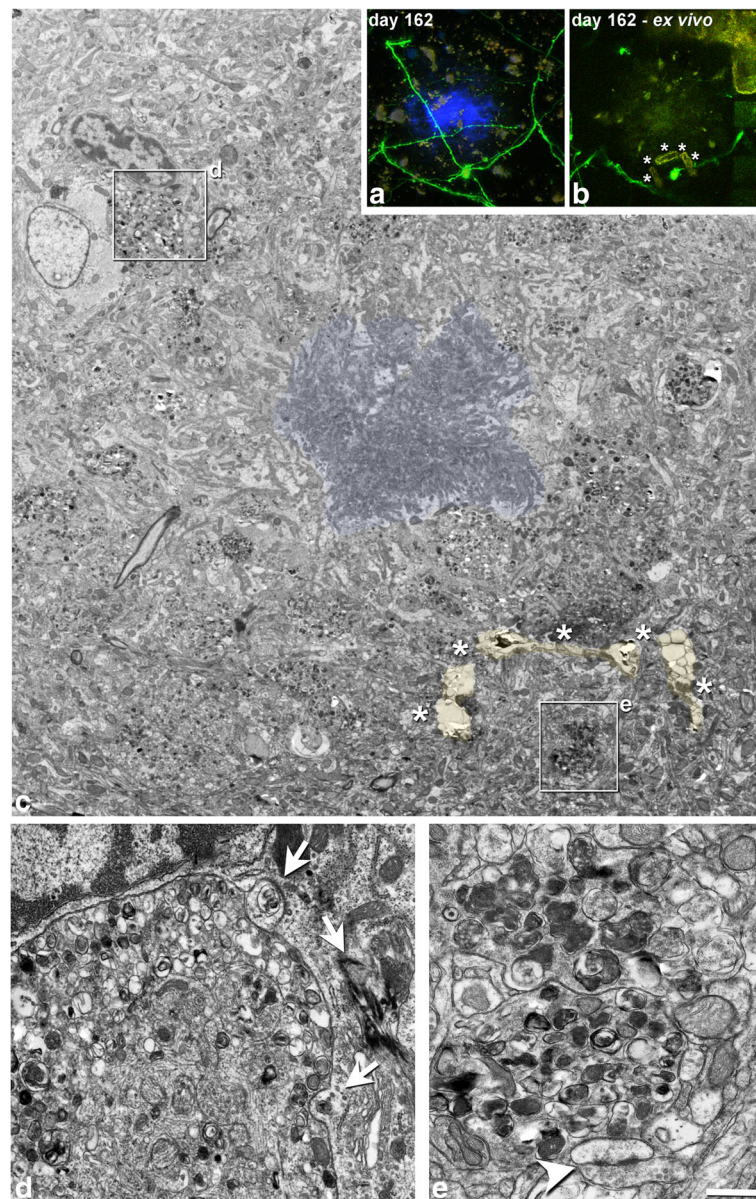


Fig. 7 Correlative two-photon microscopy and TEM of an Aβ plaque. **(a)**, Maximum projection of images taken from a GFP-expressing AxD near an Aβ plaque stained with Methoxy-X04 (blue) on day 162 (the same AxD (dys 7) as in Fig. 1a-c – red arrow). **(b)**, Ex vivo single plane of the AxD (note that some NIRB marks were made around the region of interest to locate it in subsequent processing steps; marks have been labeled with asterisks). **(c)**, Low-magnification electron micrograph showing the Aβ plaque (the central core formed by fibrillar Aβ peptide has been pseudocolored in blue). The GFP-expressing AxD (dys 7) that was imaged in vivo is surrounded by the laser marks (pseudocolored in orange and labeled with asterisks). Rectangles delimit the regions shown at a higher magnification in panels **d**, **e**. **(d)**, Image showing a microglial cell with numerous phagocytic inclusions (arrows) in close apposition to an AxD, suggesting that this cell is participating in phagocytosis of the AxD. Microglial cell was identified based on its ultrastructural characteristics. **(e)**, Higher magnification of dys 7. Note that autophagic vacuoles take up a large area of the AxD contents, and also that the AxD is almost devoid of any normal-looking organelles. A normal-looking asymmetric synapse can be observed in close apposition to the AxD (arrowhead). Scale bar (in **e**): 23.1 μm in **a**, **b**; 3 μm in **c**; 0.61 μm in **d**; 0.52 μm in **e**

period —only 15% of them were present from the first day of imaging (day 100). At the end of the imaging period, around 70% of AxDs had been lost, in most cases due to the disappearance of the whole axon (76%) (Fig. 8f, Additional file 6 a-f).

Discussion

In our study, we observed that around 22 and 28% of the axons adjacent to Aβ plaques developed dystrophic pathology in the dE9 and APP-PS1, respectively. This is an interesting finding since it indicates that most of the

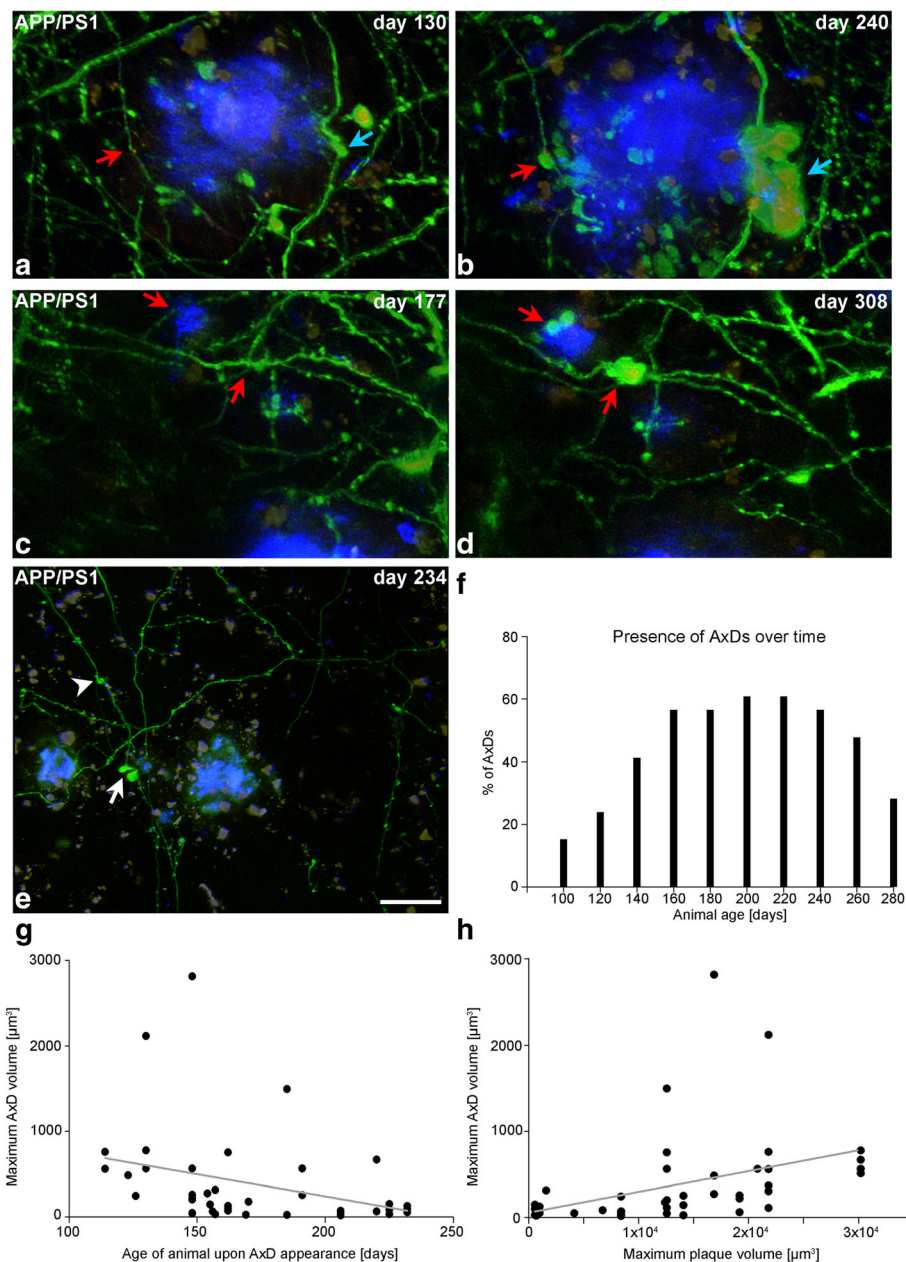


Fig. 8 Relationship between A β plaques and AxDs formation and development. **(a, b)**, Maximum projection of images (120 images, $z = 0.3 \mu\text{m}$) showing the presence of a large AxD (blue arrow) and a small AxD (red arrow) (GFP, green) close to a large plaque stained with Methoxy-X04 (blue) **(b)**. Note that the larger AxD starts to develop around day 130 (animal age). **(c, d)**, Maximum projection of images (120 images, $z = 0.3 \mu\text{m}$) showing the presence of smaller AxDs (red arrows) (GFP, green) close to a small A β plaque stained with Methoxy-X04 (blue) **(d)**. These two smaller AxDs appear around day 232 (animal age). **(c)**, Panoramic images that show the regions in panels **a - d** are in the Additional file 6. **(e)**, Maximum projection of images (134 images, $z = 0.3 \mu\text{m}$) showing GFP-expressing neurites and A β plaques stained with Methoxy-X04 (blue). There is an axon with two AxDs: one small AxD that is not associated with A β plaques (arrowhead), and another which is close to an A β plaque stained with Methoxy-X04 (arrow). The days shown refer to the animal age (the imaging began on day 100 of the animal lifetime). **(f)**, Graph showing the percentage of the total number of AxDs ($n = 47$) that are present over time. Days in X correspond to the bin center (bin width = 20 days). **(g)**, Correlation (Spearman $r = -0.4711$, $p = 0.0022$) between the maximum AxD volume and the day of AxD appearance, indicating that larger AxDs develop earlier than smaller AxDs in the animal lifetime. **(h)**, Correlation (Spearman $r = 0.6173$, $p < 0.0001$) between the maximum volume that an AxD reaches and the maximum volume of the A β plaque it is associated with. Large AxDs are present only around large A β plaques. Scale bar (in **e**): $25.1 \mu\text{m}$ in **a-d**; $28.4 \mu\text{m}$ in **e**

axons near the A β plaques are resistant to this pathology. Thus, this raises the question as to why some axons (a minority) seem to be more susceptible than others to the dystrophic pathology.

Using the GFP-M model, it was possible to analyze supragranular layers axons which have been reported [16] to originate mainly from neurons whose soma are located in cortical layers II/III/V (type A3 axon), layer VI (type A2 axon) and thalamus (type A1 axon). These axons are morphologically very similar to thin-EPB, TB and thick-EPB axons, respectively, as defined in the present study. In previous *in vivo* studies regarding bouton turnover in axons present in layer I of the mouse barrel cortex, it was found that axons from layer VI were highly plastic, followed by axons from layer II/III/V that showed intermediate levels of plasticity and thalamocortical axons in which most of the boutons were persistent [16]. In the present study, we found dystrophic pathology in all these types of axons. However, the majority of axons in contact with A β plaques did not develop AxDs. In this regard, it is important to take into account that pyramidal neurons from different layers and even those located in the same layer have different morphological, neurochemical and physiological properties (e.g., [54]). Thus, it is possible that particular types of neurons located in layers II/III/V, layer VI and in the thalamus are more susceptible to developing dystrophic pathology. Indeed, previous studies mainly using a variety of neurochemical markers showed that there are some subpopulations of neurons selectively vulnerable to the AxD development, e.g., those cortico-cortical fibers that express SMI-312 and GAP-43 [37], or neurofilament triplet proteins (NF) [18, 44]. Furthermore, we analyzed only the supragranular layers and it is possible that the susceptibility of the axons in contact with A β plaques in layers IV to VI is different to the observations in the present study in the supragranular layers. Thus, further studies are necessary to identify the subpopulation(s) of pyramidal cells that are more susceptible to this pathology.

The relationship between the formation of extracellular A β deposits and their associated AxDs remains elusive. For years it has been considered that the formation of AxDs was a consequence of A β deposits or microglia activation, but not an active participant in the pathogenesis of the A β plaques (see [20]). However, this view is changing and there are increasing data suggesting that beta-secretase 1 (BACE1) elevation and associated A β overproduction occurs inside the AxDs [26, 27, 46, 55, 64] (see Additional file 8). Moreover, A β is a possible cause of the alterations in axonal transport [50]. If a partial transport defect allows more time for axonal APP processing as suggested [55], then this could generate more A β , feeding back into a worsening transport defect and progressive enlargement of both A β

plaques and AxDs. These facts—together with anomalous mitochondrial function and oxidative stress, autophagy and altered lysosomal processing considered in synthesis with the mechanisms of disrupted axonal transport—suggest that AxDs are an important source of extracellular amyloid deposits (see [20]). The plaque induction of neuritic changes and the contribution of AxDs to A β deposition are probably not mutually exclusive and could occur concomitantly even in the same AxD.

Several authors have also contributed to the *in vivo* study of AxDs, providing information about their formation near A β plaques and their probability of recovery after different treatments [13, 15, 23, 53, 59]. However, in these studies, the pathology was followed over relatively short time periods (3 days to 5 weeks maximum) and no detailed morphometric studies were performed. Plasticity and axonal sprouting has been observed around amyloid plaques performing *in vitro* and *ex vivo* studies using different IHC markers (e.g., GAP-43) ([38, 40, 47, 49, 65] see [5] for a review). The existence of many growth factors around the A β plaques has been studied and sprouting has been proposed as a compensatory mechanism for the synaptic alterations that take place near A β plaques [39, 45, 63]. However, this plasticity phenomenon had not been detailed described and quantified *in vivo* to date. An important advantage of our study was that the AxDs were followed over long periods of time (up to 210 days). A great number of axonal segments were followed and AxDs were studied individually to further analyze the heterogeneous changes between different AxDs and in the same AxD over time (plasticity of AxDs). The individual study of the axons and their dystrophies was possible by means of the GFP-M transgenic model that has a low density of neurons expressing GFP. Moreover, the use of specialized tools allowed the performance of 3D reconstruction and measurement of volumes to carry out a detailed quantitative study. Most AxDs were formed and developed during the imaging period, and numerous AxDs had already disappeared by the end of this period (Additional file 9). We were able to observe that AxDs had long lifetimes (commonly more than 100 days). In the APP-PS1 mouse, amyloid pathology and related dystrophic neuritic changes around the A β plaques developed earlier than in the dE9 mouse (A β plaque deposition in the neocortex begins around the age of 6 months in the dE9 [30] and 2 months in the APP-PS1 mouse [48]). However, we observed in both models similar findings regarding the high AxD plasticity over time. The most important observations are the following: i) AxDs did not grow steadily—their volume increased and decreased over time, showing dramatic volume differences at distinct time points; ii) AxDs located at the end of the axon could also become fully reversed while the parental axon remained

and a new AxD could be generated after a variable period of time; iii) Axonal sprouting was a common event: prominent morphological changes occurred in larger AxDs over time and interestingly the re-growth of long axonal segments from axons that were cut at a dystrophic point was observed in the APP-PS1 mouse. This is interesting since it has been recently observed in vivo that, depending on the cell type, some ablated axons spontaneously re-grow and although they never reconnect to their original targets, axons consistently form new boutons at comparable pre-lesion synaptic densities, implying the existence of intrinsic homeostatic programs, which regulate synaptic numbers on regenerating axons [14]. We cannot rule out the possibility that the absence of this phenomenon in dE9 could suggest that the sample size was not sufficient, or an intrinsic difference of the amyloid pathology between the two mouse lines.

Taking these results together, the existence of this neuronal plasticity (especially around A β plaques) increases the likelihood that the synaptic abnormalities associated with the A β plaques can be reversed within a certain time window before most AxDs and their axons have disappeared. Thus, this opens up the possibility that early prevention or elimination of the A β plaques with appropriate therapeutic strategies might prevent disease progression and promote functional axon regeneration and the recovery of neural circuits.

Conclusion

AxDs were formed only in a quarter of GFP-expressing axons near A β -plaques, which indicates a selective vulnerability. AxDs, especially those reaching larger sizes, had long lifetimes and appeared as highly plastic structures with large variations in size and shape and axonal sprouting over time. We observed that most AxDs were formed and developed during the imaging period, and numerous AxDs had already disappeared by the end of this time. This work is the first in vivo study analyzing quantitatively the high plasticity of the axonal pathology around A β plaques. We hypothesized that a therapeutically early prevention of A β plaque formation or their growth might halt disease progression and promote functional axon regeneration and the recovery of neural circuits.

Additional files

Additional file 1: Figure S1. Location of auto-fluorescent spots. (PDF 371 kb)

Additional file 2: Table S1. Table showing the number of imaging positions that was successfully imaged weekly during near 6 months. (PDF 260 kb)

Additional file 3: Figure S2. Correlative light and FIB/SEM microscopy. (PDF 317 kb)

Additional file 4: Figure S3. Size ratio of dystrophic segments. (PDF 393 kb)

Additional file 5: Figure S4. Re-formation of AxDs and sprouting phenomenon (re-growth) in the APP-PS1 mouse. (PDF 341 kb)

Additional file 6: Figure S5. Relationship between A β plaques and AxDs formation and development. Quantitative analysis of different types of A β plaques. (PDF 463 kb)

Additional file 7: Figure S6. Behavior of auto-fluorescent spots after the elimination of an AxD. (PDF 204 kb)

Additional file 8: Figure S7. Quantitative study of the neurochemical characteristics of the AxDs. (PDF 351 kb)

Additional file 9: Figure S8. Schematic representation of A β plaques and AxDs development over time. (PDF 200 kb)

Abbreviations

3D: Three-dimensional; AD: Alzheimer's disease; APP-PS1: Amyloid Precursor Protein – Preseniline 1; AxDs: Axonal dystrophies; A β : Amyloid β ; BP: Bandpass; EPB: En Passant Bouton axons; FIB/SEM: Focused ion beam/scanning electron microscopy; GFP-M: Green fluorescent protein – M; NFTs: Neurofibrillary tangles; NIRB: Near infrared branding; SP: Short pass; TB: Terminal Bouton axons; TEM: Transmission electron microscopy

Acknowledgment

We would like to thank Matthias Jucker who kindly provided the APP-PS1 mice used in this study.

Funding

The work was supported by grants from the Spanish Ministry of Economy and Competitiveness (MINECO) (BFU2012-34963 to JF), the Centre for Networked Biomedical Research on Neurodegenerative Diseases (CIBERNED, CB06/05/0066) (to JF), a grant from the Alzheimer's Association (ZEN-15-321663) (to JF) and the Humboldt Research Fellowship for Postdoctoral Researchers (LBL).

Availability of data and materials

The datasets used and/or analysed during the current study available from the corresponding author on reasonable request.

Authors' contributions

LBL: Conception or design of the work, Data collection, Data analysis and interpretation, Drafting the article, Critical revision of the article, Final approval of the version to be published. SVF: Data collection, Data analysis and interpretation, Critical revision of the article. EFR: Data collection, Data analysis and interpretation, Critical revision of the article. AMP: Data collection, Data analysis and interpretation, Critical revision of the article. JRR: Data collection, Data analysis and interpretation, Critical revision of the article. MMD: Critical revision of the article. JF: Critical revision of the article, Final approval of the version to be published. JH: Critical revision of the article, Final approval of the version to be published. All authors read and approved the final manuscript.

Competing interests

The authors declare that they have no competing interests.

Consent for publication

Not applicable.

Ethics approval and consent to participate

Not applicable.

Author details

¹German Center for Neurodegenerative Diseases-Munich site (DZNE-M) and Center for Neuropathology and Prion Research (ZNP), Ludwig-Maximilians University, Munich, Feodor-Lynen-St 23, 81377 Munich, Germany.

²Laboratorio Cajal de Circuitos Corticales, Centro de Tecnología Biomédica, Universidad Politécnica de Madrid, Madrid, Spain. ³Departamento de Arquitectura y Tecnología de Sistemas Informáticos, Escuela Técnica Superior de Ingenieros Informáticos, Universidad Politécnica de Madrid, Madrid, Spain.

⁴Instituto Cajal, Consejo Superior de Investigaciones Científicas, Madrid, Spain. ⁵Centro de Investigación Biomédica en Red sobre Enfermedades Neurodegenerativas (CIBERNED), ISCIII, Madrid, Spain. ⁶Munich Cluster of

Systems Neurology (SyNergy), Ludwig-Maximilians University, Munich, Germany. ⁷Departamento de Psicobiología, Facultad de Psicología, Universidad Nacional de Educación a Distancia (UNED), C/Juan del Rosal 10, 28040 Madrid, Spain.

Received: 12 December 2016 Accepted: 26 January 2017

Published online: 07 February 2017

References

- Alzheimer A (1907) Über eine eigenartige Erkrankung der Hirnrinde. *Allgemeine Zeitschrift für Psychiatrie und Psychisch-gerichtliche Medizin* 64:146–148
- Adalbert R, Nogradi A, Babetto E, Janeckova L, Walker SA, Kerschensteiner M, Misgeld T, Coleman MP (2009) Severely dystrophic axons at amyloid plaques remain continuous and connected to viable cell bodies. *Brain J Neurol* 132:402–416
- Alpar A, Ueberham U, Bruckner MK, Seeger G, Arendt T, Gartner U (2006) Different dendrite and dendritic spine alterations in basal and apical arbors in mutant human amyloid precursor protein transgenic mice. *Brain Res* 1099:189–198
- Alpar A, Ueberham U, Seeger G, Arendt T, Gartner U (2007) Effects of wild-type and mutant human amyloid precursor protein on cortical afferent network. *Neuroreport* 18:1247–1250
- Arendt T (2001) Alzheimer's disease as a disorder of mechanisms underlying structural brain self-organization. *Neuroscience* 102:723–765
- Arendt T (2009) Synaptic degeneration in Alzheimer's disease. *Acta Neuropathol* 118:167–179
- Bishop D, Nikic I, Brinkoetter M, Knecht S, Potz S, Kerschensteiner M, Misgeld T (2011) Near-infrared branding efficiently correlates light and electron microscopy. *Nat Methods* 8:568–570
- Bittner T, Burgold S, Dorostkar MM, Fuhrmann M, Wegenast-Braun BM, Schmidt B, Kretschmar H, Herms J (2012) Amyloid plaque formation precedes dendritic spine loss. *Acta Neuropathol* 124:797–807
- Bittner T, Fuhrmann M, Burgold S, Ochs SM, Hoffmann N, Mitteregger G, Kretschmar H, LaFerla FM, Herms J (2010) Multiple events lead to dendritic spine loss in triple transgenic Alzheimer's disease mice. *PLoS One* 5:e15477
- Blanchard V, Moussaoui S, Czech C, Touchet N, Bonici B, Planche M, Canton T, Jedidi I, Gohin M, Wirths O et al (2003) Time sequence of maturation of dystrophic neurites associated with Abeta deposits in APP/PS1 transgenic mice. *Exp Neurol* 184:247–263
- Blazquez-Llorca L, Hummel E, Zimmerman H, Zou C, Burgold S, Rietdorf J, Herms J (2015) Correlation of two-photon in vivo imaging and FIB/SEM microscopy. *J Microsc* 259:129–136
- Braak H, Thal DR, Ghebremedhin E, Del Tredici K (2011) Stages of the pathologic process in Alzheimer disease: age categories from 1 to 100 years. *J Neuropathol Exp Neurol* 70:960–969
- Brendza RP, Bacskai BJ, Cirrito JR, Simmons KA, Skoch JM, Klunk WE, Mathis CA, Bales KR, Paul SM, Hyman BT et al (2005) Anti-Abeta antibody treatment promotes the rapid recovery of amyloid-associated neuritic dystrophy in PDAPP transgenic mice. *J Clin Invest* 115:428–433
- Canty AJ, Huang L, Jackson JS, Little GE, Knott G, Maco B, De Paola V (2013) In-vivo single neuron axotomy triggers axon regeneration to restore synaptic density in specific cortical circuits. *Nat Commun* 4:2038
- D'Amore JD, Kajdasz ST, McLellan ME, Bacskai BJ, Stern EA, Hyman BT (2003) In vivo multiphoton imaging of a transgenic mouse model of Alzheimer disease reveals marked thioflavine-S-associated alterations in neurite trajectories. *J Neuropathol Exp Neurol* 62:137–145
- De Paola V, Holtmaat A, Knott G, Song S, Wilbrecht L, Caroni P, Svoboda K (2006) Cell type-specific structural plasticity of axonal branches and boutons in the adult neocortex. *Neuron* 49:861–875
- DeFelipe J, Fairen A (1993) A simple and reliable method for correlative light and electron microscopic studies. *J Histochem Cytochem* 41:769–772
- Dickson TC, King CE, McCormack GH, Vickers JC (1999) Neurochemical diversity of dystrophic neurites in the early and late stages of Alzheimer's disease. *Exp Neurol* 156:100–110
- Feng G, Mellor RH, Bernstein M, Keller-Peck C, Nguyen QT, Wallace M, Nerbonne JM, Lichtman JW, Sanes JR (2000) Imaging neuronal subsets in transgenic mice expressing multiple spectral variants of GFP. *Neuron* 28:41–51
- Fiala JC (2007) Mechanisms of amyloid plaque pathogenesis. *Acta Neuropathol* 114:551–571
- Fiala JC (2005) Reconstruct: a free editor for serial section microscopy. *J Microsc* 218:52–61
- Fuhrmann M, Mitteregger G, Kretschmar H, Herms J (2007) Dendritic pathology in prion disease starts at the synaptic spine. *J Neurosci Off J Soc Neurosci* 27:6224–6233
- Garcia-Alloza M, Borrelli LA, Rozkalne A, Hyman BT, Bacskai BJ (2007) Curcumin labels amyloid pathology in vivo, disrupts existing plaques, and partially restores distorted neurites in an Alzheimer mouse model. *J Neurochem* 102:1095–1104
- Geddes JW, Anderson KJ, Cotman CW (1986) Senile plaques as aberrant sprout-stimulating structures. *Exp Neurol* 94:767–776
- Geddes JW, Monaghan DT, Cotman CW, Lott IT, Kim RC, Chui HC (1985) Plasticity of hippocampal circuitry in Alzheimer's disease. *Science* 230:1179–1181
- Gouras GK, Tampellini D, Takahashi RH, Capetillo-Zarate E (2010) Intraneuronal beta-amyloid accumulation and synapse pathology in Alzheimer's disease. *Acta Neuropathol* 119:523–541
- Gouras GK, Willen K, Faideau M (2014) The inside-out amyloid hypothesis and synapse pathology in Alzheimer's disease. *Neurodegener Dis* 13:142–146
- Grutzendler J, Helmin K, Tsai J, Gan WB (2007) Various dendritic abnormalities are associated with fibrillar amyloid deposits in Alzheimer's disease. *Ann N Y Acad Sci* 1097:30–39
- Hof PR, Young WG, Bloom FE, Belichenko PV, Celio MR. Comparative cytoarchitectonic atlas of the C57Bl/6 and 129/SV mouse brains. 2000. Elsevier, New York City
- Jankowsky JL, Slunt HH, Gonzales V, Jenkins NA, Copeland NG, Borchelt DR (2004) APP processing and amyloid deposition in mice haplo-insufficient for presenilin 1. *Neurobiol Aging* 25:885–892
- Klunk WE, Bacskai BJ, Mathis CA, Kajdasz ST, McLellan ME, Frosch MP, Debnath ML, Holt DP, Wang Y, Hyman BT (2002) Imaging Abeta plaques in living transgenic mice with multiphoton microscopy and methoxy-X04, a systemically administered Congo red derivative. *J Neuropathol Exp Neurol* 61:797–805
- Knafo S, Alonso-Nanclares L, Gonzalez-Soriano J, Merino-Serrais P, Feraud-Espinosa I, Ferrer I, DeFelipe J (2009) Widespread changes in dendritic spines in a model of Alzheimer's disease. *Cereb Cortex* 19:586–592
- Knafo S, Venero C, Merino-Serrais P, Feraud-Espinosa I, Gonzalez-Soriano J, Ferrer I, Santpere G, DeFelipe J (2009) Morphological alterations to neurons of the amygdala and impaired fear conditioning in a transgenic mouse model of Alzheimer's disease. *J Pathol* 219:41–51
- Koffie RM, Meyer-Luehmann M, Hashimoto T, Adams KW, Mielke ML, Garcia-Alloza M, Micheva KD, Smith SJ, Kim ML, Lee VM et al (2009) Oligomeric amyloid beta associates with postsynaptic densities and correlates with excitatory synapse loss near senile plaques. *Proc Natl Acad Sci U S A* 106:4012–4017
- Luebke JI, Weaver CM, Rocher AB, Rodriguez A, Crimins JL, Dickstein DL, Wearne SL, Hof PR (2010) Dendritic vulnerability in neurodegenerative disease: insights from analyses of cortical pyramidal neurons in transgenic mouse models. *Brain Struct Funct* 214:181–199
- Masliah E, Alford M, Adame A, Rockenstein E, Galasko D, Salmon D, Hansen LA, Thal LJ (2003) Abeta1-42 promotes cholinergic sprouting in patients with AD and Lewy body variant of AD. *Neurology* 61:206–211
- Masliah E, Mallory M, Deerinc T, DeTeresa R, Lamont S, Miller A, Terry RD, Carragher B, Ellisman M (1993) Re-evaluation of the structural organization of neuritic plaques in Alzheimer's disease. *J Neuropathol Exp Neurol* 52:619–632
- Masliah E, Mallory M, Hansen L, Alford M, Albright T, DeTeresa R, Terry R, Baudier J, Saitoh T (1991) Patterns of aberrant sprouting in Alzheimer's disease. *Neuron* 6:729–739
- Masliah E, Xie F, Dayan S, Rockenstein E, Mante M, Adame A, Patrick CM, Chan AF, Zheng B (2010) Genetic deletion of Nogo/Rtn4 ameliorates behavioral and neuropathological outcomes in amyloid precursor protein transgenic mice. *Neuroscience* 169:488–494
- McKinney RA, Debanne D, Gahwiler BH, Thompson SM (1997) Lesion-induced axonal sprouting and hyperexcitability in the hippocampus in vitro: implications for the genesis of posttraumatic epilepsy. *Nat Med* 3:990–996
- Merchan-Perez A, Rodriguez JR, Alonso-Nanclares L, Schertel A, Defelipe J (2009) Counting synapses using FIB/SEM microscopy: a true revolution for ultrastructural volume reconstruction. *Front Neuroanat* 3:18
- Merino-Serrais P, Benavides-Piccione R, Blazquez-Llorca L, Kastanauskaitė A, Rabano A, Avila J, DeFelipe J (2013) The influence of phospho-tau on dendritic spines of cortical pyramidal neurons in patients with Alzheimer's disease. *Brain J Neurol* 136:1913–1928
- Merino-Serrais P, Knafo S, Alonso-Nanclares L, Feraud-Espinosa I, DeFelipe J (2011) Layer-specific alterations to CA1 dendritic spines in a mouse model of Alzheimer's disease. *Hippocampus* 21:1037–1044

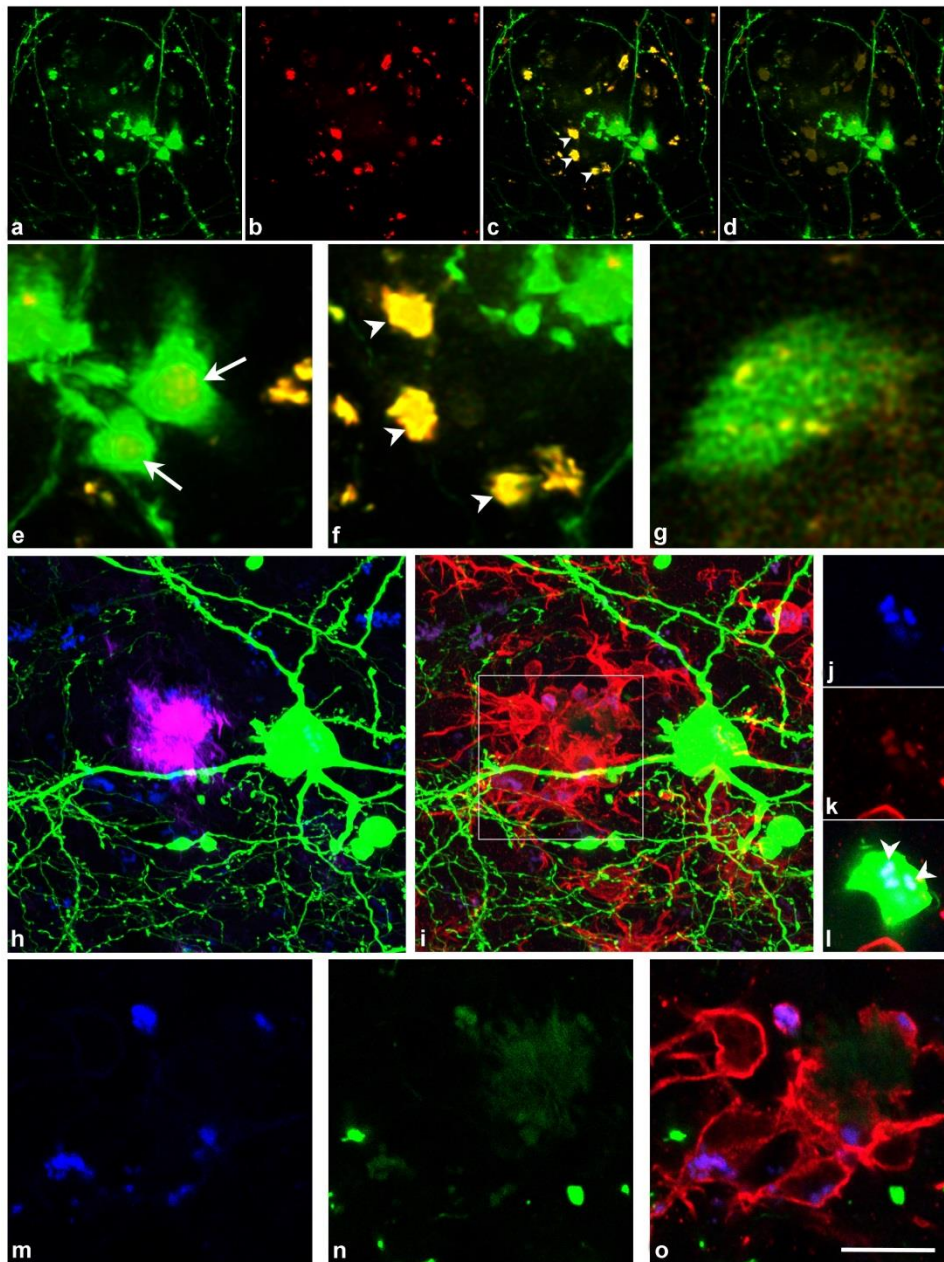
44. Mitew S, Kirkcaldie MT, Dickson TC, Vickers JC (2013) Neurites containing the neurofilament-triplet proteins are selectively vulnerable to cytoskeletal pathology in Alzheimer's disease and transgenic mouse models. *Front Neuroanat* 7:30
45. Nelson AR, Kolasa K, McMahon LL (2014) Noradrenergic sympathetic sprouting and cholinergic reinnervation maintains non-amyloidogenic processing of Aβ. *J Alzheimers Dis* 38:867–879
46. Nixon RA (2006) Autophagy in neurodegenerative disease: friend, foe or turncoat? *Trends Neurosci* 29:528–535
47. Phinney AL, Deller T, Stalder M, Calhoun ME, Frotscher M, Sommer B, Staufenbiel M, Jucker M (1999) Cerebral amyloid induces aberrant axonal sprouting and ectopic terminal formation in amyloid precursor protein transgenic mice. *J Neurosci Off J Soc Neurosci* 19:8552–8559
48. Radde R, Bolmont T, Kaeser SA, Coomaraswamy J, Lindau D, Stoltze L, Calhoun ME, Jaggi F, Wolburg H, Gengler S et al (2006) Aβ42-driven cerebral amyloidosis in transgenic mice reveals early and robust pathology. *EMBO Rep* 7:940–946
49. Roisen FJ, Bartfeld H, Nagele R, Yorke G (1981) Ganglioside stimulation of axonal sprouting in vitro. *Science* 214:577–578
50. Rui Y, Tiwari P, Xie Z, Zheng JQ (2006) Acute impairment of mitochondrial trafficking by beta-amyloid peptides in hippocampal neurons. *J Neurosci Off J Soc Neurosci* 26:10480–10487
51. Sanchez-Varo R, Trujillo-Estrada L, Sanchez-Mejias E, Torres M, Baglietto-Vargas D, Moreno-Gonzalez I, De Castro V, Jimenez S, Ruano D, Vizuete M et al (2012) Abnormal accumulation of autophagic vesicles correlates with axonal and synaptic pathology in young Alzheimer's mice hippocampus. *Acta Neuropathol* 123:53–70
52. Spires-Jones TL, Meyer-Luehmann M, Osetek JD, Jones PB, Stern EA, Bacskai BJ, Hyman BT (2007) Impaired spine stability underlies plaque-related spine loss in an Alzheimer's disease mouse model. *Am J Pathol* 171:1304–1311
53. Spires TL, Meyer-Luehmann M, Stern EA, McLean PJ, Skoch J, Nguyen PT, Bacskai BJ, Hyman BT (2005) Dendritic spine abnormalities in amyloid precursor protein transgenic mice demonstrated by gene transfer and intravital multiphoton microscopy. *J Neurosci Off J Soc Neurosci* 25:7278–7287
54. Spruston N (2008) Pyramidal neurons: dendritic structure and synaptic integration. *Nat Rev Neurosci* 9:206–221
55. Stokin GB, Lillo C, Falzone TL, Brusch RG, Rockenstein E, Mount SL, Raman R, Davies P, Masliah E, Williams DS et al (2005) Axonopathy and transport deficits early in the pathogenesis of Alzheimer's disease. *Science* 307:1282–1288
56. Streit WJ, Kreutzberg GW (1988) Response of endogenous glial cells to motor neuron degeneration induced by toxic ricin. *J Comp Neurol* 268:248–263
57. Su JH, Cummings BJ, Cotman CW (1993) Identification and distribution of axonal dystrophic neurites in Alzheimer's disease. *Brain Res* 625:228–237
58. Su JH, Cummings BJ, Cotman CW (1998) Plaque biogenesis in brain aging and Alzheimer's disease. II. Progressive transformation and developmental sequence of dystrophic neurites. *Acta Neuropathol* 96:463–471
59. Tsai J, Grutzendler J, Duff K, Gan WB (2004) Fibrillar amyloid deposition leads to local synaptic abnormalities and breakage of neuronal branches. *Nat Neurosci* 7:1181–1183
60. Vickers JC, Chin D, Edwards AM, Sampson V, Harper C, Morrison J (1996) Dystrophic neurite formation associated with age-related beta amyloid deposition in the neocortex: clues to the genesis of neurofibrillary pathology. *Exp Neurol* 141:1–11
61. Vickers JC, King AE, Woodhouse A, Kirkcaldie MT, Staal JA, McCormack GH, Blizzard CA, Musgrove RE, Mitew S, Liu Y et al (2009) Axonopathy and cytoskeletal disruption in degenerative diseases of the central nervous system. *Brain Res Bull* 80:217–223
62. Woodhouse A, Vickers JC, Adlard PA, Dickson TC (2009) Dystrophic neurites in TgCRND8 and Tg2576 mice mimic human pathological brain aging. *Neurobiol Aging* 30:864–874
63. Zhan SS, Kamphorst W, Van Nostrand WE, Eikelenboom P (1995) Distribution of neuronal growth-promoting factors and cytoskeletal proteins in altered neurites in Alzheimer's disease and non-demented elderly. *Acta Neuropathol* 89:356–362
64. Zhang XM, Cai Y, Xiong K, Cai H, Luo XG, Feng JC, Clough RW, Struble RG, Patrylo PR, Yan XX (2009) Beta-secretase-1 elevation in transgenic mouse models of Alzheimer's disease is associated with synaptic/axonal pathology and amyloidogenesis: implications for neuritic plaque development. *Eur J Neurosci* 30:2271–2283
65. Zhang XM, Xiong K, Cai Y, Cai H, Luo XG, Feng JC, Clough RW, Patrylo PR, Struble RG, Yan XX (2010) Functional deprivation promotes amyloid plaque pathogenesis in Tg2576 mouse olfactory bulb and piriform cortex. *Eur J Neurosci* 31:710–721

Submit your next manuscript to BioMed Central and we will help you at every step:

- We accept pre-submission inquiries
- Our selector tool helps you to find the most relevant journal
- We provide round the clock customer support
- Convenient online submission
- Thorough peer review
- Inclusion in PubMed and all major indexing services
- Maximum visibility for your research

Submit your manuscript at
www.biomedcentral.com/submit





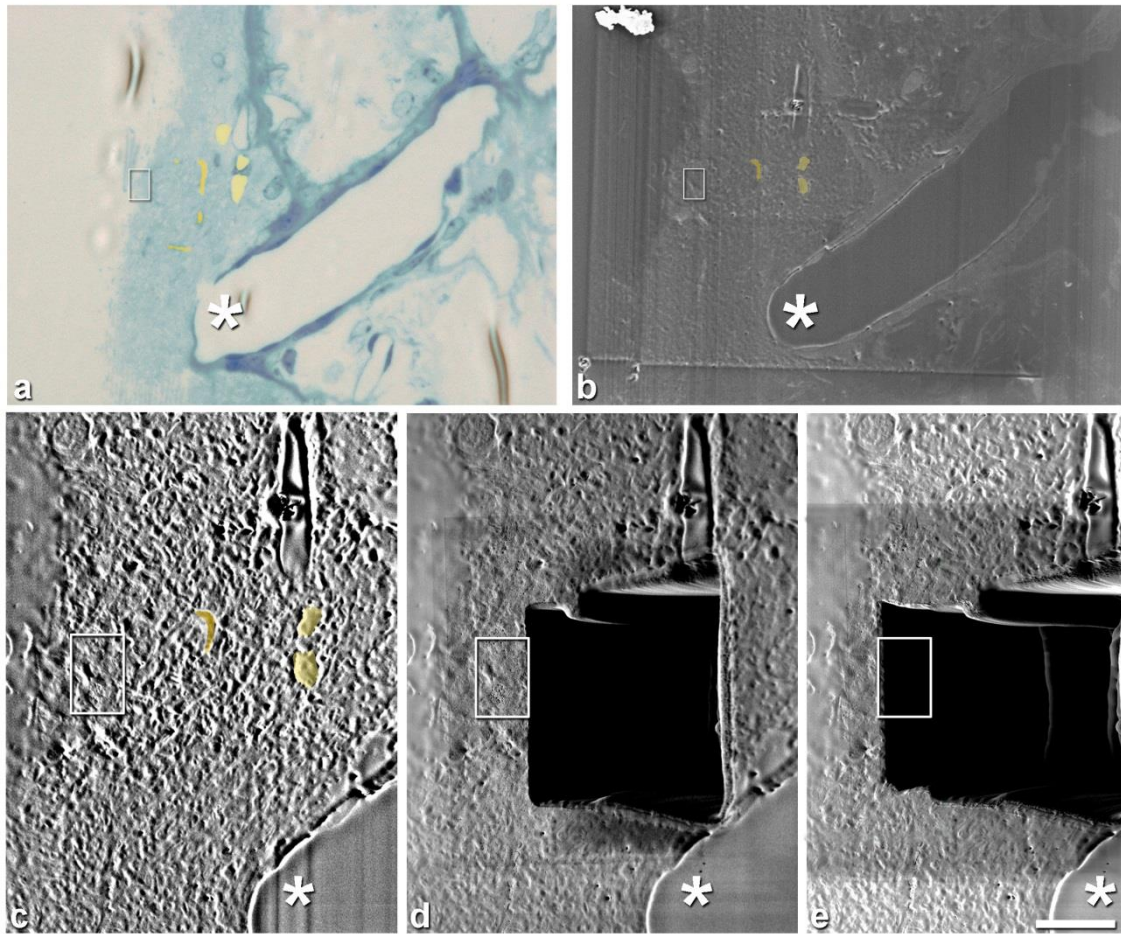
Supplementary Fig. 1 Location of auto-fluorescent spots. (a–d), Two-photon *in vivo* images of the same GFP-expressing AxD (dys 1) around an Aβ plaque stained with Methoxy-X04 (blue) in the somatosensory cortex of the dE9 mouse (the same AxD is shown in Fig. 2). Two-photon excitation of GFP-expressing neuronal structures was performed at 880 nm and the signal was detected using a bandpass (BP) 500–550 nm filter (a). To exclude false positive fluorescent spots from the analysis, we also recorded emissions at 590–650 nm (b). By combining both images, the auto-fluorescent spots can be visualized as yellow structures (arrowheads, the same as in f) (c). When necessary, Photoshop was used to facilitate the visualization of GFP-expressing structures by manually darkening those auto-fluorescent structures that were alone in the neuropil and not inside any GFP-expressing structure (d). (e–g), Higher magnification of two-photon *in vivo* images showing that the auto-fluorescent spots can be inside GFP-expressing AxDs (arrow, e), in the neuropil (arrowheads, f) and inside neuronal cell bodies (lipofuscin, g). (h–o), Immunohistochemistry for Iba-1 (red) was performed to better define the presence of the auto-fluorescence. (h), Maximum projection of images (44 images, $z = 0.4 \mu\text{m}$) showing a GFP-expressing pyramidal neuron and numerous neuronal processes (green) near an Aβ plaque stained with Methoxy-X04 (magenta). The far-red fluorescence was also recorded to facilitate the visualization of auto-fluorescent spots (blue). (i), Same stack of images and field of view as in h adding the fluorescence recorded for Alexa 594 (immunofluorescence of Iba-1, red) and excluding the fluorescence recorded for Methoxy-X04 (Aβ plaque, magenta). (j–l), Single optical section showing a higher magnification of the neuronal body of the pyramidal neuron in (h, i). Auto-fluorescent spots (recorded with far-red fluorescence (j), Alexa 594 (k) and GFP channel (l)) are inside the neuronal cell body (lipofuscin (white), arrowheads) (l). (m–o), Single optical section showing a higher magnification of the region in i that was delimited by a square. Auto-fluorescent spots (arrowheads, recorded with far-red (m), GFP (n) and Alexa 594 channel (o)) are enclosed within microglial processes (red) (o). Scale bar (in o): 25.5 μm in a–d; 5.2 μm in e–g; 12.5 μm in h, i; 6 μm in j–l; 6.3 μm in m–o

Images properties	Aim	Mouse model	Number of imaging positions	Number of time points / Total number of images	Number of dystrophic axons	Total number of axons	Number of A β plaques
High magnification images (logical size 512 \times 512 pixels; physical size x, y, z: 84.9 x 84.9 x 40 μ m; z-step = 1 μ m)	The 3D reconstruction of AxDs over time	dE9 (number of animals, n = 6)	#1	19 / 19	1	6	1
			#2	19 / 19	4	11	1
			#3	19 / 19	1	5	1
			#4	19 / 19	1	8	1
			#5	18 / 18	2	10	1
			#6	18 / 18	1	6	1
			TOTAL	18 - 19 / 112	10	46	6
		APP-PS1 (number of animals, n = 7)	#1	17 / 17	3	9	1
			#2	23 / 23	5	14	1
			#3	23 / 23	3	9	1
			#4	23 / 23	3	11	1
			#5	19 / 19	1	8	1
			#6	19 / 19	1	7	1
			TOTAL	17 - 23 / 124	16	58	6
Panoramic high-resolution images (logical size 1400 \times 1400 pixels; physical size x, y, z: 202.3 x 202.3 x 39.9 μ m; z-step = 0.3 μ m)*	The spatiotemporal relationship between A β plaques and AxDs	APP-PS1 (number of animals, n = 7)	#1	23 / 23	14	-	6
			#2	23 / 23	6	-	4
			#3	23 / 23	3	-	2
			#4	23 / 23	9	-	7
			#5	23 / 23	11	-	6
			#6	21 / 21	4	-	4
			#7	17 / 17	5	-	4
			TOTAL	17 - 23 / 153	52	-	33

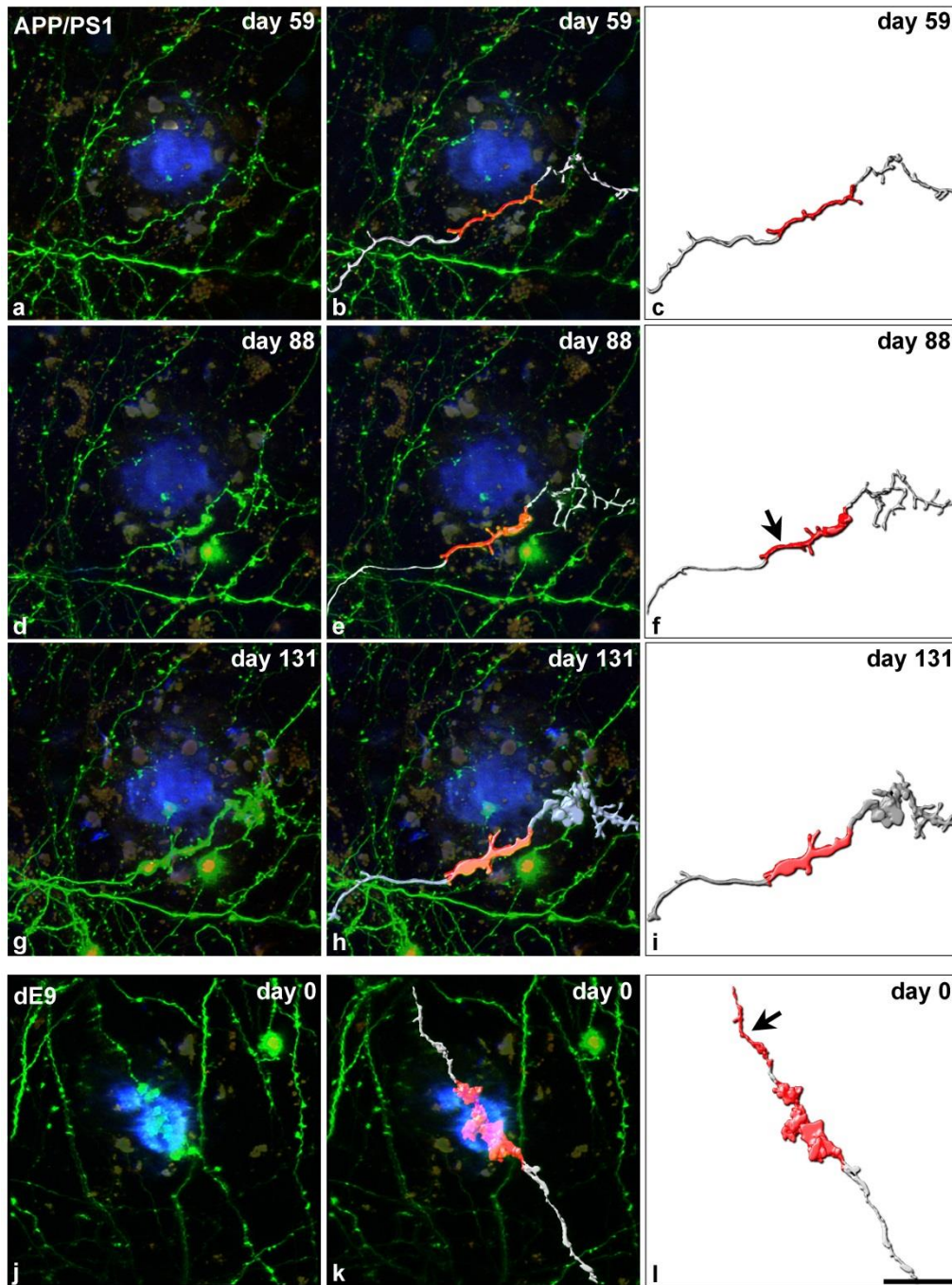
Supplementary Table 1 Table showing the number of imaging positions that was successfully weekly imaged during near 6 months. For each imaging position is also shown: the number of images acquired over time (time points), and the number of dystrophic axons, axons and A β plaques present in each imaging position.

Two types of images were acquired to carry out the aims of the work.

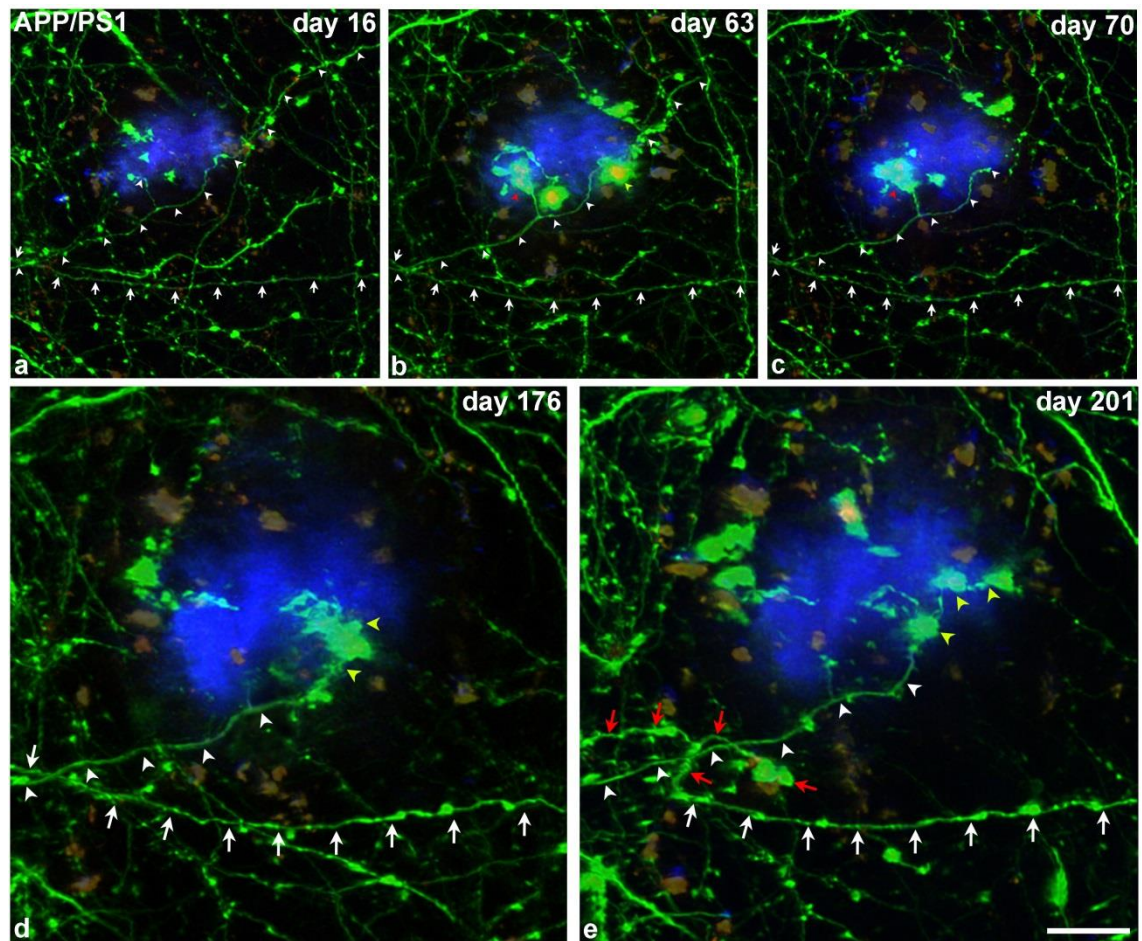
*Note that data from panoramic high-resolution images (lifetime of AxDs and type of axon where AxDs are formed) were also used in Aim “The 3D reconstruction of AxDs over time”.



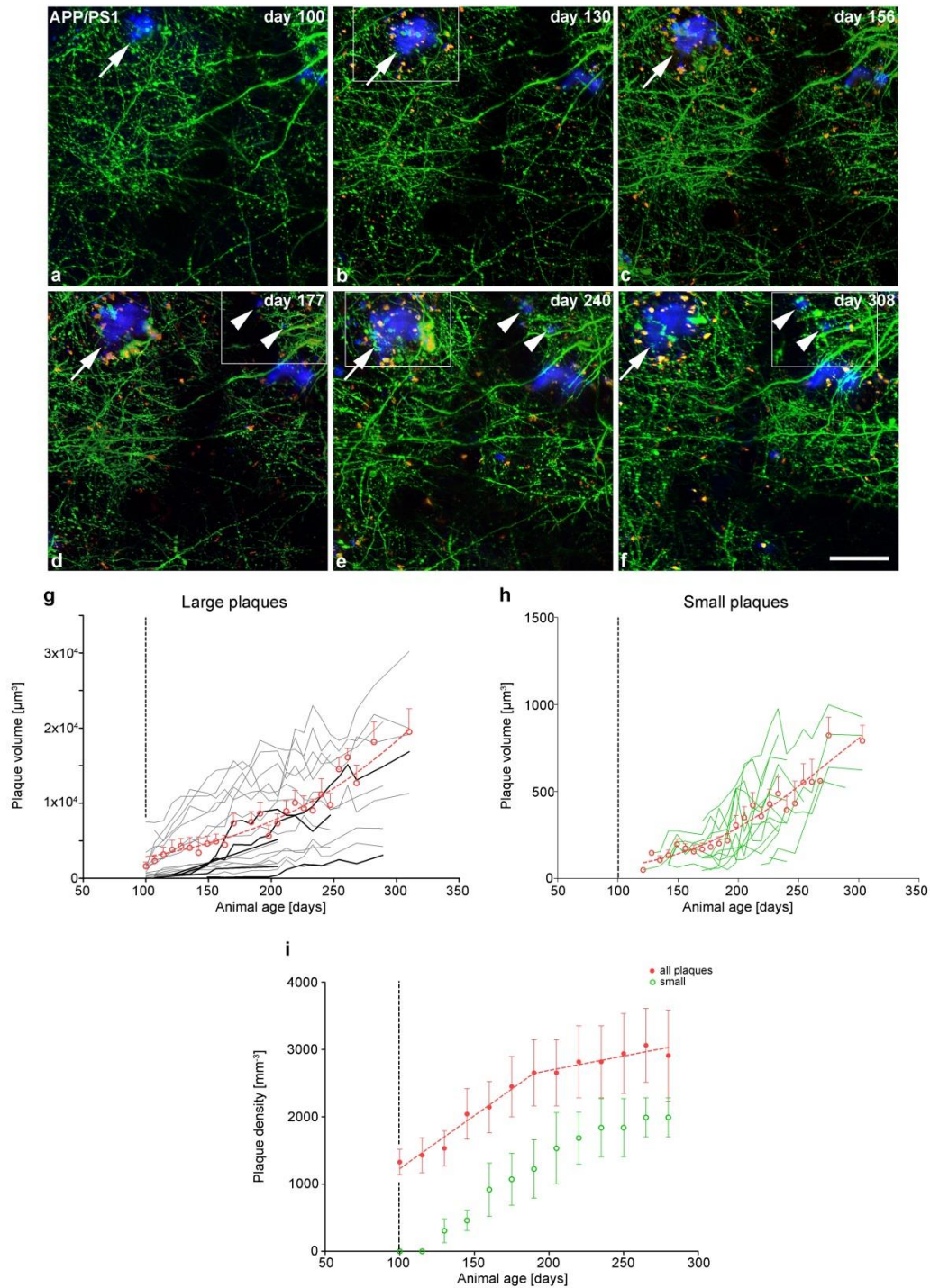
Supplementary Fig. 2 Correlative light and FIB/SEM microscopy. (a), Photograph of the final Toluidine blue stained semithin section that was taken from the surface of the block containing the region of interest shown in Fig. 6 and that was further analyzed using FIB/SEM microscopy. NIRB marks are visible (pseudocolored in yellow and orange; see Fig. 6 c). (b), Same field of view as in a showing the correlative laser marks on the surface of the block used for FIB/SEM (pseudocolored in yellow and orange). (c–d), Higher SEM image magnification of the region of interest (rectangle), before (c) and after (d) milling of the trench needed to obtain back-scattered electron images. d shows the beginning of acquisition of the stack of electron microscopy images and e shows the trench after the region of interest has been fully reconstructed. The rectangle in all images shows the position and the x, z dimensions of the FIB/SEM stack that was obtained. The asterisk points out the same blood vessel. Scale bar (in e): 44.5 μm in a, b; 15 μm in c–e



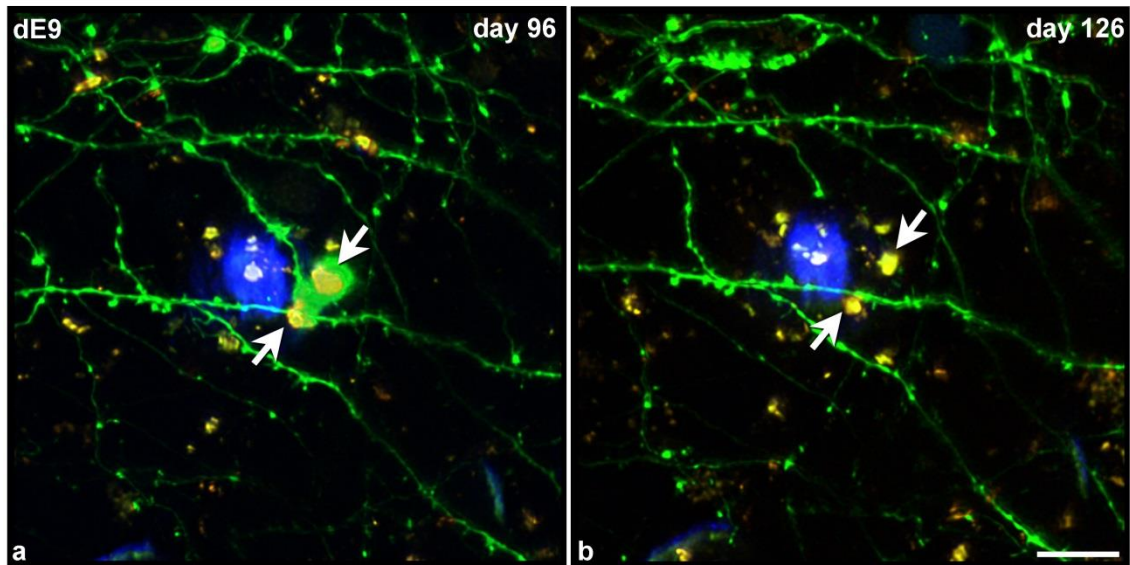
Supplementary Fig. 3 Size ratio of dystrophic segments. (a–i), Two-photon *in vivo* images of a GFP-expressing AxD (dys 7) near an A β plaque stained with Methoxy-X04 (blue) in the somatosensory cortex of the APP-PS1 mouse at three different time points (a, d, g). The axon was reconstructed using Imaris software (b, e, h, respectively). The reconstruction can be observed in isolation in c, f, i, respectively. The dystrophic segment is shown in red. To obtain the size ratio: the “normal axon volume” was determined by taking, if possible, the average volume of 3 axonal segments at three different time points, prior to the AxD formation. Segments were of the same length and in the same position as the maximum AxD segment that will later appear (c). In i, the maximum AxD segment can be observed. Note that in f the region pointed out by the arrow is still non-dystrophic. (j–l), Two-photon *in vivo* images of a GFP-expressing AxD (dys 1) around an A β plaque stained with Methoxy-X04 (blue) in the somatosensory cortex of the dE9 mouse (same as in Fig. 2). The axon was reconstructed using Imaris software (k). The reconstruction can be observed in isolation in l. The dystrophic segment is shown in red, as is the “normal-looking axon segment” (arrow). In those cases where the AxD was present from the first day of imaging, the segments taken as “normal” were those that were from the same normal-looking axon, with the same length as the maximum AxD segment and which were situated outside the A β plaque. Scale bar (in l): 23.1 μ m in a–l



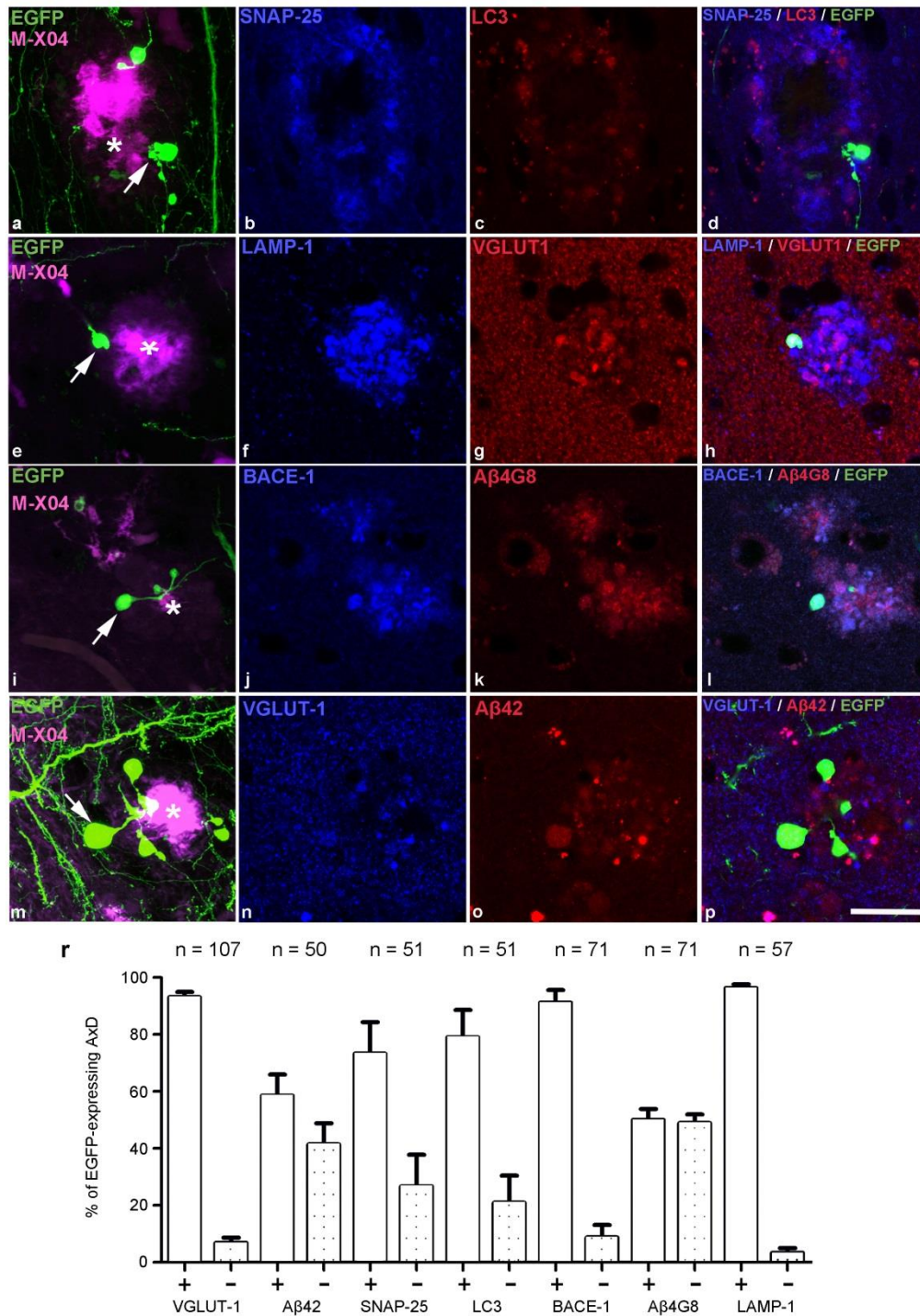
Supplementary Fig. 4 Re-formation of AxDs and sprouting phenomenon (re-growth) in the APP-PS1 mouse. (a–e), Maximum projection of a stack of images (40 images; z-step: 1 μm) taken with the two-photon microscope in the supragranular layers of the somatosensory cortex of the APP-PS1 mouse at five different time points showing some neurites expressing GFP around an A β plaque stained with Methoxy-X04 (blue). There are two axons of interest, one is marked with arrowheads (axon 1) and the other with arrows (axon 2). Axon 1: At the beginning, axon 1 looks normal (a). Days later, the middle part of the axon becomes dystrophic (yellow arrowhead – dys 2a), as does a short branch (red arrowhead – dys 1). Moreover, a distal portion of axon 1 disappears and so the axon as a whole is shortened (b). One week later, the AxD in the middle part has disappeared and axon 1 is cut at this point (c). Days later, the AxD at the short branch (dys 1) has disappeared and another AxD (dys 2b) appears at the edge of axon 1 where dys 2a was previously present (d). The morphology of this AxD changes over time (e). Axon 2: At the beginning, axon 2 looks normal (a–b). Days later, this axon gets thicker (c–d) and, at some point, the axon is cut and then re-grows through the A β plaque. The new re-growth segment (32 μm) becomes dystrophic (e, red arrows). Scale bar (in e): 19.5 μm in a–c; 10.3 μm in d–e



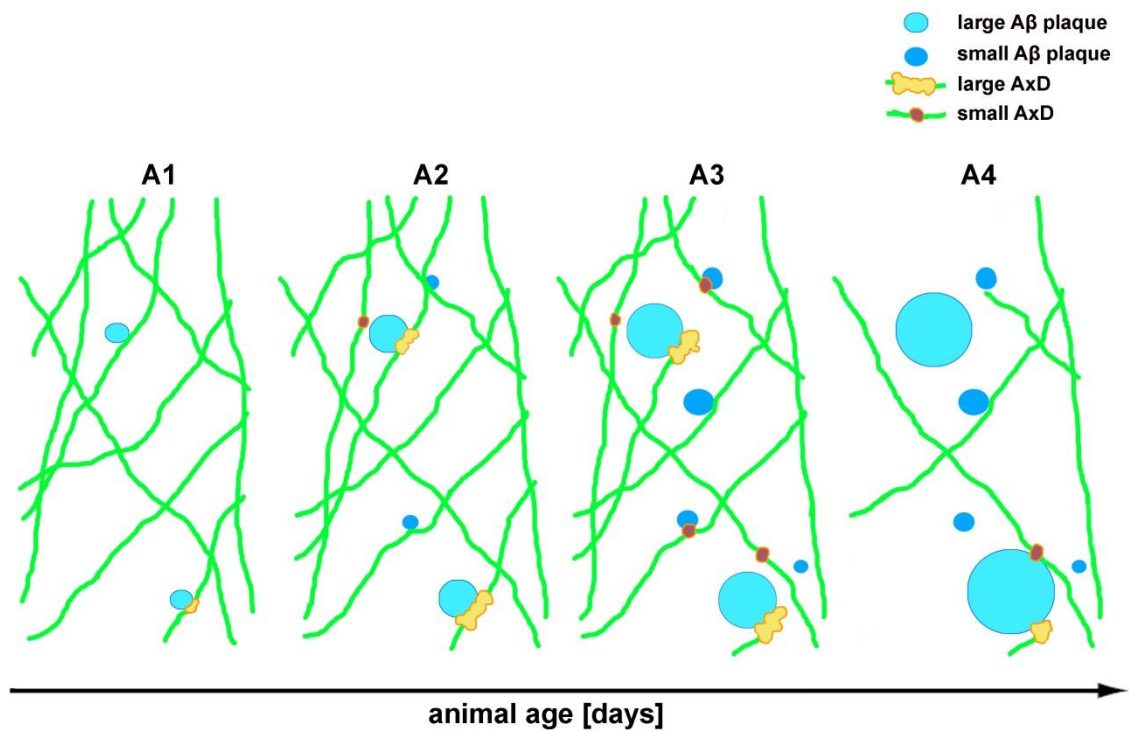
Supplementary Fig. 5 Relationship between Aβ plaques and AxDs formation and development. Quantitative analysis of different types of Aβ plaques. (a-f), Maximum projection of images (136 images, $z = 0.3 \mu\text{m}$) showing GFP-expressing neurites and the formation and growth of different types of Aβ plaques over time in the supragranular layers of the somatosensory cortex of the APP-PS1 mouse (two-photon microscopy). An Aβ plaque that reaches a large volume is pointed out by an arrow. Arrowheads point out small plaques. Rectangles in b, e surround the region shown in Fig. 8 a, b, respectively. Rectangles in d, f surround the region shown in Fig. 8 c, d, respectively. Note that most AxDs were formed and developed during the imaging period, and numerous AxDs had already disappeared by the end of this time (see Aβ plaque pointed out by an arrow). (g, h), Graphs showing the volume of large Aβ plaques (both pre-existing plaques, gray lines; and plaques that appeared during the imaging period, black lines) (g) and small Aβ plaques (h) in the animal lifetime. Open red circles show the mean \pm SEM volume over time for large (g) and small (h) Aβ plaques. Dashed red line shows the fitted sigmoid curve for large (R^2 0.36) and small Aβ plaques (R^2 0.45): the inflection point of the function is expected at day 408 in g and at day 271 in h. (i), Graph showing the density of Aβ plaques in the animal age (mean \pm SEM) (red circles). Dashed red lines correspond to the two fitted regression lines (R^2 0.28); both lines intercept at day 190. The slope is $15.75 \pm 6.34 \mu\text{m}^3/\text{day}$ for the first line and $4.28 \pm 5.45 \mu\text{m}^3/\text{day}$ for the second line. The density of small Aβ plaques against animal age (mean \pm SEM) (green open circles) has been also represented. Scale bar (in f): $42.7 \mu\text{m}$ in a-f



Supplementary Fig. 6 Behavior of auto-fluorescent spots after the elimination of an AxD. (a, b), Maximum projection of a stack of images (40 images; z-step: 1 μm) taken with the two-photon microscope in the supragranular layers of the somatosensory cortex of the dE9 mouse at two different time points, showing some neurites expressing GFP around an $\text{A}\beta$ plaque stained with Methoxy-X04 (blue). This AxD is the same one showed in Fig. 4. It can be observed that the auto-fluorescence (yellow spots) inside the GFP-expressing AxD (in a) remains at the same location after the loss of the AxD (in b). The arrows point out the region of interest. Scale bar (in b): 12.4 μm in a, b



Supplementary Fig. 7 Quantitative study of the neurochemical characteristics of the AxDs. Confocal images of the supragranular layers of the somatosensory cortex in coronal sections of the dE9 mouse brain (~ 12 months) in which immunohistochemistry was performed with different antibodies. (a, e, i, m), Maximum projection ($z = 0.4 \mu\text{m}$) to display the AxDs present in axons of pyramidal neurons expressing GFP (white arrows) in close proximity to an A β plaque stained with Methoxy-X04 (magenta, white asterisks). (b, c), Single plane of the stack taken in the region in a showing immunoreactivity for SNAP-25 (blue) and LC3 (red), respectively. (f, g), Single plane of the stack taken in the region in e showing immunoreactivity for LAMP1 (blue) and VGLUT 1 (red), respectively. (j, k), Single plane of the stack taken in the region in I showing immunoreactivity for BACE 1 (blue) and A β 4G8 (red), respectively. (n, o), Single plane of the stack taken in the region in m representing immunoreactivity for VGLUT-1 (blue) and A β 42 (red), respectively. (d, h, l, p), Same optical plane in b–c, f–g, j–k and n–o, respectively, in which the image showing the expression of GFP in this plane has been digitally added. (r), Quantification of the expression of VGLUT-1, A β 42, SNAP25, LC3, BACE1, A β 4G8 and LAMP1 in AxDs expressing GFP in the dE9 mouse. Scale bar (in p): 21.7 μm in a–p



Supplementary Fig. 8 Schematic representation of Aβ plaques and AxDs development over time. Initially, Aβ plaques develop (A1). Larger AxDs appear associated with Aβ plaques that will become large (A1, A2). Smaller Aβ plaques are formed next to pre-existing large Aβ plaques. Small AxDs develop around both small and large Aβ plaques. Large Aβ plaque volume increases rapidly (A3). Finally, numerous axons and AxDs disappear. Large Aβ plaques continue increasing their volume whereas plaque density is stabilized (A4). Neurites are represented in green

3.2. Transcallosal deafferentation induces contralesional cortex reorganization after stroke

Every year 15 million people suffer a stroke. Of these, six millions die and five millions survive with permanent disabilities. This makes stroke the fifth most frequent cause of death and the most frequent cause for long-term disability worldwide. The dimension of the problem becomes even more evident considering that the total number of stroke survivors will rise from 33 million in 2010 to a staggering 70 million by 2030. In the past decades tremendous clinical and pre-clinical efforts were undertaken to understand the acute, life-threatening consequences of stroke and to develop novel therapeutic options. However, even today very little is known about the mechanisms responsible for long-term impairments after stroke and therefore no pathophysiology-based therapeutic options are available. Current knowledge suggests that stroke does not cause only local damage, but also affects the performance of the whole brain by destabilizing the microanatomy and physiology of healthy, remote brain regions connected to the infarcted brain. This process that also occurs in the contralateral hemisphere may limit or even actively suppress functional recovery after stroke. Here we want to address the mechanisms of this destabilization in the contralateral cortex and its contribution to functional recovery. To mimic stroke, we will use an already well established model where we occlude for one hour the MCA (medial cerebral artery) by inserting a filament. After 60 min the filament is removed leading to reperfusion. Neurons connected to the infarct will be labeled using virus tracing (AAV expressing GFP) and their dendritic arbor will be visualized through a cranial window glued with dental cement in the contralateral hemisphere with a diameter of 4mm. The cranial window as well as the virus injection, were done 1 month prior to stroke induction.

Using this experimental paradigm, we will analyze changes in the arborization and synapses of the neurons connected to the infarcted tissue and reorganization of these cells and their associated network over time. The detailed investigation of these processes will allow us to better understand how the brain responds and reorganizes after injury and to develop measures to enhance or possibly inhibit this remodeling in order to develop novel therapeutic strategies for patients suffering from brain injury.

Contribution of V.F.S to this work: I performed all surgical procedures (cranial window implantation and stroke induction), lesion standardization, development and implementation of post-operative care protocol together with behavior testing, retro-virus injections, laser speckle imaging (CO₂ challenge, whisker stimulation and heatmap generation), chronic 2P imaging, immunostainings and confocal imaging. Furthermore, I contributed to all data acquisition and analysis together with the writing and correcting of the manuscript under the supervision of H.F and P.N. (please see section 8 for further details)

Transcallosal deafferentation induces contralesional cortex reorganization after stroke

Susana Valero-Freitag ^{1,4}, Fatma B Seker ^{1,4}, Bernhard K Groschup ^{1,4}, Athanasios Lourbopoulos ^{1,4}, †, Benno Gesierich ^{2,4}, Antonia Wehn ^{1,4}, Igor Khalin ^{1,4}, Marco Düring ^{2,4}, Martin Dichgans ^{3,4}, Farida Hellal ^{1,4#} & Nikolaus Plesnila ^{1,4#}

1) Experimental Stroke Research, University of Munich Medical Center, Munich, Germany

2) Vascular Cognitive Impairment, University of Munich Medical Center, Munich, Germany

3) Translational Stroke and Dementia Research, University of Munich Medical Center, Munich, Germany

4) Institute for Stroke and Dementia Research Munich, , University of Munich Medical Center, Munich, Germany

† Current address: Neurointensive Care Unit, Schön Klinik Bad Aibling, Bad Aibling, Germany

These authors contributed equally to this study.

Corresponding authors:

Farida.hellal@med.uni-muenchen.de

Phone: +49 (0)89 4400 - 46200

Fax: +49 (0)89 4400 – 46010

Nikolaus.Plesnila@med.uni-muenchen.de

Phone: +49 (0) 89 4400 46 219 or 220

Fax: +49 (0) 89 4400 46 113

Abstract

Stroke induces neuronal deafferentation leading to remote anatomical and functional changes (diaschisis) via mechanisms not yet fully understood. The current study aimed to characterize the long-term effect of cerebral ischemia on contralesional cortical reorganization and dendritic dynamics and to correlate these changes to sensorimotor behavior and neural activity.

To achieve these aims, we performed the following experiments: We (i) characterized the consequences of deafferentation of neurons of origin in the contralesional cortex using anterograde and retrograde viral labeling up to three months after cerebral ischemia, (ii) investigated dendritic spine turnover in the contralesional hemisphere by repetitive 2-photon *in vivo* imaging, in correlation with behavioral analysis using an optimized long-term survival mouse model depicting large stroke and sustained sensorimotor deficit, and (iii) mapped the contralesional neural activity by functional hyperemia using laser speckle imaging.

Three months after stroke, we found significant contralesional cortical thinning (-11%; $p < 0.001$) in the absence of substantial cell loss or neuronal body shrinkage but a decrease of neuropil fraction (-14%). Throughout stroke recovery, which plateaued after three weeks (40% residual deficit), the deafferented neurons displayed dynamic dendritic spine turnover. In parallel with changes in relative excitatory/inhibitory balance between both hemispheres, we also observed decreased contralesional spine density in apical dendrites of transcallosal neurons (-35%), which became prone to hyperexcitability. This structural reorganization is accompanied by increased functional hyperemia up to one month, followed by a normalization phase at three months, further implicating changes in neural activity and synaptic transmission in the contralesional cortex. Our data reveal that stroke-induced transhemispheric diaschisis is mediated by

the deafferentation of transcallosal neurons. Affected transcallosal neurons remodel their dendritic spines and trigger contralesional cortex structural and functional reorganization.

One sentence summary:

Deafferentation of transcallosal neurons induces contralesional cortex reorganization after ischemic stroke.

INTRODUCTION:

Stroke is the second cause of lifelong disability, primarily affecting the aged population but also increasingly younger adults worldwide (1, 2). Clinical and preclinical studies on ischemic stroke have helped to deepen our understanding on gray matter injury and neuronal loss, however, more recently it was recognized that white matter injury may also contribute to stroke outcome (3, 4). White matter lesions elicit further progression of the structural damage and functional loss, putting the surviving victims at the highest risk for severe disability and increased physical dependence. Indeed, injury to white matter fiber tracts may underlie the progressive nature of stroke (5-7).

Brain coordinated function relies on the dense anatomical connections of white matter tracts to transmit information rapidly both locally and to somewhat distant locations. Therefore, fiber damage by ischemia can result in deafferentation and interruption of functional connectivity in regions that are remote from the stroke lesion (8-10). Lateralization of the infarct, as seen in middle cerebral artery stroke alters the dynamics of exchange and connections between the two hemispheres. This interhemispheric communication, which is inhibitory, is primarily occurring through the corpus callosum (11). Consecutively widespread symptoms of dysfunctions referred to as diaschisis will appear within and across both hemispheres, seemingly unrelated to the location of the initial infarct (10, 12). Crossed cerebellar and transcallosal diaschisis are primarily reported in human stroke and are associated with perfusion and metabolism alterations in the contralesional hemisphere (10). The underlying anatomical changes orchestrating these dysfunctional events, including alterations onto the transcallosal neurons, are yet not fully understood. Despite compelling data of their implication in the recovery of function, only a macroscale representation of their contribution to stroke pathology has emerged (12). It is also not clear how diaschisis and the transcallosal pathways evolve

during stroke recovery, specifically at the more chronic stages. Only a few longitudinal experimental stroke studies have engaged in examining how the damaged corpus callosum contributes to contralesional cortical alterations beyond the sub-acute phase, and with conflicting results (13, 14).

Here we aimed to characterize the contribution of the transcallosal pathway to long-term contralesional alteration after stroke. To this end, we subjected mice to one hour MCA occlusion followed by reperfusion (fMCAo) to mirror the mechanical thrombectomy intervention in humans (15). In our hands, this model has the benefit of presenting the entire spectrum of stroke severity and a sustained chronic sensorimotor deficit enabling to determine the contribution of the contralesional hemisphere to the long-term functional outcome (16). To better understand the structural underpinnings of remote alterations of transcallosal deafferentation seen in subcortical stroke, we extended our investigation to a cortical stroke model induced by distal MCA occlusion (dMCAo).

Using anterograde and retrograde viral labeling, we unequivocally traced transcallosal neurons damaged by stroke and characterized the consequences of their deafferentation up to three months after cerebral ischemia. We investigated dendritic spine turnover and density in the contralesional hemisphere *ex-vivo* and longitudinally by repetitive 2-photon *in vivo* imaging in parallel with monitoring of the neurological deficit. We analyzed the impact on neuronal transmission. We finally mapped the contralesional neural activity upon whiskers stimulation by functional hyperemia using laser speckle imaging.

RESULTS:

Chronic ischemic stroke is characterized by sustained neurological impairment

In order to investigate chronic diaschisis after ischemic stroke in association with functional recovery, we needed to optimize a severe experimental stroke model that would display assessable long-term neurological impairment. One major impediment of large stroke experimental models, such as the mouse fMCAo model, is mortality (15-17). We previously demonstrated that the fMCAo model in mice is accompanied by cachexia and a high mortality rate, specifically during the critical period encompassing the acute and sub-acute phases of stroke pathophysiology (16). To overcome this critical period, we developed a post-operative care protocol supporting the animals to recover from anesthesia and the surgical procedure which permitted to reach 100% of survival (Fig. 1A). We monitored the behavior of the animals, using a single composite score paralleling the NIH Stroke Scale (18) which provides a separate readout for general health and neurological deficits (16). We found that the sickness behavior peaked during the first day after surgery. The effect was, however, more prominent in the fMCAo group as compared to sham operated animals (3.5 fold). After one week, all mice recovered and became asymptomatic (Fig. S1B). We evaluated the neurological deficit through scoring of 12 items, including body asymmetry, gait, and balance abilities (16). Stroke animals, in comparison to the sham group, presented substantial and sustained neurological impairment with the most severe deficit during the first day (9.5 disability points versus 0.37 for the sham group). Although a spontaneous recovery occurred during the first week, it plateaued at this point, remaining at about 40% of the initial level ($p < 0.0001$) up to 9 weeks after fMCAo (Fig. 1B). Altogether the post-operative care protocol by reducing the burden of surgery and anesthesia permitted to

keep the entire spectrum of stroke severity reflected by sustained long term impairment paralleling the human condition (18).

Chronic sustained neurological impairment is correlated with tissue atrophy in both ipsilesional and contralesional hemispheres

Ipsilesional and contralesional hemispheric volume, as well as surface across the cerebrum, were analyzed in PFA fixed brains isolated from mice at three months after fMCAo and age matching controls. The lesion area in the ipsilesional hemisphere extended from the cortex to other vital structures such as the corpus callosum, hippocampus, and thalamus (Fig. 1C-F). The MRI performed at three months following fMCAo showed that the initial infarct has evolved to atrophy extending to the entire hemisphere in the chronic phase (31% of the control hemisphere). Interestingly, the volume of the contralesional hemisphere was also affected and displayed a statistically significant reduction of about 9 % in comparison to controls (Fig. 1D).

We also analyzed the profile of cross-sectional areas along the rostrocaudal axis. We aimed to understand whether there was a specific change of cross-sectional areas in the contralesional hemisphere in regards to the lesion core (homotopic area in Fig. 1E). Indeed we found that the area change in the contralesional hemisphere was not uniform. In the corresponding sections homotopic to the lesion, the contralesional hemisphere area was significantly reduced while the area size increased in the next caudal sections (average Bregma - 2.5 mm to - 3.5 mm in Fig. 1E). These results indicate that the process of remodeling occurring in the ipsilesional hemisphere after stroke extends to the contralesional hemisphere. Since transcallosal neurons show also a homotopic representation we hypothesized that this process is mediated through the interhemispheric connectivity and the transcallosal pathway.

Transcallosal deafferentation leads to contralesional cortical thinning and neuropil shrinkage

To better understand the individual contribution of interhemispheric transcallosal connections to structural changes in the contralesional hemisphere, we induced an ischemic stroke by occluding the distal part of the MCA (dMCAo). This type of stroke generates lesion confined to the primary somatosensory cortex S1 and barrel field and the immediate subcortical region, which in the mouse is mainly the corpus callosum (19, 20).

We first performed histological analysis at two months after dMCAo to analyze the contralesional cortex response. We measured the contralesional cortical thickness on Nissl-stained sections through cortical regions spanning the sensorimotor cortex. We observed a significant thinning of the contralesional cortex after dMCAo of 11% ($p=0.0001$; Fig. 2A), a finding well in line with our previous findings in humans by MRI (21, 22). When analyzing the barrel cortex, the homotopic region to the infarct, we did not find any overt alterations in the cortical layering (data not shown), nor significant changes in the total cell or neuronal density (Fig. 2B). Also, we did not observe variations in the overall neuronal cell body size distribution (Fig. 2C). The most striking finding was, however, a 14% shrinkage of the cortical neuropil, the fraction of the brain parenchyma which harbors synapses, axons, and dendrites ($p<0.0001$; Fig. 2D and E). From these findings we conclude that transcallosal deafferentation elicits contralesional cortical thinning by a refinement of the cellular processes of the cortical neurons projecting into the tissue damaged by ischemic stroke, as also indicated by morphological changes of their soma.

To further characterize the consequences of transcallosal deafferentation, we specifically examined neurons of the contralesional cortex sending processes to the

infarcted tissue through the corpus callosum. We labeled these neurons using viral labeling with AAV1-hSyn-EGFP. The virus was injected one month before stroke to allow recovery. The use of a pressure injection system allowed us to generate sparse labeling (Fig. 3A). Up to two months after stroke, we found dystrophic axons and varicosity-like structures in the ipsilesional cortex that persisted along the corpus callosum, which may suggest ongoing damage to the axonal fiber bundles (Fig. 3B). Then we traced back through the corpus callosum the soma and dendrites of these deafferented transcallosal neurons in the contralateral hemisphere. Indeed along the callosal path some alterations were present within the fiber bundles (Fig. 3C) as well as its surface (Fig. 3D). Their soma identified via the viral labeling in contrast to other cortical neurons displayed signs of atrophy and condensation in a number of cells indicative of cellular reorganization (Fig. 3E and F). Moreover, the apical dendrites of these transcallosal neurons depicted a significant spine density decrease of 35% ($p=0.008$; Fig. 4A and B). This massive loss of apical spines suggests a significant disruption of intracortical synaptic connections within the contralateral hemisphere.

Transcallosal dendritic spine dynamics underlie diaschisis

We then examined whether this contralesional cortex network disruption occurred in association with changes in spine functionality by visualizing spine dynamics of transcallosal neurons in the cerebral cortex contralateral to the ischemic lesion by 2-photon imaging (Fig. 4C and D). To unambiguously trace the dendritic tufts of transcallosal neurons, we injected a retrograde viral tracer (rAVV-CAG-GFP) in the cortex later on subjected to cerebral ischemia. The mice were implanted with a cranial glass window and, after one month, were subjected to fMCAo or sham surgery (Fig. 4C). Under our experimental conditions, stroke did not alter the number of stable spines (Fig. 4E) while the number of lost spines seems tend to be more prominent than

the gained spines (Fig. 4F). Overall, the spines tended to be more dynamic over time (Fig. 4H) presenting more transient spines ($p=0.04$) (Fig. 4G). At two months post-stroke the spine density decreased together with loss of dendritic branches in the homotopic region mirroring the residual lesion core in the ipsilesional cortex ($p=0.02$) (Fig. 4I). We found that most appearing spines survived for at most one imaging session (2 weeks). Similarly spines present at the baseline and surviving more than 4 weeks were prone to survive longer until 8 weeks. Hence the stable and transient fractions do not relatively transfer and likely belong to independent populations with potentially different functions.

Transcallosal deafferentation promotes increased contralesional cortical inhibition

We next aimed to characterize how transcallosal neuron deafferentation and spine reorganization affect the contralesional cortical synaptic transmission. We, therefore, quantified the number of inhibitory and excitatory punctates present in the barrel field column by immunofluorescence using gad65-67 and vGlut1 as specific markers for total inhibitory and excitatory synapses, respectively (Fig. 5A). Twenty-four hours after stroke both Gad65-67- and vGlut1-positive synapses decreased as a sign of acute deafferentation from the infarct area (Fig. 5B and C), but recovered to sham levels within seven days after stroke. Gad65-67 expression was stable until two weeks after stroke, but showed a drastic increase three months after the insult (Fig. 5B), while Vglut1 showed a dramatic decrease at this time point (Fig. 5C). These changes in excitatory and inhibitory synapses and, hence, neurotransmission, were reflected by the regulation of contralesional hemisphere GABAA receptor subunit expression on the RNA level.

In order to reflect the global changes of inhibition, we plotted the average expression levels of the GABAA receptor subunits for phasic ($\alpha 1-3$ and $\gamma 2$) and tonic ($\alpha 4-5$ and δ) inhibition. Stroke induced decrease of both phasic and tonic inhibition at 24h in

ipsilesional ($p=0.005$) and contralesional ($p=0.01$) cortices (Fig. 5D and E). The levels were however higher in the contralesional cortex. While the phasic inhibition progressively normalized for both cortices at two months poststroke, the tonic inhibition remained unstable. At 7d the tonic inhibition decreased in the contralesional cortex equalizing with the ipsilesional cortex ($p=0.009$). The levels were then restored to the sham in both cortices. However, at two months, the expression of subunits mediating tonic inhibition displayed an upregulation in the contralateral cortex compared to the ipsilateral cortex ($p = 0.019$) (Fig. 5E). So, transcallosal deafferented neurons remodeled their dendrites and refined their spines to receive more excitatory input. This initiated reorganization of the contralesional cortical synaptic transmission. While the inhibition stabilized in the ipsilateral cortex, the contralesional cortex further remodels increasing phasic inhibition in the homotopic barrel field cortex.

Deafferented transcallosal neurons are prone to hyperexcitability

To better understand the changes in interhemispheric connectivity, we also analyzed the nature of the remaining synapses contacting the deafferented transcallosal neurons. Thus, after immunofluorescence for vGlut1 and gad65-67, we counted the number of GFP positive spines contacting vGlut1 or gad65-67 punctate in the homotopic area to the lesion (Fig. 5F). We found an increasing number of vGlut1 contacts within the dendritic tuft of transcallosal neurons deafferented by fMCAo in comparison to the sham group (47% $p=0.04$, Fig. 5G). In contrast, the amount of gad65-67 contacts was reduced (Fig. 5H). The ratio of vGlut1 and Gad65-67 punctates further indicate that the deafferented transcallosal neurons remain hyperexcitable at 3 months after stroke (Fig. 5I).

Neurovascular coupling and functional connectivity are impaired in the contralesional hemisphere

To link the anatomical changes to functionality, we analyzed the cortical hemodynamics as a surrogate for neural activity. It is well recognized that a local neuronal activity results in increases in local cerebral blood flow (CBF) in the activated region, a phenomenon called functional hyperemia and mediated by a process named neurovascular coupling (NVC) (23, 24). In order to ensure that the changes in CBF reflect neuronal excitability and not alterations in vascular reactivity, we assessed vascular reactivity by the application of the direct and selective cerebral vasodilator CO₂ (25), a procedure also used in humans (26). Indeed, CO₂ inhalation induced vasodilation and increased CBF in both sham and stroke groups equally (Fig. S3) demonstrating that following stroke local cortical hemodynamics changes indeed reflect neuronal activity. We recorded the CBF response of the contralesional hemisphere upon stimulation of the ipsilesional whisker pad by laser speckle imaging at 5, 7, 14, 60, and 90 days after stroke (Fig. 6AB and Fig. S4). The average of the maximum responses to whisker stimulation (five trials) showed a gradual increase of NVC from 7d becoming statistically significant at 14d after stroke in comparison to sham ($p=0.028$). The values normalized until 30 days and fell slightly below the sham level at three-month post-stroke (Fig. 6C). To better understand the pattern of changes in the different cortical areas, we generated heatmaps to analyze the spatiotemporal evolution of CBF responses in the contralesional cortex. For all whiskers stimulated, the initial CBF response was localized to branches of the MCA spreading within the entire barrel field (Fig. 6B, Movie S2). The local response remained stable within the sham group over time while presenting a more dynamic pattern in the stroke group. At the initial assessment at 5d, the local CBF response in stroke appeared in ectopic areas independent of the barrel

field. The signal tends to increase beyond the sham topographic representation propagating over the rest of the sensorimotor cortex from 7d to 1-month post-stroke ($p=0.1$ at 7-14d) (Fig. 6G and Movie S3). The map of the signal became similar to the sham topographic representation at 3-month post-stroke (Fig. 6G and Movie S4). Altogether the local CBF response and neuronal activity fluctuate in the contralesional cortex. In parallel to remodeling of the lesion and recovery of function, the contralesional cortex responds by neuronal hyperactivation in sensorimotor regions extending the whiskers representation within the first month to finally normalizing three months after stroke.

DISCUSSION:

In the present study, we investigated long-term transcallosal diaschisis after ischemic stroke. We found that chronic stroke is characterized by tissue atrophy which encompasses the original lesion site, the ipsilesional hemisphere as a whole, and the contralesional hemisphere. These structural changes are accompanied by decreased neuronal activity in the contralateral region homotopic to the infarct site. We could demonstrate that the transcallosal pathway connecting the ipsilateral and contralesional hemispheres is the substrate for this change. Stroke damage and deafferent fibers of transcallosal neurons that remodel their dendritic spines to retain the excitatory input onto their dendrites triggering in the contralesional cortex increase inhibitory synaptic transmission in the homotopic barrel field.

A large body of literature has focused on tissue atrophy of the ischemic hemisphere after stroke. The atrophy occurs throughout recovery at the infarct region orchestrated by inflammation aiming at the clearance of cell debris and lesion seclusion by scar formation (16, 27, 28). The lesion progresses jeopardizing the corpus callosum integrity and the interhemispheric communication. Serial diffuse tensor imaging had revealed occurrence of Wallerian degeneration in callosal fibers after large MCA stroke and in correlation with persistence and worsening of motor disability up to 1 month after infarction (29, 30). Nonetheless, as of today, few preclinical studies have analyzed changes in remote areas within the same hemisphere and even less in the contralesional hemisphere. In fact, in most current investigations, the contralesional hemisphere is used as control tissue for normalization.

Long-term structural remodeling of contralesional white matter has been associated with subcortical infarcts in various clinical studies, including ours (3, 4, 21, 22, 31). We and others have observed contralesional cortical thinning as a hallmark response of

anatomically connected regions in subcortical stroke patients at six months after the event (22). Here we reproduced the change in cortical thickness and demonstrated that a cortical stroke lesion triggers cortical thinning via mechanisms that we could attribute to transcallosal neuron deafferentation. Cortical infarction damages the fibers running through the corpus callosum leading to progressive disconnections. Damaged to the fibers even in the absence of disconnection may as well affect the velocity, the volume of signal transmission, and mitigate the axonal functionality, which may impact the contralesional cortex. The propagation of a retrograde injury signal potentially involving dynein associated factors upon axotomy has been suggested as a potential mechanism of communication from the damaged area to the soma to explain the somatic responses such chromatolysis and changes in gene transcription (32, 33). Specific viral labeling of transcallosal neurons allowed to observe morphological signs of disconnection, including dystrophy and retraction bulbs formation along the callosal pathway (34, 35). The morphological changes of the fibers extended to the contralesional hemisphere and persisted up to three months after stroke.

In the current study we show that this deafferentation does not result in cell death in the homotopic contralesional cortex. We did not find any change in cell density or soma size distribution, which would have indicated active retrograde degeneration, a process linked to axotomy close to the cell body (36). What we revealed, in contrast, is significant neuropil alterations, which would suggest at least in part a structural reorganization of the dendritic arborization in the cortical circuit. Because the deafferentation occurs far distal from the cell body, the axotomized neurons do not shrink their soma, but their dendrites (36, 37). In fact, we found significant spine density loss in the apical dendrites of deafferented transcallosal neurons.

Dendritic remodeling after stroke has been extensively investigated in perfused peri-infarct and remote regions within the ipsilateral cortex, notably by Tim Murphy's team. Altogether extensive remodeling associated with cortical map displacement is occurring within the first three months and is presented as an adaptative mechanism assuming the functional gaps due to the lesion (38-41). In contrast, the contralesional dendritic remodeling is still debated (13, 14, 42). One of the shortcomings of previous analysis is the use of *thyl*-GFP multivariant transgenic mice, which provide a non-uniform label of neurons through layers but also regions of the cortex, including the S1 barrel field (43, 44). Using retrograde viral labeling of transcallosal neurons, we removed the ambiguity of specificity by targeting directly the transcallosal neurons deafferented by an ischemic stroke, which exhibited reduced spine density.

Interestingly, the spine loss seems to preferentially affect inhibitory input onto transcallosal neurons as most of the remaining synapses were positive for vGlut1 and were therefore excitatory. This enhanced presynaptic excitability also reported elsewhere may be mediated by a decrease in GABAergic (γ -aminobutyric acid) inhibition or an increase in glutamatergic responses, which have been found in the contralesional hemisphere (36). Our study demonstrated a heavily damaged ipsilesional hemisphere, and degeneration of transcallosal projections typically exerting inhibition. Their degeneration could explain uncovering of preexisting excitatory connections resulting in the early enhanced ipsilesional excitability (36, 37, 45, 46).

To get an insight into the functionality of the contralesional cortex, we analyzed the changes in neuronal activity through neurovascular coupling and whiskers stimulation. We found prolonged contralesional activation in the barrel field during early and late sub-acute phases post-stroke this in agreement with human fMRI data and finger-thumb opposition task (47). The activation extended the barrel field network within the first

two weeks, likely reflecting recruitment of lateral excitatory projections leading to broader disinhibition. The enhanced activation occurring at the time when the function is impaired after stroke may contribute to its partial restoration through potentiation of uncrossed cortical pathways. Conversely, in the context of interhemispheric inhibition, this hyperactive contralesional cortex, via increasing inhibition, can exert greater control over the ipsilateral cortex and hinder its functions (48). This notion at the basis of major inhibitory neuromodulation protocols in humans (48, 49) correlates with commonly reported increased ipsilateral inhibition within the same time frame, specifically for M1-dependent motor function (49). The strength of interhemispheric inhibition was found to be proportional to motor impairment, and reduction of contralesional excitability promoted recovery of hand function (50, 51).

Although within the last decade, the contribution of the contralesional cortex to stroke recovery is increasingly understood in experimental models, the part attributable to the deafferented transcallosal neurons is still not clear. Inactivation of the contralesional cortex using the GABAA receptor agonist muscimol induced by endothelin showed a biphasic effect. During the 14 day treatment period, muscimol worsened the deficit but corrected grasping performance and asymmetry of the paretic forelimb after withdrawal up to 2 months post-stroke (52). We saw that during the first 14 days, the contralesional cortex adjusted to the hyperactivity of these neurons while normalizing its activity at three months after stroke. Still, the deafferented transcallosal neurons remodeled their spines, becoming more prone to receive excitatory input within this normalized network. Attempt to inhibit the contralesional cortex at this later stage has proven not been efficient or even worsening the outcome after brain injury (53).

In conclusion, this study demonstrated that the contralesional cortex reorganizes after stroke triggered by the deafferented transcallosal neurons, which remain hyperexcitable

over the chronic phase. These findings of biphasic reorganization underlying diaschisis may give insight into the neurophysiological underpinnings through which neurorehabilitation therapies benefit to stroke recovery. Furthermore, this study provides the basis for preclinical evaluation of the transcallosal neuron path as a potential therapeutic target to alleviate chronic stroke impairment.

References and Notes:

1. Y. Bejot, B. Delpont, M. Giroud, Rising Stroke Incidence in Young Adults: More Epidemiological Evidence, More Questions to Be Answered. *Journal of the American Heart Association* **5**, (2016).
2. G. B. D. S. Collaborators, Global, regional, and national burden of stroke, 1990-2016: a systematic analysis for the Global Burden of Disease Study 2016. *The Lancet. Neurology* **18**, 439-458 (2019).
3. R. Lindenberg, R. Seitz, in *Neuroimaging - Methods*, P. Bright, Ed. (InTech, 2012), chap. 12, pp. 233-244.
4. P. W. Ho *et al.*, Is white matter involved in patients entered into typical trials of neuroprotection? *Stroke* **36**, 2742-2744 (2005).
5. H. Nonaka *et al.*, Microvasculature of the human cerebral white matter: arteries of the deep white matter. *Neuropathology : official journal of the Japanese Society of Neuropathology* **23**, 111-118 (2003).
6. M. C. Stoeckel, H. J. Wittsack, S. Meisel, R. J. Seitz, Pattern of cortex and white matter involvement in severe middle cerebral artery ischemia. *Journal of neuroimaging : official journal of the American Society of Neuroimaging* **17**, 131-140 (2007).
7. Y. Tateishi *et al.*, Large deep white matter lesions may predict futile recanalization in endovascular therapy for acute ischemic stroke. *Interventional neurology* **3**, 48-55 (2015).
8. H. Karbasforoushan, J. Cohen-Adad, J. P. A. Dewald, Brainstem and spinal cord MRI identifies altered sensorimotor pathways post-stroke. *Nature communications* **10**, 3524 (2019).
9. A. G. Guggisberg, P. J. Koch, F. C. Hummel, C. M. Buetefisch, Brain networks and their relevance for stroke rehabilitation. *Clinical neurophysiology : official journal of the International Federation of Clinical Neurophysiology* **130**, 1098-1124 (2019).
10. E. Carrera, G. Tononi, Diaschisis: past, present, future. *Brain : a journal of neurology* **137**, 2408-2422 (2014).
11. K. W. Doron, D. S. Bassett, M. S. Gazzaniga, Dynamic network structure of interhemispheric coordination. *Proc Natl Acad Sci U S A* **109**, 18661-18668 (2012).
12. G. Silasi, T. H. Murphy, Stroke and the connectome: how connectivity guides therapeutic intervention. *Neuron* **83**, 1354-1368 (2014).
13. Y. Takatsuru *et al.*, Neuronal circuit remodeling in the contralateral cortical hemisphere during functional recovery from cerebral infarction. *The Journal of neuroscience : the official journal of the Society for Neuroscience* **29**, 10081-10086 (2009).
14. D. G. Johnston, M. Denizet, R. Mostany, C. Portera-Cailliau, Chronic in vivo imaging shows no evidence of dendritic plasticity or functional remapping in the contralesional cortex after stroke. *Cerebral cortex* **23**, 751-762 (2013).
15. B. A. Sutherland *et al.*, The transient intraluminal filament middle cerebral artery occlusion model as a model of endovascular thrombectomy in stroke. *Journal of cerebral blood flow and metabolism : official journal of the International Society of Cerebral Blood Flow and Metabolism* **36**, 363-369 (2016).
16. A. Lourdopoulos *et al.*, Inadequate food and water intake determine mortality following stroke in mice. *Journal of cerebral blood flow and metabolism : official journal of the International Society of Cerebral Blood Flow and Metabolism* **37**, 2084-2097 (2017).
17. G. Llovera *et al.*, Results of a preclinical randomized controlled multicenter trial (pRCT): Anti-CD49d treatment for acute brain ischemia. *Science translational medicine* **7**, 299ra121 (2015).
18. P. Lyden *et al.*, Improved reliability of the NIH Stroke Scale using video training. NINDS TPA Stroke Study Group. *Stroke* **25**, 2220-2226 (1994).
19. G. Llovera, S. Roth, N. Plesnila, R. Veltkamp, A. Liesz, Modeling stroke in mice: permanent coagulation of the distal middle cerebral artery. *Journal of visualized experiments : JoVE*, e51729 (2014).
20. K. Zhang, T. J. Sejnowski, A universal scaling law between gray matter and white matter of cerebral cortex. *Proc Natl Acad Sci U S A* **97**, 5621-5626 (2000).
21. M. Duering *et al.*, Incident subcortical infarcts induce focal thinning in connected cortical regions. *Neurology* **79**, 2025-2028 (2012).
22. M. Duering *et al.*, Acute infarcts cause focal thinning in remote cortex via degeneration of connecting fiber tracts. *Neurology* **84**, 1685-1692 (2015).
23. D. Attwell, C. Iadecola, The neural basis of functional brain imaging signals. *Trends in neurosciences* **25**, 621-625 (2002).

24. D. J. Heeger, D. Ress, What does fMRI tell us about neuronal activity? *Nat Rev Neurosci* **3**, 142-151 (2002).
25. M. Balbi, M. J. Vega, A. Lourdopoulos, N. A. Terpolilli, N. Plesnila, Long-term impairment of neurovascular coupling following experimental subarachnoid hemorrhage. *Journal of cerebral blood flow and metabolism : official journal of the International Society of Cerebral Blood Flow and Metabolism*, 271678X19863021 (2019).
26. P. Liu, J. B. De Vis, H. Lu, Cerebrovascular reactivity (CVR) MRI with CO₂ challenge: A technical review. *NeuroImage* **187**, 104-115 (2019).
27. A. Lourdopoulos, A. Erturk, F. Hellal, Microglia in action: how aging and injury can change the brain's guardians. *Frontiers in cellular neuroscience* **9**, 54 (2015).
28. B. Puig, S. Brenna, T. Magnus, Molecular Communication of a Dying Neuron in Stroke. *International journal of molecular sciences* **19**, (2018).
29. R. K. Gupta *et al.*, Focal Wallerian degeneration of the corpus callosum in large middle cerebral artery stroke: serial diffusion tensor imaging. *Journal of magnetic resonance imaging : JMRI* **24**, 549-555 (2006).
30. J. Puig *et al.*, Wallerian degeneration in the corticospinal tract evaluated by diffusion tensor imaging correlates with motor deficit 30 days after middle cerebral artery ischemic stroke. *AJNR. American journal of neuroradiology* **31**, 1324-1330 (2010).
31. G. Liu *et al.*, Structural remodeling of white matter in the contralesional hemisphere is correlated with early motor recovery in patients with subcortical infarction. *Restorative neurology and neuroscience* **33**, 309-319 (2015).
32. I. Rishal, M. Fainzilber, Axon-soma communication in neuronal injury. *Nat Rev Neurosci* **15**, 32-42 (2014).
33. E. T. Urban, 3rd *et al.*, Gene expression changes of interconnected spared cortical neurons 7 days after ischemic infarct of the primary motor cortex in the rat. *Mol Cell Biochem* **369**, 267-286 (2012).
34. A. Erturk, F. Hellal, J. Enes, F. Bradke, Disorganized microtubules underlie the formation of retraction bulbs and the failure of axonal regeneration. *The Journal of neuroscience : the official journal of the Society for Neuroscience* **27**, 9169-9180 (2007).
35. I. Nikic *et al.*, A reversible form of axon damage in experimental autoimmune encephalomyelitis and multiple sclerosis. *Nature medicine* **17**, 495-499 (2011).
36. T. Nagendran *et al.*, Distal axotomy enhances retrograde presynaptic excitability onto injured pyramidal neurons via trans-synaptic signaling. *Nature communications* **8**, 625 (2017).
37. B. G. Kim, H. N. Dai, M. McAtee, S. Vicini, B. S. Bregman, Remodeling of synaptic structures in the motor cortex following spinal cord injury. *Exp Neurol* **198**, 401-415 (2006).
38. C. E. Brown, P. Li, J. D. Boyd, K. R. Delaney, T. H. Murphy, Extensive turnover of dendritic spines and vascular remodeling in cortical tissues recovering from stroke. *The Journal of neuroscience : the official journal of the Society for Neuroscience* **27**, 4101-4109 (2007).
39. C. E. Brown, C. Wong, T. H. Murphy, Rapid morphologic plasticity of peri-infarct dendritic spines after focal ischemic stroke. *Stroke* **39**, 1286-1291 (2008).
40. T. C. Harrison, G. Silasi, J. D. Boyd, T. H. Murphy, Displacement of sensory maps and disorganization of motor cortex after targeted stroke in mice. *Stroke* **44**, 2300-2306 (2013).
41. R. Mostany *et al.*, Local hemodynamics dictate long-term dendritic plasticity in peri-infarct cortex. *The Journal of neuroscience : the official journal of the Society for Neuroscience* **30**, 14116-14126 (2010).
42. Y. Takatsuru, J. Nabekura, N. Koibuchi, Activity of the layer II/III neurons in the somatosensory cortex (SSC) plays a critical role on functional recovery after focal stroke in the contralateral SSC. *Neuroscience letters* **543**, 168-171 (2013).
43. G. Feng *et al.*, Imaging neuronal subsets in transgenic mice expressing multiple spectral variants of GFP. *Neuron* **28**, 41-51 (2000).
44. C. Porrero, P. Rubio-Garrido, C. Avendano, F. Clasca, Mapping of fluorescent protein-expressing neurons and axon pathways in adult and developing Thy1-eYFP-H transgenic mice. *Brain Res* **1345**, 59-72 (2010).
45. K. M. Jacobs, J. P. Donoghue, Reshaping the cortical motor map by unmasking latent intracortical connections. *Science* **251**, 944-947 (1991).
46. U. Takechi *et al.*, Longitudinal changes of motor cortical excitability and transcallosal inhibition after subcortical stroke. *Clinical neurophysiology : official journal of the International Federation of Clinical Neurophysiology* **125**, 2055-2069 (2014).
47. R. S. Marshall *et al.*, Evolution of cortical activation during recovery from corticospinal tract infarction. *Stroke* **31**, 656-661 (2000).

48. N. Dancause, B. Touvykine, B. K. Mansoori, Inhibition of the contralesional hemisphere after stroke: reviewing a few of the building blocks with a focus on animal models. *Progress in brain research* **218**, 361-387 (2015).
49. K. C. Dodd, V. A. Nair, V. Prabhakaran, Role of the Contralesional vs. Ipsilesional Hemisphere in Stroke Recovery. *Frontiers in human neuroscience* **11**, 469 (2017).
50. J. Duque *et al.*, Transcallosal inhibition in chronic subcortical stroke. *NeuroImage* **28**, 940-946 (2005).
51. C. Grefkes *et al.*, Modulating cortical connectivity in stroke patients by rTMS assessed with fMRI and dynamic causal modeling. *NeuroImage* **50**, 233-242 (2010).
52. B. K. Mansoori *et al.*, Acute inactivation of the contralesional hemisphere for longer durations improves recovery after cortical injury. *Exp Neurol* **254**, 18-28 (2014).
53. D. R. Verley, D. Torolira, B. A. Hessel, R. L. Sutton, N. G. Harris, Cortical Neuromodulation of Remote Regions after Experimental Traumatic Brain Injury Normalizes Forelimb Function but is Temporally Dependent. *J Neurotrauma* **36**, 789-801 (2019).

Materials and methods and other supporting materials are available in the online version of the paper.

Acknowledgments:

We thank Dr. G. Llovera for teaching the distal cerebral ischemia model, U. Mamrak for teaching the fMCAo model, Julia Kramer and Franz Singer, our animal keepers and veterinary officer Dr. M. Schneider for technical support, Dr. F. Gualtieri and Prof. H. Potschka for their welcoming in their team for confocal imaging. The rAAV2-retro helper was a gift from Alla Karpova & David Schaffer (Addgene plasmid # 81070). This work was supported by Era-net NEURON (058 MISST), Synergy Munich Cluster for Systems Neurology, and DFG. Marie Curie Fellowship. The authors declare no competing financial interests.

Author contributions:

V.F.S., H.F., P.N., and M.D. were the main platform for scientific discussion and designed the experiment.

V.F.S., H.F., G.K.B., and S.F.B. performed the experiments, data acquisition, quantifications, and statistical analysis.

L.A., G.B., and M.U provided technical support.

V.F.S. and H.F. wrote the manuscript with input and revision from all authors

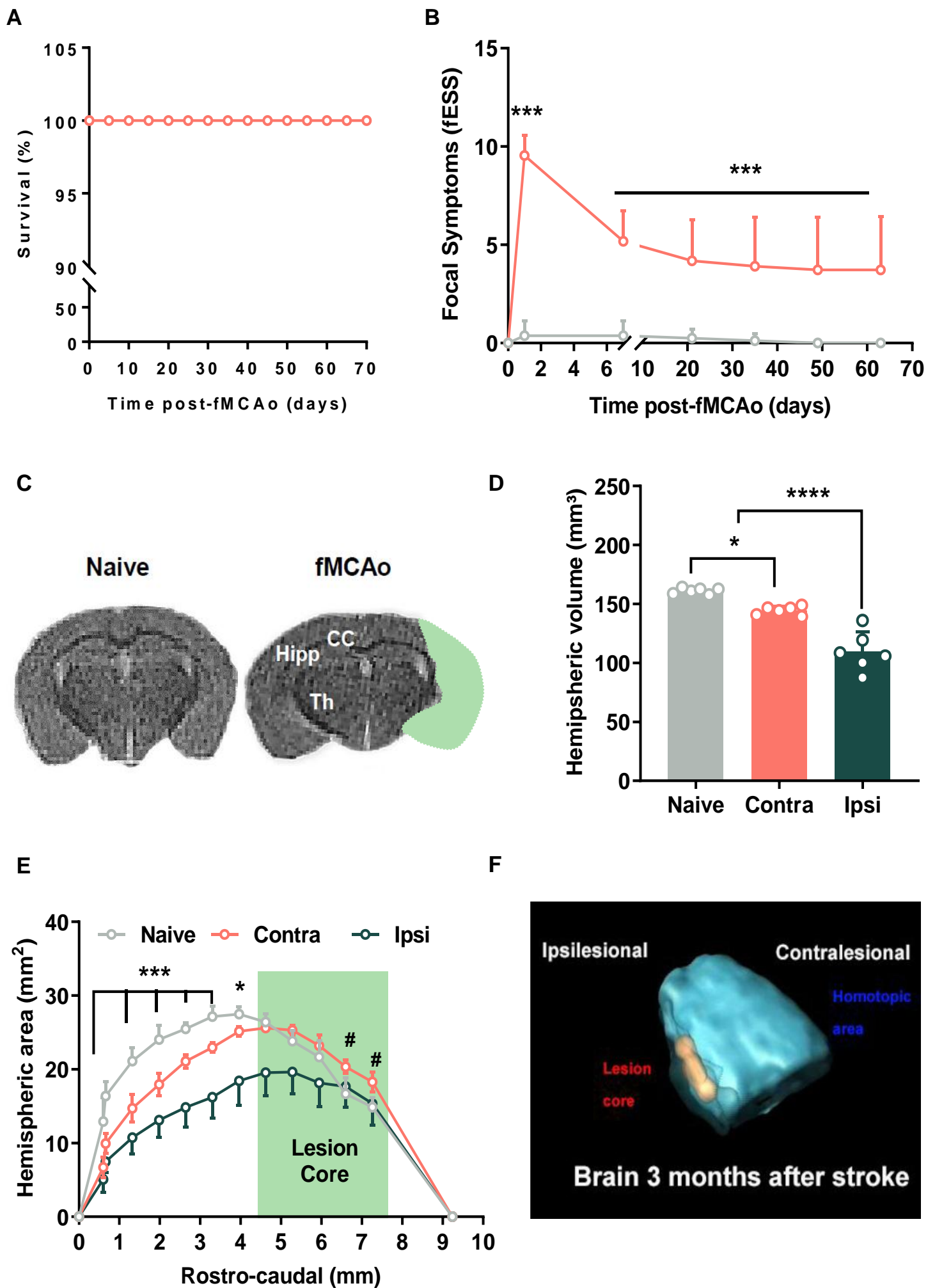
Supporting Online Material

Materials and Methods

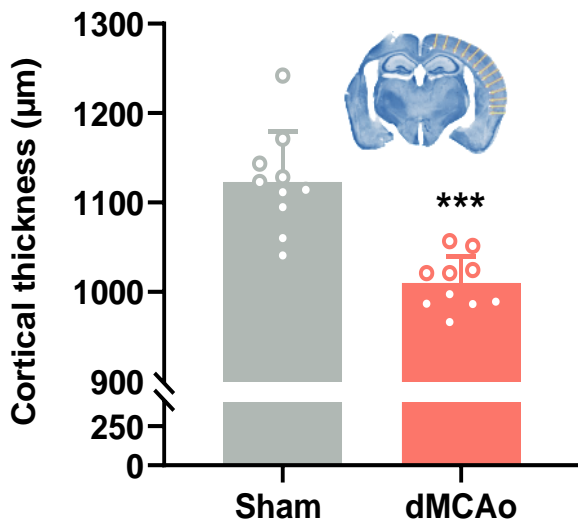
Figs. S1-S4

Tables S1

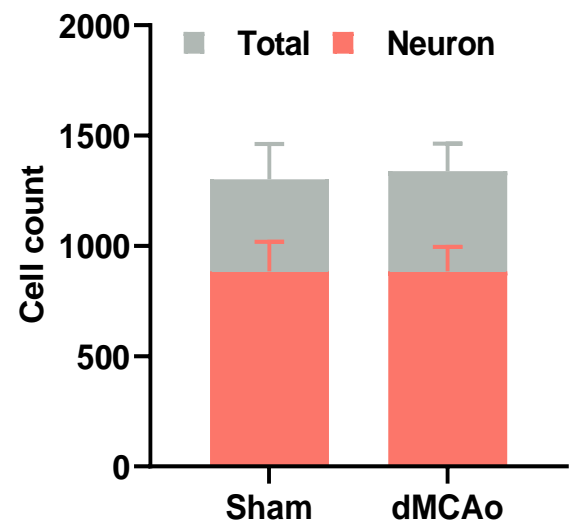
Movie Captions



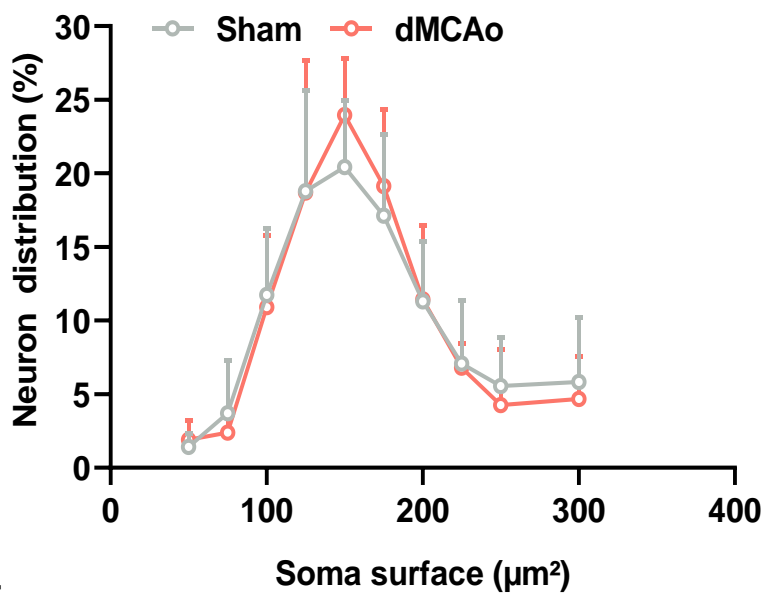
A



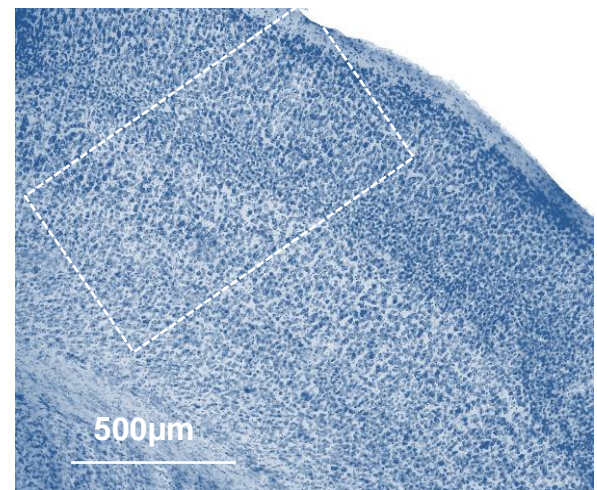
B



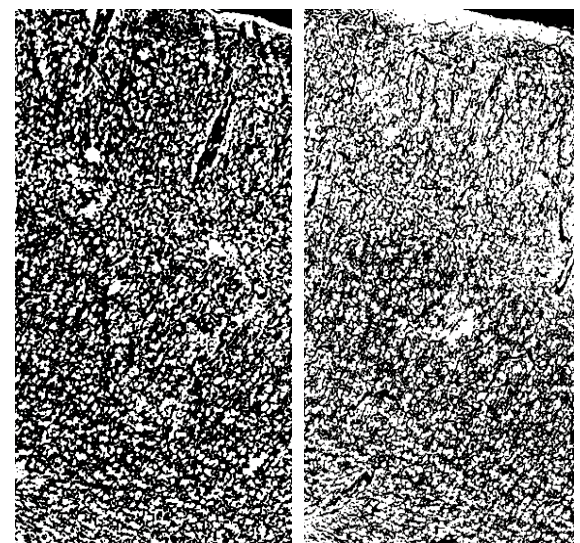
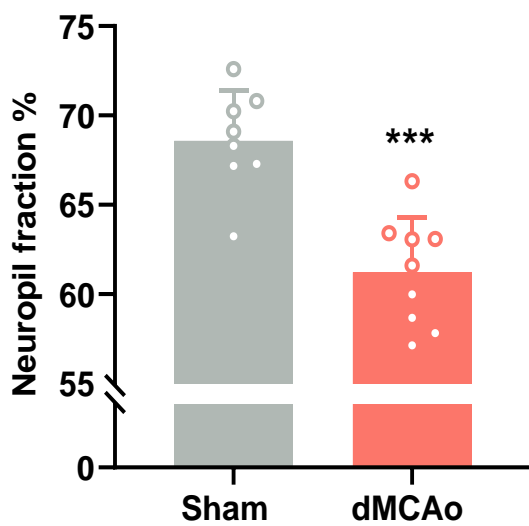
C



D



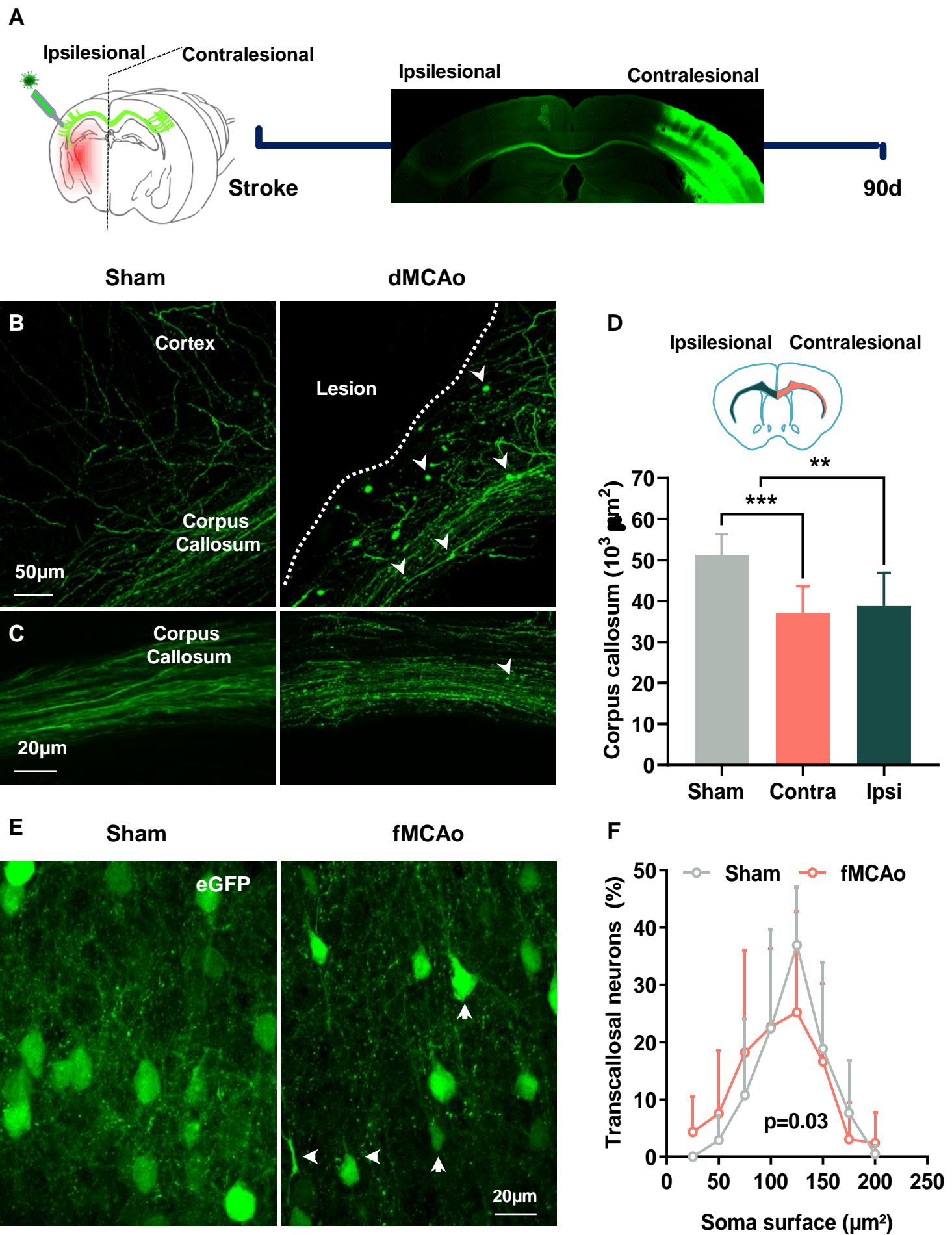
E

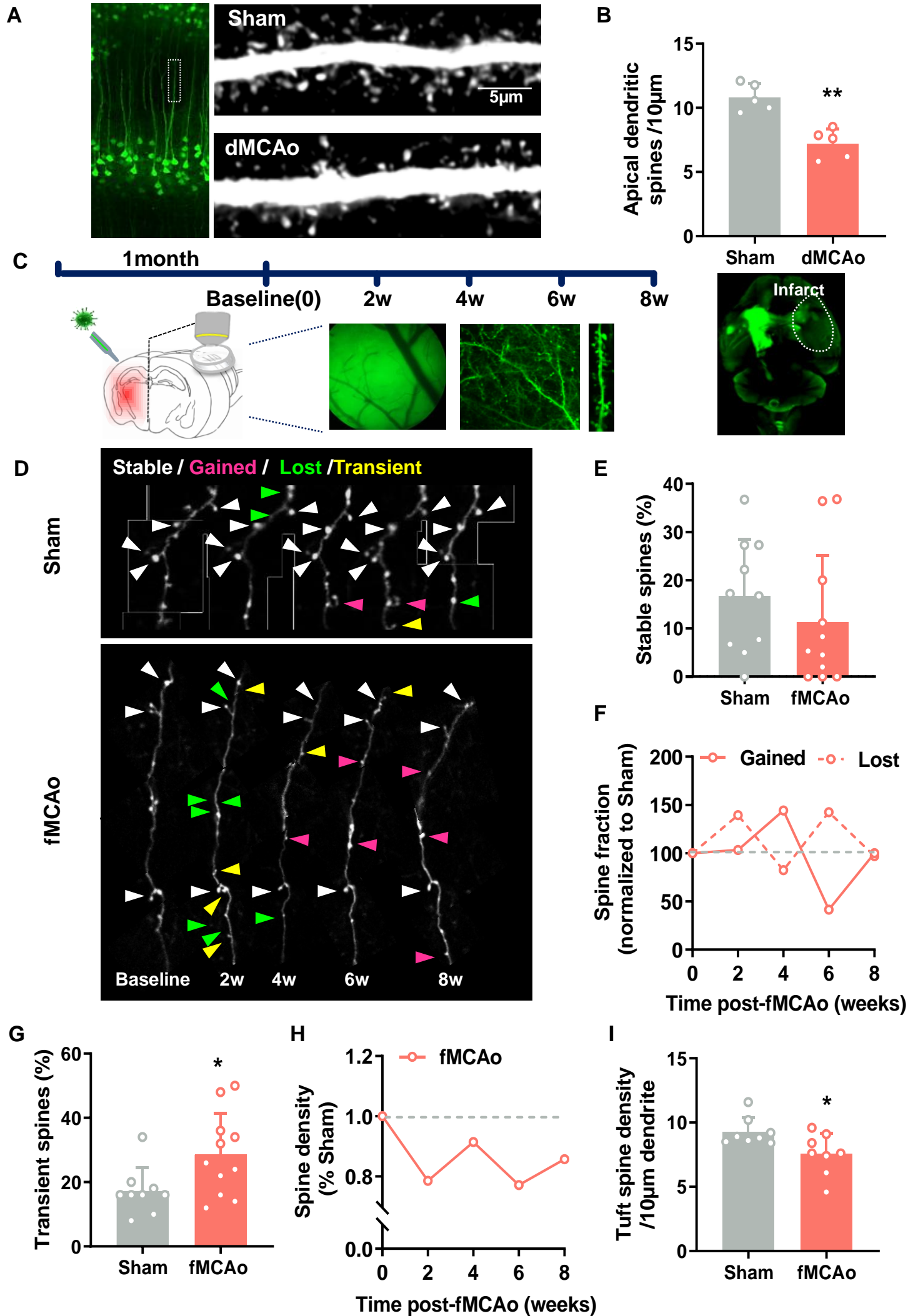


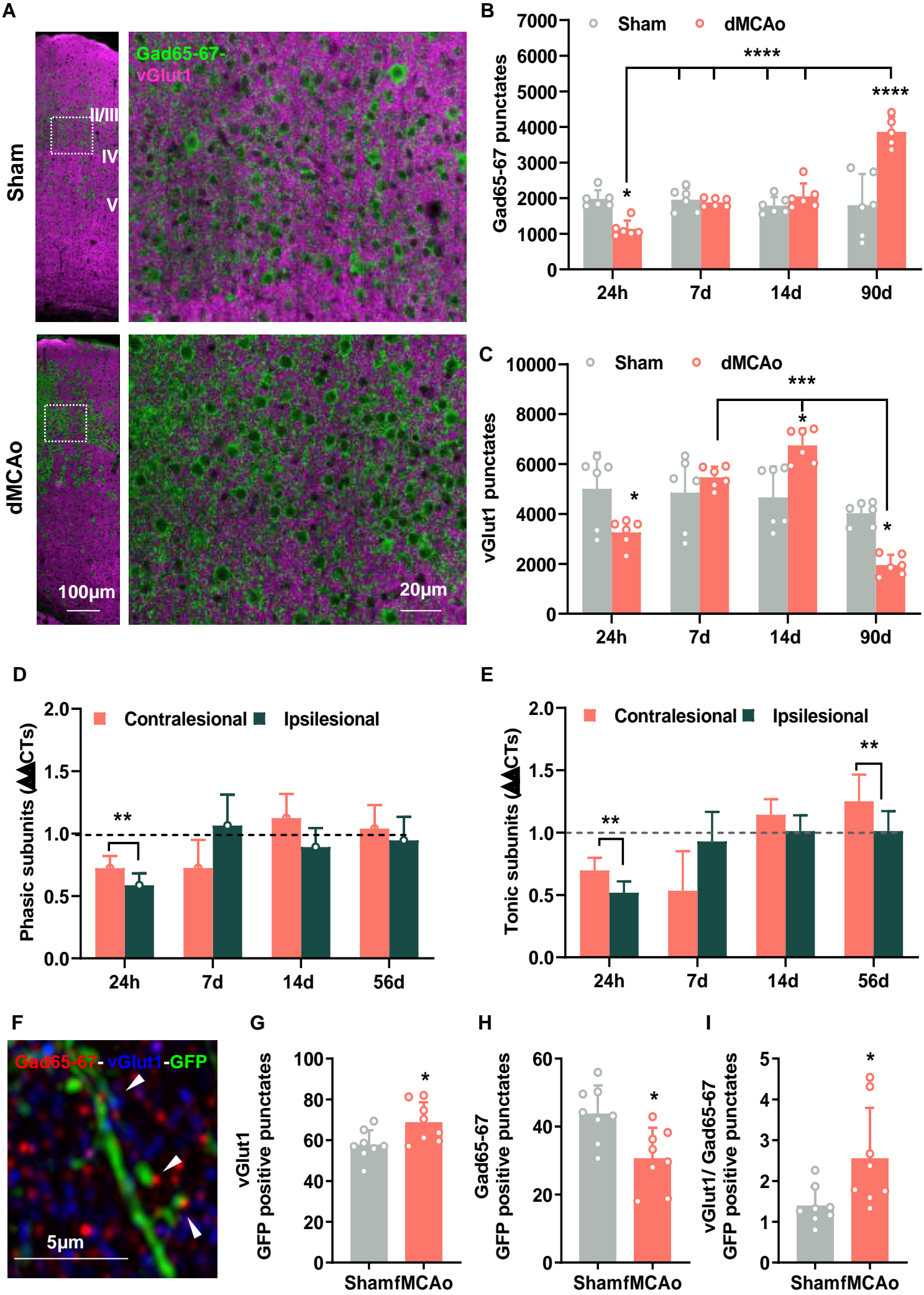
Sham

dMCAo

Valero Freitag et al, Figure 3







Valero Freitag et al, Figure 6

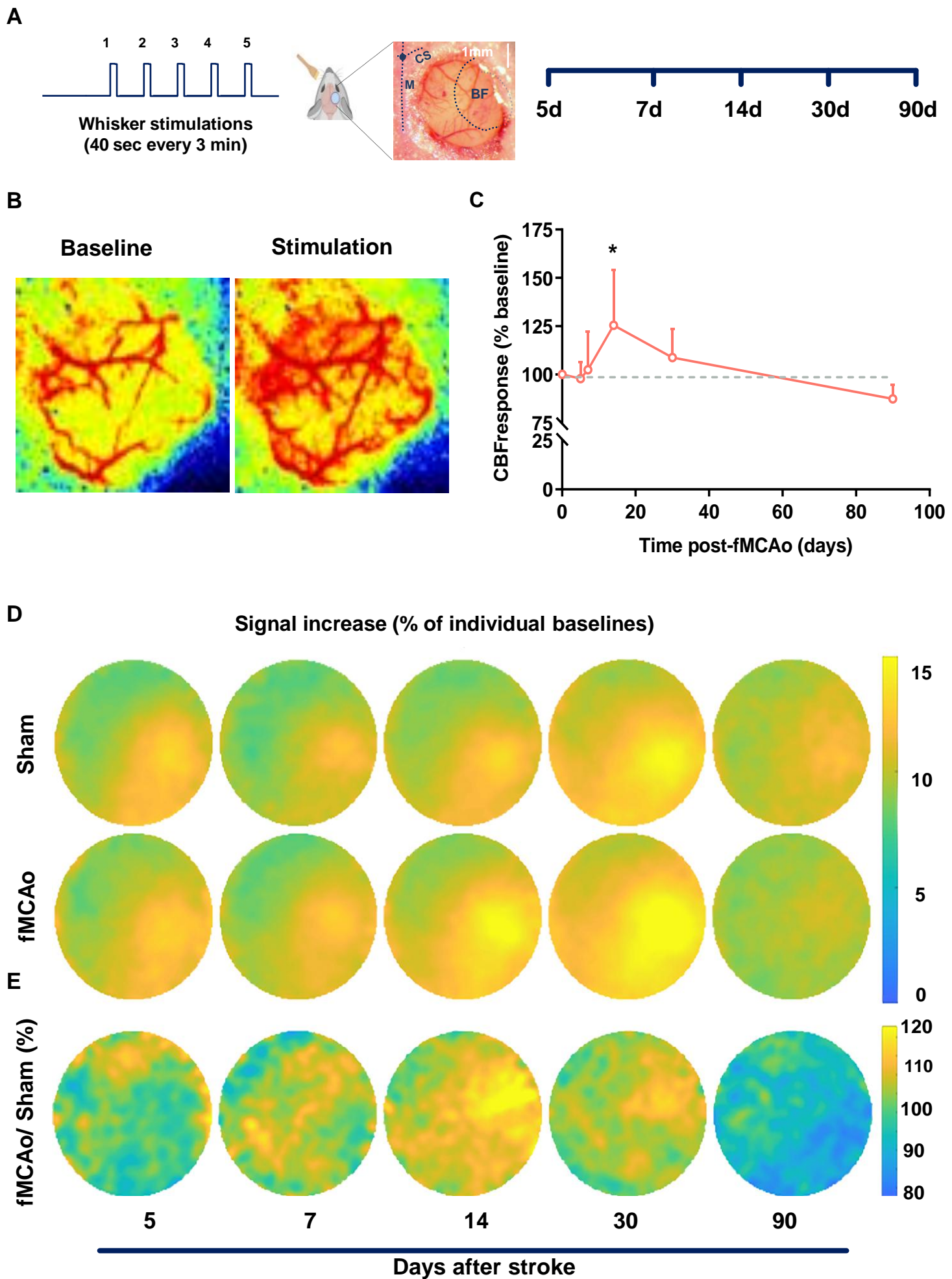


Figure Legends

Fig.1 fMCAo characterization

(A) The post-operative care protocol enabled a 100% survival rate in the chronic stroke phase. (B) Mice sustained neurological deficit up to 2 months after stroke (n= 11 fMCAo and 8 Sham) Two-way ANOVA followed by Sidak post-hoc test; means±sd; ***p<0.0001. (C) Illustration MRI imaging slice control and 3-month post-stroke (corpus callosum CC, Hippocampus Hipp, and Thalamus Th). (D) Corresponding quantification of hemispheric volume and (E) cross-sectional surface analysis Two-way ANOVA followed by Sidak post-hoc test; means±sd; *p<0.05 ***p<0.0001 stroke compared to naïve and #p<0.05 contralesional (contra) compared to ipsilesional (Ipsi). (F) 3D reconstruction of MRI image slices three months poststroke.

Fig.2 Transcallosal deafferentation leads to contralesional cortical thinning and neuropil shrinkage

(A) Quantification of contralesional cortical thickness, (B) total cell and neuronal density, (C) neuronal soma size distribution in the region of the barrel cortex (250-500 counted cells per brain), and (D) Region of the barrel cortex analyzed and neuropil extraction from Nissl stained inverted images. (E) Quantification of the neuropil fraction at two months after dMCAo (n= 10 mice/group). Data were analyzed by Mann-Whitney Rank Sum test and are presented as means ± standard deviation **** p< 0.0001, *** p< 0.001.

Fig.3 Callosal damage and soma alterations onto deafferented transcallosal neurons

(A) Schem of transcallosal neurons labeling and workflow. (BC) Cortical and callosal projections of transcallosal neurons in sham and after stroke damage where GFP positive axons present signs of degeneration and retraction bulbs (arrowheads) in the

cortex **(B)** and corpus callosum **(C)**, hallmark of degeneration and ongoing dieback at eight weeks after lesion. **(D)** Quantification of corpus callosum surfaces. **(E)** eGFP positive soma of transcallosal neurons presenting scarce atrophy. **(F)** Corresponding quantification of soma distribution (n=8-9 mice /group).

Fig.4 Contralesional transcallosal dendritic spine dynamics after stroke

(A) Contralesional transcallosal neurons labeled with AAV-EGFP portion of apical dendrite from sham-operated and injured animals two months after dMCAo. **(B)** Quantification *ex-vivo* of spine density in apical dendrites (region taken at least 100 μ m away from soma and with no branching point). Data were analyzed by a two-tailed t-test and are presented as means \pm standard deviation (n=5/ group; average of 700) *** $p < 0.001$. **(C)** Scheme of the workflow and illustrations of viral labeling. **(D)** 2-photon microscope acquired pictures of the same dendrites followed over different time points in the same animal. Quantification of **(E)** stable spines number **(F)** dynamic of gained and lost spine fractions **(G)** percentage of transient spines, **(H)**. Data were analyzed by a two-way ANOVA followed by Sidak post-hoc test (n= 8-11 Sham and fMCAo, respectively).

Fig.5 Contralesional excitation-inhibition balance

(A) Contralesional cortical column in the barrel field at 12 weeks poststroke labeled with Vesicular glutamate transporter 1 (vGlut1) and the glutamic acid decarboxylase 65/67 (Gad65/67) and blow up in the layer II/III in sham and stroke brain respectively. Quantification of **(B)** Gad65/67 and vGlut1 **(C)** punctate within the cortical column (n=7/group).

Relative expression of GABAA receptor subunits mediating phasic **(D)** and tonic **(E)** inhibition in the ipsilesional peri-infarct and contralesional homotopic region *versus* the sham group (dashed line). Illustration of inhibitory (red) and excitatory (blue) contacts

(F) together with quantification of vGlut1 (G) and Gad65/67 (H) punctate onto dendrites of deafferented transcallosal neurons in the homotopic area to the lesion. (I) Ratio of vGlut1/Gad65-67 synapses (n=8-9 mice /group). Data were analyzed by one-way ANOVA followed by Bonferroni post-hoc test and Student t-Test (ipsilesional *versus* contralesional), and are presented as means \pm standard deviation * $p<0.05$, *** $p<0.001$; **** $p<0.0001$.

Fig.6 Contralesional neurovascular coupling and functional connectivity impairment

(A) Timeline of the left whiskers stimulations (five trials) and cranial window on the contralesional cortex (CS, cortical suture; M, midline, BF, barrel field, blue dot shows the Bregma). (B) CBF at baseline and during stimulation. (C) Quantification of the average of maximum response. Data are presented as means \pm sd; Student t-Test *: $p<0.05$. (D) Heat maps averaging the response of all animals in each group and (E) stroke component of the response *versus* sham.

Supplementary material

Materials and Methods

Animals:

Animals were housed in our animal facility, under a 12/12hrs light/dark cycle, and were provided food and water ad libitum. Adult male C57BL/6N mice (12-16 weeks old, 23-26 g of body weight, Charles Rivers Laboratories) were used for the study. All surgical procedures and experiments were approved by the Ethics Review Board of the Government of Upper Bavaria in compliance with the ARRIVE (Animal Research: Reporting In Vivo Experiments) criteria (1). All experiments were performed and analyzed following randomized and blinded protocols.

Surgical procedures:

Virus injections and cranial window implantation:

Mice were anesthetized with an intraperitoneal (i.p.) triple combination injection of Medetomidin (0.5 mg/kg), Midazolam (5mg/kg) and Fentanyl (0.05 mg/kg). Stereotaxic virus injections were performed as previously described (2) with some modifications as follow. In brief, after placing the animal in the stereotaxic frame (David Kopf apparatus) on a warm pad, the skin was incised at the midline to expose the skull. A trepanation (3x4 mm) were carried out on the left or right side of the sagittal suture for the retrograde and anterograde labeling respectively. Mannitol (250 µl of 20%, B Braun Mesulgen) was injected intraperitoneally to facilitate virus penetration. About 10⁹ copies in 1µl of Adeno-associated viruses (AAV1-hSyn-EGFP or retroAAV2-CAG-EGFP) per mouse were distributed through pulled glass micropipettes (outside diameter at tip of about 30-40 µm) attached to a picospritzer (Twenty air-driven pulses per site,

20 PSI; 5-15 ms; General valve). Six defined locations (0.5 mm in depth to reach the layer II/III) were selected to include cortical areas that innervate the forelimbs and the whisker pad. After the injections the removed piece of bone was glued back with dental cement and Crazy glue. The anesthesia was then antagonized with a combination of Atipamezol (2.5 mg/kg), Flumazenil (0.5 mg/kg) and Naloxon (1.2 mg/kg) subcutaneously. Cranial window implantation was performed on the right hemisphere 2-3 days after the injections and one-month prior stroke surgery as previously described (3) with the following modifications. In brief, buprenorphine (100µg s.c. Temgesic Schering-Plough, Germany) was injected 30 minutes before the surgery. The mice were anesthetized with a combination of 2% Isoflurane/70%air/30% O₂ and received an injection of 200µg of Dexamethasone (s.c. to prevent brain swelling before trepanation (4 mm diameter). The dura mater was carefully removed with a thin forceps, and a circular cover glass (4 mm diameter) was placed directly on the surface of the brain. The cover glass was fixed to the cranial bone using a mixture of dental cement (Cyano Veneer) and Crazy glue. A plastic ring (100µg of weight) used for the fixation of the head during imaging was then firmly glued to the cranial bone. Animals were placed in a pre-heated recovery chamber (32°C) until all the vital functions had been recovered. All animals received daily analgesia up to 3 days (100µg s.c. Temgesic Schering-Plough, Germany) and Enrofloxacin (10 mg/kg; Baytril 50mg/ml Bayer, Germany) for five consecutive days.

2-Photon imaging and spine dynamics evaluation

Starting one month after cranial window implantation, dendritic tufts in upper layer II/III were imaged five times at two weeks interval. Imaging experiments were performed under light sedation Anesthesia was induced by subcutaneous bolus injection of medetomidin (0.05mg / kg) 10 min before experimentation and maintained through a

mask with a combination of 0.5-1 % isoflurane/70% air/30% oxygen (4). The dendritic tufts of transcallosal neurons connected to the infarct were imaged using a water immersion Plan-Apochromat 20x/NA 1.0 objective mounted on A Carl Zeiss LSM-7 MP, Oberkochen, Germany equipped with a Li:Ti laser (Chameleon, Coherent, USA). Repetitive imaging of the same dendrites could be achieved with the mouse head fixed with the plastic ring to a custom-made imaging setup. Superficial vessels were used as initial landmarks, and overview images (stack image $\approx 200\mu\text{m}$, x: $424.89\mu\text{m}$, y: $424.89\mu\text{m}$) were taken to relocate the dendrites of interest (3-5 per mouse). Dendrites selected for imaging were located at superficial levels of the cortex ($\approx 30\mu\text{m}$ depth; x: $87.23\mu\text{m}$, y: $87.23\mu\text{m}$) and a z-stack (Laser power varied between 5-10%, speed 8, Long Pass 570) was acquired. Also, the imaging lasted a maximum of 1 hour per session to preserve the EGFP signal over the imaging sessions (Fig.S2A,B). Besides, the heart rate and peripheral oxygen saturation were monitored by pulse oximeter on Lab Chart Reader. At the end of the imaging sessions, the mice were left to recover in 32°C recovery chamber prior returning to their home-cage. Spine quantifications: Spine density overtime was measured by dividing the total number of spines on the dendritic branch by its length for each time point. Spines were counted as stable when persisting during all imaging sessions. Transient spines were defined as spines appearing in single timepoint excluding baseline and the last time point (8 weeks). Gained and lost fractions of spines were calculated over the total number of spines. The spine density at three months was measured ex-vivo by counting the number of spines per $10\mu\text{m}$ dendritic length.

Cerebral ischemia models

The mice were anesthetized with 4% isoflurane, (balanced with 30% O_2 , and 65% N_2) and maintained with 1.5-2% isoflurane for the duration of surgery. The body

temperature was maintained at 37°C using a feedback-controlled heating pad. Permanent focal cerebral ischemia (dMCAo) was induced by electrocoagulation of the distal part of the middle cerebral artery (MCA) as previously described (5). In brief, 30 minutes before surgery, the mice received subcutaneous of Buprenorphine (100µg s.c.; Temgesic Schering-Plough, Germany) for analgesia. The skin was excised to expose the skull, a burr hole was drilled in the temporal bone, and the MCA was permanently occluded using high-frequency electrocoagulation forceps. This model causes less than 5% mortality. Transient cerebral ischemia (referred as fMCAo) was induced by occlusion of the left middle cerebral artery for 60 min followed by reperfusion using the filament model (silicon-coated filament #701912PK5Re, Doccol) as previously described (6, 7). Certainty of the occlusion was confirmed by decreased regional cerebral blood flow (CBF) monitored by a laser Doppler probe fixed to the skull above the MCA territory (Fig.S1C). Vital parameters were controlled by pulse oximeter (Fig.S1DE). Wounds were treated with Povidone-iodine and sutured; the mice received an injection of saline (1 ml s.c.; B Braun Mesulgen) and were placed in 32°C recovery chamber until full recovery of motor function. Then the mice were returned to their home cage with free access to water and food. Sham surgeries were performed following the same surgical procedures without occlusion of the MCA.

Post-operative care:

To minimize mortality after tMCAo, we applied post-operative care based on the feeding protocol we previously described (7) with the following modifications (Fig.S1A). During the first three days following surgery, the mice received daily injections of Buprenorphine (4 mg/kg s.c.) as analgesic and 0.2% Glucose (G-20 B Braun Mesulgen) up to 14 days until stabilization of the body weight. In addition to the regular food and water supply, Petri dishes containing freshwater gel slices were placed

a the bottom of the cage along with daily refreshed gel formulated food containing 12.8 KJ/g of metabolizable energy (regular mouse/rat maintenance powdered food (V1530, Ssniff Germany) mixed with water (1:3 ratio). Bodyweight was monitored before surgery, daily for the first week, and weekly after that until five weeks after stroke induction as an indicator of animal welfare (data not shown). Only animals which showed less than 20% body weight loss were included in the study.

Behavior assessment:

Sickness and sensorimotor behavioral deficits (also called modified Neurological Severity Score mNSS) were assessed as previously described (7) starting from the day of stroke surgery and every two weeks in alternate with the 2-photon imaging sessions for nine weeks.

Whisker stimulation and Laser speckle imaging:

Wisker stimulation was performed under light sedation, as described above. The left whiskers were stimulated five times with a frequency of 1-2 Hz for 40 seconds with 3 minutes interval while the CBF response was recorded on the right somatosensorial cortex through the cranial window previously used for the imaging. PeriCam PSI High-Resolution Laser Speckle was used for acquisition of whisker stimulation responses at a resolution of 44 frames/sec (Movie S2). Numerical values were generated using the PIMSoft program. For each 30 sec of stimulation, the CBF response was normalized to an individual baseline corresponding to the 20-sec recording before stimulation (Movie S2, see TOI). Individual and averaged responses for sham and stroke groups were analyzed.

CO₂ challenge:

Vasomotor reactivity was evaluated using CO₂ as a vasoactive stimulus, as previously described (8). Animals were kept under light sedation as described above to record the baseline and exposed to 10% CO₂ for 5 min to induce a hypercapnic blood flow response (Fig.S3A). Inhaled CO₂ was controlled by microcapnometry (Fig.S3B). The contralesional CBF response was monitored before and after CO₂ inhalation (Fig.S3C) until recovery of baseline (4 min) by laser speckle imaging.

Heat map acquisition:

Laser Doppler perfusion imaging (LDPI) was used to capture 2-D images of the perfusion in the cortex contralateral to the infarct while stimulating the ipsilateral forepaw. For each mouse, a series of images were acquired with an acquisition rate of 4.4Hz and image matrix 245 x 245 pixels. Image acquisition started 2 minutes before the first forepaw stimulation. Stimulations lasted 30 seconds and were repeated five times with an inter-stimulus-interval of 3 minutes. Perfusion images were analyzed in MATLAB (R2016b, The MathWorks, Natick, MA) using custom scripts. First, a spherical region of interest (ROI), containing the exposed cortex, was defined manually. For each pixel within the ROI, the perfusion signal time-series was highpass filtered with a cutoff frequency of 0.004 Hz, in order to remove signal drift. This filter was implemented using the MATLAB functions `cheby1` and `filtfilt` to design a Chebyshev Type I filter of order 2 and to perform zero-phase digital filtering. Then a threshold was defined using Otsu's method, in order to detect stimulation periods automatically. The correct detection of stimulation periods was verified visually. To account for a potentially ramp-like increase of the perfusion signal at the beginning of the stimulation, the perfusion signal was averaged within 10 and 30 seconds after the automatically detected stimulation onset and normalized to the baseline perfusion signal, defined

individually for each stimulation period as the average signal within 40 to 10 seconds before the automatically detected stimulation onset. The hereby resulting, normalized response of the perfusion signal to the stimulation was then averaged across stimulation periods, first individually for each animal, and then across animals within each experimental group. To allow averaging across animals, the images, cropped around the spherical ROI, were resized to an image matrix of 120 x 120 pixels. One animal of the sham group was excluded due to signal fluctuations, not being related to the stimulation periods. For a better understanding of the individual responses, heat maps were also acquired for individual animals (Fig. S4). Given the within sham group variation in the response to stimulation we had to implement exclusion criteria. We included datasets only if at least a connected area of pixels, covering at least 5% of the total area in the spherical ROI and having response to stimulation above 10% of baseline intensity (data not shown).

Tissue processing and imaging:

Animals were anesthetized by intraperitoneal injection of mix midazolam (5mg/kg; Braun, Melsungen, Germany), fentanyl (0.05mg/kg; Jansen-Cilag, Neuss, Germany), and medetomidine (0.5mg/kg; Pfizer, Karlsruhe, Germany) and transcardially perfused with saline followed by 4% paraformaldehyde in 0.1 M sodium phosphate buffer pH 7.4 (PBS). Brains were removed and post-fixed the same fixative for 24h and transfer to PBS for further processing. After a brief wash in PBS, the brains were either embedded in 4% low melting temperature agarose for vibratome sectioning or kept in graded solutions of sucrose (10-30%) and froze in dry-ice chilled isopentane for cryosectioning. Serial free-floating 50µm thick coronal sections were cut through the cerebrum with a Leica VS1200 vibratome and collected in cryoprotectant solution (polyethylene glycol 400 and glycerol TBS/0.05% sodium azide). Serial cryo-sections

(20 μ m) were cut on Thermo Shandon 620 Cryostat collected on Superfrost plus slides. All samples were stored at -20°C until further processing.

Brain thickness and neuropil fraction measurements

To explore the extent of brain atrophy, the thickness of the contralesional cortex and corpus callosum were assessed at bregma 0, -0.5 and -1.5 levels covering the infarct in Nissl-stained sections. Sections mounted onto Superfrost slides were air-dried overnight, and incubated for 45 minutes at 60°C in a solution of 0.05% Cresyl fast violet /0.05% acetic acid, rinsed in distilled water, and differentiated through a graded series of alcohols before clearing in xylene and coverslipped with DPX. To evaluate the cortical thickness, 15 perpendicular lines extending from white matter to pial surface were placed on the sections using a 5X objective covering cortical regions spanning the sensorimotor cortex including the primary visual, primary motor, and lateral entorhinal cortices according to the landmarks described by Paxinos and Franklin. Ipsilesional and contralesional (until midline) corpus callosum surfaces were measured at bregma level slices, as previously described using ImageJ software (9). The average of three sections was then calculated for each animal and used for statistical comparison between groups. Results were expressed as the mean cortical thickness in μ m and surface coverage for corpus callosum.

The Nissl-stained volume fraction corresponds to cell bodies of neurons, glia, and endothelial cells. The non-stained area represents the neuropil space containing the glial and neuronal dendrites and axons, which provides an indirect readout of connectivity coverage. The neuropil fraction was evaluated in layers II/III from high-resolution images taken in the homotopic region to the lesion. The area covered by the neuropil was extracted in the inverted images after conversion to 8 bit and binarization (erode

and dilate) using Image J software. The average of three sections was then calculated for each animal and used for statistical comparison between groups.

Cell density and soma size:

To determine the neuronal and non-neuronal cell densities, three brain sections (bregma 0, -0.5 and -1.5 levels) were stained with NeuN and Dapi. Four regions per section were delimited and imaged in homotopic region to the lesion in the contralesional cortex (layer II/III and V). Manual counting of the number of Dapi stained cells NeuN positive or NeuN negative was performed after blinding for the sham and stroke groups. Neuronal soma size area was traced and measured using Image J software. Frequency distribution of the neuronal soma sizes was generated using Excel software.

Immunofluorescence and confocal imaging

Immunofluorescent stainings were performed on vibratome sections as previously described (10) using guinea pig anti -Vesicular glutamate transporter 1(vGlut1; Millipore AB5905; and the rabbit anti- glutamic acid decarboxylase 65/67 (Gad65/67; Sigma G5163) both at the dilution 1:5000 followed by Donkey anti Guinea pig Alexa 647 and Donkey anti rabbit Alexa 488 (1:1000) secondary. Fluorescence images were acquired with EC Plan-Neofluar 40x/1.30 Oil DIC M27, and the Plan-Apochromat 100x/1.46 Oil DIC objectives mounted on confocal laser scanning microscope (LSM 880, Carl Zeiss) equipped with the GaAsP and Airyscan detectors.

Quantification of vGlut1 and Gad 65/67 punctate was performed in the homotopic contralesional cortex on 3 representative sections (bregma 0, -0.5 and -1.5 levels). 7 regions of interested (30µm z-stack; 42.43 µm width); delineating a full cortical column from marginal zone to corpus callosum) were defined per section. Total number of

vGlut1 and Gad 65/67 punctates were counted using the macro Find Maxima from FIJI Image J software (Noise tolerance 15 and 20 respectively). The average of three sections was then calculated for each animal and used for statistical comparison between groups. We also manually counted the number of vGlut1 and gad65/67 overlapping with contacting the GFP positive spines from labeled transcallosal neurons in the anterior and posterior region homotopic to the lesion (see neurovascular coupling result section for details).

Ex-vivo MRI acquisition

In vivo MRI was performed using a 3T nanoScan® PET/MR (Mediso, Münster Germany). The magnet is equipped with a 3 Tesla cryogen-free system (bore size 2350 mm, > 450 mT/m maximum gradient) and a 42 mm internal diameter quadrature mouse body coil was used. The brains stored in PBS in 15 ml falcon tubes were fixed on custom-made holder during MRI scanning. Coronal MRI sections of the entire cerebrum were performed. T2-weighted imaging (T2WI) were acquired with the following parameters: 2D fast-spin echo (FSE); TR/TE = 3000/65.3 ms; number of averages 17; matrix size = 272×272 ; field of view = $38 \text{ mm} \times 38 \text{ mm}$; resolution $140 \times 140 \times 660 \mu\text{m}^3$. To determine the stroke lesion area, the ROI was identified by referring to T2-weighted images. Ipsilesional and contralesional hemispheric were manually measured on 12 consecutive sections using ImageJ software (polygone tool; National Institutes of Health, Bethesda, MD). Volume was then calculated using the following equation: $V = d \cdot (A_1/2 + A_2 + A_3 \dots + A_n/2)$ with d being the distance between sections in mm and A being the measured area. 3D reconstruction of the representative MRI images was performed using Imaris Software.

Real-Time PCR

At different time-points after stroke, the brains were dissected and the lesion area in the ipsilateral cortex, as well as the homotopic corresponding area in the contralesional cortex, were collected separately using a biopsy punch (3 mm diameter) and used to isolate total RNA. Total RNA was isolated using the RNeasy Mini kit (Qiagen), according to the manufacturer's protocol and quantified by measuring optical density. A total of 1000 ng of total RNA was treated with amplification grade DNase I (Invitrogen; Karlsruhe, Germany) to eliminate residual genomic DNA from the sample, and reverse transcribed with oligo(dT)12-18 primers and Superscript II Reverse Transcriptase, using the Omniscript First-Strand Synthesis System for RT-PCR (Qiagen), according to the manufacturer's instructions. Real-Time PCR reactions were carried out with 20 ng of cDNA template and 20 pm each of forward and reverse gene-specific primer, using the LightCycler QuantiNova SYBR Green RT-PCR Kit (Qiagen). Primers for GABA_A receptor subunits $\alpha 1$, $\alpha 2$ and δ targeting phasic (extrasynaptic) and $\alpha 4$, $\alpha 5$ and $\gamma 2$ targeting tonic (synaptic) inhibition were designed spanning intronic regions to rule out contamination from genomic DNA (Table. S1). Real-time PCR reactions were performed in triplicate on a Light Cycler 480 Instrument (Roche; Mannheim, Germany). Melting curve analysis was run for each primer pair to ensure that the PCR reaction yielded a single, pure, PCR product. CP (Crossing Point) values, which correlate inversely with the log of the initial template concentration, were determined by averaging CP values from three independent Light Cycler reactions. Fold increase in expression of the transcript was calculated as a ratio of $2^{\Delta CP}$ from target gene and $2^{\Delta CP}$ from GAPDH gene. The housekeeping gene, GAPDH was used for normalization in order to compensate for variability in RNA amount and for exclusion of general transcription effects. All expression values are relative to the ones of sham operated

animals. Relative expression values of all subunits mediating phasic respectively tonic inhibition were averaged for each animal to obtain a measure for phasic and tonic inhibition.

Statistical analysis:

Sample size and statistical analysis were performed using Graphpad Prism 8 software. All plotted values were expressed as means plus standard deviation (SD). F test was applied to define similarity in variances. For comparison between two groups statistical significance was determined by two-tailed Student's t-test with Welch' correction or Mann-Whitney Rank Sum test. For multiple comparison one-way analysis of variance (ANOVA) followed by followed by Sidak post-hoc test was used. Two ANOVA followed by followed by Sidak or Bonferroni post-hoc test were applied for repeated measures as indicated in figure legends. A p-value of less than 0.05 was considered statistically significant.

Movie legends

Movie S1: 3D reconstruction of representative MRI images of a brain 3 months after stroke

Positioning of the lesion core and the corresponding homotopic region in the contralesional hemisphere.

Movie S2: Example of CBF response to whiskers stimulation in Sham- operated animal Activity of ROI (blue) versus full field of view (black). TOI (time of interest) defining the baseline and following stimulation (2 trials).

Movie S3: Example of CBF response to whiskers stimulation 14 days after stroke

Movie S4: Example of CBF response to whiskers stimulation 90 days after stroke

References

1. C. Kilkenny, D. G. Altman, Improving bioscience research reporting: ARRIVE-ing at a solution. *Laboratory animals* **44**, 377 (Oct, 2010).
2. A. Erturk *et al.*, Three-dimensional imaging of the unsectioned adult spinal cord to assess axon regeneration and glial responses after injury. *Nature medicine* **18**, 166 (Dec 25, 2011).
3. A. Holtmaat *et al.*, Long-term, high-resolution imaging in the mouse neocortex through a chronic cranial window. *Nature protocols* **4**, 1128 (2009).
4. J. V. Cramer *et al.*, In vivo widefield calcium imaging of the mouse cortex for analysis of network connectivity in health and brain disease. *NeuroImage* **199**, 570 (Jun 7, 2019).
5. G. Llovera, S. Roth, N. Plesnila, R. Veltkamp, A. Liesz, Modeling stroke in mice: permanent coagulation of the distal middle cerebral artery. *Journal of visualized experiments : JoVE*, e51729 (Jul 31, 2014).
6. G. Llovera *et al.*, Results of a preclinical randomized controlled multicenter trial (pRCT): Anti-CD49d treatment for acute brain ischemia. *Science translational medicine* **7**, 299ra121 (Aug 5, 2015).
7. A. Lourbopoulos *et al.*, Inadequate food and water intake determine mortality following stroke in mice. *Journal of cerebral blood flow and metabolism : official journal of the International Society of Cerebral Blood Flow and Metabolism* **37**, 2084 (Jun, 2017).
8. M. Balbi *et al.*, Dysfunction of mouse cerebral arteries during early aging. *Journal of cerebral blood flow and metabolism : official journal of the International Society of Cerebral Blood Flow and Metabolism* **35**, 1445 (Sep, 2015).
9. R. H. Andres *et al.*, Human neural stem cells enhance structural plasticity and axonal transport in the ischaemic brain. *Brain : a journal of neurology* **134**, 1777 (Jun, 2011).
10. M. Ghosh *et al.*, Pericytes are involved in the pathogenesis of cerebral autosomal dominant arteriopathy with subcortical infarcts and leukoencephalopathy. *Annals of neurology* **78**, 887 (Dec, 2015).

Fig. S1.

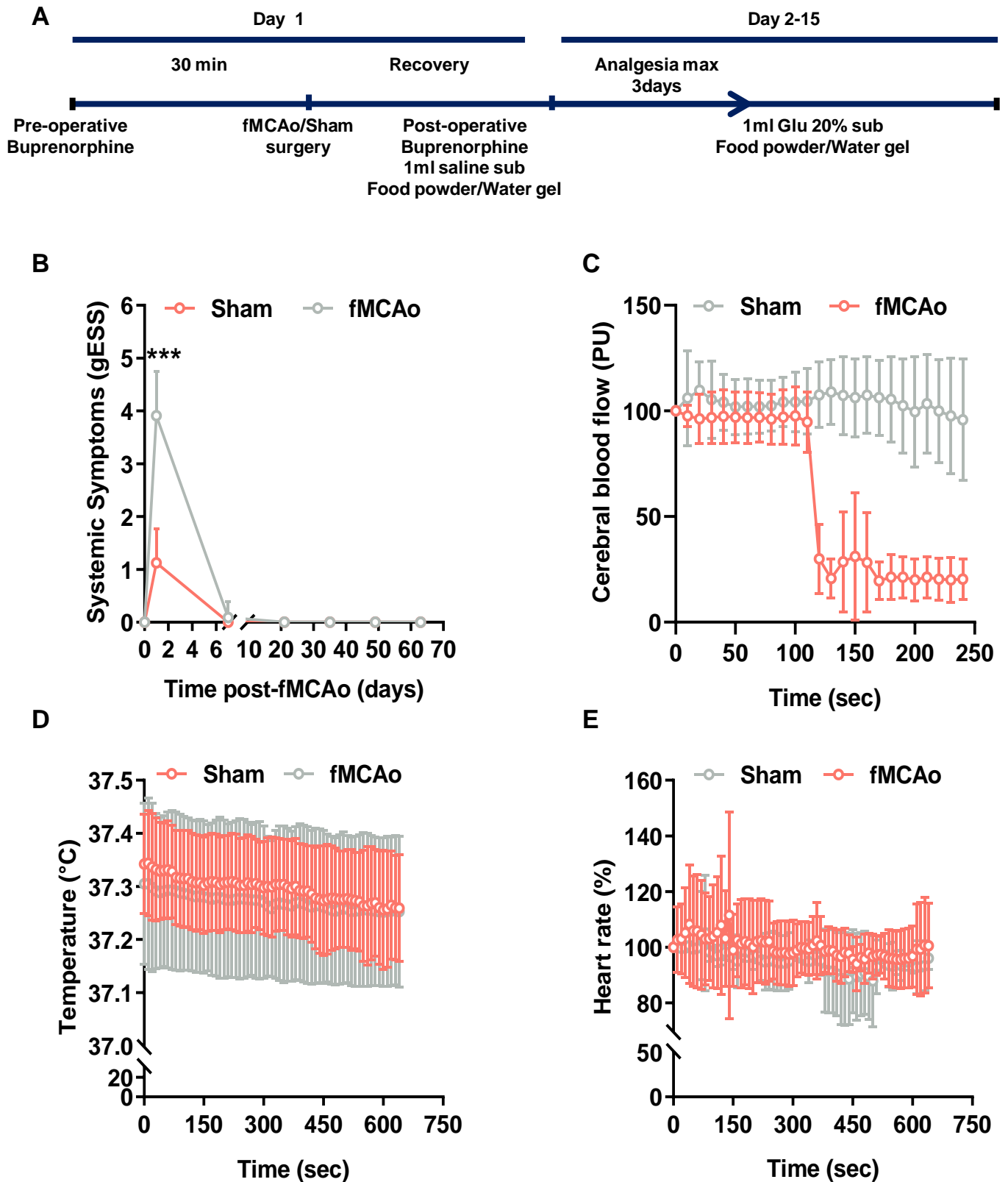


Fig. S1. Post-operative care workflow, sickness behavioral recovery and vital parameters (A) Protocol for optimum survival. **(B)** Sickness behavior recovery overtime. **(C)** Drop in cerebral blood flow at the MCA during the occlusion. **(D)** Rectal temperature and **(E)** heart rate are not altered. Data is analyzed by Two-way ANOVA followed by Sidak post-hoc test and presented as means \pm standard deviation ***p<0.001; (n = 8-11/group).

Fig. S2.

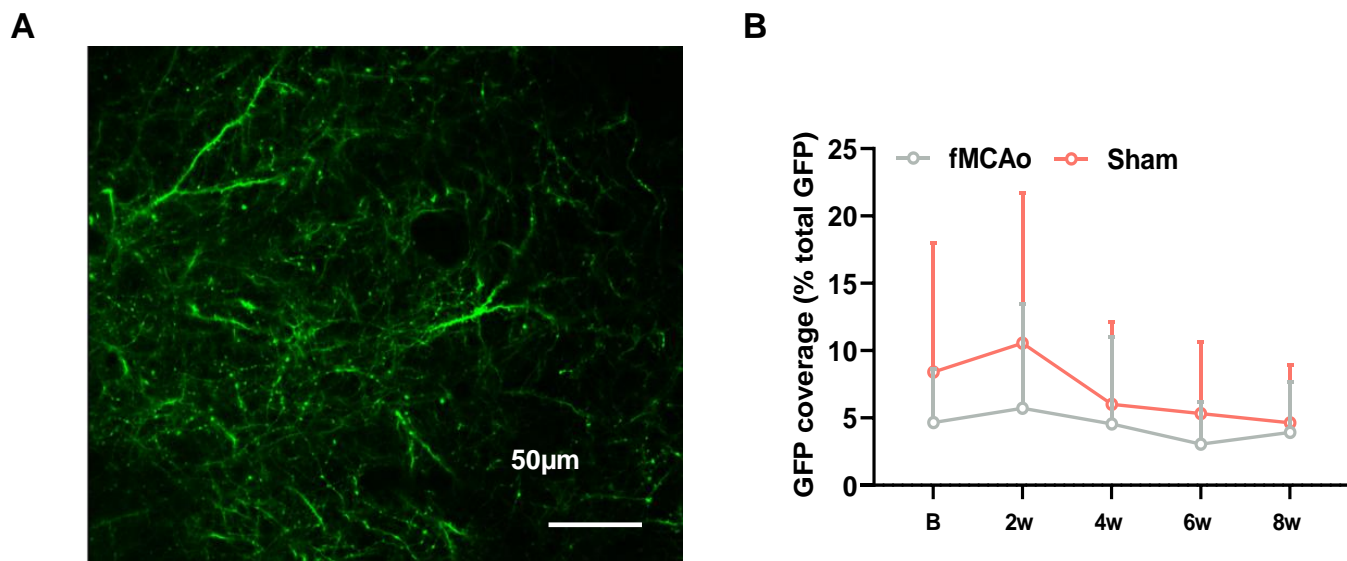


Fig. S2. Analysis of fluorescence over the course of time

(A) 2-photon overview picture of GFP positive dendritic tufts of transcallosal neurons connected to the lesion (B) GFP coverage does not vary over the repetitive imaging sessions. Data are presented as means \pm standard deviation ($n = 7/\text{group}$).

Fig. S3.

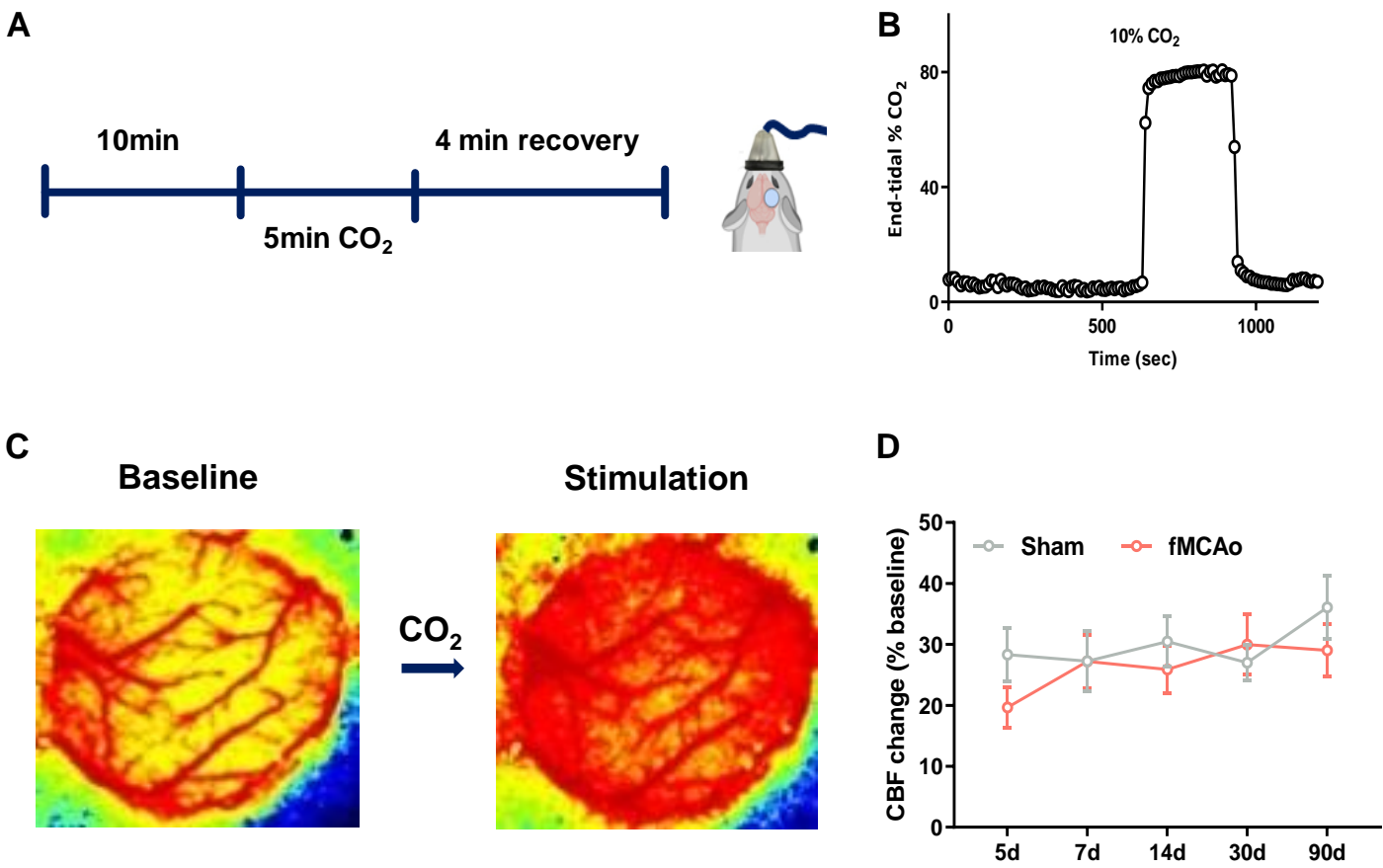


Fig. S3.

E

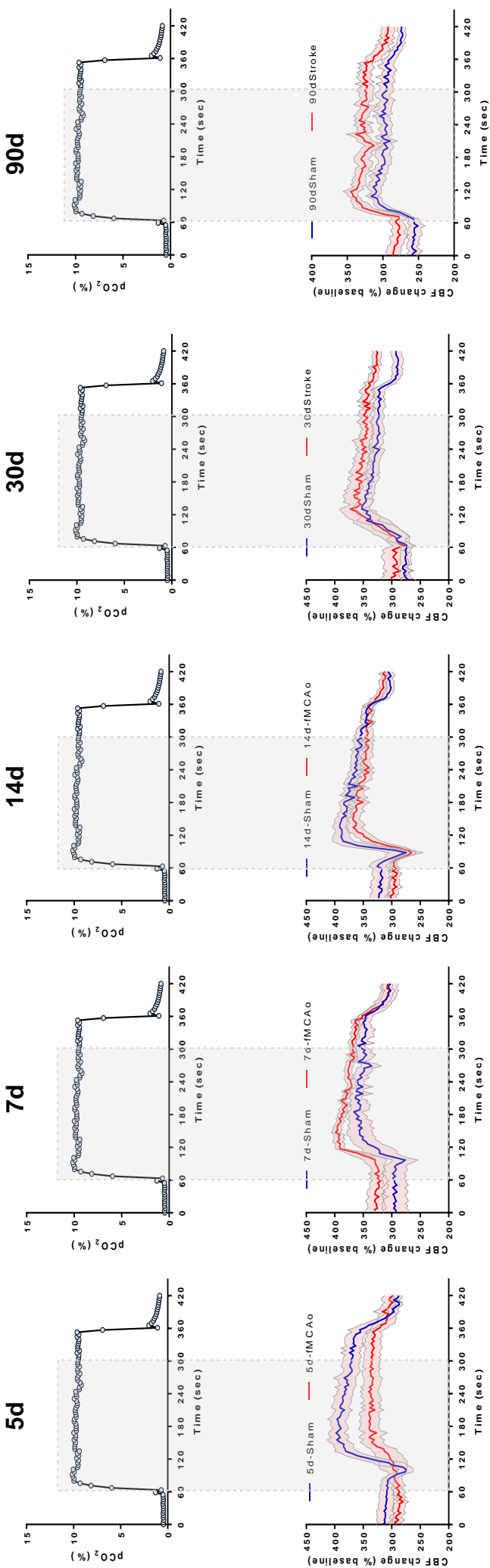


Fig. S3. CO_2 inhalation and vessel reactivity assessment

(A) CO_2 challenge timeline and (B) illustration of increased CBF upon stimulation (C) End-tidal $p\text{CO}_2$ changes during CO_2 inhalation (C) Response measured as area under the curve over time. (E) Averaged CBF responses to 10% CO_2 inhalation. Data are presented as means \pm standard deviation (n = 7-8/ group).

Fig. S4.

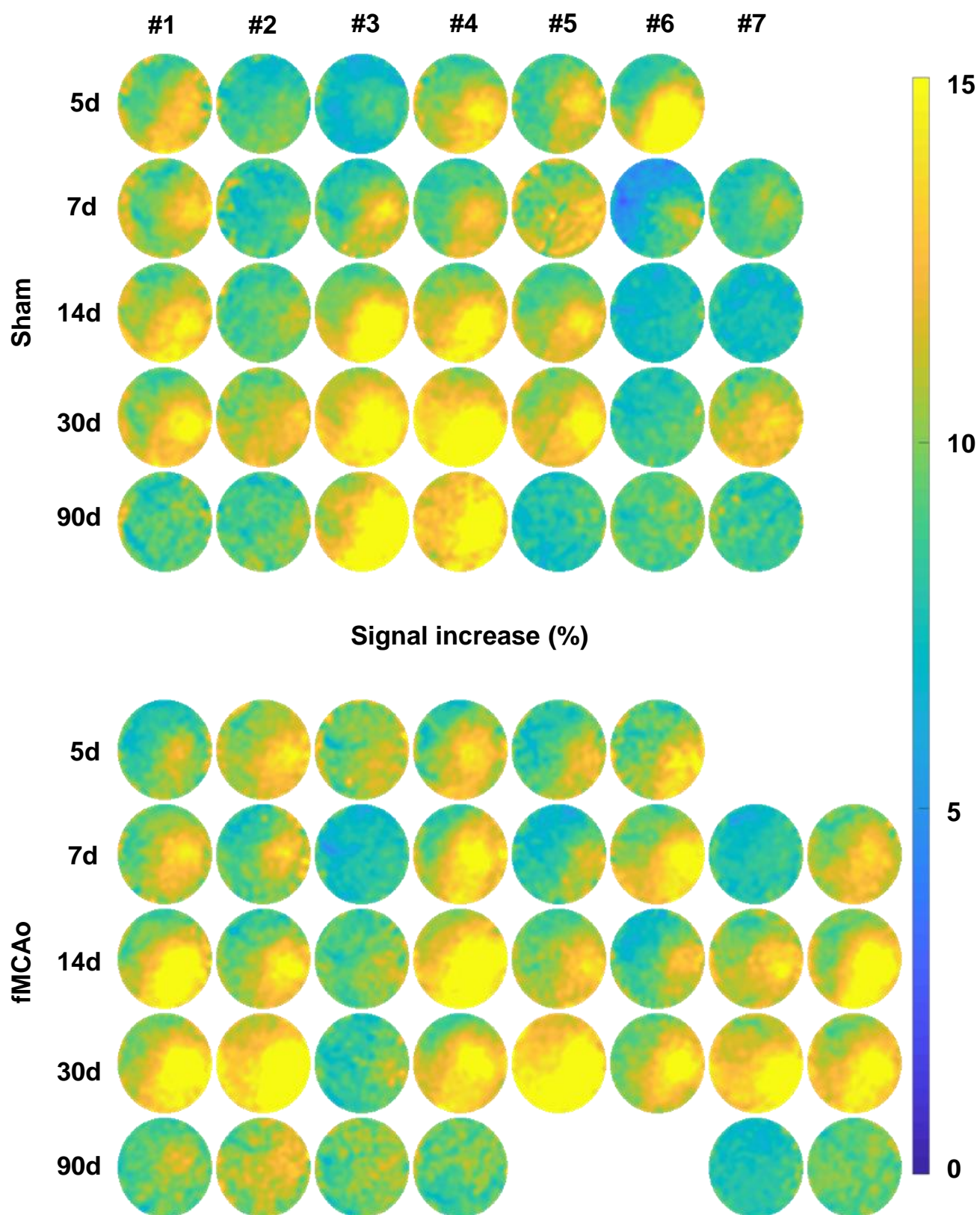


Fig. S4. Individual heat maps

Mouse individual heat maps (5 averaged stimulations). Missing signals are from animals presenting blurry infected cranial windows which had to be terminated.

Table. 1 qPCR primers

Gene	Gene product	Forward	Reverse
<i>Gabra1</i>	GABA Receptor A subunit α 1	GCCCACTAAAATTCGGAAGC	CTTCTGCTACAACCACTGAACG
<i>Gabra2</i>	GABA Receptor A subunit α 2	TTCACAAAAAGAGGATGGGC	TGACGGAGCCTTTCTCTTTT
<i>Gabra3</i>	GABA Receptor A subunit α 3	TGGCACTTTTATGTGACCAGA	CATGCTTGGGAGAGATGCCT
<i>Gabra4</i>	GABA Receptor A subunit α 4	AAAGCCTCCCCCAGAAGTT	CATGTTCAAATTGGCATGTGT
<i>Gabra5</i>	GABA Receptor A subunit α 5	GACGGACTCTTGGATGGCTA	ACCTGCGTGATTCGCTCT
<i>Gabrd</i>	GABA Receptor A subunit delta	CAAGGTCAAGGTCACCAAGC	GGGAGATAGCCAACCTCCTGA
<i>Gabrg2</i>	GABA Receptor A subunit gamma 2	GGAATACAACTGAAGTAGTGA AGACAA	TTCTGCTCAGATCGAAGTACAC A
<i>Gapdh</i>	Glyceraldehyde-3-phosphate dehydrogenase	ATTGTCAGCAATGCATCCTG	ATGGACTGTGGTCATGAGCC

4. Discussion

4.1. Critical reasoning of the results

Our results characterized the long-lasting and high plasticity undergoing in neurites in pathological conditions. As the main components of the synapses, the alterations axons and dendrites undergo has a great impact on synaptic strength, number, and function (Lin and Koleske, 2010; Araya et al., 2014) worsening the pathological condition. Synaptic pathology has been previously studied in neurodegenerative diseases and psychiatric disorders (van Spronsen and Hoogenraad, 2010), highlighting the importance of the structural and molecular organization of synapses for brain function and recovery.

We can summarize our results on axonal pathology in AD, in two main points according to the experiments developed *in vivo* and *ex vivo*. The three-dimensional reconstruction and study of dystrophic axons expressing GFP followed *in vivo*, allowed us to observe the possible existence of two subpopulations of dystrophies, both with a long life span. On the one hand, a more "active" population characterized by more significant variations in size over time that reach higher volumes. Interestingly, in this population, both the disappearance and formation of new dystrophies in the same parental axon as well as "sprouting" or abnormal axonal growth can be observed. On the other hand, we find other more stable or "passive" dystrophies that present less variation over time. With the *ex vivo* analysis, we were able to observe that most of the dystrophies that express GFP express markers of a presynaptic nature as well as lysosomal and autophagy markers. We also found that A β peptide is expressed in only 60% of the GFP-expressing dystrophies.

Previous research has focused on imaging neurites in the vicinity of amyloid plaques (D'Amore et al., 2003; Tsai et al., 2004; Garcia-Alloza et al., 2006; Serrano-Pozo et al., 2011; Sadleir et al., 2016). DN's were observed over short periods (3 days to 5 weeks maximum) as a pathological hallmark near plaques analyzing their nature and potential origin. Also, dystrophies were imaged before and after applying antioxidants (Garcia-Alloza et al., 2006), A β antibodies (Brendza et al., 2005), or BACE inhibitors as treatments (Peters et al., 2018).

An essential contribution of our study was the follow-up of individual dystrophies over a long period (5.5 months). This enabled the analysis of long-lasting heterogeneous changes that take place between different dystrophies or in the same dystrophy. We observed that they are present for a longer time than previously thought and do not grow steadily, but show "waves" of growth and decrease. They can also disappear while the parental axon remains and generate new dystrophy.

Although DN's apply to both morphological changes in axons and dendrites, in our model, the dystrophies expressing GFP were predominant axonal as by their characteristics seen *in vivo* and by immunostaining and co-localization with the common synaptic markers (Vglut-1, BACE-1, and SNAP-25).

Moreover, we observed that almost all DN's expressing GFP had immunoreactivity for BACE-1 (92%). However, in the case of A β and APP peptide, only 60% of the GFP expressing dystrophies expressed A β 42, which recognizes monomeric forms of A β . 50% of the GFP expressing dystrophies were positive for A β 4G8, which recognizes both APP and some forms of A β peptide. This is probably why only about half of the dystrophies could be explained by the presence of BACE-1 and the generation of A β . However, we cannot exclude that A β formation

may be a transitory event in DNs since we have observed that over time they are very flexible structures.

As described in other studies, we also found the colocalization of DNs with lysosomal and autophagy markers. Therefore, the accumulation of autophagic vesicles in DNs is essential in their formation. However, it remains unclear what exactly leads to the formation of these abnormalities in the axons near the plaques in AD.

In our study, we observed that about 22% of the axons crossing near the amyloid plaque developed a dystrophic pathology. This is an interesting finding since most axons seem to be resistant to the pathology. Until recently, cortical pyramidal neurons have been considered a homogeneous class of cells. This concept is now changing and different pyramidal cell types have been recognized. Cortical regions, layers, or even within the same layer pyramidal neurons could differ in morphology, neurochemistry, and physiological properties (Molnar and Cheung, 2006; Schubert et al., 2006; Hattox and Nelson, 2007). These different properties may explain the different susceptibility to dystrophic pathology.

Furthermore, the relationship between extracellular amyloid deposits and the formation of dystrophies is not known. Are DNs a cause or a consequence of the plaque formation? For years, it has been considered that the formation of DNs was a consequence of amyloid deposition or microglia activation but not an active participant in the pathogenesis of the plaques. This view is changing and instead suggest that the processing of the A β peptide in DNs contributes to the formation of the plaques (Nixon et al., 2005). This fact, together with the disruption of axon transport, abnormal mitochondrial function, oxidative stress, autophagy, and altered lysosomal processing, places DNs as a possible nest for plaque formation (Fiala, 2007).

We found two subpopulations of DNs: stable or "passive" dystrophies versus a more "active" type. The existence of these two types seems to suggest that both situations can coexist and that the dystrophies can be cause or consequence of the plaques, being the "active" ones those that contribute more pronounced to the formation of the plaque and the "passive" ones, the dystrophies that would originate in a second way.

In the same line, our neurochemical analyses suggest the existence of two populations of dystrophies that express GFP, those that present APP and A β (over 50%), and others that do not. The first may correspond to those formed by the intracellular presence of BACE-1 and the generation of A β and which would actively participate in the formation of the plaque, while the others may be those, which originate secondarily from the effect of the A β of the plaque.

Taking into account all these results and the existence of this neuronal plasticity, especially around the amyloid plaques, the possibility that synaptic abnormalities associated with amyloid plaques may be reversible within a specific time window increases. To that end, the two-photon *in vivo* technique and the use of appropriate tools for the development of detailed three-dimensional reconstructions can help to establish the guidelines for future research to promote axonal functional regeneration and the restoration of neuronal circuits.

Regarding our stroke research, we demonstrate that damaged and deafferented transcallosal neurons remodel their dendritic spines underlying the observed diaschisis in the contralesional hemisphere. The ongoing atrophy at the level of the infarcted hemisphere (ipsilesional) would lead to an extension of the damage to the contralesional side through the transcallosal pathway. The first effect we could see was a decrease in the cortical thickness, which has also been observed in previous clinical studies (Duering et al., 2015; Cheng et al., 2020).

The thinning took place without any cell death since no change in the cell density nor in the soma size was seen. Interestingly, we found a significant decrease in the neuropil fraction, together with a decrease in spine density in the apical dendrites of transcallosal neurons after stroke. The dendritic reorganization of these neurons might explain this remote effect.

Previous studies have focused on dendritic alterations in the contralesional hemisphere, but it remains unclear if there is remodeling or not (Takatsuru et al., 2009; Johnston et al., 2013). The controversy might lie in differences in the observed cortical area and the use of thy1-GFP multivariant transgenic mice, which provides non-uniform labeling through layers as well as cortical regions (Porrero et al., 2010). One crucial aspect of our work, also contributing to lower the level of ambiguity in the field, was the use of retrograde labeling to target specifically the transcallosal neurons deafferented by an ischemic stroke.

Moreover, the structural changes observed were related to the functional outcome by measuring the response to whisker's stimulation using laser speckle imaging. Based on the NVC principle, activated and more functional neurons demand more blood supply and induce an increase in the hemodynamic signal that is recorded by the laser speckle. Structural alterations would translate at the same time into different functionality/responding patterns.

The homotopic area presented a peak of activity at 14 days post-ischemia, followed by a decrease at three months. Surprisingly to our previous findings (decreased response to whisker stimulation at three months), our immunostainings revealed an imbalance towards more excitation in the homotopic region after stroke. This might be related to the fact that the signal obtained with the laser speckle shows a global response of the whole imaged window, which could be indeed decreased. In contrast, in our staining, we focused just on the GFP expressing transcallosal neurons that displayed a higher level of excitation. A similar situation has been observed before in cultured neurons where distal axonal injury (axotomy) was followed by spine loss and an increase in excitability. A cascade of events leading to a retrograde axon-to-soma signaling and then trans-synaptic signaling from the injured neuron to uninjured presynaptic neurons might be responsible for the synaptic changes and enhanced excitability (Nagendran et al., 2017).

The detailed investigation of dendritic changes allows us to understand better how the brain responds and reorganizes after injury and to develop measures to enhance or possibly inhibit this remodeling from developing novel therapeutic strategies for patients suffering from a stroke.

4.2. Technical considerations

For both studies, we chose the longitudinal two-photon imaging through a chronic cranial window as a technical approach. For the visualization of neuronal structures, we made use of transgenic models or retrograde viral labeling. Two-photon laser scanning microscopy (TPLSM) is a well-known tool used since the 1990s for the imaging of structural dynamics of dendritic and axonal arbors (Denk et al., 1990; Svoboda and Yasuda, 2006). An advantage of two-photon microscopy is that by using long wavelength-excitation light, it provides a depth penetration of several micrometers (~800 μm) into the intact nervous tissue (Rochefort and Konnerth, 2012). Usually, for the imaging of spines, the spatial resolution is limited to around 300 nm, although current super-resolution techniques such as STED microscopy overcome this resolution barrier (Nagerl et al., 2008).

In general, TPLSM offers great advantages for the observation of brain structures. However, the strong scattering caused by the skull over the cortex can hinder the observation of fluorescently labeled neuronal structures or microvasculature (Kneipp et al., 2016). For this

reason, we performed a craniotomy and removed the bone before implanting the chronic glass window.

The procedure offers, on the one hand, higher imaging quality but is known to be related to alterations such as inflammation and microglial activation (Dorand et al., 2014). For instance, immunohistochemical analysis using glial fibrillary acidic protein (GFAP) and ionized calcium-binding adaptor molecule-1 (Iba-1) showed gliosis under the cranial window during four weeks post craniotomy (Koletar et al., 2019). Therefore, we started our imaging at least four weeks after window implantation.

In our experiment, we circumvented the craniotomy induced artifacts by following different steps. First, we avoided local damage and the resulting brain edema by using dexamethasone. This drug is a well-known corticosteroid that reduces cerebral edema (Dietrich et al., 2011) and enables the successful placement of the glass on the brain parenchyma.

Another crucial point during surgery was related to the hole drilled in the bone. By using a biopsy punch with the same diameter as the cover glass, we ensured a perfect match and adjustment of the glass on the brain. The tight coupling avoided movement artifacts during imaging caused by normal breathing and heartbeat (Paukert and Bergles, 2012).

After the surgery, the window can get infected and occluded by fibrotic scarring, periosteal dura, together with bone regrowth compromising its use for repetitive longterm imaging (Heo et al., 2016). Therefore we treated the animals with enrofloxacin the day of surgery as well as in the first postoperative days. Also known as baytril, this antibiotic owns significant post-antibiotic effect for both, Gram-negative and Gram-positive bacteria, and is active in stationary and growth phases of bacterial replication (Slate et al., 2014). Nevertheless, we still had to exclude some animals from the experiment (~28%).

For the observation of dendritic spines in our stroke experiment, we performed viral injections. To facilitate the penetration of viral cargo, we made use of mannitol. The co-infusion with this compound has been shown to improve gene transfer to neurons, increasing the distribution and the total number of transduced cells (Mastakov et al., 2001).

However, in contrast to the transgenic expression of GFP, viral labeling might be less stable and possibly bleach over the imaging sessions. We measured the stability of the GFP signal and ensured that the GFP coverage remained stable. Additionally, imaging sessions were separated for at least a week for the GFP signal to recover.

The axonal pathology was studied in two transgenic mouse lines (dE9xGFP-M and APP-PS1xGFP-M), which are well-known models in AD research (Hall and Roberson, 2012).

Heterozygous dE9 and APP-PS1 mice were crossed with heterozygous GFP-M mice resulting in triple transgenic dE9xGFP-M and APP-PS1xGFP-M mice, which express GFP in pyramidal neurons. In the dE9 model, plaques appear at six months while in the APP-PS1 mouse, it begins at two months (Hall and Roberson, 2012).

Our data showed DNs, which may contribute to the disease progression. However, it was recently shown that GFP expression might change neuronal behavior. It has been demonstrated that GFP expression increases oxidative stress (Ganini et al., 2017) as well as changes in the expression of proteins that are associated with protein folding, cytoskeletal organization, and cellular immune response (Coumans et al., 2014). Nevertheless, these studies were performed using cell culture and not in the living animal. In addition, a study that analyzed the long-term expression of GFP and its variants in transgenic mice showed a minimal toxic effect (Feng et al., 2000).

In our stroke study, we contributed to clear the controversy reached by other studies about the contralesional structural and functional remodeling. Some findings pointed out dendritic alterations while others showed the opposite results (Takatsuru et al., 2009; Johnston et al., 2013). The controversy could be due to differences in the observed cortical area and the use of thy1-GFP multivariant transgenic mice, which provides non-uniform labeling through layers as well as cortical regions (Porrero et al., 2010). With our retrograde labeling, we were able to target the transcallosal neurons and study stroke-induced deafferentation specifically.

The imaging of the spine plasticity was performed under light sedation since it can be strongly influenced by the use of anesthetics. For example, the administration of ketamine has been shown to alter dendritic filopodial dynamics (Yang et al., 2011) as well as synaptic remodeling (Crosby et al., 2010). Considering the impact of drugs, we designed our protocol to reach only a level of light sedation. Too much anesthesia could lead to no response or anesthesia-induced alterations, while too little amount could result in movement artifacts during imaging. To obtain light sedation, we based our protocol on medetomidine in combination with a low dose of isoflurane (Cramer et al., 2019). The drug medetomidine is a potent alpha 2-adrenoceptor agonist and stimulates receptors centrally to producing dose-dependent sedation. In the periphery, it causes an analgesic effect accompanied by marked bradycardia and decrease the cardiac output (Cullen, 1996).

Furthermore, to relate the structural dendritic reorganization observed in mice after ischemia to neuronal activity, we relied on the neurovascular coupling (NVC) and laser speckle imaging after the whisker's stimulation. This technique is based on similar principles than BOLD-fMRI used in patients, therefore, our experimental outcome is directly comparable to BOLD imaging and translational research. In addition, a previous study by Lecrux and collaborators (Lecrux et al., 2019) observed that sensory input, such as whiskers stimulation, evoked comparable laser-doppler flowmetry, and BOLD-fMRI signals.

Moreover, we used the filament model (fMCAo) as the method to induce an ischemic stroke. In this model, a silicone-coated filament is pushed into the internal carotid artery until the laser-doppler signal (probe placed on the skull) indicates occlusion of the MCA territory. The occlusion was performed for 60 min, followed by filament removal and reperfusion time (Groger et al., 2005). This model, broadly used in the field of experimental stroke, recapitulates most of the pathophysiology of ischemic stroke in humans (Lourbopoulos et al., 2017; Sommer, 2017). Nevertheless, it causes cortico-striatal infarcts and severe neurological deficits (Dirnagl and Endres, 2014) that are linked to a high mortality rate of 30– 90% (Ingberg et al., 2016). Previous research made by our group highlighted that mortality is not primarily caused by ischemic brain damage and infarct size, but secondarily by inadequate food and water intake (Lourbopoulos et al., 2017). We, therefore, we adapted of post-stroke nutritional support established in our laboratory to increase survival,

We could keep all mice induced with stroke and depict sustained neurological deficits allowing to characterize the subacute and chronic phases of stroke. Moreover, the improvement of long-term survival, together with the presence of chronic functional impairments, significantly increased the translational potential of our findings.

4.3. Considerations about the findings and future directions

In our study, we offer new insights into nature and progression in pathological conditions of neuritic changes. Recent studies focusing on BACE1 inhibitory drugs are currently developed to treat AD patients and showed promising results in animal models. The sequential and

increased deletion of BACE1 in an adult AD mouse model (5xFAD) was capable of completely reversing amyloid deposition. This resulted in significant improvement in gliosis and neuritic dystrophy, as well as a significant improvement of synaptic functions (Hu et al., 2018). Even if it represents an exciting pharmacological approach, the interference in BACE1 metabolism has presented side effects in the past, and further research needs to be performed for a better understanding of its role in health and disease (Vassar, 2014; Moussa-Pacha et al., 2020). Here we provide relevant cues for the discovery of novel therapeutic strategies together with information related to the optimal time window for pharmacological treatment. The therapeutic window to treat DNs is more extended than previously thought, and neurons could still be rescued also if they looked altered and dysfunctional at first sight (Adalbert et al., 2009).

Furthermore, our findings associated with the structural and functional changes after stroke provided relevant information about how and when to enhance brain repair and recovery. In contrast to the limited therapeutic window for the acute phase of stroke (thrombolytic/thrombectomy treatment), interventions during later phases of stroke display much broader applicability. For that reason, current and future research focus on the structural and functional reestablishment of the neurovascular networks as the fundamental process for stroke recovery. Combining physical interventions (rehabilitation) with other treatments (e.g., drugs, stem cell transplantation, or electrical stimulations) may enhance the brain repairing power, reestablishing the altered networks, brain functions, and contributing to counteracting the lifelong disabilities (Zhao and Willing, 2018).

Nevertheless and according to both preclinical and clinical studies, intervention timing is a sensitive issue to the restorative approach. Our findings associated with dendritic changes after stroke suggested that neurons in the contralesional hemisphere undergo very dynamics and progressive alterations. This dynamic would explain the difficulty of defining the correct time for an intervention. The dendritic reorganization and the functional outcome would suggest 14 days at the latest.

Future experimental efforts using electrophysiology recordings and calcium imaging could provide understanding to better targeting the transcallosal neurons connected to the infarct.

Stroke is often associated with cognitive decline and dementia attributed to the vascular pathology (Iadecola, 2013). Current clinical studies have documented a close relationship between cerebrovascular disease and Alzheimer's disease risk (Garcia-Alloza et al., 2011). Our work on axonal dystrophy, deafferentation, and dendritic spines alterations highlighted damages in white matter and fiber tracts. These alterations were critical and common features defining disease progression in both Alzheimer's Disease and ischemic stroke, suggesting their implication in the development of dementia-like conditions.

5. References

- Adalbert R, Nogradi A, Babetto E, Janeckova L, Walker SA, Kerschensteiner M, Misgeld T, Coleman MP (2009) Severely dystrophic axons at amyloid plaques remain continuous and connected to viable cell bodies. *Brain* 132:402-416.
- Ahmad M, Graham SH (2010) Inflammation after stroke: mechanisms and therapeutic approaches. *Transl Stroke Res* 1:74-84.
- Andrews RJ, Bringas JR, Alonzo G, Salamat MS, Khoshyomn S, Gluck DS (1993) Corpus callosotomy effects on cerebral blood flow and evoked potentials (transcallosal diaschisis). *Neurosci Lett* 154:9-12.
- Araya R, Vogels TP, Yuste R (2014) Activity-dependent dendritic spine neck changes are correlated with synaptic strength. *Proc Natl Acad Sci U S A* 111:E2895-2904.
- Atochin DN, Huang PL (2011) Role of endothelial nitric oxide in cerebrovascular regulation. *Curr Pharm Biotechnol* 12:1334-1342.
- Attwell D, Buchan AM, Charpak S, Lauritzen M, Macvicar BA, Newman EA (2010) Glial and neuronal control of brain blood flow. *Nature* 468:232-243.
- Audrey Ragagnin, Aurélie Guillemain, Nancy J. Grant and Yannick J. R. Bailly (April 17th 2013). *Neuronal Autophagy and Prion Proteins, Autophagy - A Double-Edged Sword - Cell Survival or Death?*, Yannick Bailly, IntechOpen, DOI: 10.5772/55646. Available from: <https://www.intechopen.com/books/autophagy-a-double-edged-sword-cell-survival-or-death-/neuronal-autophagy-and-prion-proteins>
- Barber PA, Davis SM, Infeld B, Baird AE, Donnan GA, Jolley D, Lichtenstein M (1998) Spontaneous reperfusion after ischemic stroke is associated with improved outcome. *Stroke* 29:2522-2528.
- Baroncelli L, Braschi C, Spolidoro M, Begenisic T, Sale A, Maffei L (2010) Nurturing brain plasticity: impact of environmental enrichment. *Cell Death Differ* 17:1092-1103.
- Battal B, Kocaoglu M, Akgun V, Bulakbasi N, Tayfun C (2010) Corpus callosum: normal imaging appearance, variants and pathologic conditions. *J Med Imaging Radiat Oncol* 54:541-549.
- Belov Kirdajova D, Kriska J, Tureckova J, Anderova M (2020) Ischemia-Triggered Glutamate Excitotoxicity From the Perspective of Glial Cells. *Front Cell Neurosci* 14:51.
- Berlucchi G, Buchtel HA (2009) Neuronal plasticity: historical roots and evolution of meaning. *Exp Brain Res* 192:307-319.
- Berry KP, Nedivi E (2017) Spine Dynamics: Are They All the Same? *Neuron* 96:43-55.
- Bertolucci F, Chisari C, Fregni F (2018) The potential dual role of transcallosal inhibition in post-stroke motor recovery. *Restor Neurol Neurosci* 36:83-97.
- Blazquez-Llorca L, Valero-Freitag S, Rodrigues EF, Merchan-Perez A, Rodriguez JR, Dorostkar MM, DeFelipe J, Herms J (2017) High plasticity of axonal pathology in Alzheimer's disease mouse models. *Acta Neuropathol Commun* 5:14.
- Bloom JS, Hynd GW (2005) The role of the corpus callosum in interhemispheric transfer of information: excitation or inhibition? *Neuropsychol Rev* 15:59-71.
- Boas DA, Dunn AK (2010) Laser speckle contrast imaging in biomedical optics. *J Biomed Opt* 15:011109.
- Boddington LJ, Reynolds JNJ (2017) Targeting interhemispheric inhibition with neuromodulation to enhance stroke rehabilitation. *Brain Stimul* 10:214-222.
- Boehme AK, Esenwa C, Elkind MS (2017) Stroke Risk Factors, Genetics, and Prevention. *Circ Res* 120:472-495.
- Borovac J, Bosch M, Okamoto K (2018) Regulation of actin dynamics during structural plasticity of dendritic spines: Signaling messengers and actin-binding proteins. *Mol Cell Neurosci* 91:122-130.

- Brainin M, Tuomilehto J, Heiss WD, Bornstein NM, Bath PM, Teuschl Y, Richard E, Guekht A, Quinn T, Post Stroke Cognition Study G (2015) Post-stroke cognitive decline: an update and perspectives for clinical research. *Eur J Neurol* 22:229-238, e213-226.
- Bredesen DE (2000) Apoptosis: overview and signal transduction pathways. *J Neurotrauma* 17:801-810.
- Brendza RP, Bacsikai BJ, Cirrito JR, Simmons KA, Skoch JM, Klunk WE, Mathis CA, Bales KR, Paul SM, Hyman BT, Holtzman DM (2005) Anti-Abeta antibody treatment promotes the rapid recovery of amyloid-associated neuritic dystrophy in PDAPP transgenic mice. *J Clin Invest* 115:428-433.
- Brown CE, Wong C, Murphy TH (2008) Rapid morphologic plasticity of peri-infarct dendritic spines after focal ischemic stroke. *Stroke* 39:1286-1291.
- Brown CE, Boyd JD, Murphy TH (2010) Longitudinal in vivo imaging reveals balanced and branch-specific remodeling of mature cortical pyramidal dendritic arbors after stroke. *J Cereb Blood Flow Metab* 30:783-791.
- Brown CE, Li P, Boyd JD, Delaney KR, Murphy TH (2007) Extensive turnover of dendritic spines and vascular remodeling in cortical tissues recovering from stroke. *J Neurosci* 27:4101-4109.
- Butz M, Steenbuck ID, van Ooyen A (2014) Homeostatic structural plasticity can account for topology changes following deafferentation and focal stroke. *Front Neuroanat* 8:115.
- Campbell BCV, De Silva DA, Macleod MR, Coutts SB, Schwamm LH, Davis SM, Donnan GA (2019) Ischaemic stroke. *Nat Rev Dis Primers* 5:70.
- Carmichael ST (2012) Brain excitability in stroke: the yin and yang of stroke progression. *Arch Neurol* 69:161-167.
- Carmichael ST, Tatsukawa K, Katsman D, Tsuyuguchi N, Kornblum HI (2004) Evolution of diaschisis in a focal stroke model. *Stroke* 35:758-763.
- Carson JA, Turner AJ (2002) Beta-amyloid catabolism: roles for neprilysin (NEP) and other metallopeptidases? *J Neurochem* 81:1-8.
- Carson RG (2005) Neural pathways mediating bilateral interactions between the upper limbs. *Brain Res Brain Res Rev* 49:641-662.
- Cirillo C, Brihmat N, Castel-Lacanal E, Le Fric A, Barbieux-Guillot M, Raposo N, Pariente J, Viguier A, Simonetta-Moreau M, Albucher JF, Olivot JM, Desmoulin F, Marque P, Chollet F, Loubinoux I (2020) Post-stroke remodeling processes in animal models and humans. *J Cereb Blood Flow Metab* 40:3-22.
- Cirrito JR, Kang JE, Lee J, Stewart FR, Verges DK, Silverio LM, Bu G, Mennerick S, Holtzman DM (2008) Endocytosis is required for synaptic activity-dependent release of amyloid-beta in vivo. *Neuron* 58:42-51.
- Clarkson AN, Huang BS, Macisaac SE, Mody I, Carmichael ST (2010) Reducing excessive GABA-mediated tonic inhibition promotes functional recovery after stroke. *Nature* 468:305-309.
- Cohen R.S. (2013) Cell Biology of the Synapse. In: Pfaff D.W. (eds) *Neuroscience in the 21st Century*. Springer, New York, NY
- Corbetta D, Sirtori V, Moja L, Gatti R (2010) Constraint-induced movement therapy in stroke patients: systematic review and meta-analysis. *Eur J Phys Rehabil Med* 46:537-544.
- Coumans JV, Gau D, Poljak A, Wasinger V, Roy P, Moens P (2014) Green fluorescent protein expression triggers proteome changes in breast cancer cells. *Exp Cell Res* 320:33-45.
- Cramer JV, Gesierich B, Roth S, Dichgans M, During M, Liesz A (2019) In vivo widefield calcium imaging of the mouse cortex for analysis of network connectivity in health and brain disease. *Neuroimage* 199:570-584.
- Crosby G, Culley DJ, Patel PM (2010) At the sharp end of spines: anesthetic effects on synaptic remodeling in the developing brain. *Anesthesiology* 112:521-523.

- Cullen LK (1996) Medetomidine sedation in dogs and cats: a review of its pharmacology, antagonism and dose. *Br Vet J* 152:519-535.
- Chen CC, Lu J, Zuo Y (2014) Spatiotemporal dynamics of dendritic spines in the living brain. *Front Neuroanat* 8:28.
- Cheng B, Dietzmann P, Schulz R, Boenstrup M, Krawinkel L, Fiehler J, Gerloff C, Thomalla G (2020) Cortical atrophy and transcallosal diaschisis following isolated subcortical stroke. *J Cereb Blood Flow Metab* 40:611-621.
- Cheng MY, Aswendt M, Steinberg GK (2016) Optogenetic Approaches to Target Specific Neural Circuits in Post-stroke Recovery. *Neurotherapeutics* 13:325-340.
- Chidambaram SB, Rathipriya AG, Bolla SR, Bhat A, Ray B, Mahalakshmi AM, Manivasagam T, Thenmozhi AJ, Essa MM, Guillemain GJ, Chandra R, Sakharkar MK (2019) Dendritic spines: Revisiting the physiological role. *Prog Neuropsychopharmacol Biol Psychiatry* 92:161-193.
- Chklovskii DB (2004) Synaptic connectivity and neuronal morphology: two sides of the same coin. *Neuron* 43:609-617.
- Chung WS, Allen NJ, Eroglu C (2015) Astrocytes Control Synapse Formation, Function, and Elimination. *Cold Spring Harb Perspect Biol* 7:a020370.
- Chuquet J, Hollender L, Nimchinsky EA (2007) High-resolution in vivo imaging of the neurovascular unit during spreading depression. *J Neurosci* 27:4036-4044.
- D'Amore JD, Kajdasz ST, McLellan ME, Bacskaï BJ, Stern EA, Hyman BT (2003) In vivo multiphoton imaging of a transgenic mouse model of Alzheimer disease reveals marked thioflavine-S-associated alterations in neurite trajectories. *J Neuropathol Exp Neurol* 62:137-145.
- Dalise S, Ambrosio F, Modo M (2014) Brain plasticity and recovery in preclinical models of stroke. *Arch Ital Biol* 152:190-215.
- del Zoppo GJ (2010) The neurovascular unit in the setting of stroke. *J Intern Med* 267:156-171.
- Deng PY, Klyachko VA (2011) The diverse functions of short-term plasticity components in synaptic computations. *Commun Integr Biol* 4:543-548.
- Denk W (1994) Two-photon scanning photochemical microscopy: mapping ligand-gated ion channel distributions. *Proc Natl Acad Sci U S A* 91:6629-6633.
- Denk W, Strickler JH, Webb WW (1990) Two-photon laser scanning fluorescence microscopy. *Science* 248:73-76.
- Dietrich J, Rao K, Pastorino S, Kesari S (2011) Corticosteroids in brain cancer patients: benefits and pitfalls. *Expert Rev Clin Pharmacol* 4:233-242.
- Dirnagl U, Endres M (2014) Found in translation: preclinical stroke research predicts human pathophysiology, clinical phenotypes, and therapeutic outcomes. *Stroke* 45:1510-1518.
- Dirnagl U, Iadecola C, Moskowitz MA (1999) Pathobiology of ischaemic stroke: an integrated view. *Trends Neurosci* 22:391-397.
- Dombeck D, Tank D (2014) Two-photon imaging of neural activity in awake mobile mice. *Cold Spring Harb Protoc* 2014:726-736.
- Dorand RD, Barkauskas DS, Evans TA, Petrosiute A, Huang AY (2014) Comparison of intravital thinned skull and cranial window approaches to study CNS immunobiology in the mouse cortex. *Intravital* 3.
- Dostovic Z, Dostovic E, Smajlovic D, Ibrahimagic OC, Avdic L (2016) Brain Edema After Ischaemic Stroke. *Med Arch* 70:339-341.
- Doyle KP, Simon RP, Stenzel-Poore MP (2008) Mechanisms of ischemic brain damage. *Neuropharmacology* 55:310-318.
- Dreier JP (2011) The role of spreading depression, spreading depolarization and spreading ischemia in neurological disease. *Nat Med* 17:439-447.
- Duering M, Righart R, Wollenweber FA, Zietemann V, Gesierich B, Dichgans M (2015) Acute infarcts cause focal thinning in remote cortex via degeneration of connecting fiber tracts. *Neurology* 84:1685-1692.

- Elder GA, Gama Sosa MA, De Gasperi R (2010) Transgenic mouse models of Alzheimer's disease. *Mt Sinai J Med* 77:69-81.
- Erturk A, Becker K, Jahrling N, Mauch CP, Hojer CD, Egen JG, Hellal F, Bradke F, Sheng M, Dodt HU (2012) Three-dimensional imaging of solvent-cleared organs using 3DISCO. *Nat Protoc* 7:1983-1995.
- Esquerda-Canals G, Montoliu-Gaya L, Guell-Bosch J, Villegas S (2017) Mouse Models of Alzheimer's Disease. *J Alzheimers Dis* 57:1171-1183.
- Farrant M, Nusser Z (2005) Variations on an inhibitory theme: phasic and tonic activation of GABA(A) receptors. *Nat Rev Neurosci* 6:215-229.
- Feng G, Mellor RH, Bernstein M, Keller-Peck C, Nguyen QT, Wallace M, Nerbonne JM, Lichtman JW, Sanes JR (2000) Imaging neuronal subsets in transgenic mice expressing multiple spectral variants of GFP. *Neuron* 28:41-51.
- Fiala JC (2007) Mechanisms of amyloid plaque pathogenesis. *Acta Neuropathol* 114:551-571.
- Fling BW, Seidler RD (2012) Task-dependent effects of interhemispheric inhibition on motor control. *Behav Brain Res* 226:211-217.
- Fling BW, Peltier SJ, Bo J, Welsh RC, Seidler RD (2011) Age differences in interhemispheric interactions: callosal structure, physiological function, and behavior. *Front Neurosci* 5:38.
- Fluri F, Schuhmann MK, Kleinschnitz C (2015) Animal models of ischemic stroke and their application in clinical research. *Drug Des Devel Ther* 9:3445-3454.
- Flynn KC (2013) The cytoskeleton and neurite initiation. *Bioarchitecture* 3:86-109.
- Frankfurt M, Luine V (2015) The evolving role of dendritic spines and memory: Interaction(s) with estradiol. *Horm Behav* 74:28-36.
- Fregni F, Boggio PS, Valle AC, Rocha RR, Duarte J, Ferreira MJ, Wagner T, Fecteau S, Rigonatti SP, Riberto M, Freedman SD, Pascual-Leone A (2006) A sham-controlled trial of a 5-day course of repetitive transcranial magnetic stimulation of the unaffected hemisphere in stroke patients. *Stroke* 37:2115-2122.
- Freret T, Bouet V, Leconte C, Roussel S, Chazalviel L, Divoux D, Schumann-Bard P, Boulouard M (2009) Behavioral deficits after distal focal cerebral ischemia in mice: Usefulness of adhesive removal test. *Behav Neurosci* 123:224-230.
- Friederici AD (2009) Pathways to language: fiber tracts in the human brain. *Trends Cogn Sci* 13:175-181.
- Galarreta M, Hestrin S (2001) Electrical synapses between GABA-releasing interneurons. *Nat Rev Neurosci* 2:425-433.
- Ganini D, Leinisch F, Kumar A, Jiang J, Tokar EJ, Malone CC, Petrovich RM, Mason RP (2017) Fluorescent proteins such as eGFP lead to catalytic oxidative stress in cells. *Redox Biol* 12:462-468.
- Garcia-Alloza M, Dodwell SA, Meyer-Luehmann M, Hyman BT, Bacskai BJ (2006) Plaque-derived oxidative stress mediates distorted neurite trajectories in the Alzheimer mouse model. *J Neuropathol Exp Neurol* 65:1082-1089.
- Garcia-Alloza M, Gregory J, Kuchibhotla KV, Fine S, Wei Y, Ayata C, Frosch MP, Greenberg SM, Bacskai BJ (2011) Cerebrovascular lesions induce transient beta-amyloid deposition. *Brain* 134:3697-3707.
- Garre-Olmo J (2018) [Epidemiology of Alzheimer's disease and other dementias]. *Rev Neurol* 66:377-386.
- Garrido C, Galluzzi L, Brunet M, Puig PE, Didelot C, Kroemer G (2006) Mechanisms of cytochrome c release from mitochondria. *Cell Death Differ* 13:1423-1433.
- Gaudet AD, Popovich PG, Ramer MS (2011) Wallerian degeneration: gaining perspective on inflammatory events after peripheral nerve injury. *J Neuroinflammation* 8:110.
- Gibson JR, Beierlein M, Connors BW (2005) Functional properties of electrical synapses between inhibitory interneurons of neocortical layer 4. *J Neurophysiol* 93:467-480.

- Giri M, Zhang M, Lu Y (2016) Genes associated with Alzheimer's disease: an overview and current status. *Clin Interv Aging* 11:665-681.
- Gold L, Lauritzen M (2002) Neuronal deactivation explains decreased cerebellar blood flow in response to focal cerebral ischemia or suppressed neocortical function. *Proc Natl Acad Sci U S A* 99:7699-7704.
- Goldey GJ, Roumis DK, Glickfeld LL, Kerlin AM, Reid RC, Bonin V, Schafer DP, Andermann ML (2014) Removable cranial windows for long-term imaging in awake mice. *Nat Protoc* 9:2515-2538.
- Gore JC (2003) Principles and practice of functional MRI of the human brain. *J Clin Invest* 112:4-9.
- Grace EA, Rabiner CA, Busciglio J (2002) Characterization of neuronal dystrophy induced by fibrillar amyloid beta: implications for Alzheimer's disease. *Neuroscience* 114:265-273.
- Groger M, Lebesgue D, Pruneau D, Relton J, Kim SW, Nussberger J, Plesnila N (2005) Release of bradykinin and expression of kinin B2 receptors in the brain: role for cell death and brain edema formation after focal cerebral ischemia in mice. *J Cereb Blood Flow Metab* 25:978-989.
- Guo C, Peng J, Zhang Y, Li A, Li Y, Yuan J, Xu X, Ren M, Gong H, Chen S (2017) Single-axon level morphological analysis of corticofugal projection neurons in mouse barrel field. *Sci Rep* 7:2846.
- Hacke W, Kaste M, Bluhmki E, Brozman M, Davalos A, Guidetti D, Larrue V, Lees KR, Medeghri Z, Machnig T, Schneider D, von Kummer R, Wahlgren N, Toni D, Investigators E (2008) Thrombolysis with alteplase 3 to 4.5 hours after acute ischemic stroke. *N Engl J Med* 359:1317-1329.
- Hall AM, Roberson ED (2012) Mouse models of Alzheimer's disease. *Brain Res Bull* 88:3-12.
- Hallett M (2001) Plasticity of the human motor cortex and recovery from stroke. *Brain Res Brain Res Rev* 36:169-174.
- Han W, Sestan N (2013) Cortical projection neurons: sprung from the same root. *Neuron* 80:1103-1105.
- Harrison TC, Silasi G, Boyd JD, Murphy TH (2013) Displacement of sensory maps and disorganization of motor cortex after targeted stroke in mice. *Stroke* 44:2300-2306.
- Hattox AM, Nelson SB (2007) Layer V neurons in mouse cortex projecting to different targets have distinct physiological properties. *J Neurophysiol* 98:3330-3340.
- Helmchen F, Denk W (2005) Deep tissue two-photon microscopy. *Nat Methods* 2:932-940.
- Henstridge CM, Tzioras M, Paolicelli RC (2019) Glial Contribution to Excitatory and Inhibitory Synapse Loss in Neurodegeneration. *Front Cell Neurosci* 13:63.
- Heo C, Park H, Kim YT, Baeg E, Kim YH, Kim SG, Suh M (2016) A soft, transparent, freely accessible cranial window for chronic imaging and electrophysiology. *Sci Rep* 6:27818.
- Hinman JD (2014) The back and forth of axonal injury and repair after stroke. *Curr Opin Neurol* 27:615-623.
- Hui T, Farzampour Z, Paz JT, Wang EH, Badgely C, Olson A, Micheva KD, Wang G, Lemmens R, Tran KV, Nishiyama Y, Liang X, Hamilton SA, O'Rourke N, Smith SJ, Huguenard JR, Bliss TM, Steinberg GK (2016) Enhanced phasic GABA inhibition during the repair phase of stroke: a novel therapeutic target. *Brain* 139:468-480.
- Ho PW, Reutens DC, Phan TG, Wright PM, Markus R, Indra I, Young D, Donnan GA (2005) Is white matter involved in patients entered into typical trials of neuroprotection? *Stroke* 36:2742-2744.
- Hobert O (2011) Regulation of terminal differentiation programs in the nervous system. *Annu Rev Cell Dev Biol* 27:681-696.
- Holtmaat A, Bonhoeffer T, Chow DK, Chuckowree J, De Paola V, Hofer SB, Hubener M, Keck T, Knott G, Lee WC, Mostany R, Mrsic-Flogel TD, Nedivi E, Portera-Cailliau C,

- Svoboda K, Trachtenberg JT, Wilbrecht L (2009) Long-term, high-resolution imaging in the mouse neocortex through a chronic cranial window. *Nat Protoc* 4:1128-1144.
- Hossmann KA (1994) Viability thresholds and the penumbra of focal ischemia. *Ann Neurol* 36:557-565.
- Howland JG, Wang YT (2008) Synaptic plasticity in learning and memory: stress effects in the hippocampus. *Prog Brain Res* 169:145-158.
- Hu X, Das B, Hou H, He W, Yan R (2018) BACE1 deletion in the adult mouse reverses preformed amyloid deposition and improves cognitive functions. *J Exp Med* 215:927-940.
- Iadecola C (2013) The pathobiology of vascular dementia. *Neuron* 80:844-866.
- Iglesias S, Marchal G, Viader F, Baron JC (2000) Delayed intrahemispheric remote hypometabolism. Correlations with early recovery after stroke. *Cerebrovasc Dis* 10:391-402.
- Ilyayeva E, Nada K, Farahi Far R, Albright K, Gujral MK, Gold M (2018) Bilateral Cerebrovascular Stroke as an Initial Presenting Symptom of Moyamoya Disease. *Case Rep Crit Care* 2018:2591494.
- Ingberg E, Dock H, Theodorsson E, Theodorsson A, Strom JO (2016) Method parameters' impact on mortality and variability in mouse stroke experiments: a meta-analysis. *Sci Rep* 6:21086.
- Isaacson JS, Scanziani M (2011) How inhibition shapes cortical activity. *Neuron* 72:231-243.
- Izumi Y, Haida M, Hata T, Isozumi K, Kurita D, Shinohara Y (2002) Distribution of brain oedema in the contralateral hemisphere after cerebral infarction: repeated MRI measurement in the rat. *J Clin Neurosci* 9:289-293.
- Jaenisch N, Liebmann L, Guenther M, Hubner CA, Frahm C, Witte OW (2016) Reduced tonic inhibition after stroke promotes motor performance and epileptic seizures. *Sci Rep* 6:26173.
- Jang SH (2013) Motor function-related maladaptive plasticity in stroke: a review. *NeuroRehabilitation* 32:311-316.
- Jankowsky JL, Slunt HH, Gonzales V, Jenkins NA, Copeland NG, Borchelt DR (2004a) APP processing and amyloid deposition in mice haplo-insufficient for presenilin 1. *Neurobiol Aging* 25:885-892.
- Jankowsky JL, Fadale DJ, Anderson J, Xu GM, Gonzales V, Jenkins NA, Copeland NG, Lee MK, Younkin LH, Wagner SL, Younkin SG, Borchelt DR (2004b) Mutant presenilins specifically elevate the levels of the 42 residue beta-amyloid peptide in vivo: evidence for augmentation of a 42-specific gamma secretase. *Hum Mol Genet* 13:159-170.
- Johansson BB (2000) Brain plasticity and stroke rehabilitation. The Willis lecture. *Stroke* 31:223-230.
- Johnston DG, Denizet M, Mostany R, Portera-Cailliau C (2013) Chronic in vivo imaging shows no evidence of dendritic plasticity or functional remapping in the contralesional cortex after stroke. *Cereb Cortex* 23:751-762.
- Kalogeris T, Baines CP, Krenz M, Korthuis RJ (2012) Cell biology of ischemia/reperfusion injury. *Int Rev Cell Mol Biol* 298:229-317.
- Kametani F, Hasegawa M (2018) Reconsideration of Amyloid Hypothesis and Tau Hypothesis in Alzheimer's Disease. *Front Neurosci* 12:25.
- Karki K, Knight RA, Shen LH, Kapke A, Lu M, Li Y, Chopp M (2010) Chronic brain tissue remodeling after stroke in rat: a 1-year multiparametric magnetic resonance imaging study. *Brain Res* 1360:168-176.
- Karnani MM, Agetsuma M, Yuste R (2014) A blanket of inhibition: functional inferences from dense inhibitory connectivity. *Curr Opin Neurobiol* 26:96-102.
- Kempermann G, van Praag H, Gage FH (2000) Activity-dependent regulation of neuronal plasticity and self repair. *Prog Brain Res* 127:35-48.

- Kepecs A, Fishell G (2014) Interneuron cell types are fit to function. *Nature* 505:318-326.
- Kerr JN, Denk W (2008) Imaging in vivo: watching the brain in action. *Nat Rev Neurosci* 9:195-205.
- Kim JY, Park J, Chang JY, Kim SH, Lee JE (2016) Inflammation after Ischemic Stroke: The Role of Leukocytes and Glial Cells. *Exp Neurobiol* 25:241-251.
- Kneipp M, Turner J, Estrada H, Rebling J, Shoham S, Razansky D (2016) Effects of the murine skull in optoacoustic brain microscopy. *J Biophotonics* 9:117-123.
- Knowles RB, Wyart C, Buldyrev SV, Cruz L, Urbanc B, Hasselmo ME, Stanley HE, Hyman BT (1999) Plaque-induced neurite abnormalities: implications for disruption of neural networks in Alzheimer's disease. *Proc Natl Acad Sci U S A* 96:5274-5279.
- Koletar MM, Dorr A, Brown ME, McLaurin J, Stefanovic B (2019) Refinement of a chronic cranial window implant in the rat for longitudinal in vivo two-photon fluorescence microscopy of neurovascular function. *Sci Rep* 9:5499.
- Labat-gest V, Tomasi S (2013) Photothrombotic ischemia: a minimally invasive and reproducible photochemical cortical lesion model for mouse stroke studies. *J Vis Exp*.
- LaFerla FM, Green KN (2012) Animal models of Alzheimer disease. *Cold Spring Harb Perspect Med* 2.
- Lai TW, Zhang S, Wang YT (2014) Excitotoxicity and stroke: identifying novel targets for neuroprotection. *Prog Neurobiol* 115:157-188.
- Lakhan SE, Kirchgessner A, Hofer M (2009) Inflammatory mechanisms in ischemic stroke: therapeutic approaches. *J Transl Med* 7:97.
- Lecrux C, Bourourou M, Hamel E (2019) How reliable is cerebral blood flow to map changes in neuronal activity? *Auton Neurosci* 217:71-79.
- Lee S, Sato Y, Nixon RA (2011) Lysosomal proteolysis inhibition selectively disrupts axonal transport of degradative organelles and causes an Alzheimer's-like axonal dystrophy. *J Neurosci* 31:7817-7830.
- Lee V, Maguire J (2014) The impact of tonic GABAA receptor-mediated inhibition on neuronal excitability varies across brain region and cell type. *Front Neural Circuits* 8:3.
- Lenzi GL, Frackowiak RS, Jones T (1982) Cerebral oxygen metabolism and blood flow in human cerebral ischemic infarction. *J Cereb Blood Flow Metab* 2:321-335.
- Leonardo CC, Hall AA, Collier LA, Ajmo CT, Jr., Willing AE, Pennypacker KR (2010) Human umbilical cord blood cell therapy blocks the morphological change and recruitment of CD11b-expressing, isolectin-binding proinflammatory cells after middle cerebral artery occlusion. *J Neurosci Res* 88:1213-1222.
- Levasseur JE, Wei EP, Raper AJ, Kontos AA, Patterson JL (1975) Detailed description of a cranial window technique for acute and chronic experiments. *Stroke* 6:308-317.
- Liepert J, Hamzei F, Weiller C (2000) Motor cortex disinhibition of the unaffected hemisphere after acute stroke. *Muscle Nerve* 23:1761-1763.
- Lin MP, Liebeskind DS (2016) Imaging of Ischemic Stroke. *Continuum (Minneap Minn)* 22:1399-1423.
- Lin YC, Koleske AJ (2010) Mechanisms of synapse and dendrite maintenance and their disruption in psychiatric and neurodegenerative disorders. *Annu Rev Neurosci* 33:349-378.
- Lo EH (2008) A new penumbra: transitioning from injury into repair after stroke. *Nat Med* 14:497-500.
- Lo RC (1986) Recovery and rehabilitation after stroke. *Can Fam Physician* 32:1851-1853.
- Lodato S, Arlotta P (2015) Generating neuronal diversity in the mammalian cerebral cortex. *Annu Rev Cell Dev Biol* 31:699-720.
- Lodato S, Shetty AS, Arlotta P (2015) Cerebral cortex assembly: generating and reprogramming projection neuron diversity. *Trends Neurosci* 38:117-125.

- Lourbopoulos A, Mamrak U, Roth S, Balbi M, Shrouder J, Liesz A, Hellal F, Plesnila N (2017) Inadequate food and water intake determine mortality following stroke in mice. *J Cereb Blood Flow Metab* 37:2084-2097.
- Malcolm MP, Vaughn HN, Greene DP (2015) Inhibitory and excitatory motor cortex dysfunction persists in the chronic poststroke recovery phase. *J Clin Neurophysiol* 32:251-256.
- Mansur CG, Fregni F, Boggio PS, Riberto M, Gallucci-Neto J, Santos CM, Wagner T, Rigonatti SP, Marcolin MA, Pascual-Leone A (2005) A sham stimulation-controlled trial of rTMS of the unaffected hemisphere in stroke patients. *Neurology* 64:1802-1804.
- Marquardt L, Anders C, Buggle F, Palm F, Hellstern P, Grau AJ (2009) Leukocyte-platelet aggregates in acute and subacute ischemic stroke. *Cerebrovasc Dis* 28:276-282.
- Masliah E, Mallory M, Hansen L, DeTeresa R, Alford M, Terry R (1994) Synaptic and neuritic alterations during the progression of Alzheimer's disease. *Neurosci Lett* 174:67-72.
- Mastakov MY, Baer K, Xu R, Fitzsimons H, During MJ (2001) Combined injection of rAAV with mannitol enhances gene expression in the rat brain. *Mol Ther* 3:225-232.
- Masters CL, Simms G, Weinman NA, Multhaup G, McDonald BL, Beyreuther K (1985) Amyloid plaque core protein in Alzheimer disease and Down syndrome. *Proc Natl Acad Sci U S A* 82:4245-4249.
- Mayeux R, Stern Y (2012) Epidemiology of Alzheimer disease. *Cold Spring Harb Perspect Med* 2.
- Meiklejohn DJ, Vickers MA, Dijkhuisen R, Greaves M (2001) Plasma homocysteine concentrations in the acute and convalescent periods of atherothrombotic stroke. *Stroke* 32:57-62.
- Meyer BU, Roricht S, Graf von Einsiedel H, Kruggel F, Weindl A (1995) Inhibitory and excitatory interhemispheric transfers between motor cortical areas in normal humans and patients with abnormalities of the corpus callosum. *Brain* 118 (Pt 2):429-440.
- Miquelajauregui A, Kribakaran S, Mostany R, Badaloni A, Consalez GG, Portera-Cailliau C (2015) Layer 4 pyramidal neurons exhibit robust dendritic spine plasticity in vivo after input deprivation. *J Neurosci* 35:7287-7294.
- Misra V, Ritchie MM, Stone LL, Low WC, Janardhan V (2012) Stem cell therapy in ischemic stroke: role of IV and intra-arterial therapy. *Neurology* 79:S207-212.
- Mitew S, Kirkcaldie MT, Dickson TC, Vickers JC (2013) Neurites containing the neurofilament-triplet proteins are selectively vulnerable to cytoskeletal pathology in Alzheimer's disease and transgenic mouse models. *Front Neuroanat* 7:30.
- Mohamed A, Posse de Chaves E (2011) Abeta internalization by neurons and glia. *Int J Alzheimers Dis* 2011:127984.
- Molnar Z, Cheung AF (2006) Towards the classification of subpopulations of layer V pyramidal projection neurons. *Neurosci Res* 55:105-115.
- Molyneaux BJ, Arlotta P, Menezes JR, Macklis JD (2007) Neuronal subtype specification in the cerebral cortex. *Nat Rev Neurosci* 8:427-437.
- Mooshagian E (2008) Anatomy of the corpus callosum reveals its function. *J Neurosci* 28:1535-1536.
- Moussa-Pacha NM, Abdin SM, Omar HA, Alniss H, Al-Tel TH (2020) BACE1 inhibitors: Current status and future directions in treating Alzheimer's disease. *Med Res Rev* 40:339-384.
- Musuka TD, Wilton SB, Traboulsi M, Hill MD (2015) Diagnosis and management of acute ischemic stroke: speed is critical. *CMAJ* 187:887-893.
- Nagendran T, Larsen RS, Bigler RL, Frost SB, Philpot BD, Nudo RJ, Taylor AM (2017) Distal axotomy enhances retrograde presynaptic excitability onto injured pyramidal neurons via trans-synaptic signaling. *Nat Commun* 8:625.
- Nagerl UV, Willig KI, Hein B, Hell SW, Bonhoeffer T (2008) Live-cell imaging of dendritic spines by STED microscopy. *Proc Natl Acad Sci U S A* 105:18982-18987.

- Naghavi FS, Koffman EE, Lin B, Du J (2019) Post-stroke neuronal circuits and mental illnesses. *Int J Physiol Pathophysiol Pharmacol* 11:1-11.
- Nixon RA, Wegiel J, Kumar A, Yu WH, Peterhoff C, Cataldo A, Cuervo AM (2005) Extensive involvement of autophagy in Alzheimer disease: an immuno-electron microscopy study. *J Neuropathol Exp Neurol* 64:113-122.
- Nudo RJ (2003) Adaptive plasticity in motor cortex: implications for rehabilitation after brain injury. *J Rehabil Med*:7-10.
- Paciaroni M, Caso V, Agnelli G (2009) The concept of ischemic penumbra in acute stroke and therapeutic opportunities. *Eur Neurol* 61:321-330.
- Pagani L, Eckert A (2011) Amyloid-Beta interaction with mitochondria. *Int J Alzheimers Dis* 2011:925050.
- Page SJ, Levine P, Leonard AC (2005) Modified constraint-induced therapy in acute stroke: a randomized controlled pilot study. *Neurorehabil Neural Repair* 19:27-32.
- Pan C, Cai R, Quacquarelli FP, Ghasemigharagoz A, Lourbopoulos A, Matryba P, Plesnila N, Dichgans M, Hellal F, Erturk A (2016) Shrinkage-mediated imaging of entire organs and organisms using uDISCO. *Nat Methods* 13:859-867.
- Paukert M, Bergles DE (2012) Reduction of motion artifacts during in vivo two-photon imaging of brain through heartbeat triggered scanning. *J Physiol* 590:2955-2963.
- Perea G, Navarrete M, Araque A (2009) Tripartite synapses: astrocytes process and control synaptic information. *Trends Neurosci* 32:421-431.
- Perez-Gracia E, Torrejon-Escribano B, Ferrer I (2008) Dystrophic neurites of senile plaques in Alzheimer's disease are deficient in cytochrome c oxidase. *Acta Neuropathol* 116:261-268.
- Perrin RJ, Fagan AM, Holtzman DM (2009) Multimodal techniques for diagnosis and prognosis of Alzheimer's disease. *Nature* 461:916-922.
- Peschillo S, Diana F, Berge J, Missori P (2017) A comparison of acute vascular damage caused by ADAPT versus a stent retriever device after thrombectomy in acute ischemic stroke: a histological and ultrastructural study in an animal model. *J Neurointerv Surg* 9:743-749.
- Petanjek Z, Judas M, Simic G, Rasin MR, Uylings HB, Rakic P, Kostovic I (2011) Extraordinary neoteny of synaptic spines in the human prefrontal cortex. *Proc Natl Acad Sci U S A* 108:13281-13286.
- Peters A, Kaiserman-Abramof IR (1970) The small pyramidal neuron of the rat cerebral cortex. The perikaryon, dendrites and spines. *Am J Anat* 127:321-355.
- Peters F, Salihoglu H, Rodrigues E, Herzog E, Blume T, Filser S, Dorostkar M, Shimshek DR, Brose N, Neumann U, Herms J (2018) BACE1 inhibition more effectively suppresses initiation than progression of beta-amyloid pathology. *Acta Neuropathol* 135:695-710.
- Porrero C, Rubio-Garrido P, Avendano C, Clasca F (2010) Mapping of fluorescent protein-expressing neurons and axon pathways in adult and developing Thy1-eYFP-H transgenic mice. *Brain Res* 1345:59-72.
- Previtali E, Bucciarelli P, Passamonti SM, Martinelli I (2011) Risk factors for venous and arterial thrombosis. *Blood Transfus* 9:120-138.
- Probst A, Brunnschweiler H, Lautenschlager C, Ulrich J (1987) A special type of senile plaque, possibly an initial stage. *Acta Neuropathol* 74:133-141.
- Radde R, Bolmont T, Kaeser SA, Coomaraswamy J, Lindau D, Stoltze L, Calhoun ME, Jaggi F, Wolburg H, Gengler S, Haass C, Ghetti B, Czech C, Holscher C, Mathews PM, Jucker M (2006) Abeta42-driven cerebral amyloidosis in transgenic mice reveals early and robust pathology. *EMBO Rep* 7:940-946.
- Rao Y, Liu ZW, Borok E, Rabenstein RL, Shanabrough M, Lu M, Picciotto MR, Horvath TL, Gao XB (2007) Prolonged wakefulness induces experience-dependent synaptic plasticity in mouse hypocretin/orexin neurons. *J Clin Invest* 117:4022-4033.
- Reitz C, Brayne C, Mayeux R (2011) Epidemiology of Alzheimer disease. *Nat Rev Neurol* 7:137-152.

- Ren M, Lin ZJ, Qian H, Choudhury GR, Liu R, Liu H, Yang SH (2012) Embolic middle cerebral artery occlusion model using thrombin and fibrinogen composed clots in rat. *J Neurosci Methods* 211:296-304.
- Ren SQ, Yao W, Yan JZ, Jin C, Yin JJ, Yuan J, Yu S, Cheng Z (2018) Amyloid beta causes excitation/inhibition imbalance through dopamine receptor 1-dependent disruption of fast-spiking GABAergic input in anterior cingulate cortex. *Sci Rep* 8:302.
- Ribas EC, Yagmurlu K, de Oliveira E, Ribas GC, Rhoton A (2018) Microsurgical anatomy of the central core of the brain. *J Neurosurg* 129:752-769.
- Ridding MC, Brouwer B, Nordstrom MA (2000) Reduced interhemispheric inhibition in musicians. *Exp Brain Res* 133:249-253.
- Risher WC, Ustunkaya T, Singh Alvarado J, Eroglu C (2014) Rapid Golgi analysis method for efficient and unbiased classification of dendritic spines. *PLoS One* 9:e107591.
- Ritter LS, Orozco JA, Coull BM, McDonagh PF, Rosenblum WI (2000) Leukocyte accumulation and hemodynamic changes in the cerebral microcirculation during early reperfusion after stroke. *Stroke* 31:1153-1161.
- Rocheffort NL, Konnerth A (2012) Dendritic spines: from structure to in vivo function. *EMBO Rep* 13:699-708.
- Roome CJ, Kuhn B (2014) Chronic cranial window with access port for repeated cellular manipulations, drug application, and electrophysiology. *Front Cell Neurosci* 8:379.
- Ruan L, Wang Y, Chen SC, Zhao T, Huang Q, Hu ZL, Xia NZ, Liu JJ, Chen WJ, Zhang Y, Cheng JL, Gao HC, Yang YJ, Sun HZ (2017) Metabolite changes in the ipsilateral and contralateral cerebral hemispheres in rats with middle cerebral artery occlusion. *Neural Regen Res* 12:931-937.
- Rusanen H, Saarinen JT, Sillanpaa N (2015) Collateral Circulation Predicts the Size of the Infarct Core and the Proportion of Salvageable Penumbra in Hyperacute Ischemic Stroke Patients Treated with Intravenous Thrombolysis. *Cerebrovasc Dis* 40:182-190.
- Sadleir KR, Kandalepas PC, Buggia-Prevot V, Nicholson DA, Thinakaran G, Vassar R (2016) Presynaptic dystrophic neurites surrounding amyloid plaques are sites of microtubule disruption, BACE1 elevation, and increased Abeta generation in Alzheimer's disease. *Acta Neuropathol* 132:235-256.
- Sanchez-Varo R, Trujillo-Estrada L, Sanchez-Mejias E, Torres M, Baglietto-Vargas D, Moreno-Gonzalez I, De Castro V, Jimenez S, Ruano D, Vizuete M, Davila JC, Garcia-Verdugo JM, Jimenez AJ, Vitorica J, Gutierrez A (2012) Abnormal accumulation of autophagic vesicles correlates with axonal and synaptic pathology in young Alzheimer's mice hippocampus. *Acta Neuropathol* 123:53-70.
- Schaapsmeeders P, Maaijwee NA, van Dijk EJ, Rutten-Jacobs LC, Arntz RM, Schoonderwaldt HC, Dorresteijn LD, Kessels RP, de Leeuw FE (2013) Long-term cognitive impairment after first-ever ischemic stroke in young adults. *Stroke* 44:1621-1628.
- Scharfman HE (2007) The neurobiology of epilepsy. *Curr Neurol Neurosci Rep* 7:348-354.
- Scheff SW, Price DA (2006) Alzheimer's disease-related alterations in synaptic density: neocortex and hippocampus. *J Alzheimers Dis* 9:101-115.
- Schubert D, Kotter R, Luhmann HJ, Staiger JF (2006) Morphology, electrophysiology and functional input connectivity of pyramidal neurons characterizes a genuine layer va in the primary somatosensory cortex. *Cereb Cortex* 16:223-236.
- Schulte T, Muller-Oehring EM (2010) Contribution of callosal connections to the interhemispheric integration of visuomotor and cognitive processes. *Neuropsychol Rev* 20:174-190.
- Seitz RJ, Azari NP, Knorr U, Binkofski F, Herzog H, Freund HJ (1999) The role of diaschisis in stroke recovery. *Stroke* 30:1844-1850.
- Serrano-Pozo A, Frosch MP, Masliah E, Hyman BT (2011) Neuropathological alterations in Alzheimer disease. *Cold Spring Harb Perspect Med* 1:a006189.

- Seubert P, Vigo-Pelfrey C, Esch F, Lee M, Dovey H, Davis D, Sinha S, Schlossmacher M, Whaley J, Swindlehurst C, et al. (1992) Isolation and quantification of soluble Alzheimer's beta-peptide from biological fluids. *Nature* 359:325-327.
- Shi Y, Kirwan P, Smith J, Robinson HP, Livesey FJ (2012) Human cerebral cortex development from pluripotent stem cells to functional excitatory synapses. *Nat Neurosci* 15:477-486, S471.
- Shih AY, Mateo C, Drew PJ, Tsai PS, Kleinfeld D (2012) A polished and reinforced thinned-skull window for long-term imaging of the mouse brain. *J Vis Exp*.
- Shim JK, Kim SW, Oh SJ, Kang N, Zatsiorsky VM, Latash ML (2005) Plastic changes in interhemispheric inhibition with practice of a two-hand force production task: a transcranial magnetic stimulation study. *Neurosci Lett* 374:104-108.
- Shoji M, Golde TE, Ghiso J, Cheung TT, Estus S, Shaffer LM, Cai XD, McKay DM, Tintner R, Frangione B, et al. (1992) Production of the Alzheimer amyloid beta protein by normal proteolytic processing. *Science* 258:126-129.
- Shors TJ, Anderson ML, Curlik DM, 2nd, Nokia MS (2012) Use it or lose it: how neurogenesis keeps the brain fit for learning. *Behav Brain Res* 227:450-458.
- Sibrian-Vazquez M, Escobedo JO, Lim S, Samoei GK, Strongin RM (2010) Homocystamides promote free-radical and oxidative damage to proteins. *Proc Natl Acad Sci U S A* 107:551-554.
- Silver J, Miller JH (2004) Regeneration beyond the glial scar. *Nat Rev Neurosci* 5:146-156.
- Slate AR, Bandyopadhyay S, Francis KP, Papich MG, Karolewski B, Hod EA, Prestia KA (2014) Efficacy of enrofloxacin in a mouse model of sepsis. *J Am Assoc Lab Anim Sci* 53:381-386.
- Sommer CJ (2017) Ischemic stroke: experimental models and reality. *Acta Neuropathol* 133:245-261.
- Sotelo C (2003) Viewing the brain through the master hand of Ramon y Cajal. *Nat Rev Neurosci* 4:71-77.
- Stern EA, Bacskai BJ, Hickey GA, Attenello FJ, Lombardo JA, Hyman BT (2004) Cortical synaptic integration in vivo is disrupted by amyloid-beta plaques. *J Neurosci* 24:4535-4540.
- Sterr A, Elbert T, Berthold I, Kolbel S, Rockstroh B, Taub E (2002) Longer versus shorter daily constraint-induced movement therapy of chronic hemiparesis: an exploratory study. *Arch Phys Med Rehabil* 83:1374-1377.
- Strong AJ, Anderson PJ, Watts HR, Virley DJ, Lloyd A, Irving EA, Nagafuji T, Ninomiya M, Nakamura H, Dunn AK, Graf R (2007) Peri-infarct depolarizations lead to loss of perfusion in ischaemic gyrencephalic cerebral cortex. *Brain* 130:995-1008.
- Svoboda K, Yasuda R (2006) Principles of two-photon excitation microscopy and its applications to neuroscience. *Neuron* 50:823-839.
- Takatsuru Y, Nabekura J, Koibuchi N (2013) Activity of the layer II/III neurons in the somatosensory cortex (SSC) plays a critical role on functional recovery after focal stroke in the contralateral SSC. *Neurosci Lett* 543:168-171.
- Takatsuru Y, Fukumoto D, Yoshitomo M, Nemoto T, Tsukada H, Nabekura J (2009) Neuronal circuit remodeling in the contralateral cortical hemisphere during functional recovery from cerebral infarction. *J Neurosci* 29:10081-10086.
- Takeuchi N, Izumi S (2012) Noninvasive brain stimulation for motor recovery after stroke: mechanisms and future views. *Stroke Res Treat* 2012:584727.
- Takeuchi T, Duzskiewicz AJ, Morris RG (2014) The synaptic plasticity and memory hypothesis: encoding, storage and persistence. *Philos Trans R Soc Lond B Biol Sci* 369:20130288.
- Tampellini D, Rahman N, Gallo EF, Huang Z, Dumont M, Capetillo-Zarate E, Ma T, Zheng R, Lu B, Nanus DM, Lin MT, Gouras GK (2009) Synaptic activity reduces intraneuronal Abeta, promotes APP transport to synapses, and protects against Abeta-related synaptic alterations. *J Neurosci* 29:9704-9713.

- Tanzi RE, Moir RD, Wagner SL (2004) Clearance of Alzheimer's Abeta peptide: the many roads to perdition. *Neuron* 43:605-608.
- Tawil SE, Muir KW (2017) Thrombolysis and thrombectomy for acute ischaemic stroke. *Clin Med (Lond)* 17:161-165.
- Trachtenberg JT, Chen BE, Knott GW, Feng G, Sanes JR, Welker E, Svoboda K (2002) Long-term in vivo imaging of experience-dependent synaptic plasticity in adult cortex. *Nature* 420:788-794.
- Tsai J, Grutzendler J, Duff K, Gan WB (2004) Fibrillar amyloid deposition leads to local synaptic abnormalities and breakage of neuronal branches. *Nat Neurosci* 7:1181-1183.
- van Spronsen M, Hoogenraad CC (2010) Synapse pathology in psychiatric and neurologic disease. *Curr Neurol Neurosci Rep* 10:207-214.
- Vassar R (2014) BACE1 inhibitor drugs in clinical trials for Alzheimer's disease. *Alzheimers Res Ther* 6:89.
- Wahl AS, Schwab ME (2014) Finding an optimal rehabilitation paradigm after stroke: enhancing fiber growth and training of the brain at the right moment. *Front Hum Neurosci* 8:381.
- Wahl M, Lauterbach-Soon B, Hattingen E, Jung P, Singer O, Volz S, Klein JC, Steinmetz H, Ziemann U (2007) Human motor corpus callosum: topography, somatotopy, and link between microstructure and function. *J Neurosci* 27:12132-12138.
- Wang DS, Dickson DW, Malter JS (2006) beta-Amyloid degradation and Alzheimer's disease. *J Biomed Biotechnol* 2006:58406.
- Wang H, Song G, Chuang H, Chiu C, Abdelmaksoud A, Ye Y, Zhao L (2018) Portrait of glial scar in neurological diseases. *Int J Immunopathol Pharmacol* 31:2058738418801406.
- Wang Y, Liu G, Hong D, Chen F, Ji X, Cao G (2016) White matter injury in ischemic stroke. *Prog Neurobiol* 141:45-60.
- Wey HY, Desai VR, Duong TQ (2013) A review of current imaging methods used in stroke research. *Neurol Res* 35:1092-1102.
- Wiley CA, Bissel SJ, Lesniak A, Dixon CE, Franks J, Beer Stolz D, Sun M, Wang G, Switzer R, Kochanek PM, Murdoch G (2016) Ultrastructure of Diaschisis Lesions after Traumatic Brain Injury. *J Neurotrauma* 33:1866-1882.
- Wisniewski HM, Ghetti B, Terry RD (1973) Neuritic (senile) plaques and filamentous changes in aged rhesus monkeys. *J Neuropathol Exp Neurol* 32:566-584.
- Witte OW, Bidmon HJ, Schiene K, Redecker C, Hagemann G (2000) Functional differentiation of multiple perilesional zones after focal cerebral ischemia. *J Cereb Blood Flow Metab* 20:1149-1165.
- Wolf F, Engelken R, Puelma-Touzel M, Weidinger JD, Neef A (2014) Dynamical models of cortical circuits. *Curr Opin Neurobiol* 25:228-236.
- Wu HY, Hudry E, Hashimoto T, Kuchibhotla K, Rozkalne A, Fan Z, Spires-Jones T, Xie H, Arbel-Ornath M, Grosskreutz CL, Bacskai BJ, Hyman BT (2010) Amyloid beta induces the morphological neurodegenerative triad of spine loss, dendritic simplification, and neuritic dystrophies through calcineurin activation. *J Neurosci* 30:2636-2649.
- Wu X, Huang L, Wu Z, Zhang C, Jiang D, Bai Y, Wang Y, Chen G (2013) Homeostatic competition between phasic and tonic inhibition. *J Biol Chem* 288:25053-25065.
- Xerri C, Zennou-Azogui Y, Sadlaoud K, Sauvajon D (2014) Interplay between intra- and interhemispheric remodeling of neural networks as a substrate of functional recovery after stroke: adaptive versus maladaptive reorganization. *Neuroscience* 283:178-201.
- Xu T, Yu X, Perlik AJ, Tobin WF, Zweig JA, Tennant K, Jones T, Zuo Y (2009) Rapid formation and selective stabilization of synapses for enduring motor memories. *Nature* 462:915-919.

- Yang G, Pan F, Gan WB (2009) Stably maintained dendritic spines are associated with lifelong memories. *Nature* 462:920-924.
- Yang G, Pan F, Parkhurst CN, Grutzendler J, Gan WB (2010) Thinned-skull cranial window technique for long-term imaging of the cortex in live mice. *Nat Protoc* 5:201-208.
- Yang G, Chang PC, Bekker A, Blanck TJ, Gan WB (2011) Transient effects of anesthetics on dendritic spines and filopodia in the living mouse cortex. *Anesthesiology* 115:718-726.
- Yang Y, Coleman M, Zhang L, Zheng X, Yue Z (2013) Autophagy in axonal and dendritic degeneration. *Trends Neurosci* 36:418-428.
- Yiu G, He Z (2006) Glial inhibition of CNS axon regeneration. *Nat Rev Neurosci* 7:617-627.
- Yoshihara Y, De Roo M, Muller D (2009) Dendritic spine formation and stabilization. *Curr Opin Neurobiol* 19:146-153.
- Yu X, Zuo Y (2014) Two-photon in vivo imaging of dendritic spines in the mouse cortex using a thinned-skull preparation. *J Vis Exp*.
- Zhang C, Feng W, Zhao Y, Yu T, Li P, Xu T, Luo Q, Zhu D (2018) A large, switchable optical clearing skull window for cerebrovascular imaging. *Theranostics* 8:2696-2708.
- Zhao LR, Willing A (2018) Enhancing endogenous capacity to repair a stroke-damaged brain: An evolving field for stroke research. *Prog Neurobiol* 163-164:5-26.
- Zhao YJ, Yu TT, Zhang C, Li Z, Luo QM, Xu TH, Zhu D (2018) Skull optical clearing window for in vivo imaging of the mouse cortex at synaptic resolution. *Light Sci Appl* 7:17153.
- Zheng H, Koo EH (2006) The amyloid precursor protein: beyond amyloid. *Mol Neurodegener* 1:5.
- Zhou Y, Danbolt NC (2014) Glutamate as a neurotransmitter in the healthy brain. *J Neural Transm (Vienna)* 121:799-817.
- Zipfel WR, Williams RM, Webb WW (2003) Nonlinear magic: multiphoton microscopy in the biosciences. *Nat Biotechnol* 21:1369-1377.

6. List of publications

- L. Blazquez-Llorca*, **S. V. Freitag***, E. F. Rodrigues, A. M. Pérez, J. R. Rodríguez, M. M. Dorostkar, J. DeFelipe, J. Herms, High plasticity of axonal pathology in Alzheimer's disease mouse models. *Acta neuropathologica communications* 5, 14 (Feb 7, 2017).
- S. V. Ovsepian, L. Blazquez-Llorca, **S. V. Freitag**, E. F. Rodrigues, J. Herms, Ambient Glutamate Promotes Paroxysmal Hyperactivity in Cortical Pyramidal Neurons at Amyloid Plaques via Presynaptic mGluR1 Receptors. *Cerebral cortex* 27, 4733 (Oct 1, 2017).

* These authors contributed equally

7. Acknowledgments

And today with a couple of scars, more white hair and somewhat thicker skin, I reach the final line of this adventure called PhD that began some years ago. I look back and I feel very satisfied with the work done, prepared and willing to venture into new professional challenges. It has not been easy but it was worth it.

First of all, I thank my supervisors Prof. Nikolaus Plesnila and Dr. Farida Hellal for giving me the opportunity and means to carry out my project and for trusting me and my abilities as a PhD student. Big thanks also to my previous supervisor Dr. Lidia Blazquez for our nice work together for teaching me how to use the two-photon microscope, perform cranial windows and many other things that helped me a lot in different experiments and projects.

Thanks to my lab mates (Sabrina, Antonia, Berni, Nina, Becky, Hanhan, Igor, Yue ...), to anyone who has contributed in some way to my project (Burcu, Thanasis, Benno, Franz, Gemma), to the members of my Thesis Advisory Committee, the workers of the animal facility (Steffi, Tamara) and the Graduated School of Systemic Neurosciences (Stefi, Lena) for being able to be part of their program of excellence as well as having been able to count on their support and activities.

I also want to highlight the great meaning that my family has had for me, especially my parents and sister Sara, as well as my closest friends (Katia, Marija, Michela, Susanne, Charoula, Marcos, Anna Lena, Alba, Sandra) during this phase of my career. Thank you very much for your support.

For everyone who reads this thesis, I hope you enjoy it and, above all, find answers to your questions or clues to continue your experiments. Nothing would make me happier than being able to contribute with my work to make progress in finding a cure for the many diseases that affect our still unknown but fascinating nervous system.

Finally, I want to mention that the present study has been carried out through the use of experimental animals, more specifically rodents according to the 3Rs rule. As a student aware of the moral and ethical factors that this entails, I have tried to use as few animals as possible, as well as pay attention to all the pre / post-operational care and procedures performed. I very much encourage all scientists to always keep this in mind.

“The important thing is to not stop questioning. Curiosity has its own reason for existing”,

Albert Einstein.

8. Declaration of author's contribution

Authors contributed to the research articles as follows:

- Lidia Blazquez-Llorca*, **Susana Valero-Freitag***, Eva Ferreira Rodrigues, Ángel Merchán-Pérez, J. Rodrigo Rodríguez, Mario M. Dorostkar, Javier DeFelipe and Jochen Herms. *equally contributed. **High plasticity of axonal pathology in Alzheimer's disease mouse models**
LBL: conception or design of the work, data collection, data analysis and interpretation, drafting the article, critical revision of the article, final approval of the version to be published. SVF: data collection, data analysis and interpretation, critical revision of the article. EFR: data collection, data analysis and interpretation, critical revision of the article. AMP: data collection, data analysis and interpretation, critical revision of the article. JRR: data collection, data analysis and interpretation, critical revision of the article. MMD: critical revision of the article. JF: critical revision of the article, final approval of the version to be published. JH: critical revision of the article, final approval of the version to be published. All authors read and approved the final manuscript.
- **Susana Valero-Freitag**, Fatma B Seker , Athanasios Loubopoulos, Bernhard K Groschup, Antonia Wehn , Benno Gesierich, Marco Düring, Martin Dichgans, Farida Hellal & Nikolaus Plesnila. **Remote contralesional cortical reorganization after experimental ischemic stroke.** V.F.S., H.F., P.N., and M.D. were the main platform for scientific discussion and designed the experiment. V.F.S., H.F., G.K.B., W.A. and S.F.B. performed the experiments, data acquisition, quantifications, and statistical analysis. L.A. and G.B., provided technical support. V.F.S. and H.F. wrote the manuscript with input and revision from all authors

Herewith, I confirm the contributions to the article/manuscripts

München,

Susana Valero Freitag

Prof. Nikolaus Plesnila
(supervisor)

Dr. Lidia Blazquez Llorca(shared first author research article 1)

9. Affidavit

Eidesstattliche Versicherung/Affidavit

Hiermit versichere ich an Eides statt, dass ich die vorliegende Dissertation _____

selbstständig angefertigt habe, mich außer der angegebenen keiner weiteren Hilfsmittel bedient und alle Erkenntnisse, die aus dem Schrifttum ganz oder annähernd übernommen sind, als solche kenntlich gemacht und nach ihrer Herkunft unter Bezeichnung der Fundstelle einzeln nachgewiesen habe.

I hereby confirm that the dissertation _____

is the result of my own work and that I have only used sources or materials listed and specified in the dissertation.

München, 19.10.2020

Susana Valero Freitag

10. Curriculum Vitae

SUSANA VALERO FREITAG

EDUCATION

LUDWIG MAXIMILIANS UNIVERSITY

Institute for Stroke and Dementia Research

Munich, Germany

Graduate School of Systemic Neurosciences

October 2016 – Present

PhD in Neurosciences

LUDWIG MAXIMILIANS UNIVERSITY

Center for Neuropathology and Prion Research (DZNE)

Munich, Germany

Oct 2013 – Oct 2014

Master's Thesis

MADRID UNIVERSITY

Madrid, Spain

Universidad Autónoma de Madrid

Oct 2012 - Oct 2014

Master in Neurosciences

GOTTFRIED WILHEM LEIBNIZ UNIVERSITY

Hannover, Germany

Oct 2010 - Mar 2011

Erasmus Scholarship (Biology)

OVIEDO UNIVERSITY

Asturias, Spain

Sep 2005 – Mar 2011

Master in Biology - Health Specialization

AWARDS

Early Career Investigator Travel Bursary for Mid-Term Symposium (ERANET) Lisbon 2019

Synergy Cluster Travel Grant for BRAIN & BRAIN PET Japan

Early Career Investigator Travel Bursary for BRAIN & BRAIN PET Japan

SyNergy Cluster Gender Program. Funding for Munich Brain Course 2018

Synergy Cluster Travel Grant for Dresden Neurorepair Conference

Synergy Cluster Travel Grant for Symposium on CBF, Metabolism and Function Berlin	2017
Best Poster Award Neurowoche München Köpfe Impulse Potenziale	2014
Grant Alvargonzález Foundation Gijón	2013
Certificate for Animal Experiments (Category C), Veterinary Office Madrid University	
Erasmus Scholarship at Gottfried Wilhelm Leibniz Universität Hannover	2011

SCIENTIFIC SKILLS

Experimental models: experience with different mouse models, handling, anesthesia/analgesia, viral injections, cranial window implantation, stroke induction, post-operative care protocols, behavior analysis, whisker stimulation and laser speckle imaging, *in vivo* 2-photon and confocal imaging

Biochemistry: Immunohistochemistry and histology

WORK HISTORY

Research Assistant	Munich, Germany
Oct 2015 – Dec 2015	Institute for Stroke and Dementia Research

Research Assistant	Munich, Germany
Dec 2014	Berstein Center for Computational Neuroscience

Research Assistant	Munich, Germany
Apr 2014 – Aug 2014	Center for Neuropathology and Prion Research

CONFERENCES AND POSTERS

1. Plaza-Alonso S, Kastanauskaite A, **Valero Freitag S**, Plesnila N, Hellal F, DeFelipe J, Merino-Serrais P
“Morphological alterations of pyramidal neurons from the contralesional hemisphere after ischemic stroke”
Cajal Institute Madrid 2019
2. **Valero Freitag S**, Groschup B, Seker FB, Gesierich B, Düring M, Dichgans M, Hellal F, Plesnila N
“Remote cortical reorganization after experimental ischemic stroke”

SFN Chicago 2019

Mid-Term Symposium ERANET-Neuron Lisbon 2019

BRAIN & BRAIN PET Japan 2019

3. **Valero Freitag S**, Lourdopoulos A, Mamrak U, Cramer J, Liesz A, Hellal F, Plesnila N
“Imaging of brain reorganization after experimental stroke by repetitive two-photon microscopy”
Dresden Neurorepair Conference 2018
4. Symposium on CBF, Metabolism and Function Berlin 2017
5. Neurowoche München Köpfe Impulse Potenziale 2014

OTHERS


Software: ZEN, Imaris, Neurobehavioral Systems (Presentation), Statistics (SPSS, R, GraphPad, SigmaPlot), LabChart, PIMSoft, Image J, Microsoft Office.

Languages: Mother tongue Spanish and German; English Fluent

Teaching: laboratory and surgical procedures (Zertifikate Hochschullehre Bayern A/B Level)

11. Copyrights

Copyright: © 2014 Risher et al. This is an open-access article distributed under the terms of the Creative Commons Attribution License, which permits unrestricted use, distribution, and reproduction in any medium, provided the original author and source are credited.



The amyloid precursor protein: beyond amyloid
Author: Hui Zheng et al
Publication: Molecular Neurodegeneration
Publisher: Springer Nature
Date: Jul 3, 2006
Copyright © 2006, Springer Nature

Creative Commons

This is an open access article distributed under the terms of the [Creative Commons CC BY](#) license, which permits unrestricted use, distribution, and reproduction in any medium, provided the original work is properly cited.

You are not required to obtain permission to reuse this article.
To request permission for a type of use not listed, please contact [Springer Nature](#)

Audrey Ragagnin, 2013

© 2013 The Author(s). Licensee IntechOpen. This chapter is distributed under the terms of the [Creative Commons Attribution 3.0 License](#), which permits unrestricted use, distribution, and reproduction in any medium, provided the original work is properly cited.

<http://creativecommons.org/licenses/by/3.0/> This work is licensed under a <http://creativecommons.org/licenses/by/3.0/> Creative Commons Attribution 3.0 Unported License.

[Stroke Res Treat. 2012; 2012: 584727.](#)
Published online 2012 Sep 25. doi: [10.1155/2012/584727](#)
- Copyright/License [Request permission to reuse](#)
[Copyright](#) © 2012 N. Takeuchi and S.-I. Izumi.
This is an open access article distributed under the Creative Commons Attribution License, which permits unrestricted use, distribution, and reproduction in any medium, provided the original work is properly cited.

Order Number: 1021083

Order Date: 03 Mar 2020

Payment Information

Susana Valero Freitag
susana.valero@med.uni-muenche
n.de

Payment method: Invoice

Billing Address:

Miss Susana Valero Freitag
Graduated School of Systemic
Neurosciences
Nymphenburgerstraße 19
4
Munich
Germany

+49 15785585613
susana.valero@med.uni-m
uenchen.de

Customer Location:

Miss Susana Valero Freitag
Graduated School of Systemic
Neurosciences
Nymphenburgerstraße 19
4
Munich
Germany

Order Details

1. Annual review of cell and developmental biology

Billing Status:
Open

Order license ID	1021083-1
Order detail status	Completed
ISSN	1530-8995
Type of use	Republish in a thesis/dissertation
Publisher	ANNUAL REVIEWS
Portion	Chart/graph/table/figure

0,00 EUR

LICENSED CONTENT

Publication Title	Annual review of cell and developmental biology	Country	United States of America
Author/Editor	ANNUAL REVIEWS, INC.	Rightholder	Annual Reviews, Inc.
Date	01/01/1995	Publication Type	e-Journal
Language	English	URL	http://arjournals.annualreviews.org/loi/cellbio

REQUEST DETAILS

Portion Type	Chart/graph/table/figure	Distribution	Worldwide
Number of charts / graphs / tables / figures requested	2	Translation	Original language of publication
Format (select all that apply)	Print,Electronic	Copies for the disabled?	No
Who will republish the content?	Academic institution	Minor editing privileges?	No
		Incidental promotional use?	No

Duration of Use	Life of current and all future editions	Currency	EUR
Lifetime Unit Quantity	Up to 499		
Rights Requested	Main product		

NEW WORK DETAILS

Title	Local and remote effects of pathological conditions on pyramidal neurites, a longitudinal two-photon in vivo study	Institution name	Graduated School of Systemic Neurosciences
		Expected presentation date	2020-03-29
Instructor name	Susana Valero Freitag		

ADDITIONAL DETAILS

The requesting person / organization to appear on the license	Susana Valero Freitag
---	-----------------------

REUSE CONTENT DETAILS

Title, description or numeric reference of the portion(s)	Introduction	Title of the article/chapter the portion is from	Introduction chapter
Editor of portion(s)	Susana Valero Freitag	Author of portion(s)	ANNUAL REVIEWS, INC.
Volume of serial or monograph	1	Publication date of portion	1995-01-01
Page or page range of portion	Introduction		

Total Items: 1		Subtotal:	0,00 EUR
		Order Total:	0,00 EUR

SPRINGER NATURE LICENSE TERMS AND CONDITIONS

Mar 11, 2020

This Agreement between Graduated School of Systemic Neurosciences -- Susana Valero Freitag ("You") and Springer Nature ("Springer Nature") consists of your license details and the terms and conditions provided by Springer Nature and Copyright Clearance Center.

License Number	4781310862685
License date	Mar 03, 2020
Licensed Content Publisher	Springer Nature
Licensed Content Publication	Springer eBook
Licensed Content Title	Cell Biology of the Synapse
Licensed Content Author	Rochelle S. Cohen
Licensed Content Date	Jan 1, 2013
Type of Use	Thesis/Dissertation
Requestor type	academic/university or research institute
Format	print and electronic
Portion	figures/tables/illustrations
Number of figures/tables/illustrations	1
Will you be translating?	no
Circulation/distribution	1 - 29
Author of this Springer Nature content	no
Title	Local and remote effect of pathological conditions on pyramidal neurites, a longitudinal two-photon study
Institution name	Graduated School of Systemic Neurosciences
Expected presentation date	Mar 2020
Portions	Cell biology of the synapse Graduated School of Systemic Neurosciences Nymphenburgerstraße 194
Requestor Location	Munich, other Germany Attn: Graduated School of Systemic Neurosciences
Total	0.00 EUR
Terms and Conditions	

Springer Nature Customer Service Centre GmbH Terms and Conditions

This agreement sets out the terms and conditions of the licence (the **Licence**) between you and **Springer Nature Customer Service Centre GmbH** (the **Licensor**). By clicking 'accept' and completing the transaction for the material (**Licensed Material**), you also confirm your acceptance of these terms and conditions.

Grant of License

The Licensor grants you a personal, non-exclusive, non-transferable, world-wide licence to reproduce the Licensed Material for the purpose specified in your order only. Licences are granted for the specific use requested in the order and for no other use, subject to the conditions below.

The Licensor warrants that it has, to the best of its knowledge, the rights to license reuse of the Licensed Material. However, you should ensure that the material you are requesting is original to the Licensor and does not carry the copyright of another entity (as credited in the published version).

If the credit line on any part of the material you have requested indicates that it was reprinted or adapted with permission from another source, then you should also seek permission from that source to reuse the material.

Scope of Licence

You may only use the Licensed Content in the manner and to the extent permitted by these Ts&Cs and any applicable laws.

A separate licence may be required for any additional use of the Licensed Material, e.g. where a licence has been purchased for print only use, separate permission must be obtained for electronic re-use. Similarly, a licence is only valid in the language selected and does not apply for editions in other languages unless additional translation rights have been granted separately in the licence. Any content owned by third parties are expressly excluded from the licence.

Similarly, rights for additional components such as custom editions and derivatives require additional permission and may be subject to an additional fee. Please apply to Journalpermissions@springernature.com/bookpermissions@springernature.com for these rights.

Where permission has been granted **free of charge** for material in print, permission may also be granted for any electronic version of that work, provided that the material is incidental to your work as a whole and that the electronic version is essentially equivalent to, or substitutes for, the print version.

An alternative scope of licence may apply to signatories of the [STM Permissions Guidelines](#), as amended from time to time.

Duration of Licence

A licence for is valid from the date of purchase ('Licence Date') at the end of the relevant period in the below table:

Scope of Licence	Duration of Licence
Post on a website	12 months
Presentations	12 months
Books and journals	Lifetime of the edition in the language purchased

Acknowledgement

The Licensor's permission must be acknowledged next to the Licenced Material in print. In electronic form, this acknowledgement must be visible at the same time as the figures/tables/illustrations or abstract, and must be hyperlinked to the journal/book's homepage. Our required acknowledgement format is in the Appendix below.

Restrictions on use

Use of the Licensed Material may be permitted for incidental promotional use and minor editing privileges e.g. minor adaptations of single figures, changes of format, colour and/or style where the adaptation is credited as set out in Appendix 1 below. Any other changes including but not limited to, cropping, adapting, omitting material that affect the meaning, intention or moral rights of the author are strictly prohibited.

You must not use any Licensed Material as part of any design or trademark.

Licensed Material may be used in Open Access Publications (OAP) before publication by Springer Nature, but any Licensed Material must be removed from OAP sites prior to final publication.

Ownership of Rights

Licensed Material remains the property of either Licensor or the relevant third party and any rights not explicitly granted herein are expressly reserved.

Warranty

IN NO EVENT SHALL LICENSOR BE LIABLE TO YOU OR ANY OTHER PARTY OR ANY OTHER PERSON OR FOR ANY SPECIAL, CONSEQUENTIAL, INCIDENTAL OR INDIRECT DAMAGES, HOWEVER CAUSED, ARISING OUT OF OR IN CONNECTION WITH THE DOWNLOADING, VIEWING OR USE OF THE MATERIALS REGARDLESS OF THE FORM OF ACTION, WHETHER FOR BREACH OF CONTRACT, BREACH OF WARRANTY, TORT, NEGLIGENCE, INFRINGEMENT OR OTHERWISE (INCLUDING, WITHOUT LIMITATION, DAMAGES BASED ON LOSS OF PROFITS, DATA, FILES, USE, BUSINESS OPPORTUNITY OR CLAIMS OF THIRD PARTIES), AND WHETHER OR NOT THE PARTY HAS BEEN ADVISED OF THE POSSIBILITY OF SUCH DAMAGES. THIS LIMITATION SHALL APPLY NOTWITHSTANDING ANY FAILURE OF ESSENTIAL PURPOSE OF ANY LIMITED REMEDY PROVIDED HEREIN.

Limitations

BOOKS ONLY: Where 'reuse in a dissertation/thesis' has been selected the following terms apply: Print rights of the final author's accepted manuscript (for clarity, NOT the published version) for up to 100 copies, electronic rights for use only on a personal website or institutional repository as defined by the Sherpa guideline (www.sherpa.ac.uk/romeo/).

Termination and Cancellation

Licences will expire after the period shown in Clause 3 (above).

Licensee reserves the right to terminate the Licence in the event that payment is not received in full or if there has been a breach of this agreement by you.

Appendix 1 — Acknowledgements:

For Journal Content:

Reprinted by permission from [the Licensors]: [Journal Publisher (e.g. Nature/Springer/Palgrave)] [JOURNAL NAME] [REFERENCE CITATION(Article name, Author(s) Name), [COPYRIGHT] (year of publication)

For Advance Online Publication papers:

Reprinted by permission from [the Licensors]: [Journal Publisher (e.g. Nature/Springer/Palgrave)] [JOURNAL NAME] [REFERENCE CITATION(Article name, Author(s) Name), [COPYRIGHT] (year of publication), advance online publication, day month year (doi: 10.1038/sj.[JOURNAL ACRONYM].)

For Adaptations/Translations:

Adapted/Translated by permission from [the Licensors]: [Journal Publisher (e.g. Nature/Springer/Palgrave)] [JOURNAL NAME] [REFERENCE CITATION(Article name, Author(s) Name), [COPYRIGHT] (year of publication)

Note: For any republication from the British Journal of Cancer, the following credit line style applies:

Reprinted/adapted/translated by permission from [the Licensors]: on behalf of Cancer Research UK: : [Journal Publisher (e.g. Nature/Springer/Palgrave)] [JOURNAL NAME] [REFERENCE CITATION (Article name, Author(s) Name), [COPYRIGHT] (year of publication)

For Advance Online Publication papers:

Reprinted by permission from The [the Licensors]: on behalf of Cancer Research UK: [Journal Publisher (e.g. Nature/Springer/Palgrave)] [JOURNAL NAME] [REFERENCE CITATION (Article name, Author(s) Name), [COPYRIGHT] (year of publication), advance online publication, day month year (doi: 10.1038/sj.[JOURNAL ACRONYM].)

For Book content:

Reprinted/adapted by permission from [the Licensors]: [Book Publisher (e.g. Palgrave Macmillan, Springer etc)] [Book Title] by [Book author(s)] [COPYRIGHT] (year of publication)

Other Conditions:

Version 1.2

Questions? customercare@copyright.com or +1-855-239-3415 (toll free in the US) or +1-978-646-2777.

SPRINGER NATURE LICENSE TERMS AND CONDITIONS

Mar 11, 2020

This Agreement between Graduated School of Systemic Neurosciences -- Susana Valero Freitag ("You") and Springer Nature ("Springer Nature") consists of your license details and the terms and conditions provided by Springer Nature and Copyright Clearance Center.

License Number	4781320535721
License date	Mar 03, 2020
Licensed Content Publisher	Springer Nature
Licensed Content Publication	Nature
Licensed Content Title	Multimodal techniques for diagnosis and prognosis of Alzheimer's disease
Licensed Content Author	Richard J. Perrin et al
Licensed Content Date	Oct 14, 2009
Type of Use	Thesis/Dissertation
Requestor type	academic/university or research institute
Format	print and electronic
Portion	figures/tables/illustrations
Number of figures/tables/illustrations	1
High-res required	no

Will you be translating? no

Circulation/distribution 1 - 29

Author of this Springer Nature content no

Title Local and remote effect of pathological conditions on pyramidal neurites, a longitudinal two-photon study

Institution name Graduated School of Systemic Neurosciences

Expected presentation date Mar 2020

Portions Figure 3

Graduated School of Systemic Neurosciences
Nymphenburgerstraße 194

Requestor Location

Munich, other
Germany
Attn: Graduated School of Systemic Neurosciences

Total 0.00 EUR

Terms and Conditions

Springer Nature Customer Service Centre GmbH Terms and Conditions

This agreement sets out the terms and conditions of the licence (the **Licence**) between you and **Springer Nature Customer Service Centre GmbH** (the **Licensor**). By clicking 'accept' and completing the transaction for the material (**Licensed Material**), you also confirm your acceptance of these terms and conditions.

1. Grant of License

1. 1. The Licensor grants you a personal, non-exclusive, non-transferable, world-wide licence to reproduce the Licensed Material for the purpose specified in your order only. Licences are granted for the specific use requested in the order and for no other use, subject to the conditions below.

1. 2. The Licensor warrants that it has, to the best of its knowledge, the rights to license reuse of the Licensed Material. However, you should ensure that the material you are requesting is original to the Licensor and does not carry the copyright of

another entity (as credited in the published version).

1. 3. If the credit line on any part of the material you have requested indicates that it was reprinted or adapted with permission from another source, then you should also seek permission from that source to reuse the material.

2. Scope of Licence

2. 1. You may only use the Licensed Content in the manner and to the extent permitted by these Ts&Cs and any applicable laws.

2. 2. A separate licence may be required for any additional use of the Licensed Material, e.g. where a licence has been purchased for print only use, separate permission must be obtained for electronic re-use. Similarly, a licence is only valid in the language selected and does not apply for editions in other languages unless additional translation rights have been granted separately in the licence. Any content owned by third parties are expressly excluded from the licence.

2. 3. Similarly, rights for additional components such as custom editions and derivatives require additional permission and may be subject to an additional fee.

Please apply to

Journalpermissions@springernature.com/bookpermissions@springernature.com for these rights.

2. 4. Where permission has been granted **free of charge** for material in print, permission may also be granted for any electronic version of that work, provided that the material is incidental to your work as a whole and that the electronic version is essentially equivalent to, or substitutes for, the print version.

2. 5. An alternative scope of licence may apply to signatories of the [STM Permissions Guidelines](#), as amended from time to time.

3. Duration of Licence

3. 1. A licence for is valid from the date of purchase ('Licence Date') at the end of the relevant period in the below table:

Scope of Licence	Duration of Licence
Post on a website	12 months
Presentations	12 months
Books and journals	Lifetime of the edition in the language purchased

4. Acknowledgement

4. 1. The Licensor's permission must be acknowledged next to the Licenced Material in print. In electronic form, this acknowledgement must be visible at the same time as the figures/tables/illustrations or abstract, and must be hyperlinked to the journal/book's homepage. Our required acknowledgement format is in the Appendix below.

5. Restrictions on use

5. 1. Use of the Licensed Material may be permitted for incidental promotional use and minor editing privileges e.g. minor adaptations of single figures, changes of format, colour and/or style where the adaptation is credited as set out in Appendix 1 below. Any other changes including but not limited to, cropping, adapting, omitting material that affect the meaning, intention or moral rights of the author are strictly prohibited.

5. 2. You must not use any Licensed Material as part of any design or trademark.

5. 3. Licensed Material may be used in Open Access Publications (OAP) before publication by Springer Nature, but any Licensed Material must be removed from OAP sites prior to final publication.

6. Ownership of Rights

6. 1. Licensed Material remains the property of either Licensor or the relevant third party and any rights not explicitly granted herein are expressly reserved.

7. Warranty

IN NO EVENT SHALL LICENSOR BE LIABLE TO YOU OR ANY OTHER PARTY OR ANY OTHER PERSON OR FOR ANY SPECIAL, CONSEQUENTIAL, INCIDENTAL OR INDIRECT DAMAGES, HOWEVER CAUSED, ARISING OUT OF OR IN CONNECTION WITH THE DOWNLOADING, VIEWING OR USE OF THE MATERIALS REGARDLESS OF THE FORM OF ACTION, WHETHER FOR BREACH OF CONTRACT, BREACH OF WARRANTY, TORT, NEGLIGENCE, INFRINGEMENT OR OTHERWISE (INCLUDING, WITHOUT LIMITATION, DAMAGES BASED ON LOSS OF PROFITS, DATA, FILES, USE, BUSINESS OPPORTUNITY OR CLAIMS OF THIRD PARTIES), AND WHETHER OR NOT THE PARTY HAS BEEN ADVISED OF THE POSSIBILITY OF SUCH DAMAGES. THIS LIMITATION SHALL APPLY NOTWITHSTANDING ANY FAILURE OF ESSENTIAL PURPOSE OF ANY LIMITED REMEDY PROVIDED HEREIN.

8. Limitations

8. 1. BOOKS ONLY: Where 'reuse in a dissertation/thesis' has been selected the following terms apply: Print rights of the final author's accepted manuscript (for clarity, NOT the published version) for up to 100 copies, electronic rights for use only on a personal website or institutional repository as defined by the Sherpa guideline (www.sherpa.ac.uk/romeo/).

9. Termination and Cancellation

9. 1. Licences will expire after the period shown in Clause 3 (above).

9. 2. Licensee reserves the right to terminate the Licence in the event that payment is not received in full or if there has been a breach of this agreement by you.

Appendix 1 — Acknowledgements:**For Journal Content:**

Reprinted by permission from [the Licensor]: [Journal Publisher (e.g. Nature/Springer/Palgrave)] [JOURNAL NAME] [REFERENCE CITATION (Article name, Author(s) Name), [COPYRIGHT] (year of publication)]

For Advance Online Publication papers:

Reprinted by permission from [the Licensor]: [Journal Publisher (e.g. Nature/Springer/Palgrave)] [JOURNAL NAME] [REFERENCE CITATION (Article name, Author(s) Name), [COPYRIGHT] (year of publication), advance online publication, day month year (doi: 10.1038/sj.[JOURNAL ACRONYM].)]

For Adaptations/Translations:

Adapted/Translated by permission from [the Licensor]: [Journal Publisher (e.g. Nature/Springer/Palgrave)] [JOURNAL NAME] [REFERENCE CITATION (Article name, Author(s) Name), [COPYRIGHT] (year of publication)]

Note: For any republication from the British Journal of Cancer, the following credit line style applies:

Reprinted/adapted/translated by permission from [the Licensor]: on behalf of Cancer Research UK: : [Journal Publisher (e.g. Nature/Springer/Palgrave)] [JOURNAL NAME] [REFERENCE CITATION (Article name, Author(s) Name), [COPYRIGHT] (year of publication)]

For Advance Online Publication papers:

Reprinted by permission from The [the Licensor]: on behalf of Cancer Research UK: [Journal Publisher (e.g. Nature/Springer/Palgrave)] [JOURNAL NAME] [REFERENCE CITATION (Article name, Author(s) Name), [COPYRIGHT] (year of publication), advance online publication, day month year (doi: 10.1038/sj.[JOURNAL ACRONYM].)]

For Book content:

Reprinted/adapted by permission from [the Licensor]: [Book Publisher (e.g. Palgrave Macmillan, Springer etc)] [Book Title] by [Book author(s)] [COPYRIGHT] (year of publication)]

Other Conditions:

Version 1.2

Questions? customercare@copyright.com or +1-855-239-3415 (toll free in the US) or +1-978-646-2777.

ELSEVIER LICENSE TERMS AND CONDITIONS

Mar 18, 2020

This Agreement between Graduated School of Systemic Neurosciences -- Susana Valero Freitag ("You") and Elsevier ("Elsevier") consists of your license details and the terms and conditions provided by Elsevier and Copyright Clearance Center.

License Number	4791880772684
License date	Mar 18, 2020
Licensed Content Publisher	Elsevier
Licensed Content Publication	Brain Stimulation
Licensed Content Title	Targeting interhemispheric inhibition with neuromodulation to enhance stroke rehabilitation
Licensed Content Author	L.J. Boddington,J.N.J. Reynolds
Licensed Content Date	March–April 2017
Licensed Content Volume	10
Licensed Content Issue	2
Licensed Content Pages	9
Start Page	214
End Page	222
Type of Use	reuse in a thesis/dissertation

Portion	figures/tables/illustrations
Number of figures/tables/illustrations	1
Format	both print and electronic
Are you the author of this Elsevier article?	No
Will you be translating?	No
Title	Local and remote effect of pathological conditions on pyramidal neurites, a longitudinal two-photon study
Institution name	Graduated School of Systemic Neurosciences
Expected presentation date	Mar 2020
Portions	Figure 1
Requestor Location	Graduated School of Systemic Neurosciences Nymphenburgerstraße 194 Munich, other Germany Attn: Graduated School of Systemic Neurosciences
Publisher Tax ID	GB 494 6272 12
Total	0.00 EUR
Terms and Conditions	

INTRODUCTION

1. The publisher for this copyrighted material is Elsevier. By clicking "accept" in connection with completing this licensing transaction, you agree that the following terms and conditions apply to this transaction (along with the Billing and Payment terms and conditions established by Copyright Clearance Center, Inc. ("CCC"), at the time that you opened your Rightslink account and that are available at any time at <http://myaccount.copyright.com>).

GENERAL TERMS

2. Elsevier hereby grants you permission to reproduce the aforementioned material subject to the terms and conditions indicated.

3. Acknowledgement: If any part of the material to be used (for example, figures) has appeared in our publication with credit or acknowledgement to another source, permission must also be sought from that source. If such permission is not obtained then that material may not be included in your publication/copies. Suitable acknowledgement to the source must be made, either as a footnote or in a reference list at the end of your publication, as follows:

"Reprinted from Publication title, Vol /edition number, Author(s), Title of article / title of chapter, Pages No., Copyright (Year), with permission from Elsevier [OR APPLICABLE SOCIETY COPYRIGHT OWNER]." Also Lancet special credit - "Reprinted from The Lancet, Vol. number, Author(s), Title of article, Pages No., Copyright (Year), with permission from Elsevier."

4. Reproduction of this material is confined to the purpose and/or media for which permission is hereby given.

5. Altering/Modifying Material: Not Permitted. However figures and illustrations may be altered/adapted minimally to serve your work. Any other abbreviations, additions, deletions and/or any other alterations shall be made only with prior written authorization of Elsevier Ltd. (Please contact Elsevier at permissions@elsevier.com). No modifications can be made to any Lancet figures/tables and they must be reproduced in full.

6. If the permission fee for the requested use of our material is waived in this instance, please be advised that your future requests for Elsevier materials may attract a fee.

7. Reservation of Rights: Publisher reserves all rights not specifically granted in the combination of (i) the license details provided by you and accepted in the course of this licensing transaction, (ii) these terms and conditions and (iii) CCC's Billing and Payment terms and conditions.

8. License Contingent Upon Payment: While you may exercise the rights licensed immediately upon issuance of the license at the end of the licensing process for the transaction, provided that you have disclosed complete and accurate details of your proposed use, no license is finally effective unless and until full payment is received from you (either by publisher or by CCC) as provided in CCC's Billing and Payment terms and conditions. If full payment is not received on a timely basis, then any license preliminarily granted shall be deemed automatically revoked and shall be void as if never granted. Further, in the event that you breach any of these terms and conditions or any of CCC's Billing and Payment terms and conditions, the license is automatically revoked and shall be void as if never granted. Use of materials as described in a revoked license, as well as any use of the materials beyond the scope of an unrevoked license, may constitute copyright infringement and publisher reserves the right to take any and all action to protect its copyright in the materials.

9. Warranties: Publisher makes no representations or warranties with respect to the licensed material.

10. Indemnity: You hereby indemnify and agree to hold harmless publisher and CCC, and their respective officers, directors, employees and agents, from and against any and all claims arising out of your use of the licensed material other than as specifically authorized pursuant to this license.

11. No Transfer of License: This license is personal to you and may not be sublicensed, assigned, or transferred by you to any other person without publisher's written permission.

12. **No Amendment Except in Writing:** This license may not be amended except in a writing signed by both parties (or, in the case of publisher, by CCC on publisher's behalf).

13. **Objection to Contrary Terms:** Publisher hereby objects to any terms contained in any purchase order, acknowledgment, check endorsement or other writing prepared by you, which terms are inconsistent with these terms and conditions or CCC's Billing and Payment terms and conditions. These terms and conditions, together with CCC's Billing and Payment terms and conditions (which are incorporated herein), comprise the entire agreement between you and publisher (and CCC) concerning this licensing transaction. In the event of any conflict between your obligations established by these terms and conditions and those established by CCC's Billing and Payment terms and conditions, these terms and conditions shall control.

14. **Revocation:** Elsevier or Copyright Clearance Center may deny the permissions described in this License at their sole discretion, for any reason or no reason, with a full refund payable to you. Notice of such denial will be made using the contact information provided by you. Failure to receive such notice will not alter or invalidate the denial. In no event will Elsevier or Copyright Clearance Center be responsible or liable for any costs, expenses or damage incurred by you as a result of a denial of your permission request, other than a refund of the amount(s) paid by you to Elsevier and/or Copyright Clearance Center for denied permissions.

LIMITED LICENSE

The following terms and conditions apply only to specific license types:

15. **Translation:** This permission is granted for non-exclusive world **English** rights only unless your license was granted for translation rights. If you licensed translation rights you may only translate this content into the languages you requested. A professional translator must perform all translations and reproduce the content word for word preserving the integrity of the article.

16. **Posting licensed content on any Website:** The following terms and conditions apply as follows: Licensing material from an Elsevier journal: All content posted to the web site must maintain the copyright information line on the bottom of each image; A hyper-text must be included to the Homepage of the journal from which you are licensing at <http://www.sciencedirect.com/science/journal/xxxxxx> or the Elsevier homepage for books at <http://www.elsevier.com>; Central Storage: This license does not include permission for a scanned version of the material to be stored in a central repository such as that provided by Heron/XanEdu.

Licensing material from an Elsevier book: A hyper-text link must be included to the Elsevier homepage at <http://www.elsevier.com>. All content posted to the web site must maintain the copyright information line on the bottom of each image.

Posting licensed content on Electronic reserve: In addition to the above the following clauses are applicable: The web site must be password-protected and made available only to bona fide students registered on a relevant course. This permission is granted for 1 year only. You may obtain a new license for future website posting.

17. **For journal authors:** the following clauses are applicable in addition to the above:

Preprints:

A preprint is an author's own write-up of research results and analysis, it has not been peer-reviewed, nor has it had any other value added to it by a publisher (such as formatting, copyright, technical enhancement etc.).

Authors can share their preprints anywhere at any time. Preprints should not be added to or enhanced in any way in order to appear more like, or to substitute for, the final versions of articles however authors can update their preprints on arXiv or RePEc with their Accepted Author Manuscript (see below).

If accepted for publication, we encourage authors to link from the preprint to their formal publication via its DOI. Millions of researchers have access to the formal publications on ScienceDirect, and so links will help users to find, access, cite and use the best available version. Please note that Cell Press, The Lancet and some society-owned have different preprint policies. Information on these policies is available on the journal homepage.

Accepted Author Manuscripts: An accepted author manuscript is the manuscript of an article that has been accepted for publication and which typically includes author-incorporated changes suggested during submission, peer review and editor-author communications.

Authors can share their accepted author manuscript:

- immediately
 - via their non-commercial person homepage or blog
 - by updating a preprint in arXiv or RePEc with the accepted manuscript
 - via their research institute or institutional repository for internal institutional uses or as part of an invitation-only research collaboration work-group
 - directly by providing copies to their students or to research collaborators for their personal use
 - for private scholarly sharing as part of an invitation-only work group on commercial sites with which Elsevier has an agreement
- After the embargo period
 - via non-commercial hosting platforms such as their institutional repository
 - via commercial sites with which Elsevier has an agreement

In all cases accepted manuscripts should:

- link to the formal publication via its DOI
- bear a CC-BY-NC-ND license - this is easy to do
- if aggregated with other manuscripts, for example in a repository or other site, be shared in alignment with our hosting policy not be added to or enhanced in any way to appear more like, or to substitute for, the published journal article.

Published journal article (JPA): A published journal article (PJA) is the definitive final record of published research that appears or will appear in the journal and embodies all value-adding publishing activities including peer review co-ordination, copy-editing, formatting, (if relevant) pagination and online enrichment.

Policies for sharing publishing journal articles differ for subscription and gold open access articles:

Subscription Articles: If you are an author, please share a link to your article rather than the full-text. Millions of researchers have access to the formal publications on ScienceDirect, and so links will help your users to find, access, cite, and use the best available version.

Theses and dissertations which contain embedded PJAs as part of the formal submission can be posted publicly by the awarding institution with DOI links back to the formal publications on ScienceDirect.

If you are affiliated with a library that subscribes to ScienceDirect you have additional private sharing rights for others' research accessed under that agreement. This includes use for classroom teaching and internal training at the institution (including use in course packs and courseware programs), and inclusion of the article for grant funding purposes.

Gold Open Access Articles: May be shared according to the author-selected end-user license and should contain a [CrossMark logo](#), the end user license, and a DOI link to the formal publication on ScienceDirect.

Please refer to Elsevier's [posting.policy](#) for further information.

18. For book authors the following clauses are applicable in addition to the above: Authors are permitted to place a brief summary of their work online only. You are not allowed to download and post the published electronic version of your chapter, nor may you scan the printed edition to create an electronic version. **Posting to a repository:** Authors are permitted to post a summary of their chapter only in their institution's repository.

19. Thesis/Dissertation: If your license is for use in a thesis/dissertation your thesis may be submitted to your institution in either print or electronic form. Should your thesis be published commercially, please reapply for permission. These requirements include permission for the Library and Archives of Canada to supply single copies, on demand, of the complete thesis and include permission for Proquest/UMI to supply single copies, on demand, of the complete thesis. Should your thesis be published commercially, please reapply for permission. Theses and dissertations which contain embedded PJAs as part of the formal submission can be posted publicly by the awarding institution with DOI links back to the formal publications on ScienceDirect.

Elsevier Open Access Terms and Conditions

You can publish open access with Elsevier in hundreds of open access journals or in nearly 2000 established subscription journals that support open access publishing. Permitted third party re-use of these open access articles is defined by the author's choice of Creative Commons user license. See our [open access license policy](#) for more information.

Terms & Conditions applicable to all Open Access articles published with Elsevier:

Any reuse of the article must not represent the author as endorsing the adaptation of the article nor should the article be modified in such a way as to damage the author's honour or reputation. If any changes have been made, such changes must be clearly indicated.

The author(s) must be appropriately credited and we ask that you include the end user license and a DOI link to the formal publication on ScienceDirect.

If any part of the material to be used (for example, figures) has appeared in our publication with credit or acknowledgement to another source it is the responsibility of the user to ensure their reuse complies with the terms and conditions determined by the rights holder.

Additional Terms & Conditions applicable to each Creative Commons user license:

CC BY: The CC-BY license allows users to copy, to create extracts, abstracts and new works from the Article, to alter and revise the Article and to make commercial use of the Article (including reuse and/or resale of the Article by commercial entities), provided the user gives appropriate credit (with a link to the formal publication through the relevant DOI), provides a link to the license, indicates if changes were made and the licensor is not represented as endorsing the use made of the work. The full details of the license are available at <http://creativecommons.org/licenses/by/4.0>.

CC BY NC SA: The CC BY-NC-SA license allows users to copy, to create extracts, abstracts and new works from the Article, to alter and revise the Article, provided this is not done for commercial purposes, and that the user gives appropriate credit (with a link to the formal publication through the relevant DOI), provides a link to the license, indicates if changes were made and the licensor is not represented as endorsing the use made of the

work. Further, any new works must be made available on the same conditions. The full details of the license are available at <http://creativecommons.org/licenses/by-nc-sa/4.0>.

CC BY NC ND: The CC BY-NC-ND license allows users to copy and distribute the Article, provided this is not done for commercial purposes and further does not permit distribution of the Article if it is changed or edited in any way, and provided the user gives appropriate credit (with a link to the formal publication through the relevant DOI), provides a link to the license, and that the licensor is not represented as endorsing the use made of the work. The full details of the license are available at <http://creativecommons.org/licenses/by-nc-nd/4.0>. Any commercial reuse of Open Access articles published with a CC BY NC SA or CC BY NC ND license requires permission from Elsevier and will be subject to a fee.

Commercial reuse includes:

- Associating advertising with the full text of the Article
- Charging fees for document delivery or access
- Article aggregation
- Systematic distribution via e-mail lists or share buttons

Posting or linking by commercial companies for use by customers of those companies.

20. Other Conditions:

v1.9

Questions? customercare@copyright.com or +1-855-239-3415 (toll free in the US) or +1-978-646-2777.
